NTNU

Norwegian University of
Science and Technology

Efficient Installation of Subsea Equipment in Deep Water

Kim Andre Tofteng

Marine Technology
Submission date: June 2018
Supervisor: Kjell Larsen, IMT
Co-supervisor: Asgeir Sørensen, IMT

Norwegian University of Science and Technology
Department of Marine Technology

NTNU Trondheim
Norges teknisk-naturvitenskapelige universitet
Institutt for marin teknikk

MASTER THESIS SPRING 2018

for

Stud. tech. Kim Andre Tofteng

Efficient installation of subsea equipment in deep water

Installasjon av undervannsutstyr på dypt vann

Background

To be able to design, install and operate a subsea oil and gas factory, a cost-effective and safe installation method is crucial. Present capital expenditure of the marine operations for a subsea production system in 300-3000m water depth is for some cases in the range 30-40% of the total capital invested.

Installation of subsea equipment is a challenge – particularly in deep water. The main challenges are:
- Plan and perform installation operations more cost-effectively while maintaining safety and accuracy. This requires that the operations must be done smarter and faster using new methods, equipment and technology.
- Existing lifting crane systems based on steel wire ropes have limitations wrt water depth and weight capacity. This is partly due to the weight of the lifting wire.
- Increase operational limits to extend the season where installation activities can be performed.
- Understand and manage the risk involved in deep water operations. An important part of this is to reduce the uncertainty of equipment and systems used.
- New and smarter installation methods must be developed.

Scope of Work

1) Review relevant literature and describe state-of-art installation methods for subsea hardware in deep water. This activity shall also include:
- A brief description of the technical challenges of the different phases of lifting by crane; from the lift-off from the deck phase until landing on the seafloor.
- A brief overview of the planning process where the importance of high operational limits, short duration of operation and large weather windows are discussed.

2) Alternative installation methods shall be briefly described. In particular, the proposed "Drop and Forget" or "Parachute Installation" method shall be discussed in detail. The discussion shall include main uncertainties, challenges and the main steps. The description shall include a proposal of the necessary equipment needed.

3) Develop a numerical simulator that can be used to assess the behavior of the installed object during the free fall and landing phase. The model shall be capable of calculating motions in six degrees of freedom.

4) Plan and perform a numerical simulation study where different objects, water depths and ocean current characteristics are considered. Extent and cases to be agreed with the supervisors. Feasibility of the "Parachute Installation" method shall be discussed based on the numerical and experimental findings.

5) Conclusions and recommendations for further work.

General information
The work scope may prove to be larger than initially anticipated. Subject to approval from the supervisor, topics may be reduced in extent.

In the project, the candidate shall present his personal contribution to the resolution of problems within the scope of work.

Theories and conclusions should be based on mathematical derivations and/or logic reasoning identifying the various steps in the deduction.

The candidate should utilise the existing possibilities for obtaining relevant literature.

Report/Delivery
The thesis report should be organised in a rational manner to give a clear exposition of results, assessments, and conclusions. The text should be brief and to the point, with a clear language. Telegraphic language should be avoided.

The report shall be written in English and shall contain the following elements: A text defining the scope, preface, list of contents, main body of the project report, conclusions with recommendations for further work, list of symbols and acronyms, reference and (optional) appendices. All figures, tables and equations shall be numerated.

The original contribution of the candidate and material taken from other sources shall be clearly defined. Work from other sources shall be properly referenced using an acknowledged referencing system.

The report shall be:
- Signed by the candidate
- The text defining the scope included
- An electronic copy to be sent to the supervisors

Ownership
NTNU has according to the present rules the ownership of the project results. Any use of the project results has to be approved by NTNU (or external partner when this applies). The department has the right to use the results as if the work was carried out by a NTNU employee, if nothing else has been agreed in advance.

Thesis supervisor**:**
Prof. II Kjell Larsen, NTNU/Statoil
Prof. Asgeir Sørensen, NTNU (co-supervisor)

Deadline: June 11th, 2018

Trondheim, February 4th, 2018

Kjell Larsen (date and signature):
June 6th 2018

Kim Andre Tofteng (date and signature):
June 11th 2018

Preface

This thesis is written by Kim Andre Tofteng as the final report in the Master's degree program in Marine Technology at the Norwegian University of Science and Technology. It was written during the fall semester of 2018.

I spent the autumn of 2017 studying fundamental concepts in marine operation related to subsea equipment installations. During my study of marine operations, I highlighted important weaknesses and expensive constraints related to the already existing methods. I suggested autonomous solutions to many of the highlighted problems to reduce the cost, which became the scope of work in my master thesis. The fundamental concepts of marine operations and highlighted problems are presented in the beginning of this report. My literature study of recent developed methods in marine operations is also presented in this report.

During my work on this thesis, it has been especially challenging to move from innovative ideas to an actual concept feasible to create. A lot of time has ben spent on thinking out methods to solve all of the observed potential problems. Changing all of the available parameters in the case study to asses potential installation conditions, and using different tuning strategies in the controller have also been very time consuming.

The field of hydrodynamics, cybernetics and marine operations are represented in the thesis, and it has been very rewarding for me to utilize what i have learned through 5 years of education in my work on this thesis.

Trondheim, June 11, 2018

Kim Andre Tofteng

Acknowledgments

I would like to express my gratitude to Kjell Larsen for fantastic guidance, discussions and motivation during my work on this thesis. I have learned a lot through weekly meetings and discussions during the year. I would also like to express my gratitude to Asgeir Sørensen for great enthusiasm on the topic, and for guidance on the cybernetics part.

Finally, I would like to thank my entire family for support throughout my education.

Abstract

This thesis presents methods to preform subsea equipment installations, and highlights problems related to the conventional crane operation used in marine operations. The crane operation faces many challenges at water depths close to 3000 m, and several recent developed methods to preform deepwater installations more efficient are presented and briefly discussed.

An autonomous method to complete a subsea equipment installation is presented and explored in the thesis. Using active control of actuators attached to the installation object, the object can be launched into the water from the support vessel, and positioned in the desired installation position by a control system. Equipment proposals for control actuators are made, and a mathematical model to control the motions of an installation object is presented in the thesis.

Several case studies are preformed on a deepwater installation of an integrated template and manifold structure (ITS), using the autonomous installation method. The control systems behaviour in different current conditions and control actuator requirements are assessed. Methods using active control together with an attached buoyancy tank or parachute are also simulated and assessed.

Based on the simulated cases, it's concluded that the presented installation method is feasible. The sensor equipment required by the control system to control the motions and postion of the installation object already exists, and are commonly used on underwater robots. A minimum of 200 [kN] is required from the control actuators in surge and sway, when the structure is submerged in 1 m/s currents, to position the a 260 tonne ITS structure in the horizontal plane, which can be produced by large attached thrusters. The roll and pitch rotations of the ITS structure is considered unfeasible to control by actuators, and the structure must therefore be stabilized passively by a buoyancy tank, parachute or some other component. Passive methods to reduce the drop velocity of the structure in water, by increasing drag damping or buoyancy is also necessary.

Sammendrag

Denne oppgaven presenterer metoder for å utføre undervannsutstyrsinstallasjoner, og fremhever problemer knyttet til konvensjonell kranoperasjon som normalt brukes i marine operasjoner. Kranoperasjonen står overfor mange utfordringer ved vanndybder nær 3000 m, og flere nylig utviklede metoder for å utføre dypvannsinstallasjoner mer effektivt presenteres og diskuteres kort i denne oppgaven.

En automatisk metode for å gjennomføre en undervannsutstyrsinstallasjon presenteres og utforskes i avhandlingen. Ved bruk av aktiv kontroll av aktuatorer som er festet til installasjonsobjektet, kan objektet slippes i vannet fra transportfartøyet og plasseres i ønsket installasjonsposisjon ved hjelp av et kontrollsystem. Utstyrsforslag til kontrollaktuatorer er presentert, og en matematisk modell for å styre bevegelsene til et installasjonsobjekt presenteres også i avhandlingen.

Flere casestudier er gjennomført på en dypvannsinstallasjon av en integrert template og manifold struktur (ITS), ved hjelp av den autonome installasjonsmetoden. Kontrollsystemets virkemåte i forskjellige strømforhold og krav til kontroll aktuatorene vurderes. Metoder, hvor aktiv kontroll sammen med en festet oppdriftstank eller fallskjerm, simuleres og vurderes også .

Basert på de simulerte casene er det konkludert med at den presenterte installasjonsmetoden er mulig å gjennomføre. Sensorutstyret som kreves av kontrollsystemet for å styre bevegelsene og posisjonen til installasjonsobjektet eksisterer allerede, og brukes ofte på undervannsroboter. Det kreves minst 200 kN fra kontrollaktuatorene i surge og sway, i 1 m/s støm, for å posisjonere den store 260 tonn ITS-strukturen i horisontalplanet, noe som kan produseres av store thrustere. Roll og Pitch bevegelsene til ITS-strukturen anses å være svært vanskelig å stabilisere ved bruk av aktuatorer, og strukturen må derfor stabiliseres passivt med en oppdriftstank, fallskjerm eller annen komponent. Passive metoder for å redusere synkehastigheten til strukturen i vann, ved å øke drag demping eller oppdrift er også nødvendig.

Contents

Nomenclature

$\alpha - factor$	Scaling factor for maximum tolerated wave hight
$\dot{v}$	fluid particle acceleration
η	Position of object
η_{ct}	Position of crane tip
$\frac{dA_{33}^{0}}{dh}$	rate of change of added mass with submergence
$\frac{dA_{33}^{\infty}}{dh}$	rate of change of added mass with submergence
∇	Volume displacement
ρ	mass density of fluid
ζ	Wave elevation
A	Cross-sectional area
A_p	Horizontal projected area of object
A_w	Water plane area
A_{ii}	Added mass
B_{lii}	Linear drag damping
B_{para}	Parachute drag damping
B_{qii}	Quadratic drag damping
C_A	Added mass coefficient
C_D	Drag coefficient in oscillatory flow
C_d	Drag coefficient
C_u	Horizontal drag
E	Young's modulus
h	Submergence relative to surface elevation
H_s	Significant wave hight
I_x	Mass moment of inertia about x
I_y	Mass moment of inertia about y
I_z	Mass moment of inertia about z
K	Total stiffness
k_c	Crane stiffness
k_s	Rigging stiffness

K_w	Wire stiffness
K_{tugger}	Stiffness in tugger lines
L_w	Length of wire
M	Mass of structure
m	Mass of wire per unit length
Op_{lim}	Maximum tolerated wave hight - Design Criterion
Op_{WF}	Maximum tolerated wave hight - Operational Criterion
$P(x)$	Cumulative distribution function
$p(x)$	Probability distribution function
S	Projected area normal to the force direction
$S(\lambda)$	Cross-product operator
$S(\omega)$	Wave spectrum
$T_\eta 3$	Eigen period in heave
T_C	Contingency Time
T_{pop}	Planned operation periode
T_R	Operation Reference Periode
U	Wind speed
V	displaced volume
v	fluid particle (waves and current) velocity
V_{curi}	Current velocity
W	Weight of structure in water
w	weight of wire, per meter wire
c θ	$\cos(\theta)$
ROV	Remotely operated vehicle
s θ	$\sin(\theta)$
SPS	Subsea Production System
t θ	$\tan(\theta)$
WoW	Waiting on Weather

List of Figures

List of Tables

Chapter 1

Introduction

1.1 Motivation and Background

In recent years, oil companies have been forced to reduce the costs of the entire life cycle of an oil production facility as they are experiencing a pressured oil price. In offshore oil production, subsea production systems is a big and important part of the oil production facility. Present capital expenditure of marine operations for a subsea production system in 300-3000m water depth is for some cases in the range $30-40\%$ of the total capital invested. This means that if subsea production systems are installed smarter and more efficient, the cost winnings could potentially be significant for the oil companies.

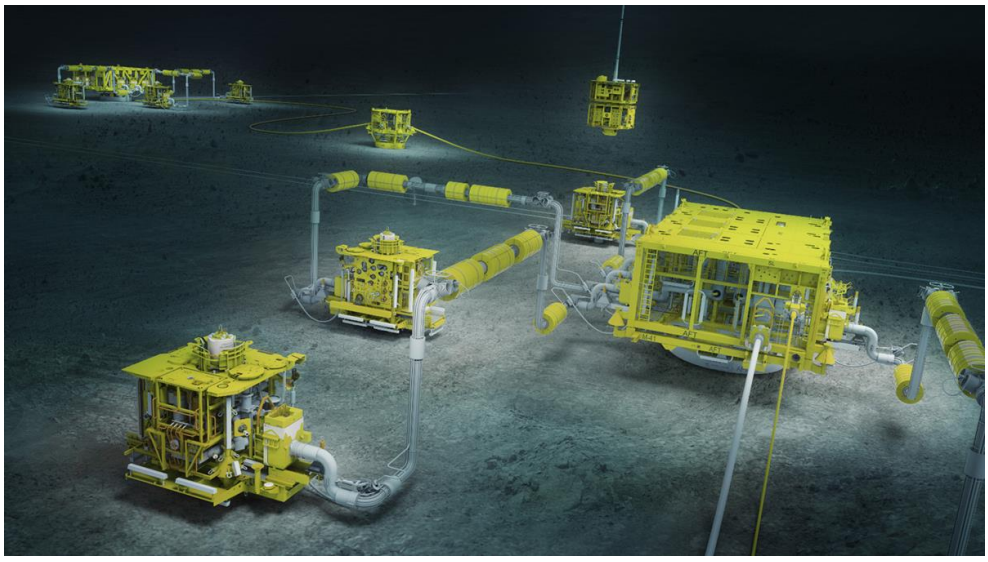

Figure 1.1: Subsea production systems (SPS) ref [1]

Oil production is a conservative business and oil companies tend to stick to methods that have provided results over the years. Therefore, not much have been changed in marine operations related to SPS installations, and the conventional "over the side" crane operation is still preferred. Offshore oil production is also moving to deeper water where the conventional "over the side" crane operation is facing new challenges.

Installation of subsea equipment have to be completed faster and smarter while maintaining safety and accuracy. New technology and installation methods have to be explored, in order to reduce

operation time and increase operation limits. In deepwater operations, the weight of the crane wire and the distance between the surface vessel and the SPS is a particularly big challenge. Installation methods more fragile to weather must be developed to extend the season where installation activities can be performed.

Recent technology development in robotics and automation have provided powerful tools to solve several industrial challenges smarter with more autonomy. Application of automation technology in marine operations could reward a significant cost winning, and have to be explored.

1.2 Objective

1. Preform a literature review of import concepts and dimensioning factors related to marine operations.
2. Highlight important problems and bottle necks constraining a subsea structure installation using a conventional crane operation, especially in deep water.
3. Preform a literature review of alternative installation method, and assess the alternative methods compared to the conventional crane operation.
4. Present a more autonomous installation method, including the necessary equipment to complete an autonomous installation of subsea structures.
5. Build a simulation model able to simulate the dynamics of a subsea structure during installation, using the presented autonomous installation method.
6. Complete several case studies using the simulation model, in order to assess the behaviour of a subsea structure when it's installed using the autonomous installation method.
7. Conclude on the feasibility of the presented installation method.

1.3 Outline of Thesis

The thesis is organized as:

Chapter 2: describes fundamental concepts related to marine operations. A thorough description of the conventional crane operation used in subsea equipment installations are also presented.

Chapter 3: presents recent developed alternative installation methods. The methods are discussed and compared to the conventional crane operation.

Chapter 4: introduces the autonomous "Drop and Forget" installation method. Several ideas on control actuators are presented, together with sensor and control system equipment requirements.

Chapter 5: describes the mathematical model used to simulate the 6 degrees of freedom motion of the subsea structure, as it's submerges using the autonomous "Drop and Forget" installation method. The control law, filter and guidance system is also presented in this chapter.

Chapter 6: 10 different case studies are presented, using the "Drop and Forget" installation method on an integrated template and manifold structure. A variety attached equipment to the installation object is simulated, and different current conditions are also tested.

Chapter 7: Concludes the thesis based on the simulated cases, and recommendations for further work are made.

Chapter 2

State of the Art

A marine operation must be designed to transfer an object from one safe condition to another. For a subsea production system (SPS) this is typically from the docks of a ship yard, to the sea bottom at the installation site. Two of the most important and cost demanding constraints of marine operations, are time and weather. The time it takes to complete the entire operation should be as short as possible. Also, the weather can not be to harsh if the operation is to be completed within a set of safety and accuracy requirements.

If one is to optimize a marine operation for minimal cost, the weather constraint has to be maximized, and the time constraint has to be minimized for the operation to be as cost efficient as possible. Both of these constraints will be discussed further in this section. A *subsea production system (SPS)* (see Figure 1.1) is often referred to in this report, and it's a common subsea structure used in oil and gas production. A typical SPS structure is an integrated template and manifold structure, containing instruments used at the sea floor in oil production.

2.1 Fundamental Concepts in Subsea Installations

2.1.1 Four Phases of the SPS Installation

A marine operation designed to install a subsea production system can according to [2] be divided into 4 phases:

1. Transportation to the installation site.
2. Lifting through splash zone
3. Submerging through the water column
4. Positioning at the sea floor.

These phases is often referred to throughout this report.

Preparation

Figure 2.1: SPS structure is loaded onto the operation vessel (ref: [3])

During the preparation phase, the SPS is loaded onto the operation vessel and the vessel is prepared for transportation to the installation site. Weldings are used to sea fasten the SPS on the operation vessel, so that the transportation can be completed in moderate waves.

Transportation to the Installation Site

When the operation vessel leaves the dock, the operation is started. In phase 1, the transportation vessel is moving towards the installation site, and the phase is completed when the operation vessel is positioned above the installation site.

Lifting Through Splash Zone

Figure 2.2: Lifting of the SPS over the side of the ship and through splash zone (ref: [4])

When the operation vessel is in position above the installation site, phase 2 starts. Welding sea fastening is released, and tugger lines are connected to the SPS to avoid pendulous motion as it's lifted over the side of the ship. The SPS is then lifted as illustrated in Figure 2.2 over the side of the ship, and into the surface water layer. In the surface water layer, the SPS enters the *splash zone* as defined in [2], which is a point where the SPS is excited by large hydrodynamic loads.

Submerging Through Water Column

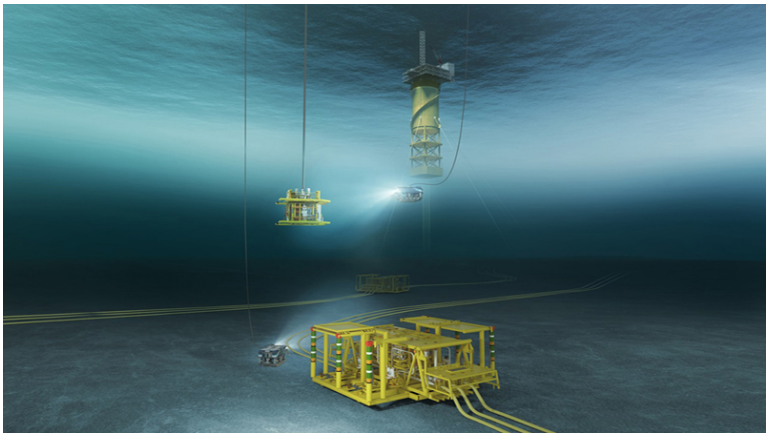

Figure 2.3: Submerging through the water column (ref: [5])

As the SPS has submerged through the top water layer, phase 3 starts. At this point the structure is slowly submerged towards the sea floor, and an ROV is used to keep track of the SPS's position in the water column.

Positioning at the Sea Floor

When the SPS is positioned right above the sea floor, phase 4 starts. At this point, the structure has to be maneuvered to the correct installation position at the sea floor by moving the surface vessel. This can typically be very time consuming in deepwater operations, as the distance between the surface vessel and the installation object is large. Finally, when the SPS has landed in the correct position, the crane wire is disconnected by an ROV and retrieved to the surface vessel. At this point the operation is finished.

2.1.2 Safe Condition

Another important concept used in marine operations, is the installation object's defined safe conditions. The safe condition is defined according to [2] as: *a condition where the object is considered exposed to "normal" risk for damage or loss. "Normal" in this context is a risk similar to the risk expected during in-place condition.* For SPS installations, there are usually two safe condition. The first is when the SPS is inside a docking facility, and the second is when the SPS is installed at the sea floor. Based on this definition, marine operations typically have according to [2] a defined *point of no return*. The point of no return is the point where the operation can't be brought back to a previous safe condition, and it has to continue to the next safe condition. For SPS installations, this point is typically after phase 2. At this point it's to complicated to bring the SPS back to the ship and bring it back to shore. Hence, after phase 3 is started, the closest safe condition is at the sea floor.

2.1.3 Weather Constraint

Weather is an important factor during the planning process of a marine operation. The weather dimensioning factor constraining the operation is Op_{lim}. Op_{lim} is the maximum tolerated wave hight, and is typically calculated independently for for each of the phases. It's for instance not possible to complete phase 2 if the waves are to high, as the risk of causing structural damage when the installation object is hanging in the crane is significant in large waves.

Op_{lim} in each phase is dependent on how fragile the planned task in the specific phase is to weather, and it's typically dependent of the size and weight of the installation object. According to [2], the operation can't start before the wave hight estimation H_s shows that Op_{lim} will not be exceeded at any point during the operation. In the North Sea where the weather is usually harsh, forecasted H_s exceeding the maximum tolerated wave hight in one of the phases is a huge issue as crane operations are very fragile to waves.

H_s estimation is done by wave statistics, and is highly connected to wind speed. For short-time operations, weather forecast is used where the estimated H_s is given by meteorologists. For longer operations, long term statistics have to be used to calculate H_s, which gives a much more conservative estimate. In Table 2.1 shown below, the H_s forecast method for different operation periods is defined according to [2].

Table 2.1: ISO 19901-6 specification for H_s estimation return period

Duration of the operation	Return periods of metocean parameters
Up to 3 days (72 hours)	Specific weather window (weather forecast)
3 days to 1 week	1 year, seasonal
1 week to 1 month	10 year, seasonal
1 month to 1 year	100 year, seasonal
More than 1 year	100 year, all year

As illustrated in Table 2.1, weather forecast can only be used to forecast H_s in operations shorter than 72 hours. If this planed operation time is exceeded, wave statistic calculations have to be made in order to forecast H_s. [6], [7] and [8] introduces several methods for estimating the wave hight H_s using wave statistics, and as shown in Table 2.1 long term sea states have to be used if the planed operation period exceeds 72 hours.

Short-Term Sea States

During short term sea states the significant wave hight H_s is assumed to be constant. Normally, meteorologists have their own models to calculate the significant wave hight H_s for a short time periods. A wave spectrum can also be used get a simple estimate of how the significant wave hight H_s is calculated in short-term sea states. An irregular wave contains a sum of many regular waves with different frequencies. The total energy inside an irregular wave can be expressed as

$$\frac{E}{\rho g} = \int_0^\infty S(\omega) d\omega \tag{2.1}$$

Where $S(\omega)$ is the wave spectrum. From this definition, several wave parameters can be deducted. There exists several standardized spectrums, and one commonly used is the Pierson-Moskowitz (PM) spectrum. This is given as

$$S(\omega) = \frac{A}{\omega^5} exp(-\frac{B}{\omega^4}) \tag{2.2}$$

$$A = 0.0081g^2 \tag{2.3}$$

$$B = 0.74(\frac{g}{V})^4 \tag{2.4}$$

where g is the gravitational acceleration, and V is the wind speed measured 19.4 m above sea level. Another commonly used standardized spectrum often used in the North Sea is the JONSWAP spectrum, and it has a form similar to the PM spectrum.
The spectral moments is defined as

$$m_n = \int_0^\infty \omega^n S(\omega) d\omega; n = 0, 1, 2.... \tag{2.5}$$

and according to [7], a simple estimate for the wave hight can be made with the use of a PM spectrum from the following equation

$$H_s = 4\sqrt{m_0} = 2(\frac{A}{B})^{0.5} = 0.0214V^2 \tag{2.6}$$

where m_0 is the $n = 0$ moment in Equation 2.5. Equaton 2.6 shows how the estimated wave hight H_s is connected to the wind speed, and that H_s is proportional to the square of the wind speed.

Long-term Sea States

For the short term sea state estimation made above, the significant wave hight is assumed constant during a short time period. For longer time periods, the significant wave hight will naturally vary, and statistical estimation methods is needed to estimate the significant wave hight H_s. To forecast H_s using long term sea states, the maximum H_s estimated to occure one time inside a specific return period has to be considered the significant wave hight H_s. In Table 2.1, the specific return period to use for the planed operation time is specified.

To find the highest wave inside a return period, a cumulative distribution function $P(H_s)$ is usually developed from a scatter diagram of measured data from the installation site. The significant wave hight H_s is an estimate for the 1/3 highest waves, and is usually assumed to be Weibull distributed. A scatter diagram with estimated H_s for a longer time period from the installation site, is often used to generate the Weibull distributed cumulative distribution function $P(H_s)$. As an example, weather data from the Heidrun field taken from [9] is shown in Figure 2.4 and 2.5.

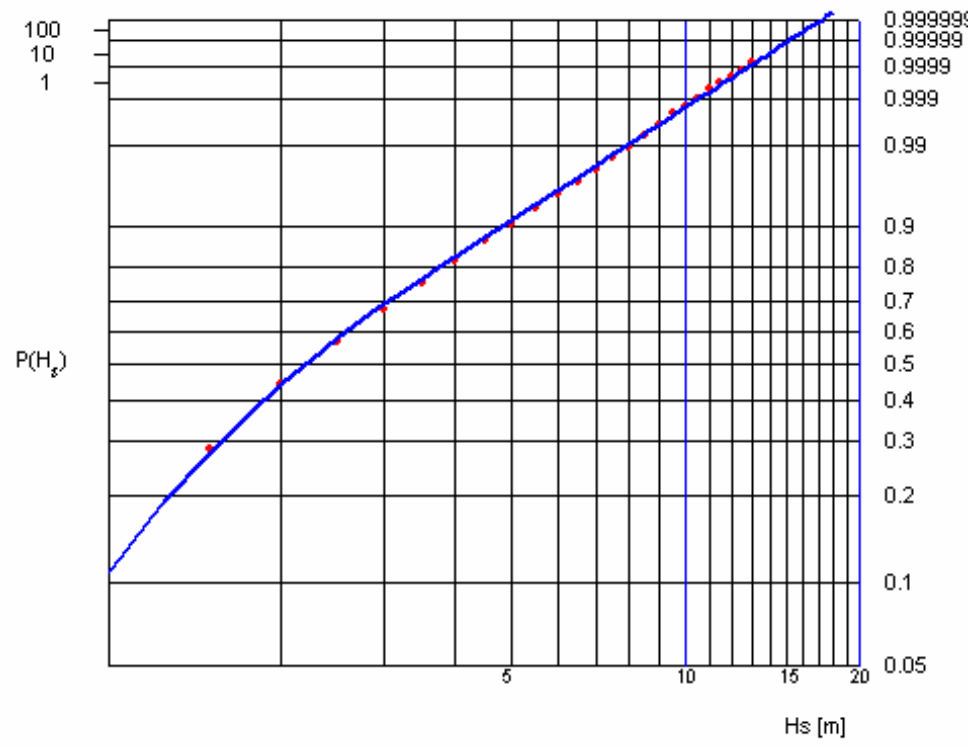

Figure 2.4: Probability of not exceeding H_s (ref: [9])

Figure 2.4 shows the cumulative distribution function of H_s, which is developed from the Weibull distribution and a scatter digram shown in Figure 2.5.

H_s	SPECTRAL PEAK PERIOD																		SUM
	0-3	3-4	4-5	5-6	6-7	7-8	8-9	9-10	10-11	11-12	12-13	13-14	14-15	15-16	16-17	17-18	18-19	19-20	<20	
0-1	55	426	1105	1561	1545	1228	849	536	319	182	101	55	30	16	9	5	3	1	2	8028
1-2	4	136	992	2957	5061	6057	5704	4553	3234	2113	1300	765	436	243	133	72	39	21	23	33843
2-3	0	5	104	678	2048	3703	4709	4670	3869	2808	1846	1127	650	359	192	100	51	26	26	26971
3-4	0	0	4	61	370	1108	2038	2639	2640	2178	1552	989	578	315	163	81	39	18	15	14788
4-5	0	0	0	3	37	208	613	1121	1438	1410	1125	765	459	249	125	59	26	11	8	7657
5-6	0	0	0	0	2	25	131	373	664	823	771	580	366	201	99	44	19	7	4	4109
6-7	0	0	0	0	0	1	17	83	225	380	444	387	267	153	75	32	13	5	2	2084
7-8	0	0	0	0	0	0	1	11	53	132	207	221	175	108	55	23	9	3	1	999
8-9	0	0	0	0	0	0	0	1	8	33	75	105	101	70	38	16	6	2	1	456
9-10	0	0	0	0	0	0	0	0	1	6	20	40	49	41	25	11	4	1	0	198
10-11	0	0	0	0	0	0	0	0	0	1	4	12	20	21	15	8	3	1	0	85
11-12	0	0	0	0	0	0	0	0	0	0	1	3	7	9	8	5	2	1	0	36
12-13	0	0	0	0	0	0	0	0	0	0	0	0	2	3	4	3	1	0	0	13
13-14	0	0	0	0	0	0	0	0	0	0	0	0	0	1	1	1	1	0	0	4
14-15	0	0	0	0	0	0	0	0	0	0	0	0	0	0	0	1	0	0	0	1
SUM	59	567	2205	5260	9063	12330	14062	13987	12451	10066	7446	5049	3140	1789	942	461	216	97	82	99272

Figure 2.5: Scatter diagram to generete $P(H_s)$ (ref: [9])

The 1, 10 and 100 year wave can then be found from Equation 2.7 by using Figure 2.4 for $P(H_s)$.

$$Q = 1 - P(H_s), \tag{2.7}$$

where

$$Q = \frac{1}{N}, \tag{2.8}$$

and

$$N = \frac{\text{return periode [s]}}{\text{average wave perode [s]}}. \tag{2.9}$$

The average wave period is the period used to calculate each H_s in the scatter diagram shown in Figure 2.5, and the return period is the amount of time you want to find the highest wave inside.

Table 2.1 also indicates if seasonal or all year wave data has to be used. When seasonal return periods are used, a cumulative distribution function similar to the one shown in Figure 2.4 can be created from a scatter diagram similar to Figure 2.5, where the scatter diagram is showing seasonal weather data. Using this method, the seasonal 1, 10 and 100 year wave can be calculated. [9] presents some calculated seasonal extreme weather data, and to illustrate how the extreme seasonal weather data varies, the data is shown in Figure 2.6.

Table 3.5 *Monthly extreme values for significant wave height [m](duration: 3 hours).*

Return period (year)	Jan	Feb	Mar	Apr	May	Jun	Jul	Aug	Sep	Oct	Nov	Dec
1	11.6	11.6	9.1	8.0	4.6	5.5	4.8	5.0	7.4	9.4	10.0	11.6
10	14.0	14.0	11.2	10.4	7.2	7.8	6.4	6.6	9.8	12.0	12.8	14.0
100	16.0	16.0	13.0	12.6	10.0	10.2	7.9	8.1	12.1	14.3	15.3	16.0

Figure 2.6: Weather data from the Heidrun field (ref: [9])

2.1.4 Time Constraint

Another fundamental constraint limiting a marine operation, is time. Long operation time is of corse expensive due to renting of equipment, operation vessels and crew. Also, Table 2.1 and the presented methods in 2.1.3 to forecast H_s using long-term wave statistics highlights the importance of time. If the total planned operation time (the time it takes from the SPS leaves the dock, to the installation is complete) exceeds 72 hours, long term wave statistics have to be used in the H_s calculation. The highest wave occurring every year is usually much higher than the one calculated from weather forecast. If you have to use the 100 year wave, the H_s estimate will be so high that it will almost be impossible to find a window the operation can be performed within.

Time Design Parameters

The time design parameter is given as T_{pop}, which is the planed time it takes to perform the operation. The planed operation time T_{pop} can be divided into four as shown in Equation 2.10, one for each phase.

$$T_{pop_{tot}} = T_{pop_1} + T_{pop_2} + T_{pop_3} + T_{pop_4} \tag{2.10}$$

As defined in [2], a contingency time also have to be calculated for each phase in order to cover any uncertainties in the operation and contingency situations. The contingency time is normally assumed to be the same as T_{pop}, and never less than 6 hours. As shown in Equation 2.11, the contingency time is calculated separately for each phase.

$$T_{c_{tot}} = T_{c_1} + T_{c_2} + T_{c_3} + T_{c_4} \tag{2.11}$$

The total planned time of the marine operation is than calculated as shown in Equation 2.12

$$T_R = T_{pop_{tot}} + T_{c_{tot}} \tag{2.12}$$

When tTable 2.1 is used, T_{pop} is used as operation period and not T_R

α-factor

To make up for uncertainties in monitoring and forecasting of environmental conditions, a scaling factor α is used. α is a function of T_{pop}, Op_{lim} together and a weather forecast level, which is chosen from tables in [10]. The design factor used for the maximum tolerated wave hight is then calculated according to Equation 2.13.

$$Op_{WF} = \alpha * Op_{lim}; \alpha < 1 \tag{2.13}$$

Op_{WF} is also calculated separately, one for each of the 4 phases. The α-factor is typically increasing with increasing Op_{lim}, and decreasing with increasing T_{pop}. The α-factor is chosen from regulations in [10] based on forecasted H_s as shown in Figure 2.7.

Table 4-1 α-factor for waves, base case

Operational Period [h]	*Design Wave Height [m]*						
	$H_s = 1$	$1 < H_s < 2$	$H_s = 2 = 2$	$2 < H_s < 4$	$H_s = 4$	$4 < H_s < 6$	$H_s \geq 6$
$T_{POP} \leq 12$	0.65	Linear Interpolation	0.76	Linear Interpolation	0.79	Linear Interpolation	0.80
$T_{POP} \leq 24$	0.63		0.73		0.76		0.78
$T_{POP} \leq 36$	0.62		0.71		0.73		0.76
$T_{POP} \leq 48$	0.60		0.68		0.71		0.74
$T_{POP} \leq 72$	0.55		0.63		0.68		0.72

Figure 2.7: DNV guidelines on choosing α

2.1.5 Waiting on Weather (WoW)

A *weather window* is defined in [2] as a time window where the forecasted H_s does not exceed Op_{wf} during the operation time T_R. The second the forecast shows that Op_{wf} will never be exceeded for each of the 4 phases, inside the planned time to complete each phase T_R, the operation can start. Therefore, a planed marine operation can not start before the forecast shows that a sufficient weather window is coming up. *Waiting on weather* is defined in [2] as the amount of time spent by stalling the operation, because a sufficient forecasted weather window is not present. In weather harsh areas like the North Sea and the Barents Sea this is a huge problem, and a lot of time and money is wasted on keeping the prepared vessel and crew on hold. Several statistical analysis have been made on the WoW issue, and Figure 2.8 and 2.9 clearly illustrates the problem. Figure 2.8 and 2.9 are based on data from the Norwegian hindcast data base NORA10, and is taken from [2].

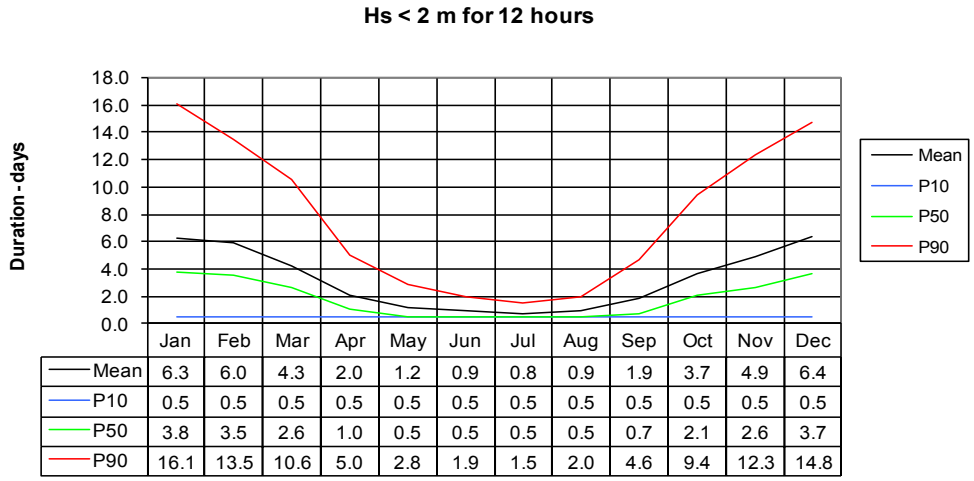

	Jan	Feb	Mar	Apr	May	Jun	Jul	Aug	Sep	Oct	Nov	Dec
Mean	6.3	6.0	4.3	2.0	1.2	0.9	0.8	0.9	1.9	3.7	4.9	6.4
P10	0.5	0.5	0.5	0.5	0.5	0.5	0.5	0.5	0.5	0.5	0.5	0.5
P50	3.8	3.5	2.6	1.0	0.5	0.5	0.5	0.5	0.7	2.1	2.6	3.7
P90	16.1	13.5	10.6	5.0	2.8	1.9	1.5	2.0	4.6	9.4	12.3	14.8

Figure 2.8: Waiting on weather $H_s < 2$

In Figure 2.8 and 2.9 it's assumed the operation is prepared at a random time, without looking at the weather forecast before preparing the operation. The probability of then having to wait a certain amount of time on the necessary weather window is illustrated in the figures. Both of Figure 2.8 and 2.9 are from the "Snøhvit" field, in the Barents Sea. The field is located far north, outside the northern coast of Norway where the weather can be really harsh. In Figure 2.8 and 2.9, P10, P50 and P90 indicates that this time is not exceeded 10%, 50% and 90% of the time. In Figure 2.8 one can see that an operation preformed in January with a T_R of 12 hours, and a $Op_{wf} < 2m$ requirement usually takes 6.3 days to complete. It is also a 10% chance that it will take 16 days to complete the operation. This indicates that a lot of time is wasted on waiting on the required weather window. The crane vessel still have to be ready the entire time, in case the weather forecast suddenly shows a sufficient weather window is coming up. During the summer months, an operation with these requirements still takes 1 day on average to complete. This means that in the best case scenario, which is only the case in 3 out of 12 months, you still have to spend $2*T_R$ on average to complete the operation.

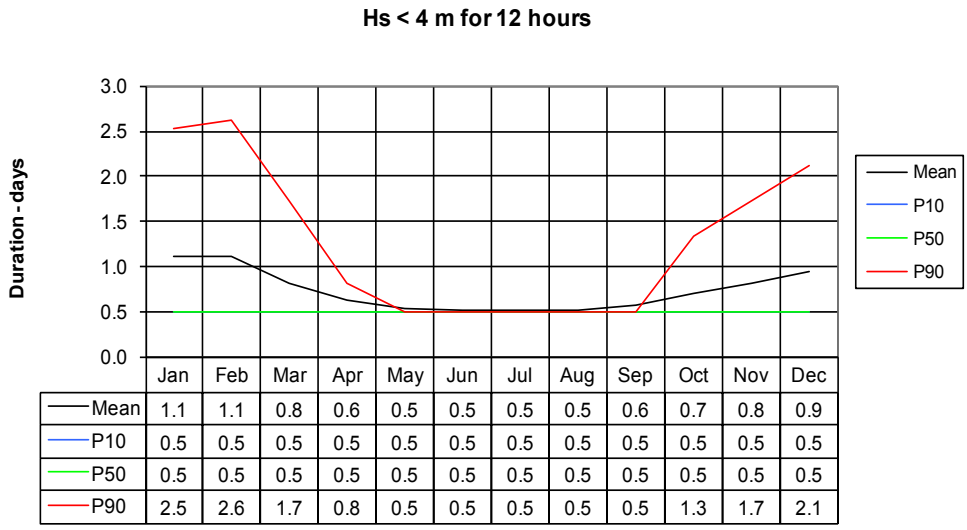

	Jan	Feb	Mar	Apr	May	Jun	Jul	Aug	Sep	Oct	Nov	Dec
Mean	1.1	1.1	0.8	0.6	0.5	0.5	0.5	0.5	0.6	0.7	0.8	0.9
P10	0.5	0.5	0.5	0.5	0.5	0.5	0.5	0.5	0.5	0.5	0.5	0.5
P50	0.5	0.5	0.5	0.5	0.5	0.5	0.5	0.5	0.5	0.5	0.5	0.5
P90	2.5	2.6	1.7	0.8	0.5	0.5	0.5	0.5	0.5	1.3	1.7	2.1

Figure 2.9: Waiting on weather $H_s < 4$

Figure 2.9 shows that when the limiting wave hight Op_{wf} is increased to 4 m, the waiting on weather time is significantly reduced. In the winter months, December and January, the operation time is only 1 day, which is $2{*}T_R$. Figure 2.9 also shows that during the summer, waiting on weather is not an issue as the operation is completed 90% of the time within the planed time T_R.

2.1.6 Discussion

If the oil industry is to produce oil at deeper water (3000m) together with a poor oil price, the installation cost of the production equipment has to be reduced. By reducing the time it takes to finish an SPS installation and increasing the maximum tolerated wave high, the operation can be less weather dependent and cheeper.

As presented earlier in this chapter, a marine operation is constrained by several design factors. Some of the design factors is possible to optimize, while many of them are set by different regulations and weather conditions.

To summarize, the tuning design factors that can be optimized is:

1. Op_{lim} - Maximum tolerated wave hight, because of weather forces and loads.
2. T_{pop} - Planned operation time

The design factors set by regulations and difficult to change is:

1. α - Weather design factor
2. T_C - Contingency time
3. H_s - Weather forecast
4. $Op_{WF}(\alpha)$ - Maximum tolerated wave hight with weather uncertainties included.
5. $T_R(T_{pop}, T_C)$ - Operation reference period

Design Factor Optimization

Op_{lim} is very dependent on the installation method used, together with the size of the SPS. Smarter installation methods can increase Op_{lim} if they are more fragile to waves. Figure 2.8 and 2.9 clearly illustrates the benefit of increasing Op_{lim}. If it's possible to change the installation method so that $Op_{lim} > 4$ for every SPS installation, the time spent on holding the operation because of unacceptable weather windows will be significantly reduced. This will give a significant cost reduction in SPS installations. Based on Table 2.7, an increase in Op_{lim} will also increase the α-factor which will give a higher Op_{WF}. it's beneficial to have Op_{WF} as close to Op_{lim} as possible, as Op_{WF} is the factor deciding the weather window.

The main requirement for T_{pop} is that it has to be held below 72 hours. Table 2.1, together with Table 2.6 clearly illustrates the issue of exceeding 72 hours in planed operation time. If one have to use long term statistics in the wave estimate, Table 2.6 shows that for the Heidrun field one have to assume a wave hight between 8-16m for 8 out of 12 months. This will make it almost impossible to find an acceptable weather window during winter, and it will be impossible to perform a SPS installation.

Faster installation methods, and more automation can give a significant reduction in T_{pop}. A reduction in T_{pop} will reduce T_C and T_R, which will reduce the time period of the needed weather window. This will reduce WoW significantly, as more weather windows will be available throughout the year. Table 2.7 also shows that a reduction in T_{pop} will increase α, which will cause an increase in Op_{WF}.

Regulation Factors

The increase in planned operation time (T_R instead of T_{pop}), and reduction in maximum tolerated waves (Op_{WF} instead of Op_{lim}) caused by scaling factors, is hard to manipulate. These scaling factors are set by regulations, and in order to change these one would have to argue that the amount of uncertainties have been reduced. More automated operations, installation methods less fragile to weather, and more failsafe installation procedures could be good arguments for an increase in the uncertainty scaling factors.

2.2 Conventional Crane Operation

The conventional way of performing aa SPS installation is by crane and crane vessel. In this section, the procedure and challenges of a typical crane operation will be discussed.

A typical crane lifting operation of an SPS installation can be divided into 5 phases.

1. Lift-off from deck
2. Object hanging in air
3. Lifting through splash zone
4. Lifting through water column
5. Landing on seabed

Each of the phases contains different challenges during the lifting operation, and the forces acting on the SPS throughout the 5 phases is presented based on information taken from [2] and [11] in this section.

2.2.1 Crane Tip Motion η_{ct}

The motion of the crane tip η_{ct} is assumed to be unaffected by the crane wire and SPS motion, and it's assumed only coupled to the ships 6 DOF motion.

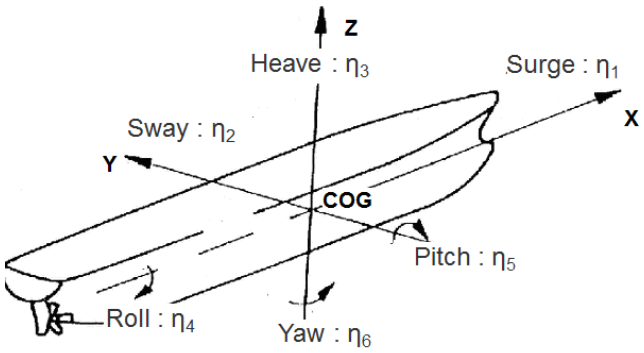

Figure 2.10: Ship coordinate system (ref:[2])

Based on the coordinate system in Figure 2.10, the surge η_{1ct}, sway η_{2ct} and heave η_{3ct} motion of the crane tip can be calculated from the Equations 2.14.

$$\begin{aligned} \eta_{1ct}(x,y,z) &= \eta_{1ship} + \eta_{5ship} * z - \eta_{6ship} * y \\ \eta_{2ct}(x,y,z) &= \eta_{2ship} - \eta_{4ship} * z + \eta_{6ship} * x \\ \eta_{3ct}(x,y,z) &= \eta_{3ship} + \eta_{4ship} * y - \eta_{5ship} * x \end{aligned} \tag{2.14}$$

The Equations 2.14 clearly illustrates how the heave motion of the crane tip η_{3ct} is connected to the heave, roll and pitch motion of the ship. The heave motion of the crane tip is especially important as it will cause a dynamic excitation force on the SPS, and a dynamic tension in the crane wire.

2.2.2 Phase 1 Lift: Lift-off From Deck

Forces

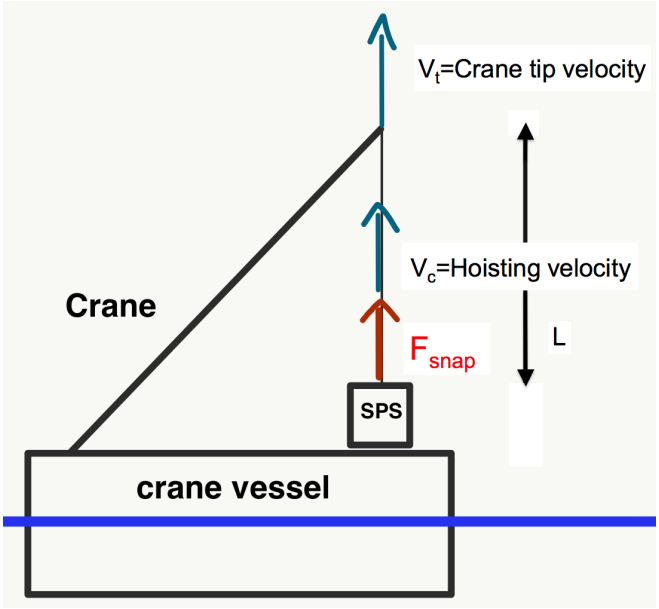

Figure 2.11: SPS is lifted off the crane vessels deck

During phase 1, the SPS is lifted from the deck on the ship and into the air. Since SPS structures usually are transported on the deck of the crane vessel, no lift of from another vessel is necessary in these operations. The load in the hoisting wire during this phase is illustrated in Figure 2.11, where the total force in the wire is shown in Equation 2.15.

$$F_{tot} = Mg + F_{snap} \tag{2.15}$$

F_{snap} is the snap load in the wire the second the crane wire is tensioned. F_{snap} is defined according to Equation 2.16.

$$F_{snap} = v_c\sqrt{KM} \tag{2.16}$$

where v_c is the hoisting velocity, K is the axial stiffness in the lifting line and M is the mass of the SPS. The snap load in this phase is caused by the winching velocity the second the hoisting wire is exciting a force on the SPS mass.

Discussion

As SPS installations usually are preformed by transporting the SPS on the crane vessels deck, not many issues or problems are related to the first phase of the crane operation. Equation 2.15 shows that as long as the winch velocity is kept relatively slow, large snap loading will be avoided and phase 1 of the crane operation will run smoothly.

2.2.3 Phase 2 Lift: Object Hanging In Air

Forces

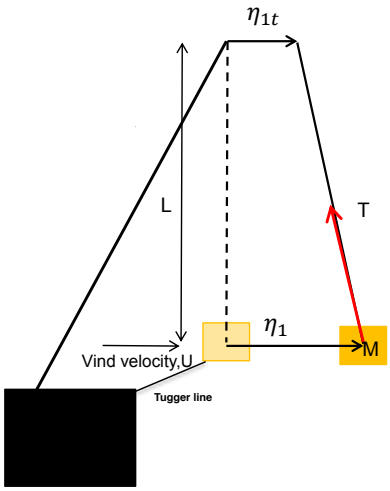

Figure 2.12: SPS is lifted over the side of the crane vessel (ref: [2])

After the SPS is in the air, it's lifted over the side of the ship. During this phase, it's very important to avoid a pendulum motion of the SPS. Tugger lines are therefore attached to the SPS and the side of the ship, in order to keep the SPS in horizontal tension when it's lifted over the side of the ship. As long as the SPS is kept in tension, no pendulum oscillation can occur and therefore impact of nearby structural elements can be avoided. The horizontal equation of motion in this phase is defined in Equation 2.17.

Horizontal 1-motion

$$M\ddot{\eta_1} + \frac{T}{L}(\eta_1 - \eta_{1ct}) + K_{tugger} * \eta_1 = C_u(U - \dot{\eta_1})^2 \tag{2.17}$$

$(\eta_1 - \eta_{1ct})$ is the relative position between the crane tip and the SPS. $(U - \dot{\eta_1})$ is the relative velocity between the wind and the SPS, T is the wire length, L is the vertical distance to the crane tip, K_{tugger} is the stiffness in the tugger lines and C_u is the horizontal drag on the SPS. The dynamic equation of motion can then be solved in order to find horizontal motion η_1 of the SPS. It is very important that η_1 is not to large so that the SPS won't hit any structural object.

The stiffness in a wire is typically

$$K = \frac{EA}{L} \tag{2.18}$$

where L is the length, E is young's modulus and A is the cross sectional area of the wire. Both the tugger lines and the crane wire will have this stiffness.

Vertical Motion

The vertical motion is not that important during this phase, which will be discussed later. The dynamic equation of motion is the shown in Equation 2.19.

$$M\ddot{\eta_3} + K\eta_3 = K\eta_{ct} \tag{2.19}$$

where K is the total stiffness of the system. The total stiffness of the system includes the crane stiffness, lifting wire stiffness and rigging stiffness, and are calculated according to Equation 2.20.

$$\frac{1}{K} = \frac{1}{k_c} + \frac{L}{EA} + \frac{1}{k_s} \tag{2.20}$$

The vertical resonance period in this phase is given in Equation 2.21 as:

$$T_{\eta 3} = 2\pi\sqrt{\frac{M + \frac{1}{3}mL_w}{K}} \tag{2.21}$$

where L_w is the length of the wire, and m is the mass of the wire per meter length.

Discussion

During phase 2, there is a problem if the wind or ship motion is able to excite a pendulum motion of the SPS. Tugger lines are attached to the SPS to avoid this problem, and the tension in these lines have to be controlled. Equation 2.17 illustrates the dynamics of the SPS in this phase. The equation shows how the horizontal motion of the crane tip is connected to the motion of the SPS, and that a horizontal motion of the crane tip will excite a force on the SPS. Hence, This phase can not be safely completed if the waves exciting the ship are to high, as the crane tips motion is highly coupled to the ships motion(given in Equation 2.14). Crane operations are usually performed in head sea, in order to avoid any roll motion of the ship. As pitch motion is significantly more resistant to exciting waves, having the ship in head sea will reduce the crane tip motion. Equation 2.17 shows that wind is also able to excite a motion of the SPS, which means it's also a weather factor that needs to be considered in a crane operation.

The vertical equation of motion is given in Equation 2.19. This equation shows that the only force able to excite a vertical motion in the SPS, is the force caused by crane tip motion. As mentioned above, the ship will be in head sea during crane operations so the motion of the crane tip will not be that large. According to Equation 2.14 heave motion on the crane tip is coupled to the roll, pitch and heave motion of the ship, which means the ship must be positioned such that heave, roll and pitch of the ship is as small as possible. Resonance is the important part to consider in this phase. Equation 2.21 shows the vertical eigen period of the system in this phase. The observations from this equation is that the wire stiffness will be really large, if the wire length is short. Equation 2.21 shows that if the stiffness K is large, and the wire length L_w is small, the eigen period is short. As crane vessels usually are large ships, they will have small amplitude oscillations with the waves. The eigen frequency of the SPS system will be much larger than the frequency of the oscillating waves and ship. Hence, the dynamic amplification factor is close to 1 and resonance is not a big issue in this lifting phase.

2.2.4 Phase 3 Lift: Lifting Through Splash Zone

Forces

Phase 3 is the part of the lifting operation where the SPS is lifted through the surface layer of the water. This is a critical phase during the crane operation, as this is the point where the SPS is exposed a high amount of excitation forces. At this point the SPS is excited by wave forces, current forces, slamming forces when it hits the water surface, it's weight in air and a buoyancy force. A summary of the forces acting on the SPS during this phase is shown in Figure 2.13.

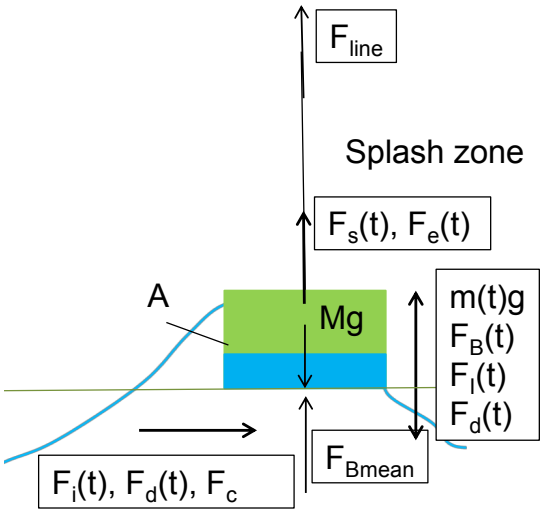

Figure 2.13: Forces on the SPS in splash zone (ref: [2])

The forces acting on the SPS shown in Figure 2.13 can be summed up to find the vertical and horizontal motion of the SPS.

Dynamic Vertical Motion

The dynamic forces in Figure 2.13 can be summed up according to the Equation 2.22, where water entry of the SPS is assumed.

$$M\ddot{\eta} = F_I(t) + F_d(t) + F_S(t) + F_B(t) + F_{line,dyn}(t) \tag{2.22}$$

The dynamic vertical equation of motion contains:

Wave Forces

$$F_I(t) = intertia\ dominated\ wave\ force = -\rho C_A V \ddot{\eta}_3 + \rho V(1 + C_A)\dot{v} \tag{2.23}$$

$$F_d(t) = drag\ dominated\ wave\ force = \frac{1}{2}\rho C_D S v|v| \tag{2.24}$$

Slamming Force

If you are lifting the SPS from air and into the water, F_S will be a slamming force and not a water exit force. The slamming force will then be

$$F_S(t) = \frac{1}{2}\rho C_S A_p(\dot{\zeta} - \dot{\eta}_3)^2 \tag{2.25}$$

$$C_S = \frac{2}{\rho A_p}\frac{dA_{33}^{\infty}}{dh}$$

Buoyancy Force

The buoyancy force is time dependent because when the SPS is lowered though the water surface, the submerged volume changes with time until the SPS is fully submerged.

$$F_B(t) = \rho g A_w \zeta \tag{2.26}$$

Equation parameters used in Equation 2.23 - 2.26 are listed in the nomenclature.

Dynamic Wire Force

$$F_{line,dynamic}(t) = K_w(\eta_{3ct} - \eta_3) \tag{2.27}$$

where K_w is the stiffness in the hoisting line. The dynamic equation of motion can then be solved numerically, and η_3 can be calculated for each time iteration.

Total Wire Force

If η_3 is calculated from the dynamic equation of motion and the crane tip motion η_{3ct} is calculated separately, the total tension in the wire can be calculated at each time iteration according to the Equation 2.28.

$$F_{wire,tot} = F_{wire,static} + F_{wire,dynamic} = Mg + M(t)g - F_{B,mean} + K_w(\eta_{ct} - \eta_3) \tag{2.28}$$

As the SPS is lowered into the water, empty wholes and spaces inside the SPS will slowly be filled with water. The increase in mass because of this is indicated as M(t) in Equation 2.28. $F_{B,mean}$ is the mean buoyancy of the SPS.

Discussion

This is the most critical phase in the crane operation as there are so many forces acting on the SPS. Equation 2.22 clearly illustrates this issue. Bad weather will cause high energy waves to excite the SPS, which can cause high motion in the SPS and therefore cause really high tension in the lifting wire. Almost every force in Equation 2.22 is either directly or indirectly connected to the waves, so the excitation forces on the SPS in this phase will be significantly increased for high wave amplitudes. The amount of dynamic forces in this phase is also dangerous, as chance of triggering a resonance motion in the SPS is significantly high. The tension in the lifting wire is especially dangerous if the waves are causing a motion in the SPS that releases tension in the wire. This will cause a high snap load on the wire when it's tensioned up again. Snap loading on the lifting wire is dangerous, and could cause failure of either the wire or the crane.

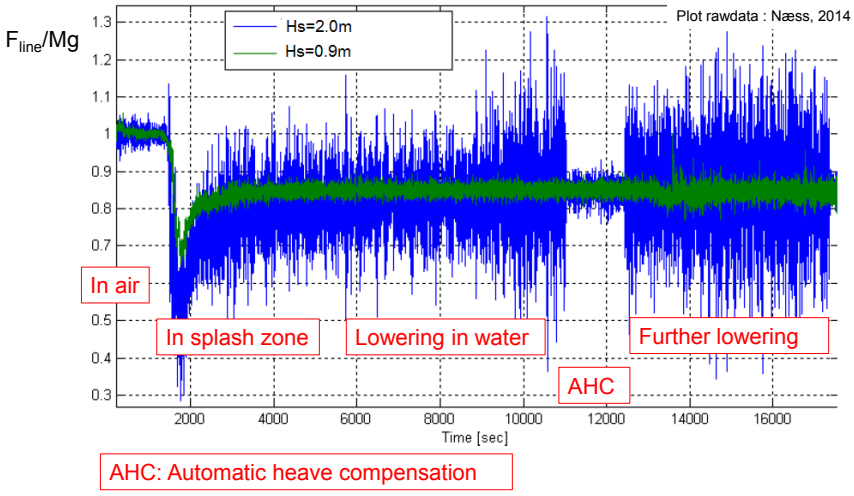

Figure 2.14: Force in hoisting line during submerging (ref: [2])

Figure 2.14 illustrates the tension in the hoisting line during lowering of the SPS for two different wave heights H_s. In the splash zone, one can clearly see that at certain time iterations for $H_s = 2$ the tension in the hoisting wire is close to zero. This indicates that waves higher than $H_s = 2$ m will probably be able to release the tension in the wire, which will cause a very dangerous snap load on the wire when it is tensioned back up. Hence, the SPS structure simulated in Figure 2.14 can

probably not complete phase 3 of the crane operation in waves higher than 2 m. An installation of this SPS will therefore have a very limited amount of weather windows it can be performed within.

The horizontal motion in this phase is not that problematic, as the ship usually lays in head sea during crane operations. Hence, the SPS will get a parallel motion to the ship, as the main horizontal excitation force will be waves exciting a parallel motion of the SPS compared to the ship. Horizontal motion is only dangerous if the SPS is moving towards the crane vessel, as it can cause structural damage. The second the SPS is dropped in the water it will also have a significant viscous damping from the water, which will reduce the horizontal motion.

2.2.5 Phase 4 Lift: Lifting Through Water Column

Forces

When the SPS is lifted through the splash zone and fully submerged a few meters down the water column, phase 4 is stared. At this point the wave loads will have minimal impact on the SPS, and the main loads working on the SPS is the vertical wire force, and the horizontal current force. The vertical wire force is causing a tension in the hoisting wire and a load on the crane. The horizontal current force is making the SPS drift off in the horizontal direction.

Vertical Motion

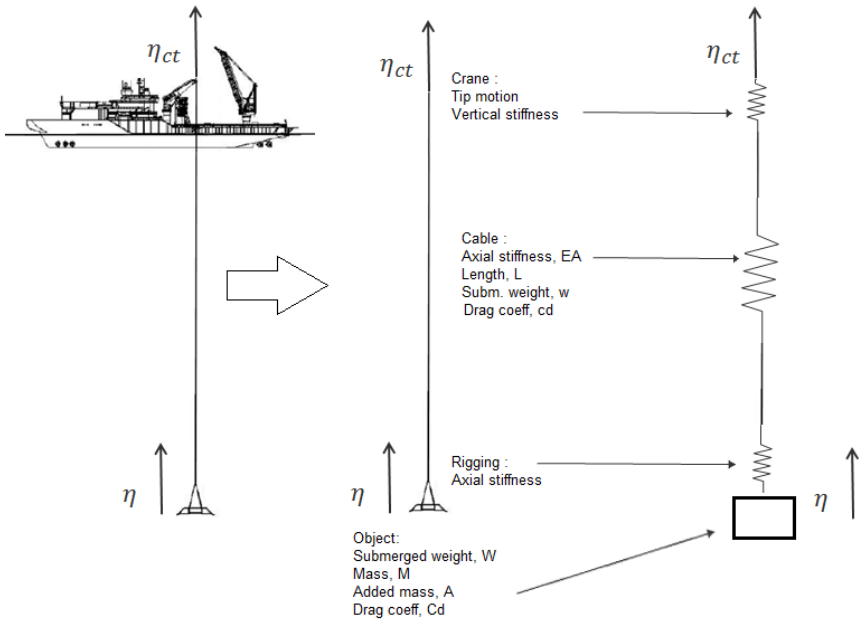

Figure 2.15: SPS is lifted through water column (ref: [2])

The dynamic equation of motion in the vertical direction if the wire is the dominant soft stiffness is shown in Equation 2.29.

$$(M + \frac{1}{3}mL + A_{33})\ddot{\eta_3} + \frac{1}{2}\rho C_D A_p \dot{\eta_3}|\dot{\eta_3}| + K\eta_3 = K\eta_{ct} \tag{2.29}$$

where K is the total stiffness of the system. It includes the crane stiffness, lifting wire stiffness and rigging stiffness.

The important property to be extracted from this equation of motion is the resonance period $T_{\eta 3}$, which is shown in Equation 2.30.

$$T_{\eta 3} = 2\pi\sqrt{\frac{M + \frac{1}{3}mL_w + A_{33}}{K}} \tag{2.30}$$

Equation 2.29 can be solved numerically to find η_3, and the total tension in the crane wire can be found using Equation 2.31.

$$F_{wire,tot} = W + wL_w + K(\eta_{ct} - \eta_3) \tag{2.31}$$

W [N] is the weight of the SPS in water, wL_w [N] is the weight of the wire and $K(\eta_{ct} - \eta_3)$ [N] is the dynamic wire tension.

There will also be an elongation in the wire in the vertical direction, due to elasticity. The formula for the elongation is not presented in this report, as it is considered to not cause any significant trouble to the lifting operation.

Horizontal Offset

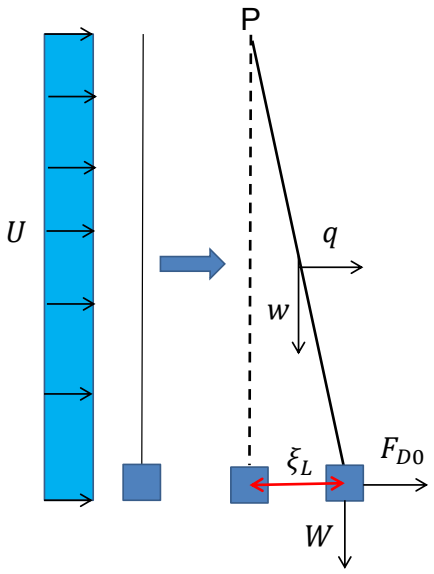

Figure 2.16: SPS offset due to currents (ref: [2])

The horizontal offset of the SPS as it submerges through the water column is found according to Equation 2.32.

$$\varepsilon_L = L_w \frac{\lambda + 0.5\frac{q}{w}}{\kappa + 0.5} \; [m] \tag{2.32}$$

where

$$\kappa = \frac{W}{wL_w}$$

and

$$q = \frac{1}{2}\rho C_{dl} D U^2$$

C_{dl} is the drag coefficient corresponding to the wire, D is the wire diameter and U [m/s] is the current speed. λ is defined as

$$\lambda = \frac{\frac{1}{2}\rho C_{D0} A U^2}{w L_w}$$

C_{D0} is the drag coefficient corresponding to the SPS, and A is the drag area of the SPS. The lifting line is assumed to be straight.

Discussion

Phase 4 of a crane operation is really time consuming, especially for deepwater operations. Equation 2.29 and 2.31 shows the equation of motion and total wire tension during this phase. A heave compensating system is usually used, in order to reduce the motion of the SPS to minimize the wire tension. This is causing a time increase of approximately 25% in the time duration of this phase. The eigen period of the system while the SPS submerges through the water column is shown in Equation 2.30, and is really important in this phase. In Equation 2.30 one can see that the eigen period will increase as the hoisting wire length is increased. The stiffness will be reduced, and the numerator in the equation will be increased because of L_w. The eigen frequency will eventually be equal to the crane tip heave oscillating frequency, and you will have vertical resonance in the system. In deep water operations the resonance depth is impossible to avoid, and an active heave compensating system is really important in order to avoid extreme tension in the lifting wire. Equation 2.31 shows that a high amplitude oscillation of the SPS motion will cause a significant wire tension.

Figure 2.14 shows that for the simulated SPS, the oscillation amplitude is increasing as the SPS is lowered in the water. This clearly illustrates this issue. Figure 2.14 also shows how the resonance oscillations are avoided by using active heave compensation.

Equation 2.31 also shows how the wire tension will increase with wire length. Deepwater installations naturally requires a long crane wire, which will eventually cause a significantly large tension in the wire, thus a large load on the crane. This is another issue related to crane operations in deep water, where the most recent solution is to use fibre rope wire instead of a steel wire. The fibre rope has a lower mass per length, which makes it much more suitable for deep water lifting. Equation 2.31 shows that a really big crane is needed, in order to cary the wire tension as the lifting depth increases. As a result, very expensive large crane vessels have to be used in deepwater operations.

As this phase is time consuming, the water currents will have a long time to give the SPS a significant horizontal offset. Equation 2.32 shows how the horizontal motion will increase with wire length. If Equation 2.32 is simulated for the submerging time, the results will show a significant horizontal offset when the SPS is closing in on the sea floor. This is a huge time consuming issue, as this offset has to be corrected if the SPS is to be placed inside the correct position.

2.2.6 Phase 5 Lift: Landing on Seabed

Forces

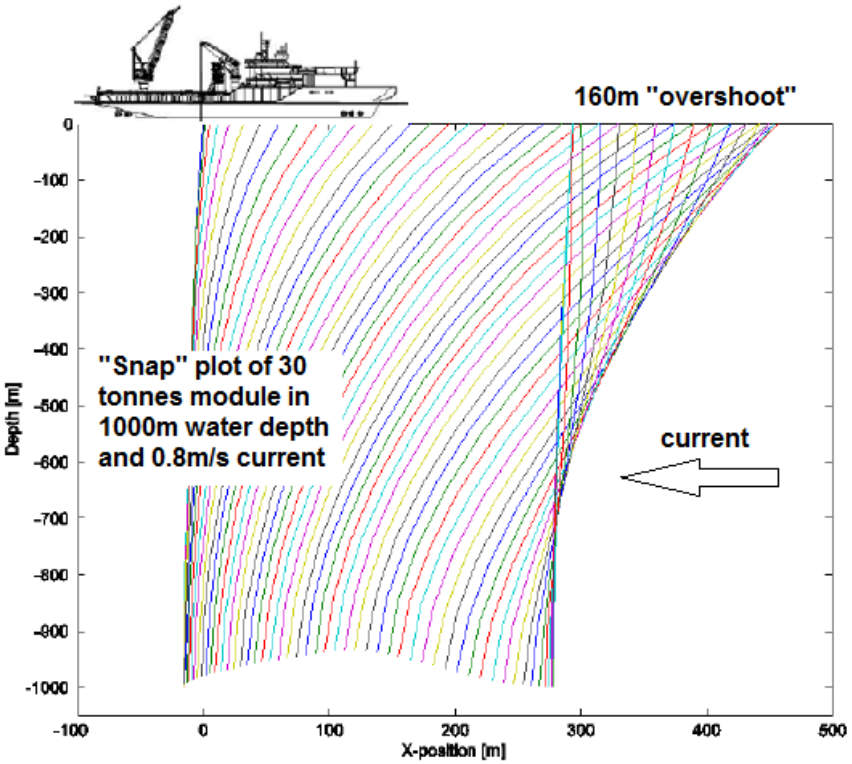

Figure 2.17: Manuvering of the SPS (ref: [2])

The last phase of a lifting operation is to land the SPS on the sea bed within the correct position. As the SPS will have a horizontal offset when it's exposed to currents, it's normally in the wrong position when it reaches the sea bed, and has to be maneuvered to the correct position by moving the crane vessel. For deepwater crane operations there will be a significant time delay from the point where the crane vessel is moved, to the point where the SPS has reached it's new position. As the crane vessel slowly moves in order to maneuver the SPS, the SPS will typically first be lifted up in the water column, before it slowly follows the ships horizontal movement. The movement of the SPS as the crane vessel moves is shown in Figure 2.17. The figure illustrates how the SPS is lifted up, before it slowly follows the movement of the vessel.

The movement of the crane vessel will be very slow, so minimal snap loading on the SPS will occur, and constant tension in the wire connecting the support vessel and the SPS is assumed. The forces acting on the crane and in the wire during this phase will look similar to Equation 2.31, where the dynamic motion can be found from Equation 2.29.

Discussion

The last part of a crane operation is to place the SPS inside its intended position. When the SPS reaches this phase of the crane operation, the heave compensation system is set to zero out the vertical movement of the SPS, so that the SPS can be smoothly lowered to the sea floor.

If the offset from Equation 2.32 is really big, which it will be especially in deep water operations,

this part will also be really time consuming. The only way to excite a force to move the SPS in a crane operation, is by moving the crane vessel. Figure 2.17 illustrates the movement of the SPS as the crane vessel is moved. The figure clearly shows how slow the SPS responds to a surface movement of the vessel. As a result, the crane vessel has to be moved back and forth until the SPS is at the correct horizontal position. In Figure 2.17 the SPS is at 1000 m depth and the response to a vessel movement is still very slow. If the installation depth is 3000 m, one have to assume that this maneuvering method is close to impossible to complete, and in the best case extremely time consuming.

2.2.7 Summary Crane Operation

As discussed in this 2.2, a crane operation contains many time consuming phases and are very fragile to weather. Deepwater installations is especially hard to complete using the conventional crane operation. Vessels with expensive heave compensating systems has to be used, the vessel need to be equipped with a really large crane, the operation requires relatively good weather and the operation time is high. One of the main problems of a crane operation is that the SPS motion is coupled to the ships motion during the entire operation. All of the equations of motion for the crane operation clearly illustrates this issue, and this is mainly what makes the crane operation very fragile to weather.

Lifting by crane requires the crane to cary heavy loads when large structures are installed. Hence, in order to perform deepwater SPS installations using the crane operation, a very large and therefore expensive crane vessel is needed. There are not to many of these vessels available, which makes them expensive to rent and significantly increases the cost of an SPS installation.

The time it takes to complete Phase 5 of the lifting operation will probably be huge if the installation depth is close to 3000 m, which will significantly increase the operation time. The submerging method used by feeding out crane wire is also very slow, which is something that is causing long operation time.

A timeline on the different phases of a crane operation, performed at 1300 m in the North Sea is provided by Equinor and shown in Figure 2.18 and 2.19. The phases referred to are the ones presented in 2.1.1.

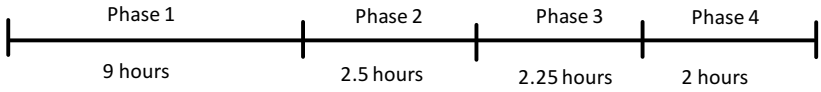

Figure 2.18: Timeline crane operation at 1300 m depth (ref: Equinor internal data)

Phase 1	• Transport is from shore (transport ready vessel), to the installation site. • 200 km transport distance • Transport velocity 12kn = 6.168 m/s
Phase 2	Includes • realesing of sea fastening • connection of tuggerlines • lifting in air over vessel side • Lifitng through splash zone
Phase 3	Lowering to seabed • Lowering velocity 0.2-0.5 m/s. Assumed 0.2 m/s. • Time increase by a factor 1.25 because of heave compensation system • Water depth = 1300 m
Phase 4	• Positioning at seabed Assumed 2hours for 1300 m depth

Figure 2.19: Installation paarameters (ref: Equinor internal data)

The first phase is time consuming because the SPS has to be transported 200 km offshore. This phase will not be that weather dependent, and is therefore not considered to be a big issue. Lifting through splash zone is very complicated, where several tasks have to be completed by the crew. Hence, this part is completed in 2.5 hours, which is a long time with a low Op_{WF} requirement.

The timeline also illustrates that phase 3 and 4 is a significantly large part of the operation time, even though the installation depth is only 1300 m in this case. If the installation depth is increased to 3000 m, the duration of phase 3 can be multiplied by 2.5. At this depth the duration of phase 4 will be a lot longer, as it will be really difficult to maneuver the SPS by moving the crane vessel at this depth. Also, since the surface motion of the crane vessel is coupled to the SPS during the entire crane operation, Op_{WF} will be relatively low for phase 2, 3 and 4. This is a huge problem if the operation time in phase 3 and 4 is significantly increased in deepwater operations.

Chapter 3

Alternative Installation Methods

In Chapter 2 of this report, several challenges connected to a SPS installations was discussed. Op_{lim} has to be increased and the operation time T_R has to be reduced in order to get a significant cost reduction in SPS installations. The conventional way of doing a SPS installation is to transport the SPS on the crane vessels deck, and lower it to the sea floor by crane. In order to try and reduce the const of SPS installations, several alternative installation methods have been proposed in different papers. They will be presented and briefly discussed in this chapter. The different phases of a SPS installation was presented in chapter 2, and will be often referred to in this chapter. To summarize, the different phases of a SPS installation is

Four Phases

1. Transportation to the installation site.
2. Lifting through splash zone
3. Submerging through the water column
4. Positioning at the sea floor.

Also, the conventional crane operation have three main challenges

1. Coupled motion between the crane vessels motion and the SPS during the entire operation. As a result, low Op_{wf}.
2. Very time consuming method to complete Phase 3 and 4. As a result, high T_R.
3. Requires large expensive crane vessel to handle the heavy loads.

3.1 Pendulous Method (PIM)

The description of this method is taken from [12], and further discussed in [13].

3.1.1 Description

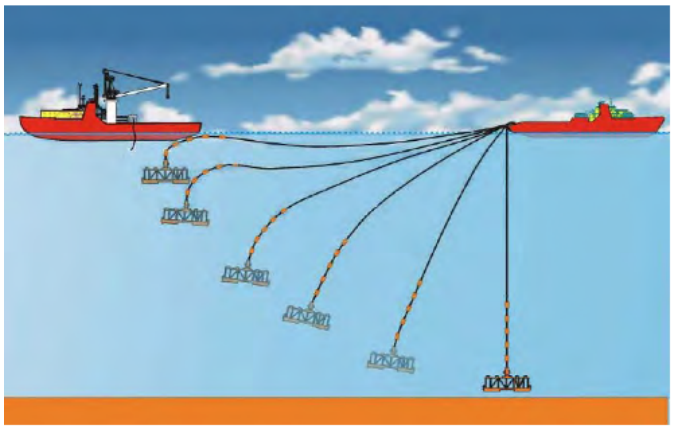

Figure 3.1: Pendulous Method (ref: [12])

The Pendulous Installation Method (PIM) is another non-conventional method developed by Petrobras due to the low availability and high cost of deepwater construction vessels and heavy lift vessels. The PIM method is to use conventional small vessels without special riggings and a FRDS system, which allows deployment of 300Te heavy equipment in deep waters up to 3,000m. The PIM method requires two small installation vessels to launch and deploy a subsea structure onto the seabed.

Different from traditional vertical launch, the PIM method uses a conventional steel wire winch system as a launch line to launch the structure in a pendulous motion while using a polyester rope as deployment line to finally deploy the structure onto the seabed. The first installation vessel uses its crane to lift off and overboard the manifold into water and through slash zone, and then transfer the load from the crane to the launch winch wire at a certain water depth, say 50m below surface. The deployment line is pre-rigged with the lifting slings of the manifold and equipped with a number of buoyancy elements to reduce the winching capacity requirement for both the launch winching system and the deployment winching system. The deployment line is pre-deployed with a certain length which shall ensure that the manifold should maintain a vertical position approximately 50m above the seabed. The elongation of the deployment polyester rope under load tension shall be taken into account to avoid any premature touchdown. Upon transferring the load from the crane to the launch winch wire, the launch winch can start paying out the launch line while maintaining the deployment winch at the braking mode. Through a pendulous movement, the load will gradually transfer from the launch line to the deployment line. When the pendulous motion is completed and the manifold will swing from the bottom of the first vessel, 50m below water surface, to the bottom of the second vessel, 50m above the seabed.

The polyester rope is gradually tensioned up to the full load. This will prevent axial resonance by using ropes much longer than the lengths that would fall into the resonance region when lowering through water column and allow ropes to undergo gradual tension after pre-paid. After the pendulous launch, the launch line can be disconnected by using ROVs to pull the trigger sling. Then the deployment winch can continue deploy the manifold vertically, position and land it into the target box on the seabed with a conventional way. This PIM method is cost effective compared to utilization of scarce specialized deepwater installation vessels or drilling rigs. It should

be pointed out that, due to complex geometry of the manifold, hydrodynamic instability may rise during launch operation.

3.1.2 Discussion

This method is mainly designed to increase the submerging speed during phase 3, and reduce the load on the crane during phase 3 and 4. As a result, the time it takes to complete phase 3 is significantly reduced. This will also cause the currents to have less time to create a horizontal offset of the SPS, which means the SPS will most likely be closer to the target position when phase 4 is started. This method also do not require the crane to carry the load from the entire wire length and the SPS during phase 3 and 4. Therefore, a smaller crane vessel can be used. Since the SPS is released in a free fall pendulum motion, the SPS is decoupled from the vessel for most of this time and the resonance depth is avoided. Hence, no heave compensating system have to be used during phase 3. The wire will only be in tension at the end of this phase.

On the negative side, this method still uses a crane to lift through splash zone, which will maintain high weather constraints in phase 2. The method also requires two vessels, which is expensive. Phase 4 is completed the same way as the crane operation, which can be very time consuming and problematic in deepwater operations.

3.2 Pencil Buoy Method (PBM)

The description of this method is taken from [12].

3.2.1 Description

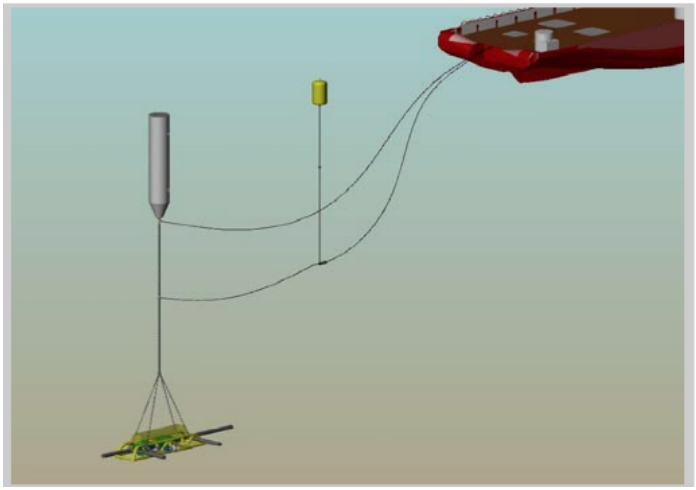

Figure 3.2: Pencil Buoy Method (ref: [12])

The Pencil Buoy Method (PBM) is a subsurface transportation and installation method developed Aker Solutions. The PBM method requires a crane barge to lift the structure from the transportation barge at a nearby inshore transfer location with sufficient water depth. Then transfer the structure weight from the crane barge to an top class AHTS vessel. After rigging the structure with the tug winch wire and the tubular buoyancy tank shaped as a pencil, the pencil buoy is then launched from the stern deck by paying out of the towing winch line while the tug moves slowly

forward. The structure and the rigging weight are suspended from the Pencil Buoy during wet tow.

The Pencil Buoy is a steel structure with internal ring stiffeners. The buoy is subdivided into many watertight compartments to meet the requirement of one-compartment damage. Normally a wet tow speed of 3.0 to 3.5 knots is maintained. Upon arrival at the installation site the towing wire is winched in while transferring the structure weight from the Pencil Buoy back to the towing winch wire. Then the buoy can be disconnected. The AHTS tug shall move slowly forward during load transfer and therefore ensure no contact between the tug stern and the buoy. A passive heave compensator is used during lowering of structure to seabed. The lifting off and lowering through splash zone are performed inshore sheltered area rather than offshore operations. The subsurface wet tow is designed for typical unrestricted summer storms. The lowering operation is a standard offshore operation similar to other deepwater installations.

3.2.2 Discussion

This method is designed to avoid the problems related to phase 2. Phase 2 is performed inshore in quiet water conditions by a crane barge before the operation is started, so no crane vessel is needed for this installation method. Therefore, the main advantage of this method is that a highly available AHTS vessel can be used to perform the entire operation. This will reduce the vessel renting cost. The weather restrictions related to phase 2 is also removed, so more weather windows are available to this phase.

On the negative side, this method uses a submerged tow to transport the SPS to the installation site. As mentioned in the description, the submerged towing speed is 3.0-3.5 knots. A regular transport on the vessels deck can be performed at 12 knots, so the submerged tow will significantly increase the time it takes to complete phase 1. Phase 1 will also be more fragile to waves when a submerged tow is used, which will reduce Op_{wf} in phase 1. Phase 3 and 4 is performed the same way as the crane operation, except that a crane do not have to cary the weight and motion loads from the SPS and the wire. Hence, most of the crane operation issues during phase 3 and 4 will still be present in this method.

3.3 Floating Installation Device (FID)

Part of the description of this method is taken from [14].

3.3.1 Description

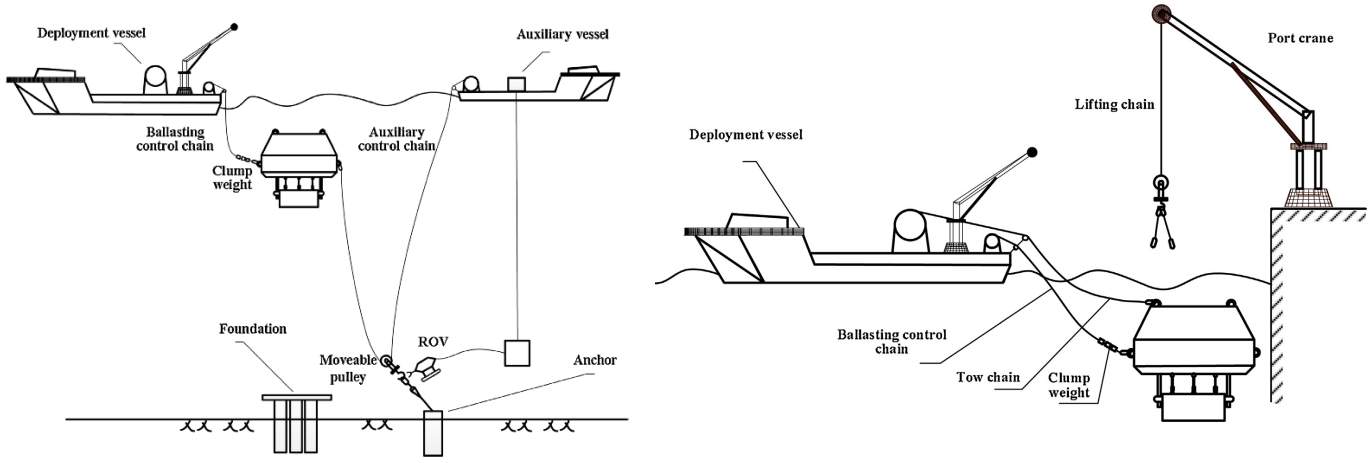

(a) SPS installation using a floating installation device (FID).

(b) Floating installation device is connected to transportation vessel inside dock facility

Figure 3.3: Floating installation device (ref: [14])

The concept of the designed method originated from the PBM. The new method utilizes an FID to support the SPS in the transportation and installation process. The device is mainly made of solid buoyant material, which has low density (lower than water), high compressive strength, a low water absorption rate and other properties. Thus, the transportation can be a wet tow process, and the need for a large deck space is eliminated, which is similar to the PBM.

In general, the method is to connect a Floating Installation device (FID) to a transportation vessel inside a docking facility. This is shown in 3.3b. The SPS and the FID is then transported to the installation site, using a submerged tow. At the installation site, an anchor first has to be installed at the sea floor before the FID is connected to an auxiliary vessel through the anchor. The SPS attached to the FID is then lowered to the sea floor, by ballasting the FID with a chain deployed by the deployment vessels crane. This procedure is shown in fig 3.3a. During the submerging of the SPS and the FID, the FID is kept in balance by adjusting the wires connected to the auxiliary and deployment vessel. When the FID have reached it's destination at the sea floor, the SPS is disconnected by a ROV and the ballasting chain is removed so that the FID will float back up. Further description can found in [14].

3.3.2 Discussion

Similar to the PBM method, this method is completing phase 2 inshore in quiet weather conditions, which is significantly increasing Op_{wf} in phase 2. The big difference from the PBM method is that this method is keeping the motion of the SPS decoupled from the support vessels motion during phase 3 and 4. Hence, the FID method will aslo gain an increase in Op_{wf} in phase 3 and 4.

The negative side of this method is mainly that it's very complicated to complete. It requires two support vessels, where one of them needs to be equipped with a crane. It also requires an anchor to be installed at the sea floor, and wires to be connected through the anchor and to the FID. See

Figure 3.3a. This seems to be very time consuming and subject to complications and errors. The winnings from increasing Op_{wf} in phase 2, 3 and 4 might be compensated by a significant increase in operation time T_R. This method will also have the same problems related to the submerged tow, as the PBM method.

3.4 Heave Compensated Landing System (HCLS)

The description of this method is taken from [15].

3.4.1 Description

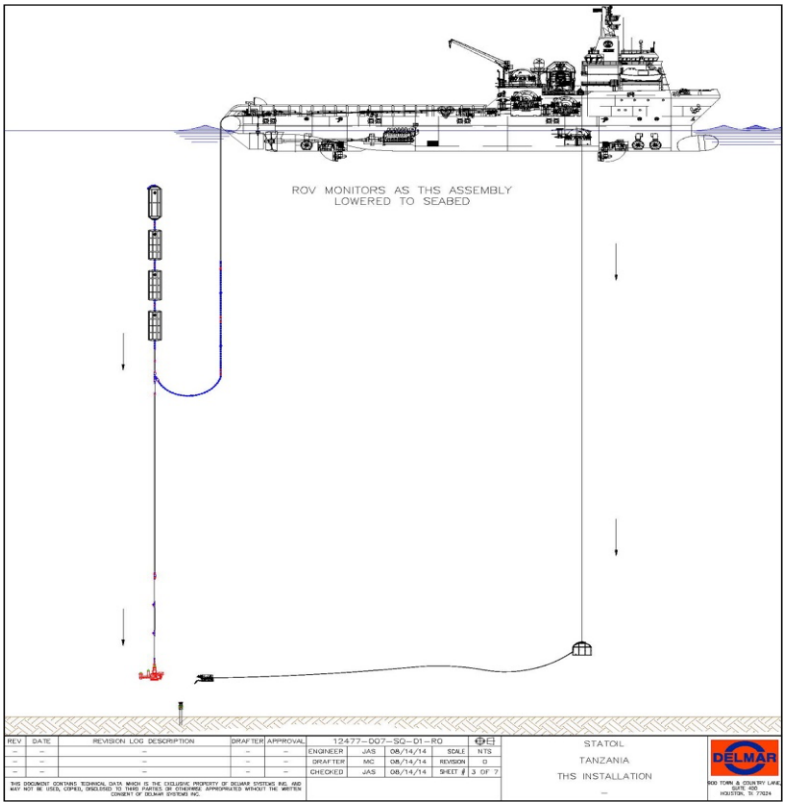

Figure 3.4: Heave Compensated Landing System (ref: [15])

The HCLS is a passive system that requires no active damping systems. The concept originated from early pipeline intervention methods'. Nearly all the components are readily available, and most can be leased.

The HCLS decouples vessel motion from the payload by supporting the payload from a buoy below the wave zone. Because the buoy is below the wave action and its associated turbulence, there is little energy and therefore little tendency for inherent motion. The buoy is connected to the vessel by chain and wire. The short chain section (-400 ft) is attached to the buoy and hangs to form a "belly" before rising toward the vessel.

The chain serves many purposes. The chain "belly" allows the workboat to heave independently of the buoy. Also, because the chain's weight is supported by both the buoy and the vessel, the buoy will naturally come to equilibrium with the sum of its buoyancy, payload and partial chain weight. Thus, the chain automatically facilitates trim adjustment for small weight inaccuracies.

The chain is also used to transfer weight to or from the buoy after the payload is landed or recovered. For example, consider the case of a 4,000 Ib. control pod being lowered and landed on a subsea manifold. After setting the pod on the manifold, 4,000 Ib. of chain weight (-105 ft of 2 inch chain) can be transferred to the buoy by paying out additional cable from the deployment system. As more chain weight is transferred to the buoy's side of the chain "belly," the equivalent payload weight is transferred to the subsea landing base. The payload can be released from the running tool, and the system will remain in equilibrium.

As the vessel stem heaves up and down, the neutral point in the chain "belly" shifts and transfers chain weight to and from the buoy. This load transfer could theoretically cause the buoy to move up and down, defeating the purpose of the HCLS system. However, this type of motion can be eliminated by engineering the HCLS around the resonant periods of each sub-system. When properly designed, the chain load is transferred to and from the buoy too quickly for the buoylpayload package to respond. This effectively decouples the buoy from the vessel. Specific attention must be paid to the environmental conditions.

Another possible function of the chain is to eliminate "snap loading" on the deployment wire under overboarding or retrieval operations. Under some conditions, especially when line loads are light or payload sail area is large, the subsea system could be traveling upward while the vessel stem is moving downward. This transition from tensile to a zero load, then back to a tensile load is known as a "snap" load. These loads can damage or break the wire and/or rigging. Increasing the load at the end of the wire with an added chain section can assist in keeping the wire in tension at all times, and thereby reduce the snap load tendency.

3.4.2 Discussion

This method presents another solution to try and keep the SPS motion decoupled from the support vessels motion during phase 3 and 4. This will increase Op_{wf} in these two phases, and will give these phases of the operation more available weather windows. it's an elegant method to decouple the motion, and it only requires a simple buoyancy structure attached to the SPS.

The method still leaves a lot of problems related to the operation unanswered. The buoyancy structure and the SPS needs to be lifted through the splash zone, assumed that it's transported to the installation site on the support vessels deck. This method will aslo probably submerge the SPS through the water column relatively slow, so there will be a significant offset when the operation reaches phase 4. Currents could also potentially cause the buoyancy structure to drift far off, if it's not held in place in some way.

This method do not present a way to maneuver the SPS during phase 4, which is a huge issue. The SPS is decoupled from the support vessels, so an active force needs to be directly applied to the SPS in order to maneuver it during phase 4. The HCLS installation method do not present a solution to this issue.

3.5 Subsea Deployment System (SDS)

The description of this method is taken from [16].

3.5.1 Description

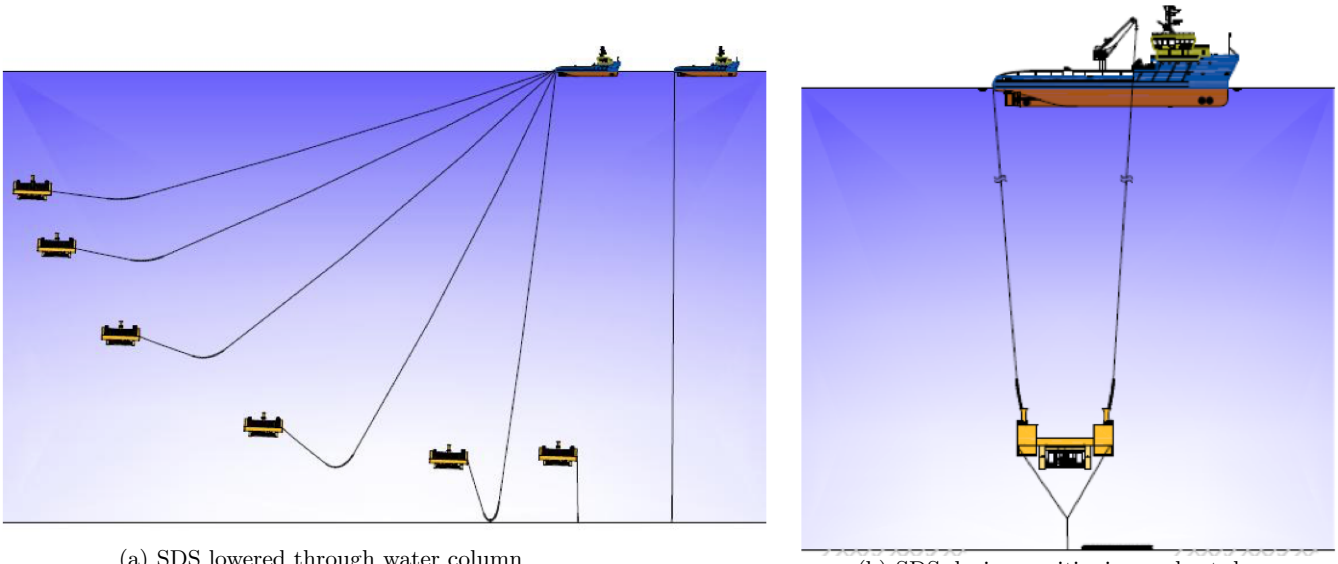

(a) SDS lowered through water column

(b) SDS during positioning and set down

Figure 3.5: Subsea deployment system (ref: [16])

The method utilizes a floating structure attached to the SPS. A typical installation will consist of the following steps:

1. Load-out
2. Shallow Draught Surface Tow
3. Ballasting and Trimming
4. Deep Draught Surface Tow
5. Submerged Tow
6. Positioning
7. Set-down
8. Ballasting
9. Float-off

Load-out: The structure may be loaded-out into the Subsea Deployment Vehicle (SDV) by a variety of methods depending on the available equipment and draught. Load-out options include:-

- Direct Lift
- Lift, Submerge and Float-over
- Float-over in a dry dock
- Submerge and Float-over using a floating dock or submersible barge

- Submerged Docking

Shallow Draught Surface: The shallow draft surface tow mode is used when there is limited water depth at the load-out location. During this phase the side hulls are dry. The SDV and structure will be towed in shallow draught surface tow mode until reaching a suitable location for flooding the hulls.

Ballasting and Trimming: At an inshore location with suitable draught, the SDV is ballasted down by flooding the hulls. The amount of solid buoyancy is such that the SDV will float with only the castles and chain towers breaking the water surface once the hulls are flooded. The water plane area of the castles is relatively small so that the net buoyancy can be accurately measured and adjusted as necessary by adding or removing ballast from the corner lockers.

Deep Draught Surface Tow Having checked and adjusted the ballast as necessary the SDV and structure are towed in deep draught surface tow mode with only the castles and control chain towers breaking surface.

Submerged Tow: When the water depth is suitable, the tow vessel pays out the tow wire and tow chain clump weight causing the SDV to submerge fully. The tow vessel can adjust its speed and the length of the tow wire to maintain the SDV at a suitable depth. The position and inclination of the SDV is monitored throughout by acoustic interrogation. On approaching the field, the tow vessel slows down and adjusts the tow wire keeping the tow chain clump weight off the seabed until in a designated parking area. The tow vessel then pays out the tow wire until the clump weight rests on the seabed. The SDV and structure is now safely "anchored" and floats above the seabed. Ideally the length of tow wire between the clump weight and SDV will be marginally greater than the distance between the parking area and the final target location. This allows final set-down without the need to lift and re-position the tow chain clump weight. In such cases it's possible to perform the entire installation operation with a single surface vessel.

Positioning: The SDV is positioned by means of two control chains suspended from the installation vessel and lowered into the chain towers. The height of the SDV is adjusted by raising or lowering the control chains and the position and orientation of the SDV is adjusted by moving the installation vessel and / or the crane. In deeper water the tow vessel may also be utilized to aid in positioning and heading control by lifting the tow wire and chain clump weight clear of seabed.

Set-down: Once the SDV is in the correct position and orientation the structure is landed by lowering the control chains until the structure rests on the seabed. The control chains are then fully lowered into the chain towers and temporarily disconnected. The control chain connector will be located on the top of the chain tower ready for reconnection after ballasting. The weight of the control chains contributes to the initial on-bottom stability, i.e. prior to ballasting.

Ballasting: Ballast weights are added to the SDV ballast chain lockers by the surface vessel crane to balance the weight of the structure. Once all the ballast is added the SDV is slightly negatively buoyant and will rest on the structure. The SDV is now disconnected from the structure.

Float-off: The installation vessel re-connects to the control chains and raises them until the SDV is neutrally buoyant. Further raising of the control chains lifts the SDV clear of the structure. The SDV is maneuvered in a near reverse of the installation procedure until clear of any subsea assets. The control chains are then removed completely from the towers allowing the SDV to float above the seabed while still anchored by the tow chain clump weight.

3.5.2 Discussion

Similar to the PBM and the FID method, the SDS method is performing phase 2 inshore in quiet water conditions, which increases Op_{wf} in phase 2. The SDS method performs phase 3 similar to the pendulous method, where the SDS is submerged through the water column in a pendulum motion. This is a fast and efficient way of completing phase 3, which keeps the SPS decoupled from the support vessels heave motion and increases Op_{wf} in phase 3. Having the SPS submerge in a pendulum motion will also reduce the horizontal offset when phase 4 is started, and this method

also only requires a small crane vessel. In phase 4, the SPS is maneuvered by moving two control chains, which means the SPS is not directly coupled to the support vessels heave motion.

This method is solving many of the issues related to the conventional crane operation in a very good way. Phase 2 and 3 will gain a significant increase in Op_{wf}, and will not be very time consuming. Problems during phase 4 may still occur using this method. If the SPS has a significant offset when it reaches the sea floor, and the control chains maneuvering the floating device attached to the SPS is excited by strong currents, it might be problematic to land the SPS inside the correct position. The method also faces problems related to a submerged tow, similar to the PBM.

3.6 Pendulous Installation with Submarine

3.6.1 Description

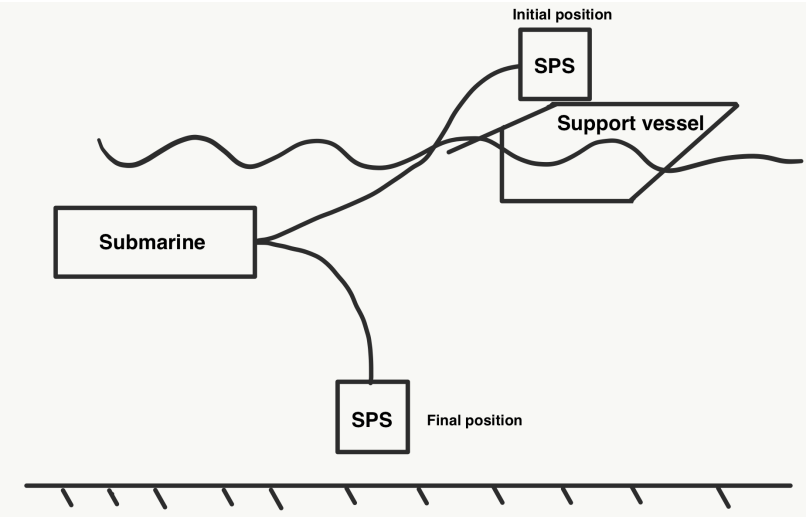

Figure 3.6: Submarine installation

A pendulous installation with a submarine is a hypothetical method, and not much testing have been performed on this method. The idea is that the SPS can be transported on a smaller support vessel without crane during phase 1. When the vessel reaches the installation site, a submarine structure is dropped into the water with a wire attached to the SPS. The SPS is on the support vessels deck at this time, and a ramp is then released in the back end of the support vessel. After the ramp is released, the support vessel is trimmed so that the back end of the ship is closer to the water. The ship will now make full speed ahed so that the SPS will slide into the water.

The SPS will submerge through the splash zone, and move in a pendulum motion towards the sea floor. This part is similar to the Pendulous method except that the SPS is now attached to a submerged submarine. Since the submarine is floating a few meters below the water surface, it's not exposed to waves. This will significantly reduce the motion of the submarine which will reduce the motion of the SPS while it submerges through the water column. The wire length between the submarine and the SPS is set, so that the pendulum motion will be over when the SPS is right above the sea floor. At this point, the submarine is feeding out wire to land the SPS at the sea floor. A simple sketch of this procedure is shown in Figure 3.6.

3.6.2 Discussion

First of all, this method will complete phase 1 and 2 very efficient as the SPS is transported on the support vessels deck, and dropped into the water at the installation site. Phase 1 and 2 will be completed in a short amount of time, and will have a high Op_{wf}. It will also only require one small transportation vessel. Phase 3 is preformed similar to the pendulous method, which is a efficient way of completing phase 3 with a high Op_{wf}.

The submarine will be at a water depth where it will have minimal wave excitation forces acting on it, so the heave motion on the submarine will be minimal. Since the SPS is coupled to the submarine in phase 4, the motion of the SPS will also be minimal. This will make it easier to land the SPS at the sea floor, but a method to position SPS in the landing phase is still needed.

This method is a very hypothetical one, and several engineering problems have to be solved on the submarine structure for this installation method to be possible. The submarine has to be able to cary the weight of the SPS structure, and be kept stable as the wire force from the SPS changes attack angle. It also has to be held in place in some way, so the SPS won't drag it far out of position.

Chapter 4

Drop and Forget Installation Method

This chapter is written to present several ideas on how to preform a "Drop and Forget" installation of an SPS, and the requirements related to the suggested methods are discussed. Several problems related to this installation method is also discussed. The "Drop and Forget" installation method is further tested throughout this report, and proposed solutions to the problems presented in this chapter are discussed based on the test results.

A "Drop and Forget" installation of a subsea production system is a proposed installation method where the subsea structure is launched into the water in free fall, and the submerging and landing within the installation site is completed without any help from the support vessel. An installation skid containing all the necessary equipment needed to preform a fully automatic free fall installation is used, and retrieved back to the surface vessel when the installation is completed.

The "Drop and Forget" installation is assumed to give a significant increase in Op_{wf} as no crane is used at any point during the installation, and the motion of the SPS is totally decoupled from the surface support vessel during submerging. The goal of the installation method is to achieve an $Op_{wf} > 4m$ requirement, as the cost winnings are assumed to be significant if this requirement is achieved. The operation time T_R is also assumed to be significantly reduced compared to the conventional crane operation, especially in deepwater operations.

A typical SPS installation object and its 6 degrees of freedom motion is shown in the Figure 4.1.

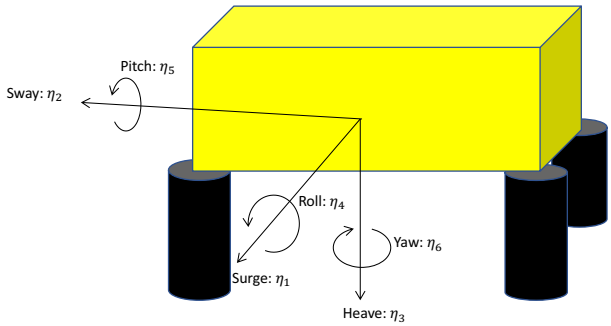

(a) Motions of the SPS in 6 DOF

(b) Integrated template and manifold structure (ref:[**?**])

Figure 4.1: Subsea production system and its motions.

4.1 Installation Procedure

Preparation

During the preparation phase, an installation skid is attached to the installation object, and the installation object with the attached installation skid is loaded onto the transportation vessel. Only a simple transportation vessel with a launching ramp is needed in this installation method, which means a vessel equipped with a large crane is not required.

Phase 1: Transportation to the Installation Site

The installation object is transported to the installation site on the support vessel. No submerged tow is used, and welding sea fastening of the installation object is used to make sure this phase is completed safely. This phase is assumed to have a high Op_{wf} requirement, and it's completed within a minimal amount of time. When the transportation vessel reaches the installation site, it's positioned above the sea floor installation site using DP, and it's positioned such that the roll motion is minimized.

Phase 2: Launch of the Installation Object Into The Water

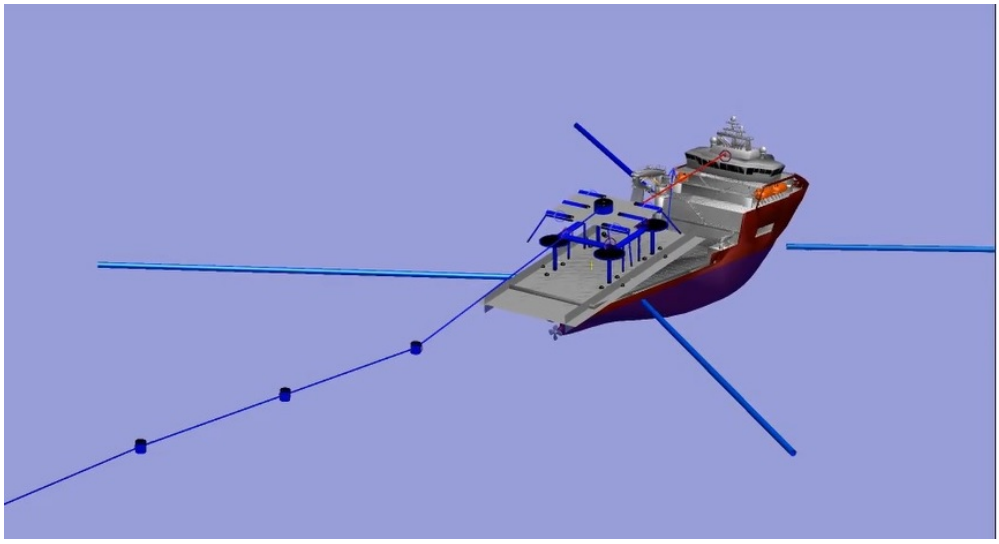

Figure 4.2: Launch of SPS from the support vessel (ref: [2])

During launching of the installation object into the water, the sea fastening is released and the ramp behind the ship is tilted such that the installation object will slide into the water. The support vessel can also use it's thrusters to accelerate forward, so that the installation object will drop into the water. Figure 4.2 illustrates the launch of the installation object from the support vessel. Even though no crane is used in this phase, it's still considered a critical phase as the installation object will drop into the water with angular velocity while it's exerted by wave forces. This will result in heavy loads on the different parts of the installation object, and it will submerge through the splash zone with large rotations. As illustrated in Figure 4.2, a line in tension attached to buoyancy tanks might have to be used to reduce the rotations of the installation object as it submerges through the splash zone. Op_{wf} requirements in this phase will highly depend on the maximum allowed motion on the support vessel when the installation object is launched of the ramp. It will also depend on how much loading and hydrodynamic forces the equipment on installation skid can handle. The operation time T_R is assumed to be very low in this phase.

Phase 3: Submerging Through Water Column

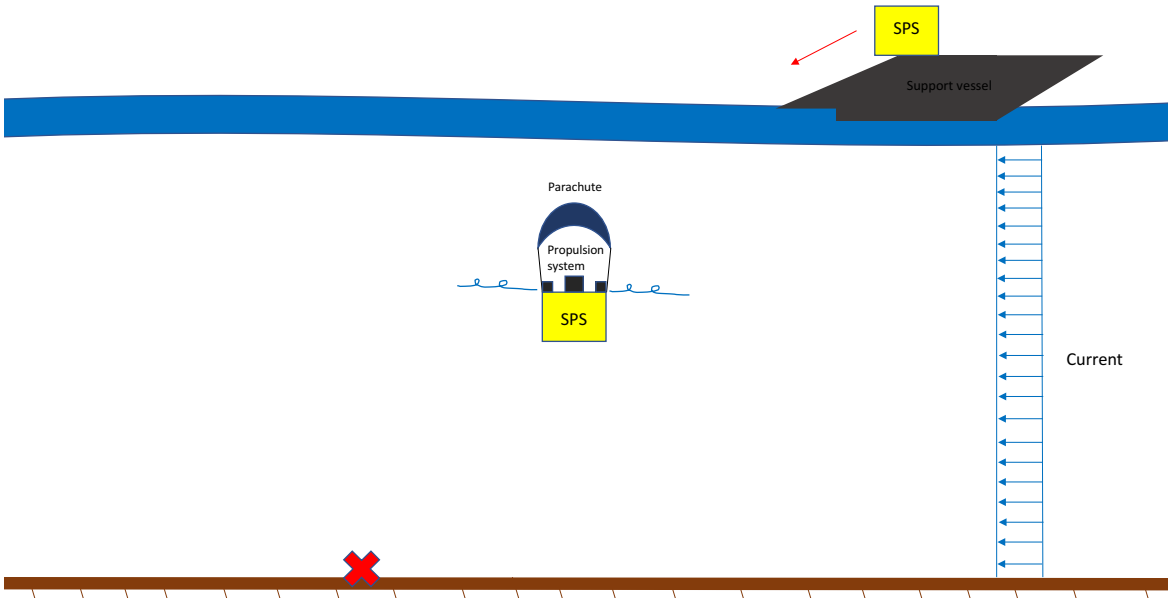

Figure 4.3: Submerging of installation object through water column

When the installation object has submerged through the splash zone, the equipment of the installation skid will start to stabilize the rotations of the object using the attached actuators. It will also slowly start to move the installation object towards the horizontal installation position at the sea floor. Figure 4.3 illustrates how this phase is completed. In Figure 4.3 a parachute is used to stabalize the roll and pitch motion of the installation object, and the parachute will also increase drag damping during submerging to reduce the drop velocity of the installation object. Figure 4.3 also shows that propellers are used to position the installation object in the horizontal plane as it submerges towards the sea floor. Op_{wf} is assumed to be significantly higher in this phase compared to the crane operation, as the submerging installation object is totally decoupled from the surface waves, and only exerted by ocean currents. The operation time T_R is also going to be low compared to the crane operation, and it is shown in [17] that phase 3 is completed within 0.5-1 hour depending on the drop velocity.

Phase 4: Landing on the Sea Floor

The installation skid attached to the installation object will slowly move the object to the correct installation position in the horizontal plane during phase 3, so no maneuvering of the object is needed in phase 4. The object will just land inside the correct position when it reaches the sea floor. When the object is installed, the installation skid attached to the object is realised by an ROV, and retrieved back to the surface vessel. This phase will have significantly shorter operation time T_R compared to the crane operation, especially in deepwater operations. As discussed in Chapter 2, positioning of the installation object at the sea floor is considered problematic and time consuming when it's maneuvered using the surface vessel, especially in deepwater operations. Therefore, using actuation directly on the installation object at the sea floor is a huge advantage.

4.2 Control Actuation Hardware Design

The main hardware requirements for the control actuators on an installation skid, designed to use in the "Drop and Forget" installation method is:

1. It has to be able to stabilize the roll and pitch motion of the object relatively fast, and it must be able to do this when the object has relatively large initial angles.
2. It has to be able to stabalize the yaw motion of the object after some time, but yaw is not as critical as the roll and pitch motion.
3. It has to be able to position the object in the correct installation position within the submerging time.
4. It has to be able to reduce the drop velocity to an acceptable impact velocity at the sea floor.

4.2.1 Propulsion Skid

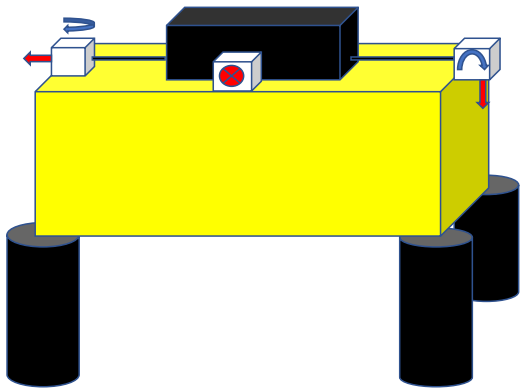

Figure 4.4: Installation skid containing propellers and motor on top of the SPS

The most direct method to provide control actuation, is to attach propellers and a motor on top of the installation object. As the installation object usually don't have any hollow elements, the object has it's centre of buoyancy and centre of gravity in the same point. Thus, the structure is hydrostatic unstable and the control actuators have to be able to provide moment in roll and pitch to stabilize the structure. The control actuators also have to provide a positive force in surge and sway to position the structure in the horizontal plane, without creating a destabilizing moment in roll and pitch. Also, the propellers must be able to counteract large rotations in yaw.

One example of how this design can look like is illustrated in Figure 4.4. If rotatable thrusters are attached on the top of the structure, connected to a motor in the middle, they will be able to provide a moment in roll, pitch and yaw, which can be used to stabilize the structure in these motions. The problem with the propeller set up in Figure 4.4, is that one have to assume the propellers need to provide a positive force in surge and sway during the entire submerging of the structure because of water current and positioning in the horizontal plane. If, for instance the left propeller in Figure 4.4 is providing the control force to position the structure in sway, it will also provide a moment in roll. This means that the right propeller has to provide an equal force downwards, in order to zero out the moment in roll produced by the left propeller.

A solution to the above mentioned problem is to use retractable thrusters found in [18] in the propulsion skid, to provide control actuation underneath the main body of the structure. An illustration of how this design can look like is shown in the figure below.

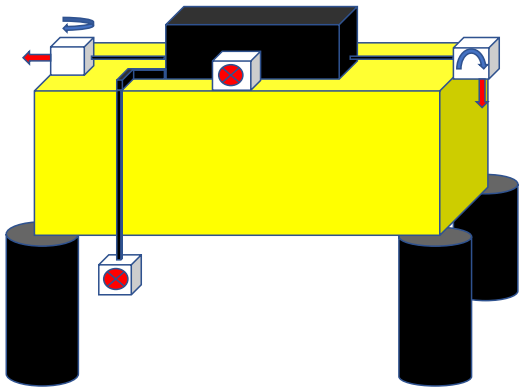

Figure 4.5: Propulsion skid using retractable thrusters

In the propeller set up illustrated in Figure 4.5, it's possible to use the force from two propellers to produce a large resulting force in surge, without creating any destabilizing moment in pitch. This will increase the maneuverability of the structure, and at the same time provide better use of control energy.

Positioning of the propellers and the amount of propellers needed have to be carefully chosen on designing a propulsion skid as shown in Figure 4.4 and 4.5. The installation skid has to be able to efficiently control the motion of the structure in surge, sway, roll, pitch and yaw, and the total set up requirements for the propellers is further explored and discussed throughout this report. Also, different propeller types to maneuvre the structure have to be explored. Azimuth thrusters presented in [18] is a good choice as they provide great directional control, and can be attached as rotatable thrusters. Water jets is also something that have to be considered, as they provide great maneuvrability by the use of nozzles, and they might be able to produce full control force faster than a conventional thruster. The time the control actuators use to produce the needed control force is also very important.

Enormous amount of control energy is required to reduce the drop velocity using only propellers [17]. Hence, using only propellers on the installation skid will require the structure to handle a relatively large impact velocity upon landing. The propellers also need to be able to produce full control force in vertical direction when the installation is completed, in order to transport the installation skid back to the sea surface.

4.2.2 Propulsion Skid and Buoyancy Tank

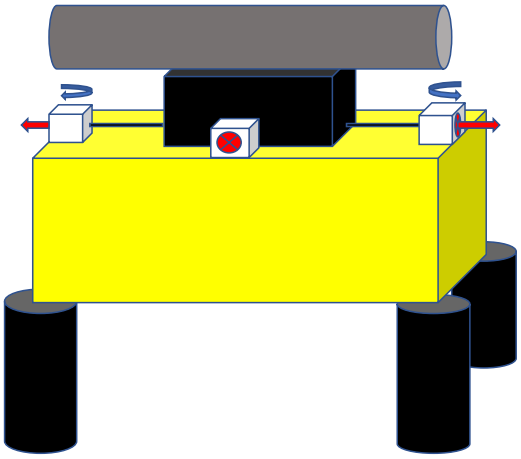

Figure 4.6: Propulsion skid and buoyancy tank

In order to reduce the actuation requirements to the installation skid containing only propellers, a hollow tank can be attached on top of the structure. The buoyancy tank will provide hydrostatic stability in roll and pitch by producing a restoring moment, as it will move the centre of buoyancy of the total structure above the centre of gravity. Thus, the propellers only need to provide actuation in surge, sway and yaw. The restoring moment of the buoyancy tank will also stabilize the structure in roll and pitch when the control force in surge and sway produces a destabilizing moment, because of the thrusters placed on top of the structure as illustrated in Figure 4.6.

Another important contribution from the buoyancy tank is the reduced drop velocity because of increased buoyancy. This will increase the submerging time, which will give the controller more time to position the structure in the horizontal plane. It will also reduce the impact velocity of the structure upon landing on the sea floor, which will reduce the impulse load on the structure upon landing. When the structure has landed, the installation skid can be removed, and the positive buoyancy from the tank will make sure the installation skid is floating back up to the sea surface.

The main issue related to the use of a buoyancy tank, is the extreme pressure it will have to resist in deep water. The installation skid has to be able to preform installations at 3000 m water depths, and at this depth the buoyancy tank has to withstand a pressure of approximately 300 bar. Therefore, the feasibility of designing a buoyancy tank able to withstand at least 300 bar pressure have to be explored. A huge block of buoyancy foam used in underwater vehicle also have to be explored, as it might be better suited to handle extreme hydrostatic pressure.

4.2.3 Propulsion Skid and Parachute

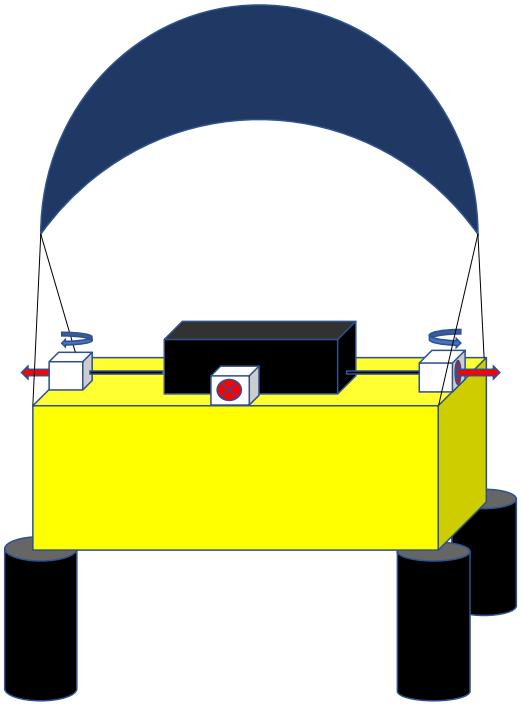

Figure 4.7: Propulsion skid and parachute

Another idea for an installation skid, is to use a parachute instead of a buoyancy tank. The parachute will function similar to the buoyancy tank, as the roll and pitch motion will be kept in tension by the parachute wires. As the parachute stabilizes the roll and pitch motion, the propellers only need to provide actuation in surge, sway and yaw. The parachute will also provide extra drag damping to the submerging structure, which will reduce the drop and impact velocity. The main benefit from using a parachute instead of a buoyancy tank, is that it functions the same as the buoyancy tank, but the extreme pressure in deep water is not an issue.

The main issue by using a parachute is handling of the parachute in water. The parachute has to be released in the water before launching of the structure in phase 2, so that it will stabilize above the structure as it submerges through the water column. Alternatively, a releasing mechanism has to be designed, so that the parachute can be released similar to the release of a parachute in air when the structure has submerged through the splash zone. This will again require that the structure is stabilized in roll and pitch by the propellers before the parachute is released. Assembling of the parachute at the sea floor after the installation so that it can be returned to the sea surface, and hydrodynamic instabilities around the parachute are also issues that have to be explored.

4.2.4 Underwater Glider and Helicopter

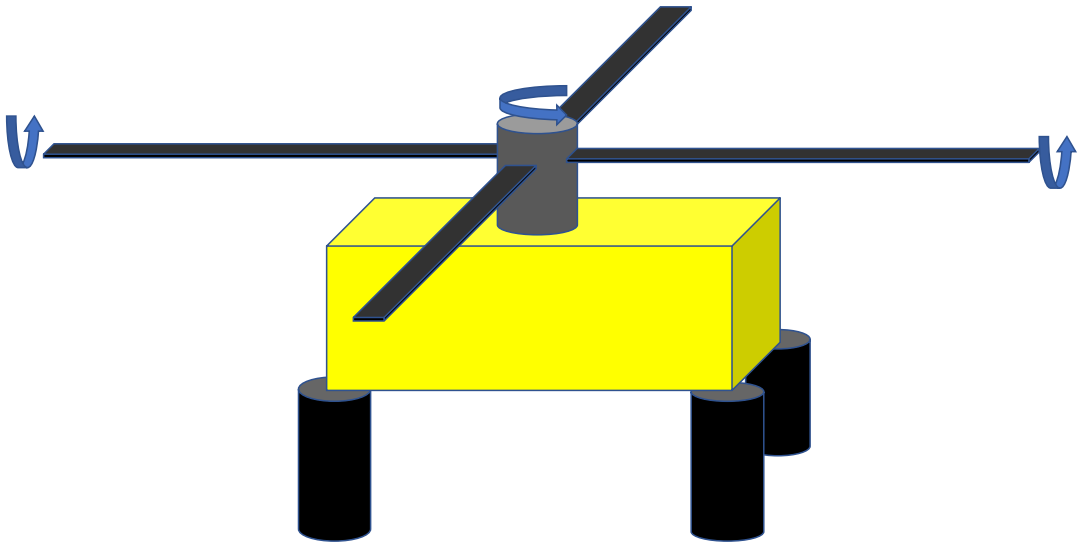

Figure 4.8: Installation skid with adjustable wings

One of the more ambitious ideas on an installation skid, is to utilize the surrounding fluid flow around the structure as it submerges to produce lift and drag by using attached wings. The 4 wings are at first fixed, such that they can't rotate in yaw. As the structure submerges during phase 3, the wings are rotated in roll and pitch to change the attack angle towards the fluid flow to adjust the lift and drag force on the wings. The adjustable lift and drag force will provide control actuation to stabilize the structure in roll, pitch and yaw, and position the structure in the horizontal plane. When the structure is almost at it's destination at the sea floor, the fixed yaw motion of the 4 wings are released so that they can work as a helicopter to produce a thrust upwards and reduce impact velocity.

Maneuvrability of this method might be an issue, as it's hard to tell how well the wings will provide actuation in each DOF. The 4 wings also might have problems on stabilizing the structure in roll and pitch if the structure has large rotations after it has submerged through the splash zone. Another issue is the use of relatively long wings, which will be excited by large hydrodynamic loads upon impact with the sea surface during launching and submerging through the splash zone.

4.3 Control System Hardware and Software Design

An installation skid containing actuators to position the structure has to be controlled by a fully embedded computer system placed on to the installation skid. The control system computer must have the ability to preform all the necessary calculations, communicate with the actuators and sensors. Communication between the installation skids computer and the surface vessel is also beneficial, in order to monitor the operation. A fully embedded computer system attached to the structure to control the actuators must be equipped with the following:

- **Structure Dynamics Representation:** Equation of motion representation of the dynamics of the structure and the installation skid in 6 DOF.
- **Controller:** Controller to command the needed control force in each DOF to achieve the desired position and attitude. When a specific actuation set up is chosen, the controller must

include the actuator dynamics producing the commanded control force. Low pass filtering also have to be considered in the controller if high frequent error measurements are an issue.

- **Sensors:** Sensors to measure data to send as feedback into the control system must be included.
- **Observer:** An observer to filter out sensor measurement bias, together with unmodeled disturbances in the dynamics of the structure have to be included. The observer ability to calculate all of the states in the dynamics of the structure using only a few sensor measurements, is also very important. This will provide redundancy if sensor measurements are lost.
- **Guidance system:** The guidance system has to be able to bring the installation object to it's intended position at the sea floor, using as little control energy as possible. No advanced maneuvring of the installation object is needed.

4.3.1 Sensors

In general it's desirable to have as many state measurements as possible, together with their first and second derivatives, to achieve good accuracy and redundancy to the control system. Most of these variables are possible to measure using sensors commonly used in underwater vehicles. The proposed required sensors for the installation skid are presented below:

Acoustic Position Measurements using Ultra-Short Baseline (USBL)

As the structure is submerged in water, GPS can't be used as position measurement sensor. Underwater acoustic positioning systems are commonly used to triangulate the position of underwater vehicles, and can be used in a similar way to measure the position of the submerging installation object. In underwater acoustic positioning systems, an acoustic signal is sent through the water towards a transponder. The transponder returns the signal to it's origin, and the travel time and bearing angle of the acoustic signal is measured. Using the speed of sound in water, the position of the transponder relative to the origin of the signal can be calculated. 3 transponders or transducers are required to triangulate the underwater position of a submerged object, and the different methods to do this is Long Baaseling system (LBL), Short Baseline system (SBL) or Ultra Short Baseline system (USBL).

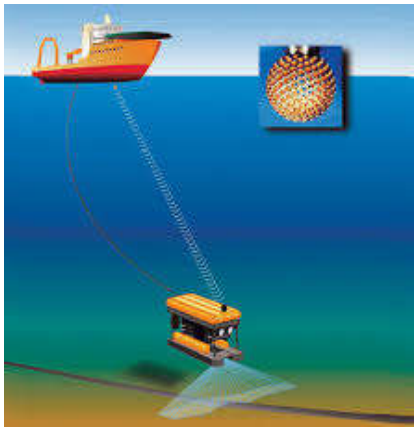

Figure 4.9: Ultra-Short Baseline (ref: [19])

Using a USBL system to measure position, one single hydrophone/transducer unit with 3 sensors is attached to the installation skid. The transducer will continuously send out an acoustic signal to a transponder located at the sea floor, which will return the signal back to the transducer

on the installation object. The 3 sensors on the transducer unit is then able to triangulate the position of the installation object relative to the transponder on the sea floor. Figure 4.9 illustrates how this works, where the hydrophone/transducer in the figure is placed on a surface vessel, and the transponder is placed on the underwater ROV. Further description on underwater acoustic positioning systems are found in [19] and [20].

Inclinometer: An inclinometer/tilt sensor is necessary to directly measure the roll and pitch angles of the structure. The structure is assumed to have large rotations during launch from deck and submerging through splash zone, so an inclinometer is recommended to support the gyroscope in rotation measurements in roll and pitch.

Inertial Measurement Unit (IMU): A 9 DOF IMU is also necessary on the installation skid. The IMU sensor consists of a 3 DOF gyroscope, 3 DOF accelerometer and a 3 DOF magnetometer. The gyroscope measures the angular rates in roll, pitch and yaw, which can be integrated in the observer to find the attitudes. The accelerometer measures the acceleration in x, y and z, which are integrated in the observer when position or velocity measurements are lost. The magnetometer utilizes Earths magnetic filed to find the heading (yaw) angle of the structure.

Doppler Velocity Log (DVL): The Doppler velocity log is another acoustic sensor with 4 transducer heads, which uses Doppler shift in the echo of the acoustic signal to calculate the velocity in x, y and z [21]. The DVL sensor will during submerging measure the relative velocity between the installation object and the surrounding water column. It can only use the sea floor as reference to measure the exact velocity of the object when the installation object is approximately 90 m above the sea floor.

Pressure Gauge: The pressure gauge sensor is used to measure the surrounding pressure of the installation object. The pressure is used in the hydrostatic pressure equation to find the exact depth of the installation object as it submerges.

Current Measurements: Current measurements can be achieved in two ways. The simples method is to to use the DVL sensor to find the relative velocity between the object and the surrounding current, together with dead reckoning calculations from the IMU sensor to find the exact velocity of the object. The IMU sensor measures the acceleration in x, y and z of the installation object, which are integrated by the observer to find the velocity. If both the relative velocity and the actual velocity of the object is known, the current velocity can easily be calculated. A more accurate alternative is to use an acoustic doppler current profiler (ADCP) attached either to the surface vessel, the sea floor or both. The main issue related to the use of an ADCP is that it won't cover the entire water column in deepwater operations if a vessel fixed ADCP is used, and it is time consuming to install an ADCP at the sea floor.

4.3.2 Installation Using Homing

Homing systems are often used when the objective is to move a vessel towards a fixed point. Homing is commonly used in docking of AUVs or autonomous ships, and methods to design homing systems are presented in [22]. Several methods to preform homing of an object already exists, and a combination of acoustic homing, optical homing and electromagnetic homing depending on the accuracy requirement are often used. As the accuracy requirement for an SPS installation is considered not to be that strict, and a position error of 0.5-1 m when the object is installed at the sea floor is assumed to be acceptable, acoustic homing is considered to be sufficient.

The USBL positioning system presented above, with the hydrophone/transducer attached to the installation object, is not able to determine the Earth fixed coordinate of the installation object during submerging because it does not have position communication with the support vessel. It can still be efficiently used in an acoustic homing system to determine the relative position between the installation object and the transponder, and an earth fixed coordinate of the installation object isn't nessesary. The accuracy of the USBL system can according to [23] be as much as 5-10 m error when the relative distance between the transducer and transponder is 3000m. Inaccurate position measurements are considered not to be a big issue at the beginning of the installation, and since

the position error will be reduced as the installation object is closing in on the transponder, the installation object will land accurately next to the transponder at the sea floor.

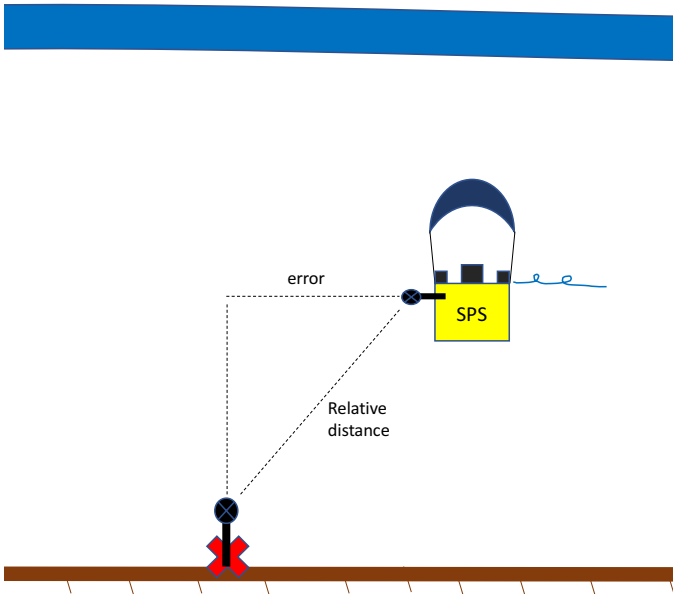

Figure 4.10: Homing of the installation object

Figure 4.10 illustrates how the homing system can be designed. A transponder is dropped from the sea surface on a spear at the exact installation position, using GPS to find the correct drop position of the spear. The transponder is assumed to drop towards the sea floor without any drift off in the horizontal plane as it is attached to a slender spear. When the transponder is installed, it's position can be measured using a vessel mounted (SBL) or (USBL) to determine the exact position of the transponder at the sea floor. If the transponder is landed in the wrong position, an ROV can move the transponder to the correct position at the sea floor.

When the installation object is dropped into the water, the attached hydrophone/transducer will communicate with the transponder at the sea floor to calculate the relative distance between the installation object and the transponder. The depth at the installation position where the transponder is located is assumed known, so the installation object can calculate the vertical distance between itself and the transponder using it's pressure sensor and transponder depth. Therefore, the horizontal relative distance between the transponder and the installation object can be calculated, and used by the guidance system to create a horizontal trajectory towards the transponder. Two transponders can also be used, in order to provide redundancy if the signal from one transponder is lost.

The main benefit of using the homing approach, is that only requires one transponder to be installed at the sea floor. Another benefit is that no communication is required between the installation object and the support vessel for position measurements, which reduces the travel time of the position measurement signals.

4.3.3 Installation Using Long Baseline

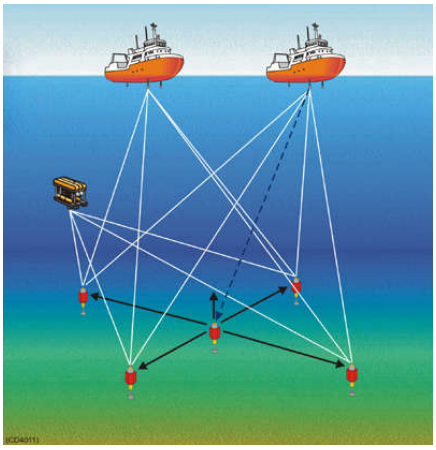

Figure 4.11: Long baseline positioning system (ref: [19])

Instead of using the USBL and homing approach, a LBL system as illustrated in Figure 4.11 can be used to obtain the exact position of the installation object during submerging. If several subsea components are to be installed at an installation site, a long baseline acoustic positioning system can be installed at the sea floor to achieve high accuracy position measurements. In the LBL system, 4 transponders are installed at the sea floor with several kilometres distance from each other, where the 4th transponder is used to provide redundancy.

In a LBL system, a communication line as illustrated in Figure 4.11 between the installation object (ROV in the figure), the 4 transponders and the support vessel is used to triangulate the exact earth fixed position of the installation object during submerging within high accuracy. An exact installation coordinate can therefore be used by the guidance system to calculate a horizontal trajectory towards the installation site. The benefit of using a LBL system is that it provides an earth fixed coordinate of the installation object as it submerges, with no uncertainty related to errors in the transponder submerging used in the homing approach. The downside is that it's more time consuming to install all the necessary equipment required to achieve long baseline position measurements.

4.4 Uncertainties and Challenges

The cost winnings of using the "Drop and Forget" installation method is assumed to be significant, but the tradeoff is increased risk of loosing control of the installation object with minimal control options from the support vessel. Transportation of the installation object to the installation site is completed very safe and with low risk of damaging or loosing control of the object. During launching of the object from the ramp illustrated in Figure 4.2, there is a chance the object will fall over the side of the ship if the roll motion is to large. Hence, the motion of the ship during this phase is very important to keep at a minimum, and methods to make sure sideways motion of the object is impossible during launch have to be considered.

When the object is launched and enters the splash zone, the most critical phase starts. Because of the large hydrodynamic loads on the installation object in this phase, the attached installation skid has to be robust in handling the heavy loads, exciting both the object and the installation skid. Unexpected heavy loads can hit the installation skid at a fragile spot, which can cause failure of fundamental components required to complete the installation. Large rotations of the object during this phase is also a big issue. Rotations of the object is considered to be the most

important motion to control, as uncontrolled rotations of the object will make it impossible for the control actuators to work properly, and large rotations upon impact at the sea floor might break the entire SPS. Therefore, redundancy to make sure the structure is stabilized in roll, pitch and yaw is important.

Unexpected situations where the control system is not able to position the object in the the horizontal plane within the correct installation position might also occur during during submerging. If the horizontal positioning fail, the object will just have to submerge to the sea floor for landing before any corrections are made. A system to communicate the estimated position and condition of the installation object to the support vessel during submerging can be implemented to monitor the installation from the support vessel. Even though the submerging of the object can be monitored from the support vessel, no human corrections are desirable during submerging as it might just increase the error. As long as the rotations are kept under control, the object will just land within the wrong position at the sea floor with minimal damage if the horizontal positioning fail.

A scenario where the component reducing the impact velocity fail, is also a possibility. Analysis to simulate the impulse loading on the structure upon impact at the sea floor at free fall velocity has to be made. Minimal damage to the SPS is desirable at free fall velocity, so that a failure of the drop velocity reduction component is acceptable without total breakage of the SPS. If the damage is to large at free fall velocity impact, methods to reduce the damage or redundancy in the drop velocity reduction component has to be implemented.

Plan B procedures to position the object at the sea floor if it's not landed within the correct position is also necessary. A proposed plan B method is to have a manual controller to control the actuators on the installation skid, and attach a cable from the support vessel to the installation object by using an ROV. The cable from the support vessel is then used to lift the object from the sea floor, and it's positioned manually to the correct position at the sea floor using the ROV camera and the manual actuator controller.

Uncertainties related to the specific choice of installation skid is also an issue. The parachute for instance have several uncertainties related to releasing of the parachute before or after the splash zone, hydrodynamics around the parachute and retrieving of the parachute at the sea floor. The buoyancy tank have uncertainties related to deformation or damage caused by the surround pressure, and the propellers have uncertainties related to failure of one or more propellers or the entire propeller motor.

Chapter 5

Simulation Model

5.1 General Description

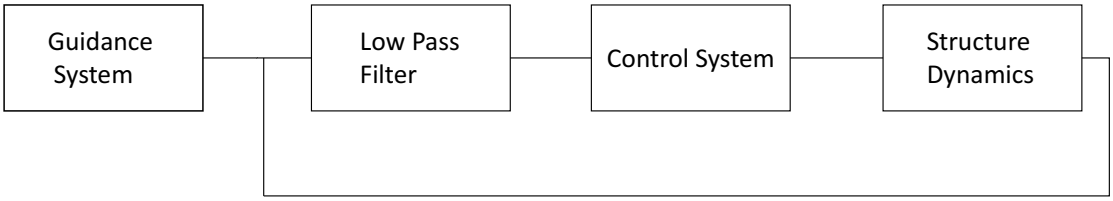

Figure 5.1: Block diagram of simulation model

The simulation model used is illustrated in Figure 5.1, and it's based on the 6 degrees of freedom marine craft equation of motion defined in [7]. The notation used in the equation of motion describing the 6 DOF motion of the installation object as it submerges, is summarized in Table 5.1.

Table 5.1: The notation of SNAME (1950) for marine vessels (ref: [7])

DOF	Forces and moments	Linear and angular velocities	Position and Euler angles
1 motions in the x direction (surge)	X	u	x
2 motions in the y direction (sway)	Y	v	y
3 motions in the z direction (heave)	Z	w	z
4 rotation about the x axis (roll, heel)	K	p	ϕ
5 rotation about the y axis (pitch, trim)	M	q	θ
6 rotation about the z axis (yaw)	N	r	ψ

Equation 5.1 and 5.2 shows the 6 DOF equation of motion in a vectorial setting, and is further described throughout this chapter.

$$\dot{\eta} = J_{\Theta}(\eta)\nu \tag{5.1}$$

$$M\dot{\nu} + C(\nu)\nu + D(\nu)\nu + g(\eta) = \tau_{control} \tag{5.2}$$

The states and forces used in the 6 DOF equation of motion shown in Equation 5.1 and 5.2 are given in Matrix 5.3, 5.4 and 5.5.

$$\eta = \begin{bmatrix} x_n, y_n, z_n, \phi, \theta, \psi \end{bmatrix}^T \tag{5.3}$$

$$\nu = \begin{bmatrix} u, v, w, p, q, r \end{bmatrix}^T \tag{5.4}$$

$$\tau = \begin{bmatrix} X, Y, Z, K, M, N \end{bmatrix}^T \tag{5.5}$$

In Matrix 5.3, 5.4 and 5.5, the matrix elements are defined in Table 5.1, where x_n, y_n and z_n is the North, East and Down position of the structure.

As the submerging structure is assumed to be affected by ocean currents, a modification is made to Equation 5.2, using relative velocity between the structure and the ocean currents. The modified equation of motion is shown in Equation 5.6.

$$M\dot{\nu_r} + C(\nu_r)\nu_r + D(\nu_r)\nu_r + g(\eta) = \tau_{control} \tag{5.6}$$

where

$$\nu_r = \nu - \nu_{current} \tag{5.7}$$

5.1.1 Assumptions

- The behaviour of the structure during impact and submerging through the water surface is not accounted for in this simulation, thus the excitation force from wind and waves are neglected. This assumption seemed reasonable as the goal of the simulation was to check the behaviour of the structure during phase 3 and 4 of the operation.
- The purpose of the simulation is assess the feasibility of the "Drop and Forget" installation method discussed in Chapter 4, so disturbance and sensor bias is not accounted for in the simulation model. Some disturbance will occur from unmodelled higher order hydrodynamic forces acting on the structure, but they are assumed to be small compared to the modelled hydrodynamic forces. Disturbance and sensor bias is best handled by an observer, and high frequency disturbances can be handled by a low pass filter. Observer design to filter sensor bias and disturbance in this control system will be similar to observer design for underwater vehicles, thus it's assumed feasible to design.
- The current speed is assumed known during submerging of the structure, as it can be measured using the doppler velocity sensor on the installation object, or an acoustic doppler current profiler (ADCP).
- The rotations of the structure are assumed to stay between -90° and 90° , so Euler angles are used to represent the attitudes and not unit quaternions, as large rotations of the structure is considered unacceptable. In reality, unit quaternions are recommended to avoid singularity problems.

- The ocean current is assumed irrotational, and without acceleration.

5.2 Coordinate System

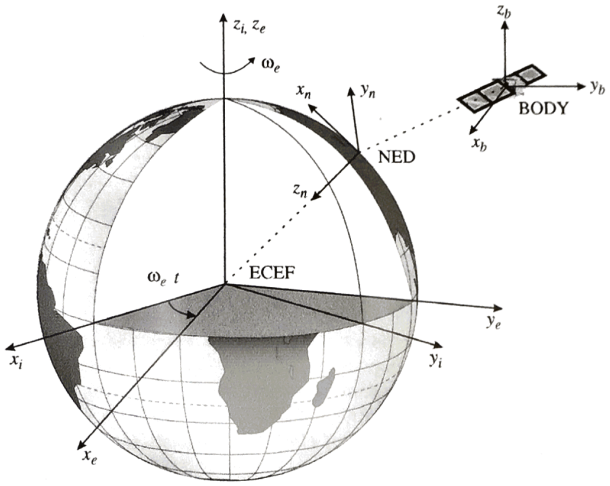

Figure 5.2: Coordinate systems ref: [7]

The coordinate systems used, is the North-East-Down (NED) coordinate system, and the body fixed coordinate system (BODY). The NED coordinate system is fixed at the drop position of the SPS from the surface vessel, and the body fixed coordinate system is fixed to the structure, and rotates with the rotation angles of the structure. Figure 5.2 illustrates the different coordinate systems. The x coordinate of the NED coordinate system is always positive northwards, the y coordinate is positive eastwards and the z coordinate is positive downwards. A transformation can also be made from the NED coordinate system to the Earth-centered-Earth-fixed coordinate system (ECEF) if the global Earth position is used.

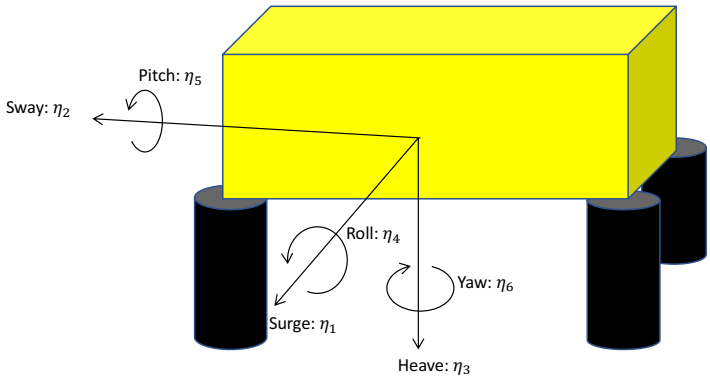

Figure 5.3: Body fixed coordinate system

Figure 5.3 illustrates the body fixed coordinate system fixed to the installation object at all time. If the installation object rotates, the body fixed coordinate system is also rotated. The benefit

of using the body fixed coordinate system is that the x velocity is always in surge motion of the structure, y velocity is always in sway motion and z velocity is always in heave motion.

The transformation between the coordinate systems is done in Equation 5.1, where the rotation matrix J_Θ is defined in Equation 5.8 according to [7].

$$J_\Theta = \begin{bmatrix} R_b^n(\Theta_{nb}) & 0_{3x3} \\ 0_{3x3} & T_\Theta(\Theta_{nb}) \end{bmatrix} \tag{5.8}$$

where

$$R_b^n(\Theta_{nb}) = \begin{bmatrix} c\psi c\theta & -s\psi c\phi + c\psi s\theta s\phi & s\psi s\phi + c\psi c\phi s\theta \\ s\psi c\theta & c\psi c\phi + s\phi s\theta s\psi & -c\psi s\phi + s\theta s\psi c\phi \\ -s\theta & c\theta s\phi & c\theta c\phi \end{bmatrix} \tag{5.9}$$

and

$$T_\Theta(\Theta_{nb}) = \begin{bmatrix} 1 & s\phi t\theta & c\phi t\theta \\ 0 & c\phi & -s\phi \\ 0 & s\phi/c\theta & c\phi/c\theta \end{bmatrix} \tag{5.10}$$

An important property of the transformation matrix J_Θ, is that it's inverse $J_\Theta^{-1} = J_\Theta^T$ is the transformation from NED coordinate system to the body frame. The transformation matrix J_Θ is often used throughout this chapter.

5.3 Structure Dynamics

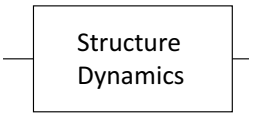

Figure 5.4: Structure dynamics block

The dynamics of the structure as it submerges through the water column is defined by its mass matrix M, damping matrix D, Coriolis centripetal matrix C and hydrostatic matrix g.

5.3.1 Mass Matrix M

The mass matrix M contains two parts. The rigid body mass matrix M_{RB} and the hydrodynamic added mass matrix M_A.

The rigid body matrix is defined as

$$M_{RB} = \begin{bmatrix} m & 0 & 0 & 0 & 0 & 0 \\ 0 & m & 0 & 0 & 0 & 0 \\ 0 & 0 & m & 0 & 0 & 0 \\ 0 & 0 & 0 & I_x & 0 & 0 \\ 0 & 0 & 0 & 0 & I_y & 0 \\ 0 & 0 & 0 & 0 & 0 & I_z \end{bmatrix} \tag{5.11}$$

In the rigid body matrix, the diagonal terms are the mass of the structure m, and the mass moment of inertia about x, y and z. The off diagonal terms are set to zero, as the origin of the structure is placed in its centre of gravity. The products of inertia $I_{xy} = I_{yx}$, $I_{xz} = I_{zx}$ and $I_{yz} = I_{zy}$ are also assumed to be zero.

The hydrodynamic added mass matrix is defined as

$$M_A = \begin{bmatrix} A_{11} & A_{12} & A_{13} & A_{14} & A_{15} & A_{16} \\ A_{21} & A_{22} & A_{23} & A_{24} & A_{25} & A_{25} \\ A_{31} & A_{32} & A_{33} & A_{34} & A_{35} & A_{36} \\ A_{41} & A_{42} & A_{43} & A_{44} & A_{45} & A_{46} \\ A_{51} & A_{52} & A_{53} & A_{54} & A_{55} & A_{56} \\ A_{61} & A_{62} & A_{63} & A_{64} & A_{65} & A_{66} \end{bmatrix} \tag{5.12}$$

The added mass force, defined by the added mass matrix multiplied by the structures acceleration, is an inertia force acting on the structure when it's accelerated as a consequence of the surrounding fluid. The added mass matrix contains the added mass constants in surge, sway, heave, roll, pitch and yaw on the diagonal, and the coupled added mass constants outside the diagonal.

The resulting mass matrix in the equation of motion is then calculated as

$$M = M_{RB} + M_A \tag{5.13}$$

5.3.2 Coriolis and Centripetal Matrix

The Coriolis and Centripetal matrix consists of the Coriolis and Centripetal forces acting on the body due to a rotation of the body frame relative to the NED frame. If the inertia matrix M_{RB}, shown in Equation 5.11 is given in the form:

$$M_{RB} = \begin{bmatrix} M_{11} & M_{12} \\ M_{21} & M_{22} \end{bmatrix} > 0 \tag{5.14}$$

where $M_{21} = M_{12}^T$, the nonlinear Coriolis centripetal matrix is defined according to [7] as

$$C_{RB}(\nu) = \begin{bmatrix} 0_{3x3} & -S(M_{11}\nu_1 + M_{12}\nu_2 \\ -S(M_{11}\nu_1 + M_{12}\nu_2) & -S(M_{21}\nu_1 + M_{22}\nu_2) \end{bmatrix} \tag{5.15}$$

where S is the cross-product operator defined in [7] as

$$\lambda \times a = S(\lambda)a \tag{5.16}$$

$$S(\lambda) = -S^T(\lambda) = \begin{bmatrix} 0 & -\lambda_3 & \lambda_2 \\ \lambda_3 & 0 & -\lambda_1 \\ -\lambda_2 & \lambda_1 & 0 \end{bmatrix}, \quad \lambda = \begin{bmatrix} \lambda_1 \\ \lambda_2 \\ \lambda_3 \end{bmatrix} \tag{5.17}$$

$\nu_1 = [u, v, w]^T$ is the linear velocity, and $\nu_2 = [p, q, r]^T$ is the angular velocity. The Coriolis and centripetal matrix can also be be calculated in a linear velocity-independent parametrization, so that it can be calculated as a function of relative velocity $C_{RB}(\nu_r)$.

Similar to the rigid body Coriolis and Centripetal matrix shown in Equation 5.15, the Coriolis and Centripetal matrix corresponding to the added mass inertia matrix can be calculated according to [7] as

$$C_A(\nu) = \begin{bmatrix} 0_{3x3} & -S(A_{11}\nu_1 + A_{12}\nu_2 \\ -S(A_{11}\nu_1 + A_{12}\nu_2) & -S(A_{21}\nu_1 + A_{22}\nu_2) \end{bmatrix} \tag{5.18}$$

if the inertia hydrodynamic added mass matrix, shown in Equation 5.12 is given in the form

$$M_A = \begin{bmatrix} A_{11} & A_{12} \\ A_{21} & A_{22} \end{bmatrix} > 0 \tag{5.19}$$

where $A_{21} = A_{12}^T$.

The Coriolis and Centripetal matrix corresponding to the inertia rigid body matrix $C_{RB}(\nu_r)$ is calculated in MATLAB using the function m2c(M_{Rb}, ν_R) in the mss toolbox [24]. Similar, the Coriolis and Centripetal matrix corresponding to the added mass inertia matrix $C_A(\nu_r)$ is calculated using the same function m2c(M_A, ν_R).

The total Coriolis and Centripetal matrix used in the equation of motion is then calculated as

$$C(\nu_R) = C_{RB}(\nu_R) + C_A(\nu_R) \tag{5.20}$$

5.3.3 Damping Matrix D

The damping matrix of the structure is the force acting on the structure, proportional to the velocity of the structure. The structure is assumed to have one quadratic damping term, and one linear damping term.

The linear damping matrix is given as

$$D_{lin} = \begin{bmatrix} D_{11}^l & D_{12}^l & D_{13}^l & D_{14}^l & D_{15}^l & D_{16}^l \\ D_{21}^l & D_{22}^l & D_{23}^l & D_{24}^l & D_{25}^l & D_{26}^l \\ D_{31}^l & D_{32}^l & D_{33}^l & D_{34}^l & D_{35}^l & D_{36}^l \\ D_{41}^l & D_{42}^l & D_{43}^l & D_{44}^l & D_{45}^l & D_{46}^l \\ D_{51}^l & D_{52}^l & D_{53}^l & D_{54}^l & D_{55}^l & D_{56}^l \\ D_{61}^l & D_{62}^l & D_{63}^l & D_{64}^l & D_{65}^l & D_{66}^l \end{bmatrix} \tag{5.21}$$

The diagonal contains the linear damping constants in surge, sway, heave, roll, pitch and yaw, and the off diagonal terms are the coupled linear damping coefficients.

The quadratic damping matrix is given as

$$D_{nlin}(\nu_r) = \begin{bmatrix} D_{11}^q|u_r| & D_{12}^q|v_r| & D_{13}^q|w_r| & D_{14}^q|p| & D_{15}^q|q| & D_{16}^q|r| \\ D_{21}^q|u_r| & D_{22}^q|v_r| & D_{23}^q|w_r| & D_{24}^q|p| & D_{25}^q|q| & D_{26}^q|r| \\ D_{31}^q|u_r| & D_{32}^q|v_r| & D_{33}^q|w_r| & D_{34}^q|p| & D_{35}^q|q| & D_{36}^q|r| \\ D_{41}^q|u_r| & D_{42}^q|v_r| & D_{43}^q|w_r| & D_{44}^q|p| & D_{45}^q|q| & D_{46}^q|r| \\ D_{51}^q|u_r| & D_{52}^q|v_r| & D_{53}^q|w_r| & D_{54}^q|p| & D_{55}^q|q| & D_{56}^q|r| \\ D_{61}^q|u_r| & D_{62}^q|v_r| & D_{63}^q|w_r| & D_{64}^q|p| & D_{65}^q|q| & D_{66}^q|r| \end{bmatrix} \tag{5.22}$$

where

$$\nu_r = \begin{bmatrix} u - u_{current} \\ v - v_{current} \\ w - w_{current} \\ p \\ q \\ r \end{bmatrix} = \begin{bmatrix} u_r \\ v_r \\ w_r \\ p \\ q \\ r \end{bmatrix} \tag{5.23}$$

Again, the diagonal contains the quadratic damping constants in surge, sway, heave, roll, pitch and yaw multiplied by the absolute value of the translational and angular velocity, and the off diagonal terms is the coupled quadratic damping coefficients multiplied by the absolute value of the translational and angular velocity.

The total damping matrix used in the equation of motion is then calculated as

$$D(\nu_R) = D_{lin} + D_{nlin}(\nu_R) \tag{5.24}$$

5.3.4 Hydrostatic Matrix g

The hydrostatic forces acting on the structure is the gravitational and buoyancy force, together with the restoring moment defined by the centre of gravity and centre of buoyancy of the structure. The hydrostatic matrix of the structure is equivalent to the spring forces in a mass-damper-spring system.

The centre of gravity vector is a vector from the origin of the structure to the centre of gravity. In the simulations presented in this report, the origin is placed in the centre of gravity of the structure, such that the CG vector is equal to zero. The centre of gravity vector is defined as

$$r_g^b = [x_g, y_g, z_g] \tag{5.25}$$

Similar, the centre of buoyancy is a vector from the origin to the centre of buoyancy, and it's defined as

$$r_b^b = [x_b, y_b, z_b] \tag{5.26}$$

The wight of the structure is

$$W = mg \tag{5.27}$$

and the buoyancy of the structure is

$$B = \rho g \nabla \tag{5.28}$$

The final hydrostatic matrix is then defined according to [7] as

$$g(\eta) = \begin{bmatrix} (W-B)sin(\theta) \\ -(W-B)cos(\theta)sin(\phi) \\ -(W-B)cos(\theta)cos(\phi) \\ -(y_gW - y_bB)cos(\theta)cos(\phi) + (z_gW - z_bB)cos(\theta)sin(\phi) \\ (z_gW - z_bB)sin(\theta) + (x_gW - x_bB)cos(\theta)cos(\phi) \\ -(x_gW - x_bB)cos(\theta)sin(\phi) - (y_gW - y_bB)sin(\theta) \end{bmatrix} \tag{5.29}$$

The z axis is positive downwards such that gravity is positive and buoyancy is negative. The mss toolbox function gvect.m [24], is used on calculating the hydrostatic matrix in MATLAB.

5.4 Control System

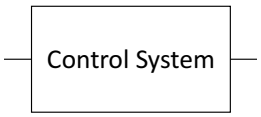

Figure 5.5: Control system block

The control system is designed to control the position of the structure, and stabilize the rotations. Feedback linearization of the Coriolis and Centripetal matrix, together with conventional PID control is used to control the surge, sway, roll, pitch and yaw motion. Maximum 70% of the Coriolis and Centripetal matrix is used as feedback in the controller, to avoid unnecessary use of control energy if the Coriolis and Centripetal matrix is measured inaccurately. No control is used in heave, as it is shown in [17] that the required control energy to reduce the fall velocity is extremely large. Also, no control allocation is done in the controller as actuation for control force is not yet decided.

5.4.1 Control Law

The control law used is shown in the equation below:

$$\tau_{control} = C(\nu_R)\nu_R * 0.7 + J_\Theta^T \tau_{PID} \tag{5.30}$$

J_Θ is defined in Equation 5.8 and C is defined in Equation 5.20. The property $J_\Theta^T = J_\Theta^{-1}$ is used on designing the control law.

The PID controller is defined as

$$\tau_{PID} = -\boldsymbol{Kp}\ \tilde{\eta} - \boldsymbol{Kd}\ \dot{\eta} - \boldsymbol{Ki} \int_0^t \tilde{\eta} dt \tag{5.31}$$

where $\tilde{\eta} = \eta - \eta_d$ is the error between real and desired position, and the matrices $\boldsymbol{Kp}$, $\boldsymbol{Kd}$ and $\boldsymbol{Ki}$ are the controller gain matrices.

As the error is given in NED, analysis of the error dynamics in body makes it convenient to use the following property for the controller gain matrices:

$$\boldsymbol{Kp} = J_\Theta \boldsymbol{Kp^*} \tag{5.32}$$

$$\boldsymbol{Kd} = J_\Theta \boldsymbol{Kd^*} J_\Theta^T \tag{5.33}$$

$$\boldsymbol{Ki} = J_\Theta \boldsymbol{Ki^*} \tag{5.34}$$

where the controller gain matrices $\boldsymbol{Kp^*}$, $\boldsymbol{Kd^*}$ and $\boldsymbol{Ki^*}$ are defined as

$$\boldsymbol{Kp^*} = \begin{bmatrix} Kp_{surge} & 0 & 0 & 0 & 0 & 0 \\ 0 & Kp_{sway} & 0 & 0 & 0 & 0 \\ 0 & 0 & Kp_{heave} & 0 & 0 & 0 \\ 0 & 0 & 0 & Kp_{roll} & 0 & 0 \\ 0 & 0 & 0 & 0 & Kp_{pitch} & 0 \\ 0 & 0 & 0 & 0 & 0 & Kp_{yaw} \end{bmatrix} \tag{5.35}$$

$$\boldsymbol{Kd^*} = \begin{bmatrix} Kd_{surge} & 0 & 0 & 0 & 0 & 0 \\ 0 & Kd_{sway} & 0 & 0 & 0 & 0 \\ 0 & 0 & Kd_{heave} & 0 & 0 & 0 \\ 0 & 0 & 0 & Kd_{roll} & 0 & 0 \\ 0 & 0 & 0 & 0 & Kd_{pitch} & 0 \\ 0 & 0 & 0 & 0 & 0 & Kd_{yaw} \end{bmatrix} \tag{5.36}$$

$$\boldsymbol{Ki^*} = \begin{bmatrix} Ki_{surge} & 0 & 0 & 0 & 0 & 0 \\ 0 & Ki_{sway} & 0 & 0 & 0 & 0 \\ 0 & 0 & Ki_{heave} & 0 & 0 & 0 \\ 0 & 0 & 0 & Ki_{roll} & 0 & 0 \\ 0 & 0 & 0 & 0 & Ki_{pitch} & 0 \\ 0 & 0 & 0 & 0 & 0 & Ki_{yaw} \end{bmatrix} \tag{5.37}$$

Using the above control law and controller gain matrices, each feedback loop can be tuned independently.

5.4.2 Controller Tuning

The strategy used on tuning the controller is to use the controller gains to tune each loop as a linear mass-damper-spring system. Analysis of the error dynamics gave the following two equations for the linear uncoupled motion of each control loop.

$$\frac{Kp^*}{M} = \omega_n^2$$
$$Kp^* = \omega_n^2 M \tag{5.38}$$

$$\frac{d + Kd^*}{M} = 2\zeta\omega_n$$
$$Kd^* = 2\zeta\omega_n M - d \tag{5.39}$$

Where ω_n is the natural frequency of the loop, and ζ is the relative damping ratio. M is the sum of the uncoupled mass and added mass term of the loop, and d is the uncoupled linear damping term. The integral gain was as a starting value set to:

$$Ki^* = \frac{\omega_n}{10} Kp* \tag{5.40}$$

and integral control force was also saturated to avoid integral windup in the controller.

Based on Equation 5.38, 5.39 and 5.40 the controller gains are chosen for each loop by setting the natural period and relative damping ratio of the linear uncoupled part of the equation of motion in surge, sway, roll, pitch and yaw. The natural frequency is calculated from the natural period using Equation 5.41.

$$\omega_n = \frac{2\pi}{T_n} \tag{5.41}$$

5.5 Current

The current is assumed to be irrotational and only have velocity in the horizontal plane. In the NED coordinate system, the current velocity is calculated as

$$\dot{\eta}_c = \begin{bmatrix} V_c cos(\beta) \\ V_c sin(\beta) \\ 0 \\ 0 \\ 0 \\ 0 \end{bmatrix} = \begin{bmatrix} u_c \\ v_c \\ w_c \\ p_c \\ q_c \\ r_c \end{bmatrix} \tag{5.42}$$

where V_c is the total current speed in [m/s], and β is the current direction. Using Equation 5.42, the current speed in the body frame is calculated using the rotation matrix from NED to body as shown in Equation 5.43.

$$\nu_c = J_\Theta(\eta)^T \dot{\eta}_c \tag{5.43}$$

Modifications are made to the current speed V_c or current direction β to simulate different current profiles.

5.6 Low-pass Filter

Figure 5.6: Low-pass filter block

A low-pass filter is used to smooth the commanded control input to get a more realistic control force signal. A propeller will for instance use some time to build up thrust, and it's not realistic to assume it can deliver full thrust in only 1-2 seconds. Very high frequent signals into the controller will also cause heavy loading on the control actuators, and the low pass filter is able to filter out high frequent disturbances in the dynamics of the structure. Both the $\tilde{\eta}$ and the $\dot{\tilde{\eta}}$ signal is filtered through the low pass filter before the signals enter the controller.

A second order Butterworth filter is used as a low pass filter, where the transfer function in the frequency domain is defined in [25] as

$$h(s) = \frac{\omega_c^2}{s^2 + \sqrt{2}\omega_c s + \omega_c^2} \tag{5.44}$$

where ω_c is the cut-off frequency. In the time domain the second order Butterworth filter is given as

$$\ddot{x}_f + \sqrt{2}\omega_c \dot{x}_f + \omega_c^2 x_f = \omega_c^2 x \tag{5.45}$$

where x_f is the filtered signal, and x is the signal to be filtered.

In order to set the cut-off frequency individually for each control loop, the time domain Equation 5.45 of the low pass filter is defined in matrix form using the matrix D and K defined below.

$$D = \sqrt{2}\begin{bmatrix} \omega_{Csurge} & 0 & 0 & 0 & 0 & 0 \\ 0 & \omega_{Csway} & 0 & 0 & 0 & 0 \\ 0 & 0 & \omega_{Cheave} & 0 & 0 & 0 \\ 0 & 0 & 0 & \omega_{Croll} & 0 & 0 \\ 0 & 0 & 0 & 0 & \omega_{Cpitch} & 0 \\ 0 & 0 & 0 & 0 & 0 & \omega_{Cyaw} \end{bmatrix} \tag{5.46}$$

$$K = \begin{bmatrix} \omega^2_{Csurge} & 0 & 0 & 0 & 0 & 0 \\ 0 & \omega^2_{Csway} & 0 & 0 & 0 & 0 \\ 0 & 0 & \omega^2_{Cheave} & 0 & 0 & 0 \\ 0 & 0 & 0 & \omega^2_{Croll} & 0 & 0 \\ 0 & 0 & 0 & 0 & \omega^2_{Cpitch} & 0 \\ 0 & 0 & 0 & 0 & 0 & \omega^2_{Cyaw} \end{bmatrix} \tag{5.47}$$

Using the matrix D and K, the dynamics of the low pass filter is defined in matrix form in the time domain as

$$\ddot{\boldsymbol{x}}_{\boldsymbol{f}} + D\dot{\boldsymbol{x}}_{\boldsymbol{f}} + K\boldsymbol{x}_{\boldsymbol{f}} = K\boldsymbol{x} \tag{5.48}$$

where $\boldsymbol{x_f} = [x_{fsurge}, x_{fsway}, x_{fheave}, x_{froll}, x_{fpitch}, x_{fyaw}]^T$ is the filtered signal, and $\boldsymbol{x} = [x_{surge}, x_{sway}, x_{heave}, x_{roll}, x_{pitch}, x_{yaw}]^T$ is the signal to be filtered. The time propagation of Equation 5.48 is calculated in discrete time using a simple Euler integration.

5.7 Guidance System

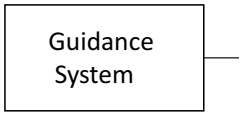

Figure 5.7: Guidance system block

The control systems objective is to move a submerging object to a desired position at the sea floor. The control system must also be able to stabilize the rotations of the structure close to zero degrees. Because of these simple requirements, no advanced maneuvring guidance system is needed. A simple guidance system is still implemented in surge and sway to smooth out the trajectory towards the desired position in the northeast plane. This is implemented so that the structure can move slowly towards the desired position in the northeast plane as it submerges through the water column, thus save some control energy in surge and sway. The guidance system in surge and sway is implemented as a first or second order Butterworth filter with very long cut-off period. The first and second order Butterworth filter equation used in the guidance system, is shown in Equation 5.49 and 5.50.

$$\dot{x}_f + \omega_c x_f = \omega_c x \tag{5.49}$$

$$\ddot{x}_f + \sqrt{2}\omega_c \dot{x}_f + \omega_c^2 x_f = \omega_c^2 x \tag{5.50}$$

5.8 Solution Method Equation of Motion

To summarize this section, the 6 DOF second order nonlinear equation of motion describing the motion of the submerging structure is given as

$$\dot{\eta} = J_\Theta(\eta)\nu \tag{5.51}$$

$$M\dot{\nu_r} + C(\nu_r)\nu_r + D(\nu_r)\nu_r + g(\eta) = \tau_{control} \tag{5.52}$$

where ν_r in Equation 5.52 is the relative velocity between the structure and the ocean currents. Using equation 5.51 and 5.52 the dynamics of the structure is simulated forward in time, using a combination of the forward and backward Euler integration. The discrete time Euler integration of Equation 5.51 and 5.52 is shown in Equation 5.53 and 5.55.

$$\nu_r[k+1] = \nu_r[k] + hM^{-1}(\tau_{control}[k] - C(\nu_r[k])\nu_r[k] - D(\nu_r[k])\nu_r[k] - g(\eta[k])) \tag{5.53}$$

$$\nu[k+1] = \nu_r[k+1] + \nu_c[k] \tag{5.54}$$

The current velocity in the body frame is assumed to remain constant within a time interval of 0.01 second, so discrete time current propagation is not included in Equation 5.54.

$$\eta[k+1] = \eta[k] + h(J_\Theta(\eta[k])\nu[k+1]) \tag{5.55}$$

The stepsize h is set to $h = 0.01$ as it is assumed sufficient accuracy. The numerical solution using the forward and backward Euler integration illustrated in Equation 5.53 and 5.55 is said to be stable for the marine craft equation of motion shown in Equation 5.51 and 5.52 in [7] and [25].

5.9 Recommendations to Expand the Simulation Model

- When a specific installation skid is chosen, include control allocation in the controller using the actuator dynamics and position on the structure. Include control actuator constraints.
- Design an Observer to estimate the states using the sensor data from the recommended sensors in Chapter 4.

- Include disturbance in the structure dynamics and current simulation. Sensor bias and sensor position on the structure also have to be included in the simulation model.

Chapter 6

Case Study

Based on the discussion in chapter 4 about proposed installation skids, several cases are simulated in this chapter using the simulation model described in chapter 5.

Simulation Objective:

1. Assess the behaviour of the structure as it submerges using active control.
2. Assess the behaviour of the structure as it submerges in different current conditions.
3. Assess the behaviour of the structure using different control strategies, in order to use as little control energy as possible.
4. Identify potential problems using the "Drop and Forget" installation method.
5. Conclude on the feasibility of the "Drop and Forget" installation method.

The simulated cases in this chapter are summarized in Table 6.1.

Table 6.1: Simulated cases

Case	Drop velocity reduction component	Roll and pitch stabilization	Horizontal positioning/ yaw stabilization	Section
Drop with unlimited control force/moment	-	Active control	Active control	6.3
Drop with saturated control force/moment	-	Active control	Active control	6.4
Drop in Brazil current profile	-	Active control	Active control	6.5
Drop in 3D current profile	-	Active control	Active control	6.6
Drop in bidirectional current profile	-	Active control	Active control	6.7
Drop in divided current profile	-	Active control	Active control	6.8
Drop in shear current profile	-	Active control	Active control	6.9
Drop using parachute	Parachute	Parachute	Active control	6.10
Drop using buoyancy tank	Buoyancy tank	Buoyancy tank	Active control	6.11
Drop of scaled structure	-	Active control	Active control	6.12

6.1 Installation Object

The installation object simulated in this chapter, is an ITS structure used in the Johan Sverdrup field in the North Sea. Structure information about the ITS structure is provided by Equinor, and hydrodynamic information about the structure is taken from [26].

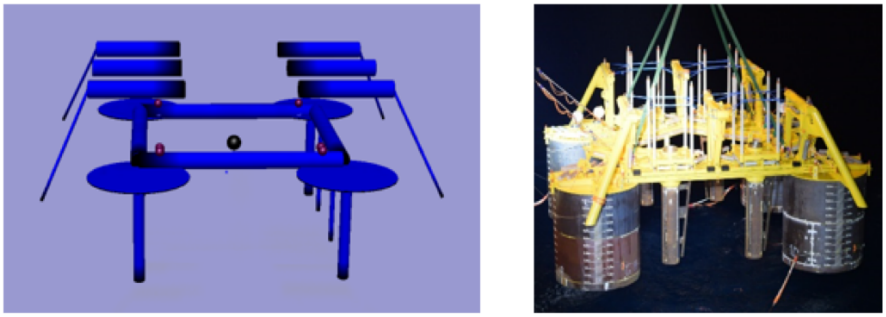

Figure 6.1: Johan Sverdrup ITS structure

Table 6.2: Johan Sverdrup ITS dimensions (ref: [26])

	Suction Anchor	Structure Body	Total
Mass [Kg]	$25 * 10^3$	$160 * 10^3$	$260 * 10^3$
Wet mass [Kg]	$21.75 * 10^3$	$139.2 * 10^3$	$226.2 * 10^3$
Height [m]	6.5	4.5	11
Length/Diameter [m]	6	18	24
Breadth/Diameter [m]	6	18	24
COG [m]	4	7.5	6.15

Using simplified hand calculations, the rigid body and hydrodynamic matrices are calculated based on the translational rigid body and hydrodynamic coefficents. Appendix A shows how the 6 DOF rigid body and hydrodynamic matrices were calculated. The structure is assumed to be coupled in surge and pitch, and sway and roll because of the asymmetrical vertical plane. It's assumed to be uncoupled in the horizontal plane because of symmetry.

6.1.1 Resulting Rigid Body and Hydrodynamic Matrices

The resulting rigid body and hydrodynamic matrices used are shown in Matrix 6.1 - 6.4.

Mass rigid body

$$\boldsymbol{M_{RB}} = \begin{bmatrix} 260000 & 0 & 0 & 0 & 0 & 0 \\ 0 & 260000 & 0 & 0 & 0 & 0 \\ 0 & 0 & 260000 & 0 & 0 & 0 \\ 0 & 0 & 0 & 8853850 & 0 & 0 \\ 0 & 0 & 0 & 0 & 8853850 & 0 \\ 0 & 0 & 0 & 0 & 0 & 42120000 \end{bmatrix} \tag{6.1}$$

Added mass

$$\boldsymbol{M_A} = \begin{bmatrix} 1417000 & 0 & 0 & 0 & 2287050 & 0 \\ 0 & 1417000 & 0 & -2287050 & 0 & 0 \\ 0 & 0 & 1277000 & 0 & 0 & 0 \\ 0 & -2287050 & 0 & 94718483 & 0 & 0 \\ 2287050 & 0 & 0 & 0 & 94718483 & 0 \\ 0 & 0 & 0 & 0 & 0 & 229554000 \end{bmatrix} \tag{6.2}$$

Linear damping

$$\boldsymbol{D_l} = \begin{bmatrix} 0 & 0 & 0 & 0 & 0 & 0 \\ 0 & 0 & 0 & 0 & 0 & 0 \\ 0 & 0 & 284000 & 0 & 0 & 0 \\ 0 & 0 & 0 & 23004000 & 0 & 0 \\ 0 & 0 & 0 & 0 & 23004000 & 0 \\ 0 & 0 & 0 & 0 & 0 & 0 \end{bmatrix} \tag{6.3}$$

Quadratic damping

$$\boldsymbol{D_q} = \begin{bmatrix} 253000 & 0 & 0 & 0 & -48613 & 0 \\ 0 & 253000 & 0 & 48613 & 0 & 0 \\ 0 & 0 & 177000 & 0 & 0 & 0 \\ 0 & 48613 & 0 & 1101067 & 0 & 0 \\ -48613 & 0 & 0 & 0 & 1101067 & 0 \\ 0 & 0 & 0 & 0 & 0 & 231093000 \end{bmatrix} \tag{6.4}$$

6.2 General Description

6.2.1 Coordinate System

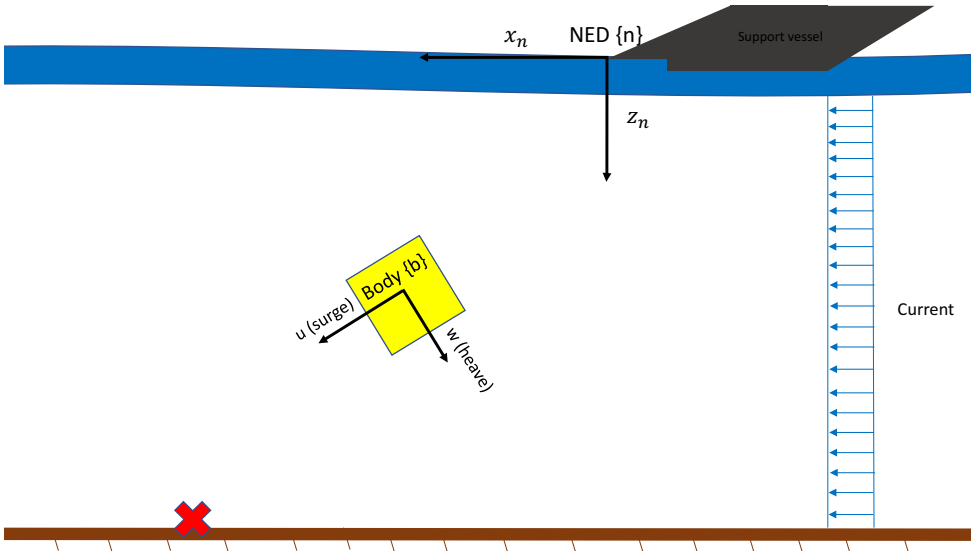

Figure 6.2: Coordinate systems used in the simulations

The coordinate system used in the simulations in this chapter, is as presented in 5.2 the NED and body coordinate system. The NED coordinate system is at all time fixed at the drop position of the installation object from the support vessel, while the body coordinate system follows the rotation

and position of the structure as it submerges. In the simulation results, position and attitude η is given in the NED coordinate system, and the velocity ν and commanded control force/moment τ is given in the body coordinate system.

6.2.2 Current Profiles

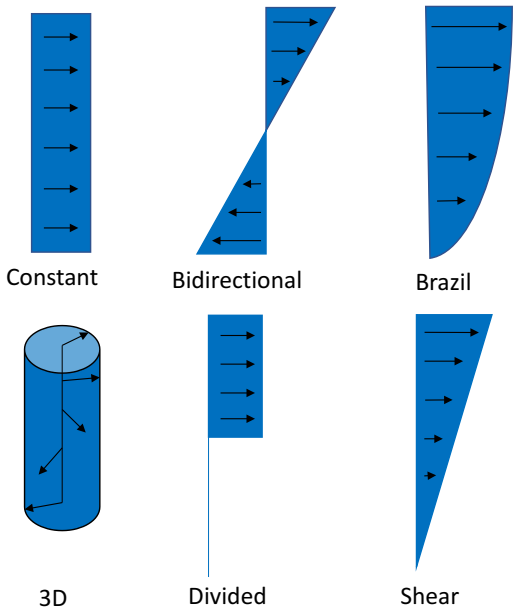

Figure 6.3: Current profiles

Several current profiles are simulated to assess the behaviour of the installation method in different current conditions. The tested current profiles are common current profiles found at relevant installation sites throughout the world, and they are illustrated in Figure 6.3. The Brazil current profile is created based on measurements from a real field development site outside Brazil, where the data is taken from [27]. As presented in 5.5, the currents are simulated by setting the total current speed V_c, and current direction β in the horizontal plane. When depth varying current profiles are simulated, the total current speed $V_c(z)$ or direction $\beta(z)$ is calculated as a function of depth using interpolation to create a function describing the current profile.

6.2.3 Control Tuning

A lot of time is spent on tuning the different simulations presented in this chapter by changing the simulation and tuning parameters. The goal has been to observe how the behaviour of the structure changes as the parameters are changed, rather than achieving perfect control of the object. Strict tracking in the north and east direction is not necessary, as the installation object has the entire submerging time to position itself in the horizontal plane.

Tuning is preformed by trial and error by changing the relative damping ratio, natural period, integrator gain and filter constants in each loop. In general, PID control is used in surge and sway, and PD control is used in roll, pitch and yaw. PID is used in roll and pitch in the simulations where steady state error in these motions was observed. As described in 5.4, the controller gains are chosen from the natural period and relative damping ratio of the linear uncoupled part of each control loop according to Equation 6.5 and 6.6.

$$Kp^* = \omega_n^2 M \tag{6.5}$$

$$Kd^* = 2\zeta\omega_n M - d \tag{6.6}$$

where $M = M_{RBii} + M_{Aii}$ and $d = D_{ii}^l$. The natural frequency is calculated from the natural period using Equation 6.7:

$$\omega_n = \frac{2\pi}{T_n} \tag{6.7}$$

The integrator gain Ki^* is adjusted based on trial and error to remove the steady state error, and at the same time avoid integrator windup. Saturation is also used on the integrator force in the simulations where integrator windup is an issue.

No active control is used in heave to reduce the free fall velocity, based on results presented in Figure 6.4 from [17].

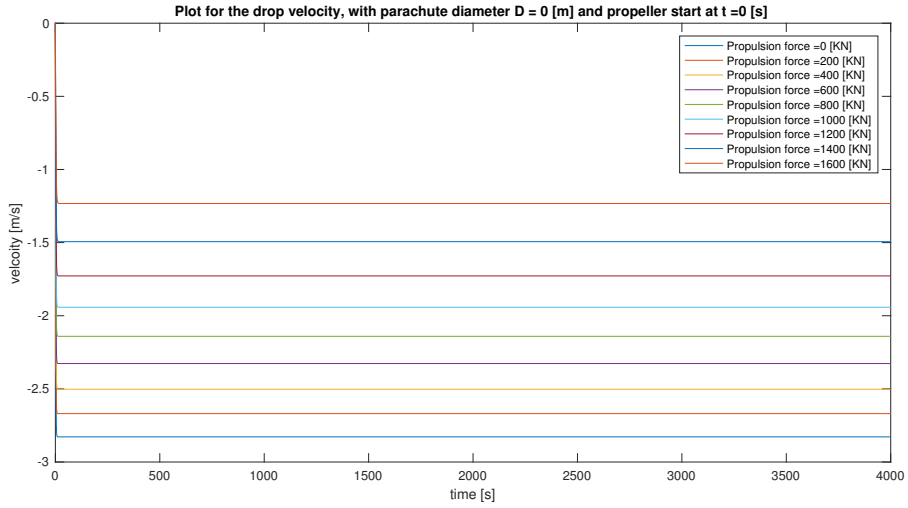

Figure 6.4: Simulation using propulsion force in vertical direction on the Johan Sverdrup ITS structure (ref: [17])

Figure 6.4 shows that an enormous amount of force is required in the vertical direction to slow down the drop velocity of the ITS structure as it submerges. It's considered unfeasible to attache thrusters of this size to an installation object, which means active control in heave is not a realistic option.

6.3 Drop with Unlimited Control Force

6.3.1 Description

A free drop installation, using control actuation in 5 DOF with unlimited control energy on the installation skid is simulated in this section. The actuators have to stabilize the structure in roll, pitch and yaw as the centre of buoyancy and gravity is located in the same point. At the same time they have to position the structure in the desired installation position. The simulation parameters and tuning constants are presented in Table 6.3 and 6.4, and the results are presented in 6.3.2. Appendix B.1 shows the remaining plots from this simulation, and Appendix C illustrates the 3D movement of the installation object as it submerges.

Table 6.3: Individual loop parameters unsaturated drop

	Surge	Sway	Roll	Pitch	Yaw
Initial Conditions η_0	0	0	20 [deg]	20 [deg]	20 [deg]
Natural period control loop T_N	110	100	27	30	800
Relative damping ratio control loop ζ	0.707	0.707	0.707	0.707	0.707
Integrator gain Ki^*	$\frac{\omega_n}{5}Kp_{Surge}$	$\frac{\omega_n}{10}Kp_{Sway}$	$\frac{\omega_n}{25}Kp_{\phi}$	$\frac{\omega_n}{5}Kp_{\theta}$	0
Cutoff period low pass filter T_C	18	15	15	20	7
Saturation control force/moment τ_{max}	-	-	-	-	-

Table 6.4: Simulation parameters unsaturated drop

Desired installation position $[\eta_d^{North}, \eta_d^{East}]^T$	$[-500, -300]^T$ [m]
Steady state drop velocity w	2.84 [m/s]
Total current velocity V_c	1 [m/s]
Current direction β	30 [deg]
Current profile	Constant
Installation depth	3000 [m]
Centre of buoyancy $r_b = [x_b, y_b, x_b]^T$	$[0, 0, 0]^T$
Centre of gravity $r_g = [x_g, y_g, z_g]^T$	$[0, 0, 0]^T$

6.3.2 Result

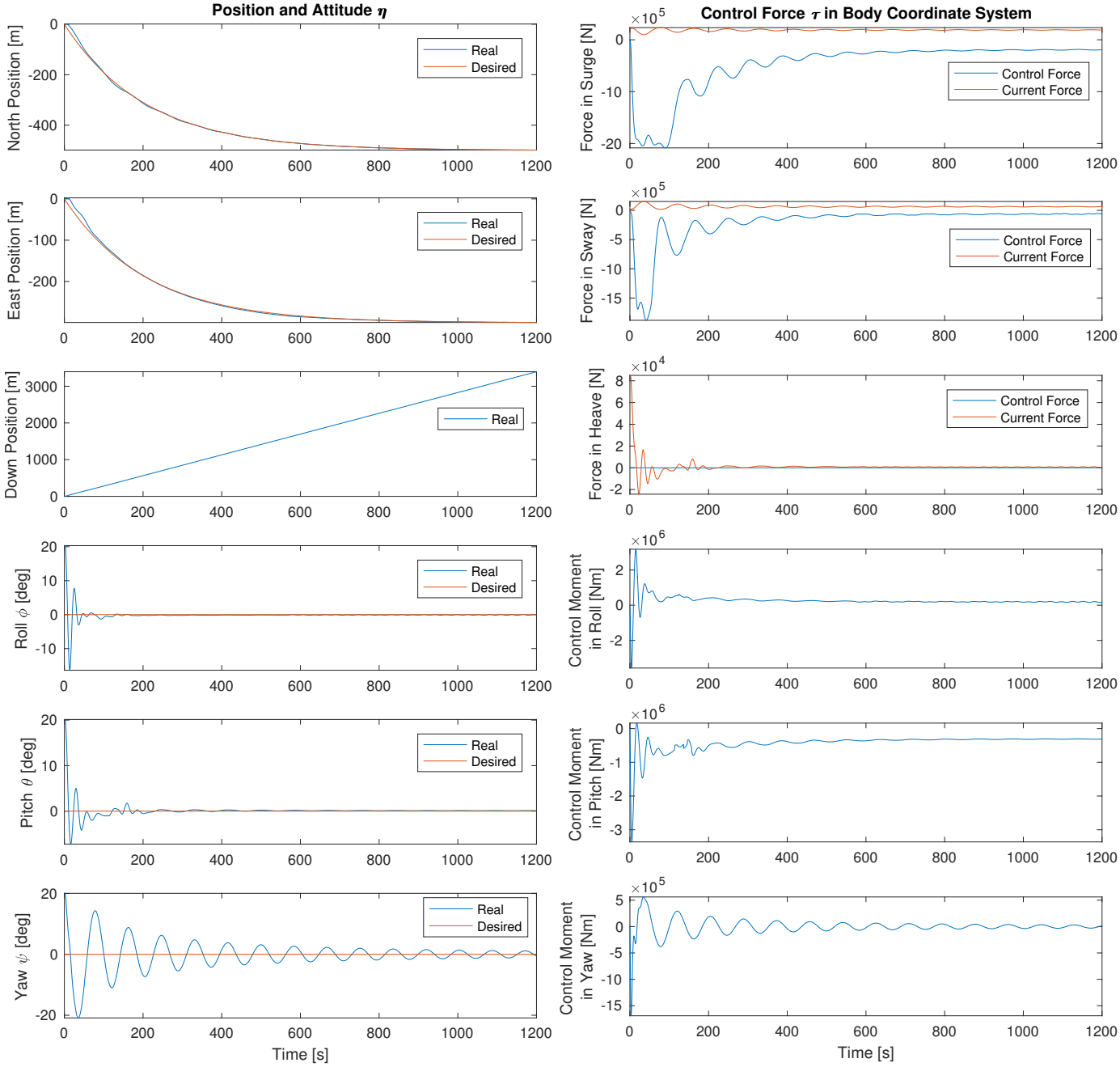

(a) Position and attitude

(b) Commanded control force

Figure 6.5: Free drop simulation result

6.3.3 Discussion

As this simulation is preformed without any component to reduce the drop velocity, the drop velocity of the structure is 2.84 [m/s]. Hence, Figure 6.5a shows that the structure is at 3000 m depth after approximately 20 min. The high drop velocity is giving the controller a limited amount of time to position the structure in the horizontal plane, and the natural period in surge and sway is chosen so that the structure will have good tracking in the horizontal plane, and be in the correct position when it reaches 3000 m depth. 2.84 [m/s] is considered to be a high impact velocity of the structure at the sea floor, and it might cause an unacceptable impulse force on the structure upon impact at the sea floor.

In this simulation, the guidance system is set to move the structure a long distance in the horizontal plane. Several simulations showed that oscillations in the controller can be a problem when the structure have to move a long distance in the horizontal plane, and at the same time has oscillating movement in yaw. It's therefore recommended to drop the structure right above the installation position, in order to avoid unnecessary problems caused by horizontal movements. Figure 6.5b also shows that the structure is moving against the ocean current, and a lot of control energy is therefore required to move the structure towards the installation position during the steep part of the trajectory. Simulations showed it was beneficial to drop the structure, such that it can drift with the ocean currents towards the installation position.

Figure 6.5b shows that the commanded control force in surge and sway has a very high peak in the beginning of the simulation, commanding approximately 2000 kN in surge and sway. This is caused by the coupled motion in surge when the pitch controller is commanding a very large moment to stabilize the structure in pitch, and the coupled motion in sway when the roll controller is commanding a large control moment to stabilize the roll motion. It's reasonable to assume large coupled inertia forces are acting on the structure when it's accelerated in roll and pitch during stabilization of these motions. The large coupled motion is causing the surge and sway controller to command a large force to counteract the coupled motion caused by the roll and pitch controller.

In the velocity plot shown in B.1 one can see a peak in surge and sway caused by the coupled motion, which is counteracted by large D-force in the controller. A solution to avoid this problem, is to start the surge and sway controller after the roll and pitch motion has been stabilized. It's desirable to avoid as much movement of the structure as possible when it's stabilized in roll and pitch, so implementations to delay the surge and sway controller a few minutes while the structure is stabilized is recommended.

Figure 6.5b also shows that a very large control moment is commanded in roll and pitch to stabilize the structure. Tuning of this simulation showed that the roll and pitch natural period have to be low for the controller to be able to stabilize these motions. The simulated structure have 4 very large suction anchors attached far from the centre of gravity of the structure, producing a very large moment about the centre of gravity. It's therefore expected that the controller must zero out the roll and pitch motion relatively fast, in order to not loose control of these motions as they gain momentum. Unstable motion is observed when the stabilization in roll and pitch is made to slow by choosing large natural period or filter cutoff period in roll and pitch. The integrator is also observed to cause very small spikes in the controller when these motions are stabilized, and methods to remove these spikes have to be considered if integrator control is used in roll and pitch.

The steady state control moment, commanded in roll and pitch is on the other hand feasible to provide. Methods where the structure is stabilized by a passive stabilization component after the splash zone, and kept stable by propellers can be considered.

In Figure 6.5b, one can se that the force required to damp the yaw motion is also very large. The yaw motion is not as critical as roll and pitch, but large yaw motion of the structure is still not desirable due to horizontal positioning and rapid movement of control actuator direction. Small oscillations are observed in the surge and pitch controller, caused by the oscillating change in surge and pitch current force because of the yaw motion. A large yaw moment is commanded in the controller in order to counteract the yaw motion before it builds up to much angular momentum.

The controllers ability to stop the yaw motion relatively fast is considered important, as large angular momentum in yaw will require a lot of control energy to counteract.

The natural period in yaw is set very high, in order to try and save control energy by using the entire submerging time to damp the yaw motion. Figure 6.5a shows that the yaw motion is not completely damped upon impact at the sea floor, as it's considered acceptable with a small yaw moment when the structure is installed. The angular velocity in yaw is observed to be very low in this simulation, but analysis to assess torsion in the structure caused by angular momentum present in the structure upon impact at the sea floor might be necessary.

The control force commanded in surge and sway, except the the force commanded in the beginning caused by roll and pitch stabilization, looks feasible. It's approximately 250 kN in surge and 100 kN in sway after 400 seconds as the guidance trajectory is closing in on the installation position, and this force can be provided by two ship propellers. The control actuator's arm to the origin of the structure can be maximum 9 m for this structure. This means a 400 [kN] thruster, which is a very large ship thruster, can produce approximately 3600 [kNm] of moment if it's positioned at the edge of the structure as illustrated in chapter 4. Figure 6.5b shows that the commanded moment is very close to this limit, which means the roll and pitch motion seems to require to much control energy for it to be feasible to control these motions with the use of thrusters. Several thrusters attached on top of the structure can be used to damp the yaw motion, so the commanded moment in yaw is feasible to produce. The time a thruster use to build up the commanded thrust is very critical, and will determine if the rotations of this structure can be stabilized using thrusters.

6.4 Drop with Saturated Control Force

6.4.1 Description

Using the same simulation parameters as the simulation presented in the previous section, a similar simulation is made where the commanded control force/moment is saturated. This simulation is made in order to assess the behaviour of the structure if its actuators are limited. Table 6.5 and 6.6 shows the simulation parameters used, and the results are presented in 6.4.2. The rest of the simulation plots are shown in Appendix B.2.

Table 6.5: Individual loop parameters saturated drop

	Surge	Sway	Roll	Pitch	Yaw
Initial Conditions η_0	0	0	20 [deg]	20 [deg]	20 [deg]
Natural period control loop T_N	110	100	27	30	800
Relative damping ratio control loop ζ	0.707	0.707	0.707	0.707	0.707
Integrator gain Ki^*	0	0	$\frac{\omega_n}{25}Kp_\phi$	$\frac{\omega_n}{5}Kp_\theta$	0
Cutoff period low pass filter T_C	18	15	15	20	7
Saturation control force/moment τ_{max}	120 [kN]	120 [kN]	700 [kNm]	700 [kNm]	500 [kNm]

Table 6.6: Simulation parameters saturated drop

Desired installation position $[\eta_d^{North}, \eta_d^{East}]^T$	$[-500, -300]^T$ [m]
Steady state drop velocity w	2.84 [m/s]
Total current velocity V_c	1 [m/s]
Current direction β	30 [deg]
Current profile	Constant
Installation depth	3000 m
Centre of buoyancy $r_b = [x_b, y_b, x_b]^T$	$[0, 0, 0]^T$
Centre of gravity $r_g = [x_g, y_g, z_g]^T$	$[0, 0, 0]^T$

6.4.2 Result

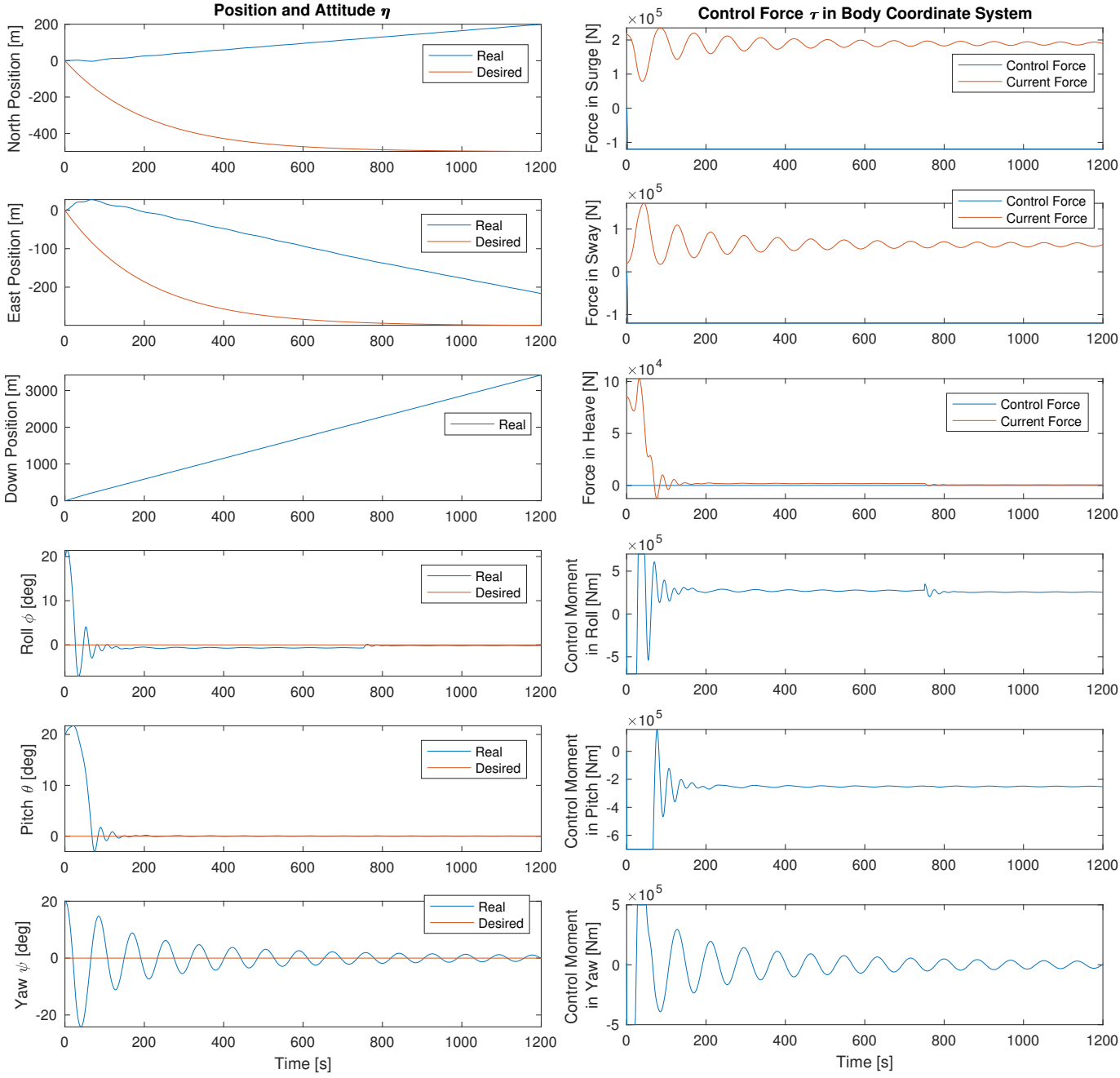

(a) Position and attitude

(b) Commanded control force

Figure 6.6: Free drop with saturated control force simulation result

6.4.3 Discussion

Figure 6.6a illustrates what will happen if the structure do not have enough control force in the horizontal plane. In the figure, one can see that the structure is not able to move against the current, and is drifting in the north direction as the structure do not have enough control force to overcome or counteract the ocean current. Figure 6.6b shows that the current force is approximately 200 kN in surge, while the control force is saturated at 120 kN. Hence, the structure will drift with the ocean current, and Figure 6.6a shows that the drift off is of significant size when the controller is lacking 80 kN of thrust. In the east direction, the controller have enough force to overcome the ocean current, but as the structure is set to move a long distance in this simulation, the force is not enough to position the structure before it reaches 3000 m.

Figure 6.6a shows a small drift off of the structure eastwards in the beginning of the simulation, before it starts to move in the negative east direction. The structure has rotations for a longer time preiod as it's saturated in roll and pitch, and the controller is using more time to stabilize these motions. At the same time, the sway controller do not have enough force to counteract the coupled motion caused by the roll stabilization, which is causing the drift off. Rotations in a longer time period in roll and pitch are also observed to cause a Coriolis and Centripetal force of significant size in surge and sway.

In Figure 6.6a and 6.6b one can see that the controller is able to stabilize the rotations when the controller is saturated in roll and pitch, and therefore using a relatively small control moment compared to the size of the structure. Smaller saturation limits were also simulated, where the the controller was unable to stablize the structure in roll and pitch. The main issue with the saturated control moment, is the speed of the commanded moment. Figure 6.6b shows that when the control moments is saturated in roll, the commanded moment changes between the saturation limits 700 kNm and -700 kN within a few seconds. The pitch and yaw moment is also changing rapidly in the beginning of the simulation, and this rapid change in commanded control moment is considered to be unfeasible to provide by thrusters. Simulations where saturations are made in the control actuators dynamics still have to be made, in order to get an exact answer to how saturation will affect the rotations.

6.5 Drop in Brazil Current Profile

6.5.1 Description

In this simulation, a free drop in the Brazil current profile is simulated. The measured current data from Brazil is shown in Appendix B.3, and the current profile is created based on the maximum measured current velocities. The Brazil current profile has a strong current speed close to the water surface, but a smoother decrease in current velocity compared to the more extreme current profiles. The simulation parameters is illustrated in the Table 6.7 and 6.8. The main simulation result is shown in 6.5.2, and the rest of the simulation plots are shown in B.3.

Table 6.7: Individual loop parameters Brazil

	Surge	Sway	Roll	Pitch	Yaw
Initial Conditions η_0	0	0	20 [deg]	20 [deg]	30 [deg]
Natural period control loop T_N	100	50	27	30	250
Relative damping ratio control loop ζ	4	1.4	0.707	0.707	0.707
Integrator gain Ki^*	$\frac{\omega_n}{5}Kp_{Surge}$	$\omega_n Kp_{Sway}$	0	0	0
Cutoff period low pass filter T_C	5	5	15	20	7
Saturation control force/moment τ_{max}	300 [kN]	300 [kN]	1000 [kNm]	1000 [kNm]	1000 [kNm]

Table 6.8: Simulation parameters Brazil

Desired installation position $[\eta_d^{North}, \eta_d^{East}]^T$	$[100, 50]^T$ [m]
Steady state drop velocity w	2.84 [m/s]
Total current velocity V_c	1.47-0.31 [m/s]
Current direction β	30 [deg]
Current profile	Brazil
Installation depth	2000 m
Centre of buoyancy $r_b = [x_b, y_b, x_b]^T$	$[0, 0, 0]^T$
Centre of gravity $r_g = [x_g, y_g, z_g]^T$	$[0, 0, 0]^T$

6.5.2 Result

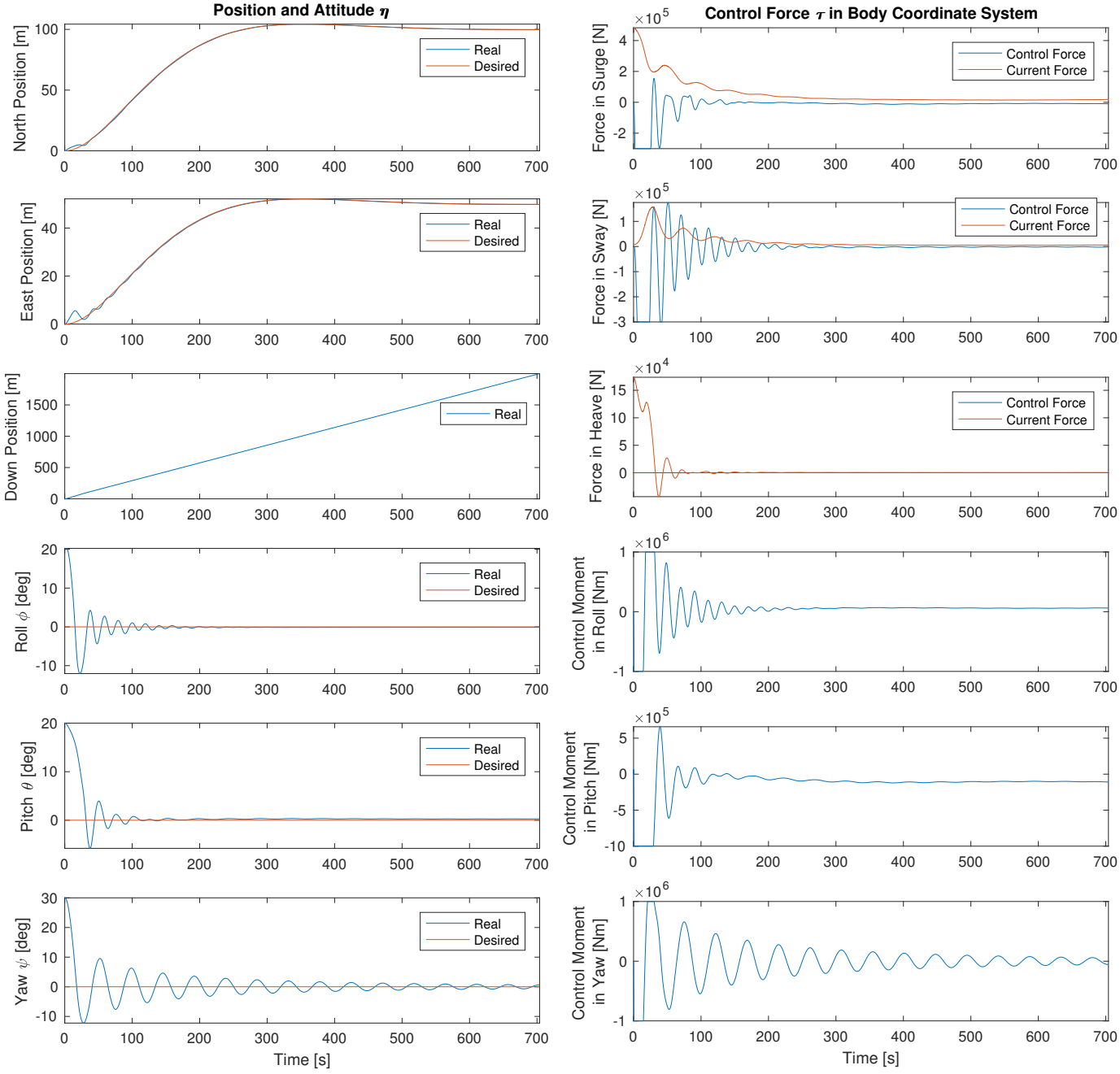

(a) Position and attitude

(b) Commanded control force

Figure 6.7: Drop in brazil current profile

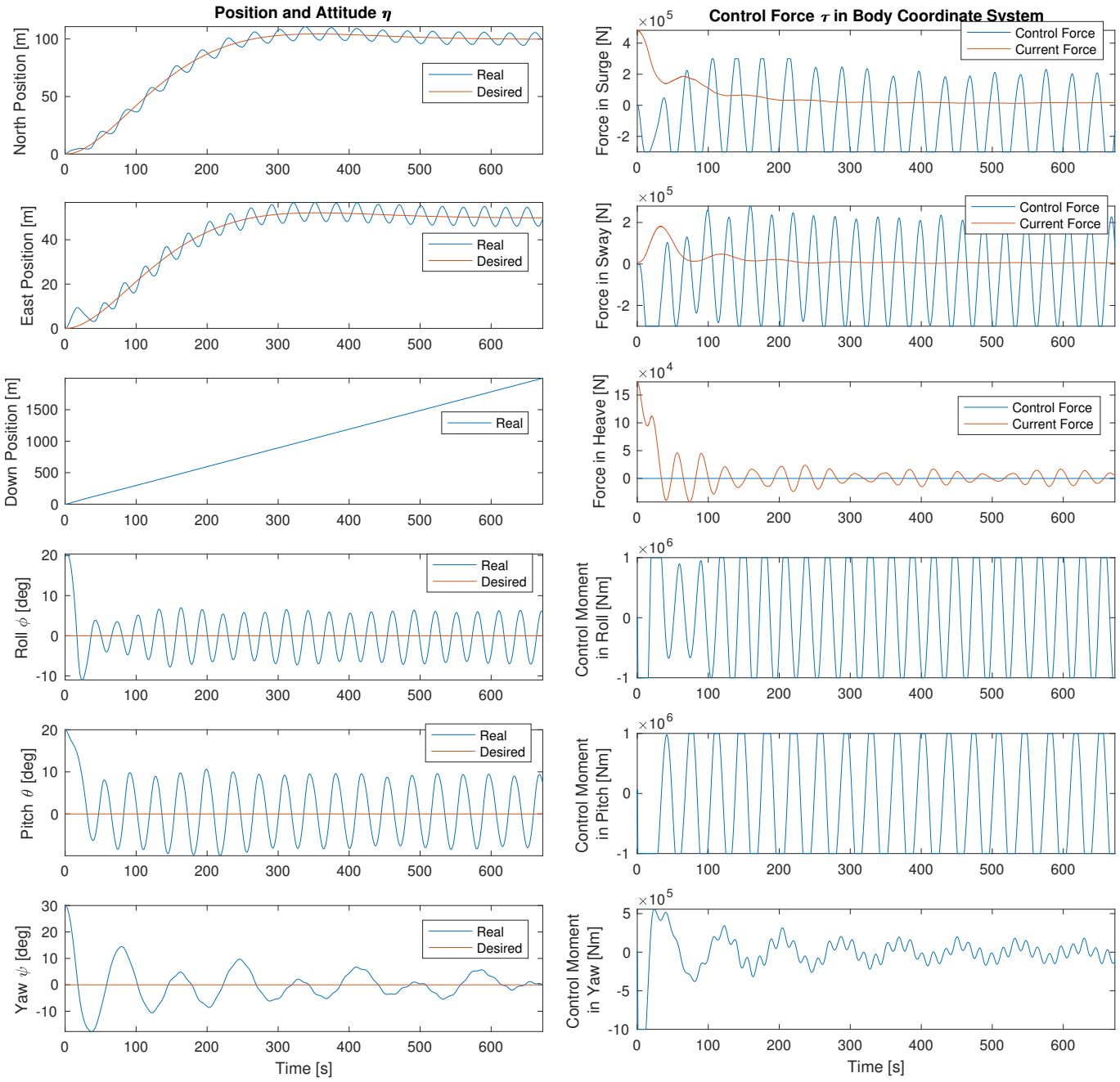

(a) Position and attitude

(b) Commanded control force

Figure 6.8: Free drop with brazil current profile using tuning from constant current simulation

6.5.3 Discussion

Figure 6.8 shows simulation results where the tuning parameters used in the constant current sumulation are used during submerging in the Brazil current profile. The figure illustrates oscillating behaviour in the controller, which are causing oscillating movement and rotations of the structure. Long natural period in surge an sway, was during tuning of the different current profiles, observed to cause oscillating behaviour in the controller during submerging in rapid changing currents. A long natural period is beneficially used in the constant current profile, in order to save control energy and achieve slow movement of the installation object in the horizontal plane. In the more rapid changing current profiles, shorter natural periods was during tuning observed to make the controller adapt better to the changing current force.

In the Brazil current profile the current speed is changing moderately fast. Figure 6.7a illustrates how well the tracking is improved using a shorter natural period in sway, and increasing the relative damping ratio in surge and sway in order to use the D-force in the controller to stop the movement of the structure if it starts gaining velocity from a large control force compared to the current force. Figure 6.7b shows how well the controller is keeping track of the changing current force in surge and sway, where the chaotic behaviour in the beginning of the simulation is caused by the roll and pitch stabilization. In Figure 6.7b, one can also see that the current force is very large next to the water surface. As a result, the commanded surge control force is saturated fast in the beginning of the simulation, but the tracking in Figure 6.7a is still very good during submerging, as the ocean current is decreasing with depth.

6.6 Drop in 3D Current Profile

6.6.1 Description

The 3D current profile is one of the more extreme current profiles, and it's considered to be a very hard operation condition to complete a free drop installation within. The installation parameters used in this simulation is shown in Table 6.9 and 6.10. The main results are presented in 6.6.2, and the rest of the simulation plots are shown in B.4.

Table 6.9: Individual loop parameters 3D

	Surge	Sway	Roll	Pitch	Yaw
Initial Conditions η_0	0	0	30 [deg]	30 [deg]	30 [deg]
Natural period control loop T_N	25	25	27	30	250
Relative damping ratio control loop ζ	3.5	1.4	0.707	0.707	0.707
Integrator gain Ki^*	0	0	0	0	0
Cutoff period low pass filter T_C	5	5	15	20	7
Saturation control force/moment τ_{max}	300 [kN]	300 [kN]	1000 [kNm]	1000 [kNm]	1000 [kNm]

Table 6.10: Simulation parameters 3D

Desired installation position $[\eta_d^{North}, \eta_d^{East}]^T$	$[50, 30]^T$ [m]
Steady state drop velocity w	2.84 [m/s]
Total current velocity V_c	1 [m/s]
Current direction β	30-210 [deg]
Current profile	3D
Installation depth	3000 m
Centre of buoyancy $r_b = [x_b, y_b, x_b]^T$	$[0, 0, 0]^T$
Centre of gravity $r_g = [x_g, y_g, z_g]^T$	$[0, 0, 0]^T$

6.6.2 Result

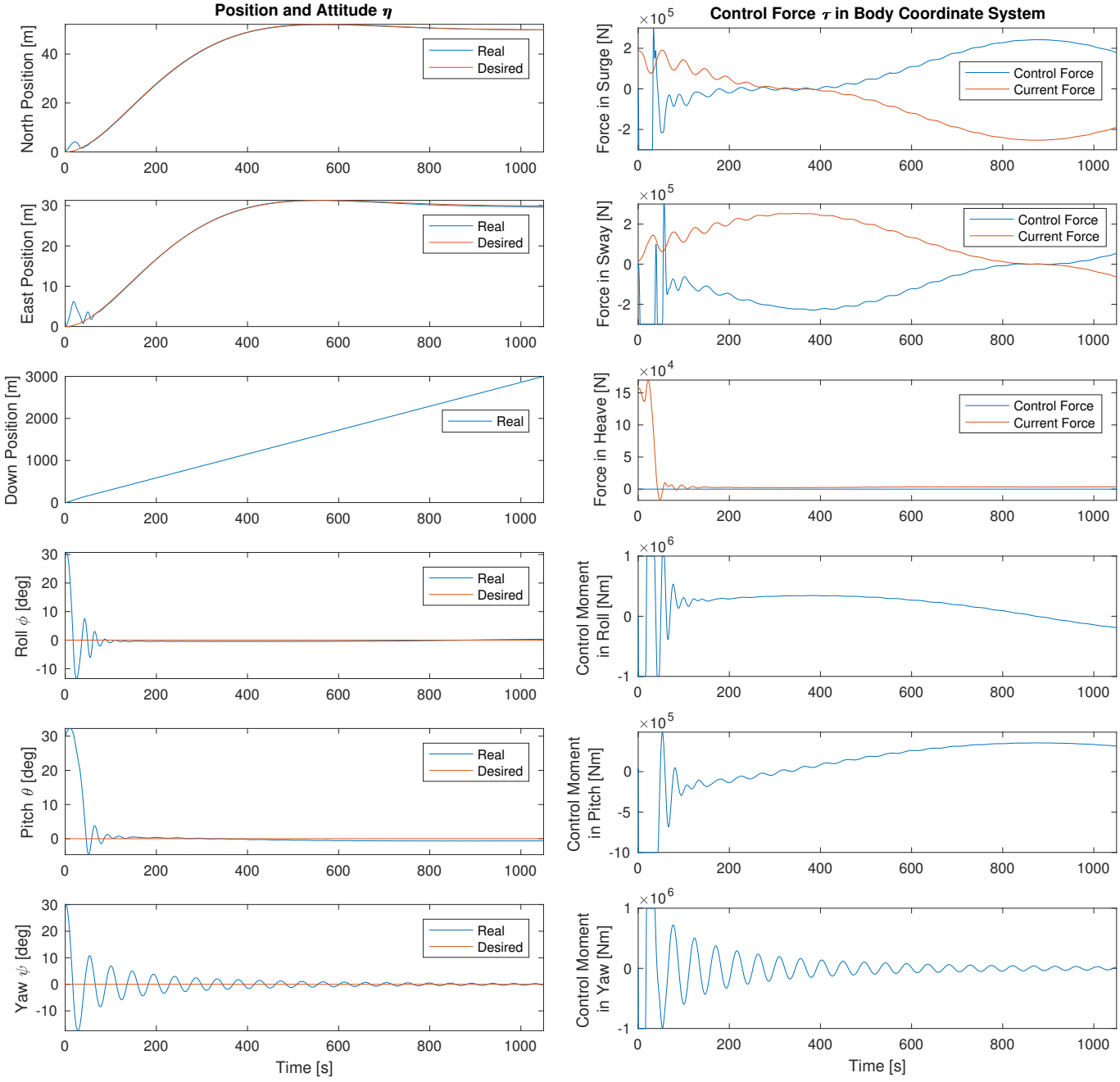

(a) Position and attitude

(b) Commanded control force

Figure 6.9: Drop in 3D current profile

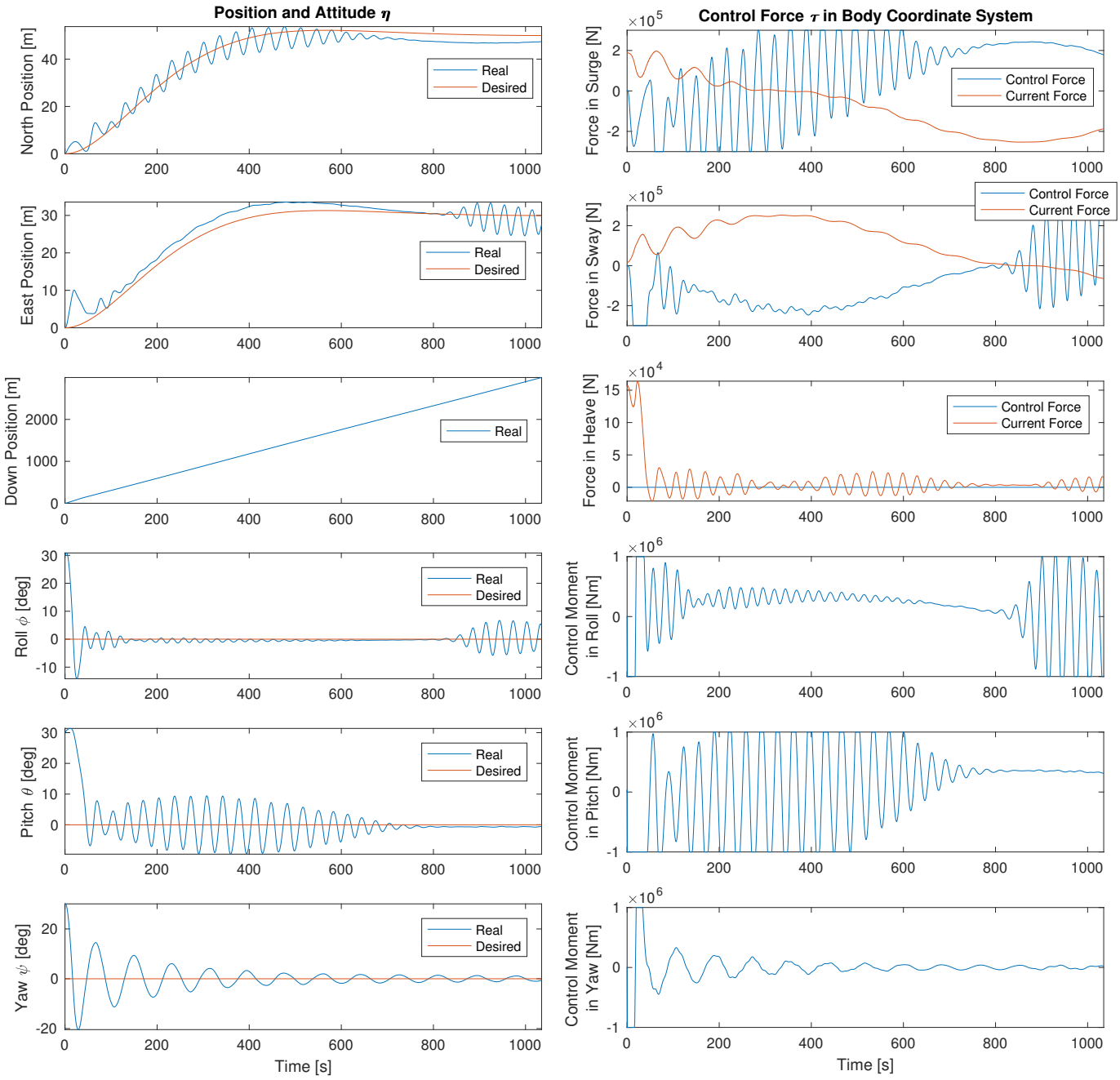

(a) Position and attitude

(b) Commanded control force

Figure 6.10: Drop in 3D current profile using tuning from constant current simulation

6.6.3 Discussion

Similar to the simulation using the Brazil current profile, Figure 6.10 shows poor tracking and oscillating behaviour in the controller, position and attitude using the controller tuning from the constant current simulation. The 3D current is changing very rapidly, so the natural period in surge and sway are set very short to achieve good results in this simulation. Figure 6.9a shows great tracking during submerging in the north and east direction, using the short natural period in surge and sway. At the same time, Figure 6.9b shows that approximately 200 [kN] of control force is required in each direction to achieve this tracking, ignoring the transient behaviour where roll and pitch are stabilized.

The tuning parameters used in this simulation gave the best results when they were tested on the other current profiles. These tuning parameters provide great tracking for all of the tested current profiles, and the only problem is the surge and sway force reaching saturation very fast in some of the profiles, and integrator windup if the integrator gains and saturations are chosen to high. Integrator force in the controller was observed to cause problems in the rapid changing current profiles, and has to be used carefully. If the integral force in the controller is to high when the current force is decreasing rapidly, the controller is not able to reduce the commanded control force as fast as the decreasing current force. As a result, windup occurs when the error becomes to large because of the poor tracking in the decreasing current profile.

6.7 Drop in Bidirectional Current Profile

6.7.1 Description

The simulation parameters in the simulation using the bidirectional current profile are shown in Table 6.11 and 6.12. The main simulation results are presented in 6.7, and the rest of the simulation plots are shown in B.5.

Table 6.11: Individual loop parameters bidirectional

	Surge	Sway	Roll	Pitch	Yaw
Initial Conditions η_0	0	0	5 [deg]	5 [deg]	0 [deg]
Natural period control loop T_N	25	25	27	30	250
Relative damping ratio control loop ζ	3.5	1.4	0.707	0.707	0.707
Integrator gain Ki^*	$\frac{\omega_n}{200} Kp_{Surge}$	$\frac{\omega_n}{200} Kp_{Sway}$	0	0	0
Cutoff period low pass filter T_C	5	5	15	20	7
Saturation control force/moment τ_{max}	300 [kN]	300 [kN]	- [kNm]	- [kNm]	- [kNm]

Table 6.12: Simulation parameters bidirectional

Desired installation position $[\eta_d^{North}, \eta_d^{East}]^T$	$[50, 30]^T$ [m]
Steady state drop velocity w	2.84 [m/s]
Total current velocity V_c	1 to -1 [m/s]
Current direction β	30 [deg]
Current profile	Bidirectional
Installation depth	3000 m
Centre of buoyancy $r_b = [x_b, y_b, x_b]^T$	$[0, 0, 0]^T$
Centre of gravity $r_g = [x_g, y_g, z_g]^T$	$[0, 0, 0]^T$

6.7.2 Result

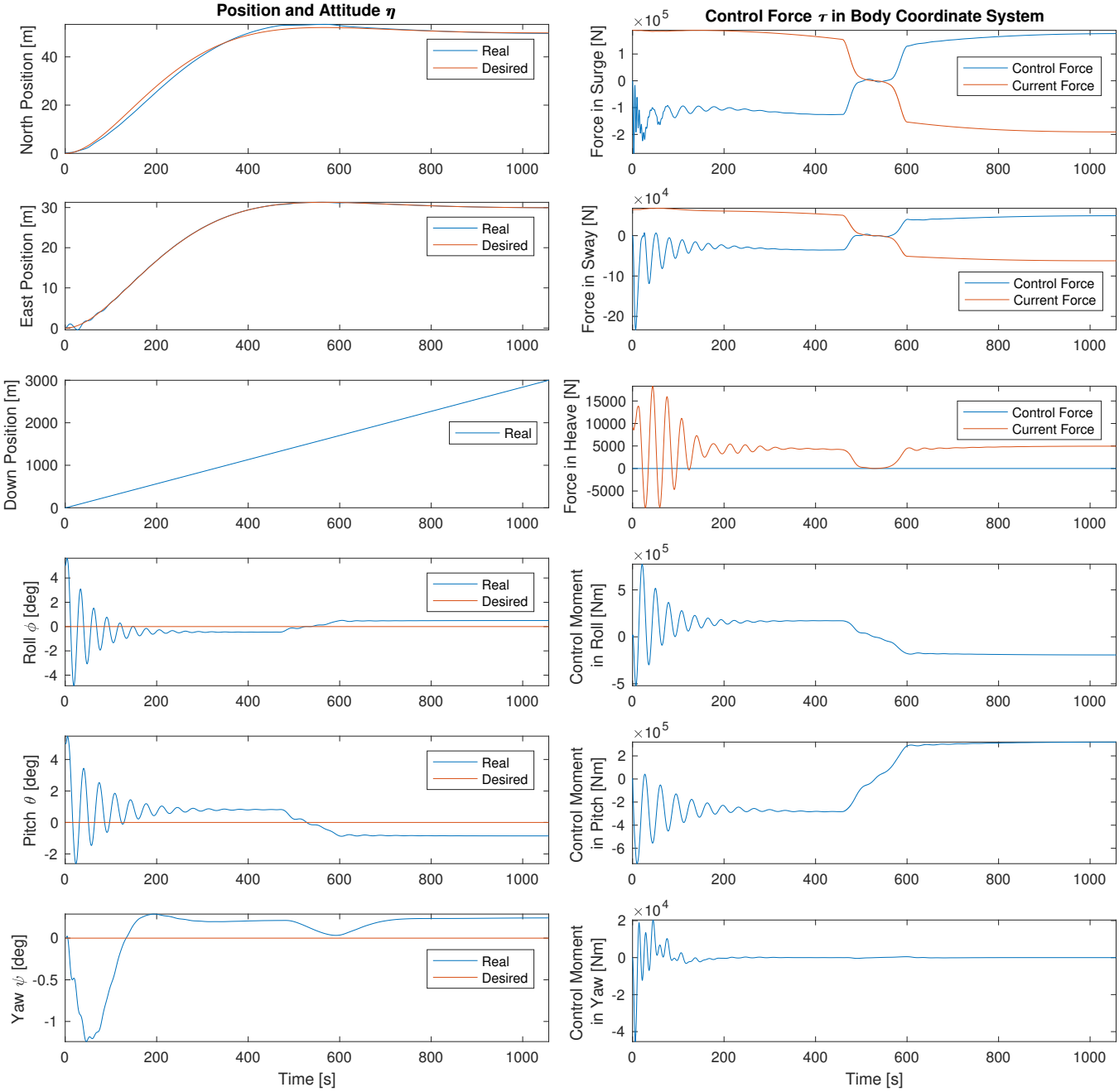

(a) Position and attitude

(b) Commanded control force

Figure 6.11: Drop in bidirectional current simulation result

6.7.3 Discussion

Figure 6.11a shows good tracking in the horizontal plane, using the tuning parameters from the 3D simulation. A small steady state error was observe in surge and sway, so very small integral gains are used to removed this steady state error. The integral gains is set such that the integral force can remove the steady state error, without making the controller unable to adapt to the changing current profile, and to avoid windup.

In Figure 6.11b, very rapid oscillations are observed in surge during roll and pitch stabilization using these tuning and filter constants, which have to be filtered out using better filtering methods. After the roll and pitch stabilization, Figure 6.11b shows that the controller is adapting well to the changing current force. The initial angles on the rotations are closer to zero in this simulation, so the commanded moment in roll, pitch and yaw shown in Figure 6.11b are not that large. Figure 6.11a shows a small steady state error in rotations during submerging, as only PD control is used.

6.8 Drop in Divided Current Profile

6.8.1 Description

The simulation parameters in the simulation using the divided current profile are shown in Table 6.13 and 6.14. The main result is presented in 6.8.2, and the rest of the simulation plots are shown in B.6.

Table 6.13: Individual loop parameters divided current

	Surge	Sway	Roll	Pitch	Yaw
Initial Conditions η_0	0	0	30 [deg]	30 [deg]	30 [deg]
Natural period control loop T_N	25	25	27	30	250
Relative damping ratio control loop ζ	3.5	1.4	0.707	0.707	0.707
Integrator gain Ki^*	0	0	0	0	0
Cutoff period low pass filter T_C	5	5	15	20	7
Saturation control force/moment τ_{max}	300 [kN]	300 [kN]	- [kNm]	- [kNm]	- [kNm]

Table 6.14: Simulation parameters divided current

Desired installation position $[\eta_d^{North}, \eta_d^{East}]^T$	$[50, 30]^T$ [m]
Steady state drop velocity w	2.84 [m/s]
Total current velocity V_c	1 - 0 [m/s]
Current direction β	30 [deg]
Current profile	Divided
Installation depth	3000 m
Centre of buoyancy $r_b = [x_b, y_b, x_b]^T$	$[0, 0, 0]^T$
Centre of gravity $r_g = [x_g, y_g, z_g]^T$	$[0, 0, 0]^T$

6.8.2 Result

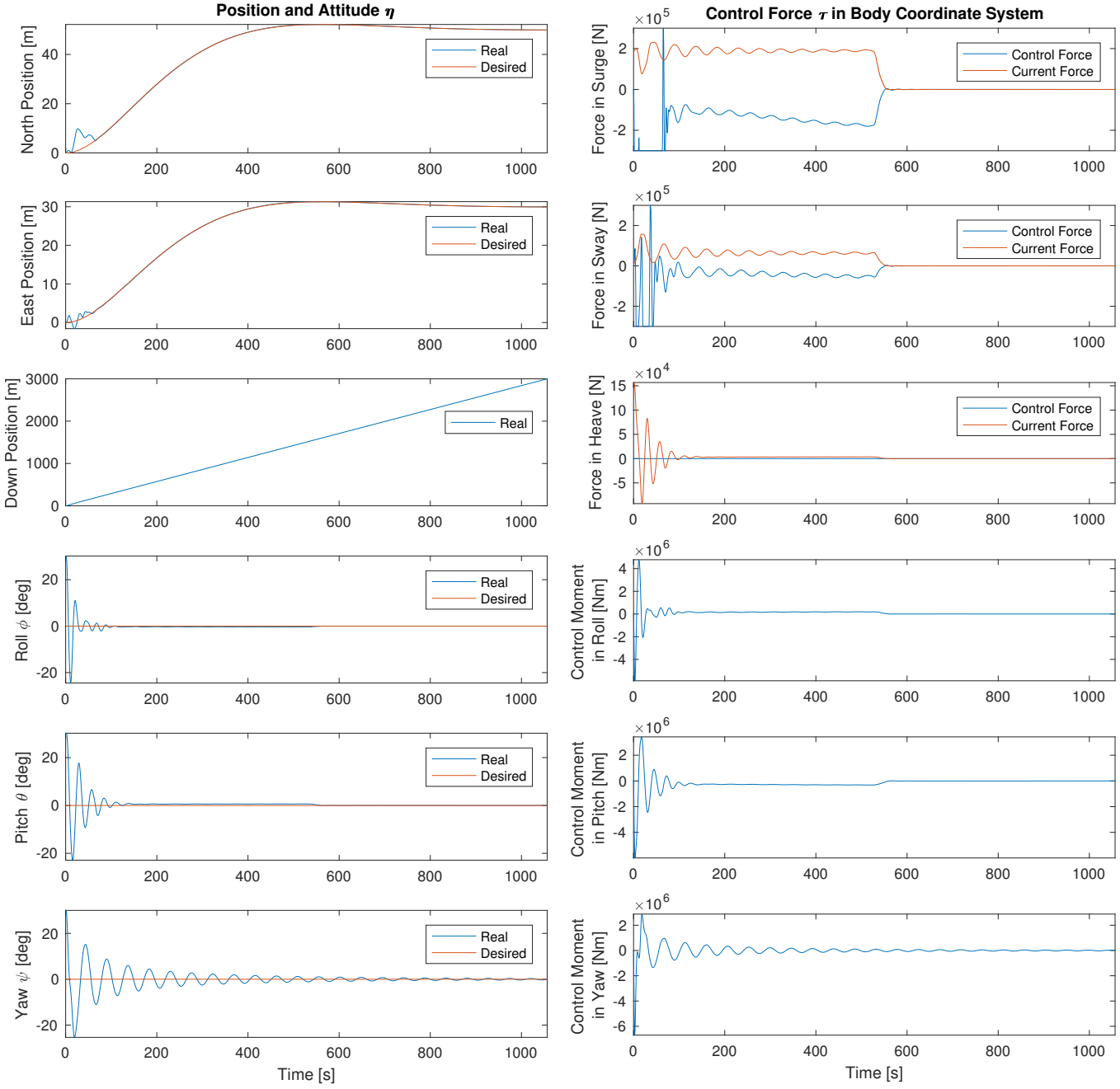

(a) Position and attitude

(b) Commanded control force

Figure 6.12: Drop in divided current profile simulation result

6.8.3 Discussion

Figure 6.12a shows great tracking in the horizontal plane using the tuning parameters from the 3D current simulation. Similar to the other varying current profiles, Figure 6.12b shows oscillation behaviour in the controller during roll and pitch stabilization, and good tracking of the changing current force after the stabilization. Figure 6.12b also shows that the low cutoff period in surge and sway in the low pass filter is making the filter unable to filter the oscillating commanded control force, caused by the yaw oscillations. Roll and pitch are stabilized perfectly, as no saturation is used.

6.9 Drop in Shear Current Profile

6.9.1 Description

The simulation parameters in the simulation using the shear current profile are shown in Table 6.15 and 6.16. The main result is presented in 6.9.2, and the rest of the simulation plots are shown in B.7.

Table 6.15: Individual loop parameters shear current

	Surge	Sway	Roll	Pitch	Yaw
Initial Conditions η_0	0	0	30 [deg]	30 [deg]	30 [deg]
Natural period control loop T_N	25	25	27	30	250
Relative damping ratio control loop ζ	3.5	1.4	0.707	0.707	0.707
Integrator gain Ki^*	0	0	0	0	0
Cutoff period low pass filter T_C	5	5	15	20	7
Saturation control force/moment τ_{max}	300 [kN]	300 [kN]	- [kNm]	- [kNm]	- [kNm]

Table 6.16: Simulation parameters shear current

Desired installation position $[\eta_d^{North}, \eta_d^{East}]^T$	$[50, 30]^T$ [m]
Steady state drop velocity w	2.84 [m/s]
Total current velocity V_c	1 - 0 [m/s]
Current direction β	30 [deg]
Current profile	Shear
Installation depth	3000 m
Centre of buoyancy $r_b = [x_b, y_b, x_b]^T$	$[0, 0, 0]^T$
Centre of gravity $r_g = [x_g, y_g, z_g]^T$	$[0, 0, 0]^T$

6.9.2 Result

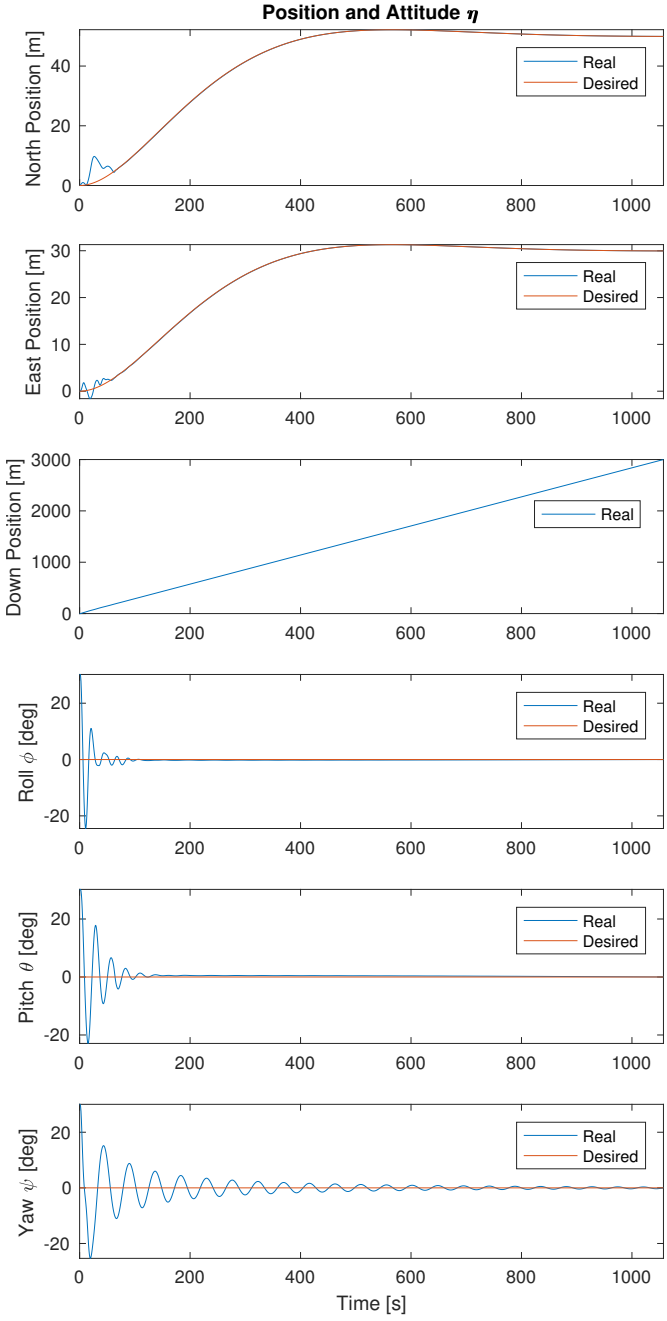

(a) Position and attitude

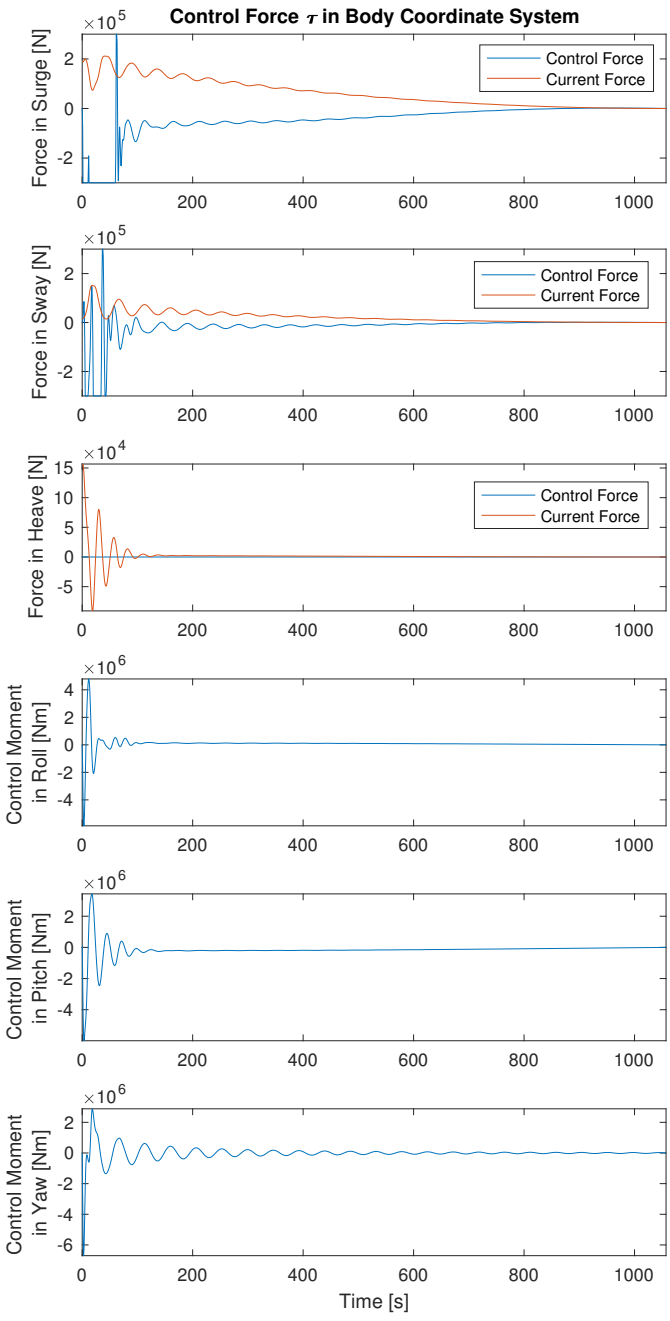

(b) Commanded control force

Figure 6.13: Drop simulation result

6.9.3 Discussion

Figure 6.13a shows great tracking in the horizontal plane during submerging in the shear current profile, and the rotations are stabilized perfectly as no saturations are used. Figure 6.13b shows the previously observed behaviour in the surge and sway controller, where chaotic oscillating control force is commanded in the controller during roll and pitch stabilization, and good control force adaptation to the current force is commanded after approximately 100 seconds.

6.10 Parachute Drop

6.10.1 Description

In this simulation, a parachute is used to stabilize the roll and pitch motion, and to reduce the drop velocity. The parachute diameter is chosen based on results from [17], and the drop velocity of the Johan Sverdrup ITS structure using different parachute diameters is illustrated in Figure 6.14.

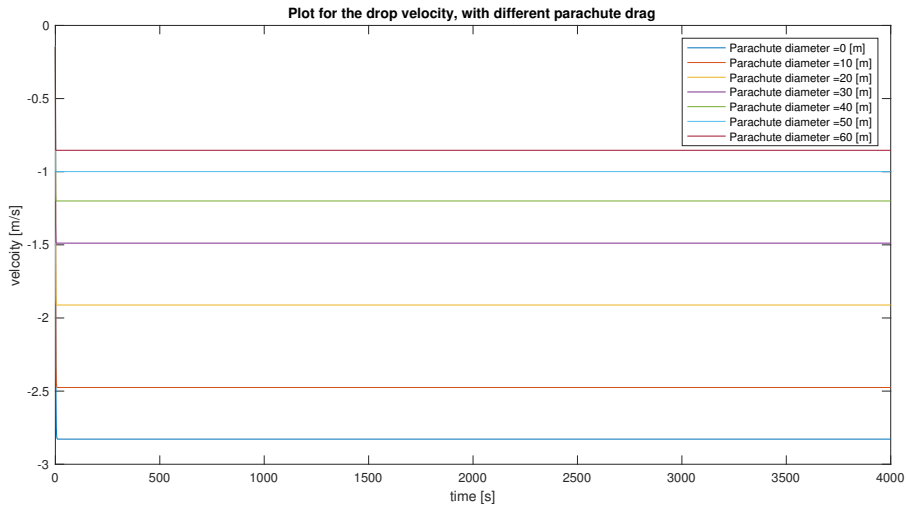

Figure 6.14: Drop velocity of the Johan Sverdrup ITS structure with different parachute diameter (ref: [17])

A parachute matrix P is used in the equation of motion to include the parachute in the structure's dynamics. The parachute is assumed to provide a restoring moment in roll and pitch, where the restoring moment is modelled as if the parachute wires attached to the edges of the installation object is providing a spring force, which will provide a restoring moment. Also, the parachute is assumed to provide extra quadratic drag damping. The parachute matrix P is defined as

$$P(\eta, \nu_r) = \begin{bmatrix} 0 \\ 0 \\ 1.75 \frac{1}{2} \rho \frac{D_{para}^2}{4} |w_r| w_r \\ \frac{EA}{L_{wire}} \frac{L_{SPS}^2}{2} \phi \\ \frac{EA}{L_{wire}} \frac{L_{SPS}^2}{2} \theta \\ 0 \end{bmatrix} \tag{6.8}$$

where $\frac{EA}{L_{wire}}$ is the spring stiffness in each of the attached parachute wires, L_{SPS} is the length and breadth of the installation object (symmetrical in the horizontal plane), and the parachute drag coefficient $Cd_{para} = 1.75$ is used [28]. The parachute matrix P is added to the equation of motion as shown in Equation 6.9.

$$M\dot{\nu_r} + C(\nu_r)\nu_r + D(\nu_r)\nu_r + g(\eta) + P(\eta, \nu_r) = \tau_{control} \tag{6.9}$$

The simulation parameters is shown in the Table 6.17 and 6.18. The main results are presented in 6.10.2, and the rest of the simulation plots are shown in B.8.

Table 6.17: Individual loop parameters parachute

	Surge	Sway	Roll	Pitch	Yaw
Initial Conditions η_0	0	0	30 [deg]	30 [deg]	30 [deg]
Natural period control loop T_N	1500	2500	-	-	700
Relative damping ratio control loop ζ	0.707	0.707	-	-	0.707
Integrator gain Ki^*	$\frac{1}{5}Kp_{Surge}$	$\frac{3}{5}Kp_{Sway}$	-	-	0
Cutoff period low pass filter T_C	350	350	-	-	7
Saturation control force/moment τ_{max}	300 [kN]	300 [kN]	-	-	1000 [kNm]

Table 6.18: Simulation parameters parachute

Desired installation position $[\eta_d^{North}, \eta_d^{East}]^T$	$[100, 50]^T$ [m]
Steady state drop velocity w	1.49 [m/s]
Total current velocity V_c	1 [m/s]
Current direction β	30 [deg]
Current profile	Constant
Installation depth	3000 m
Centre of buoyancy $r_b = [x_b, y_b, x_b]^T$	$[0, 0, 0]^T$
Centre of gravity $r_g = [x_g, y_g, z_g]^T$	$[0, 0, 0]^T$
Parachute diameter D_{para}	30 [m]

6.10.2 Result

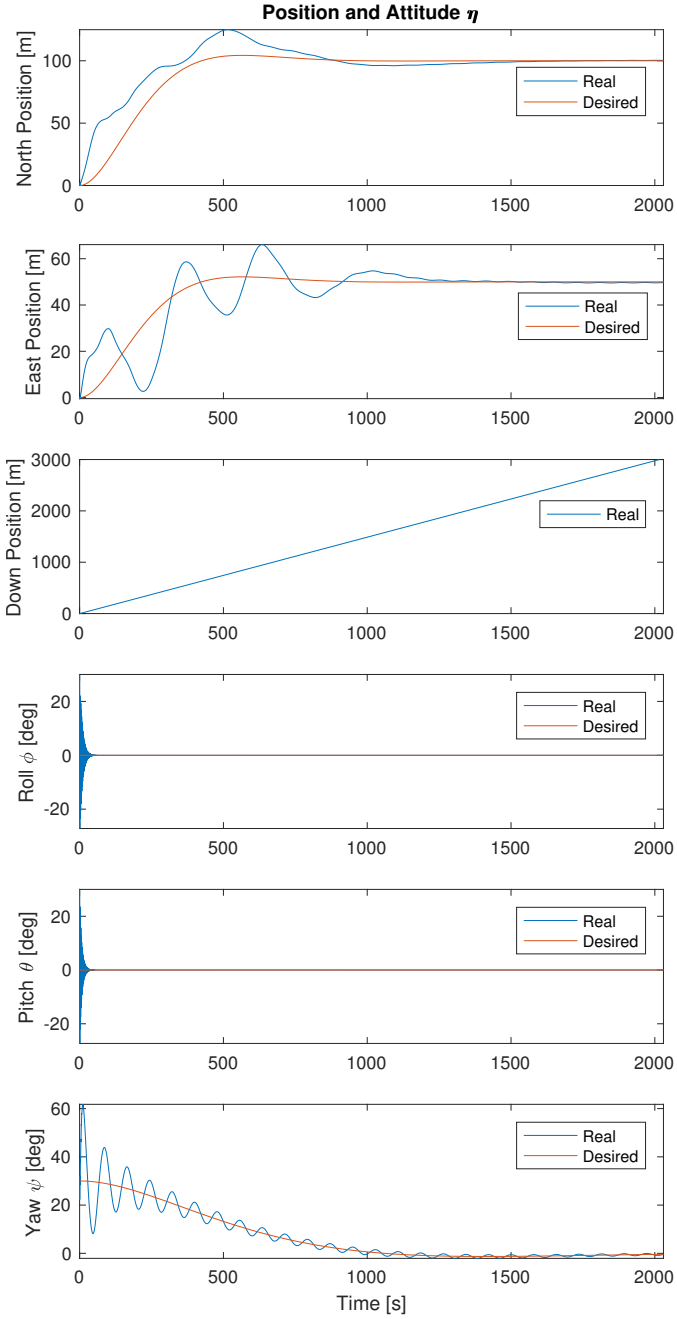

(a) Position and attitude

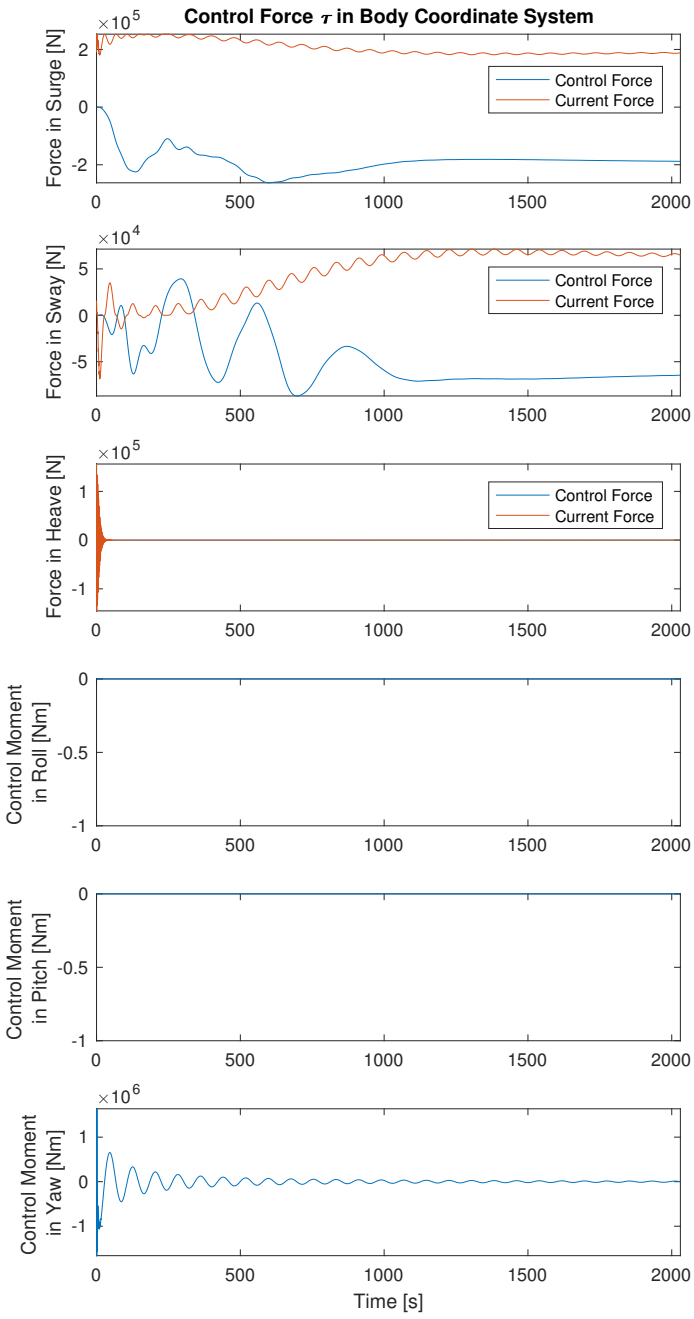

(b) Commanded control force

Figure 6.15: Free drop with attached parachute

6.10.3 Discussion

In the parachute simulation, the drop velocity is reduced because of the increased drag damping from the parachute. Hence, the controller has more time to position the structure in the horizontal plane, and a control strategy using a very long natural period in surge and sway is used. The long natural period in surge and sway is set to try and use as little control energy as possible when the installation is preformed in a constant current profile, and to achieve a very smooth movement of the structure in the horizontal plane. Figure 6.15a illustrates the control strategy used in the horizontal plane, where the low natural periods are causing the poor tracking towards the desired installation position. When the structure has moved close to the installation position, the integrator force in the controller is moving the structure to the exact installation position by removing the steady state error. When the structure is at the exact installation position, the integrator force is equal to the current force, so the controller is just counteracting the ocean current to keep the structure in place. The long cutoff period in the low pass filter is beneficially used to achieve a smooth integrator force, and to avoid integrator windup.

Figure 6.15b shows that a very smooth control force is commanded in surge and sway during the entire simulation, which is considered beneficial for the large ITS structure. The figure also shows how well the low pass filter is utilized on filtering out the high frequent oscillations in the surge and sway controller, caused by the small yaw oscillation. The yaw oscillations are causing an oscillating current force in surge and sway because of the rotating body frame, and it's not desirable for the controller to follow this high frequent oscillation. At the same time, Figure 6.15a shows that the structure has very smooth movements in the north and east direction, and it's positioned at the exact desired installation position when the structure is at 3000 m depth.

In Figure 6.15a, one can see that the roll and pitch motion is stabilized as a decaying spring without any active control. This stabilization is provided by the restoring moment from the attached parachute wires. Filtering is a must when the parachute is used to stabilize the roll and pitch motion, as the decaying spring is causing high frequent oscillations of the body frame. This oscillation has to be filtered out in surge, sway and yaw, in order to not cause unnecessary high frequent loading on the actuators. Figure 6.15b shows that this high frequent oscillation is successfully filtered out in surge and sway using the second order Butterworth filter with long cutoff period. Filtering issues are observed in the beginning of the commanded yaw moment, where the filter is unable to remove the small oscillations. The filtered error signal have very small spikes in the beginning of the simulation causing these oscillations, which indicates that the second order Butterworth filter is having issues with filtering this signal sufficiently. Hence, better filtering technics to handle the yaw signal sufficiently have is required. Control strategies, where the surge and sway controller is started after the roll and pitch stabilization is finished also have to be considered, in order to avoid potential problems in the parachute during the transient phase.

Several methods to try and save control energy in yaw was also tested in this simulation. A natural period of 700 s is used in yaw, in order to use the entire submerging time to damp the yaw motion. Long natural period in yaw was observed to reduce the commanded yaw moment, especially in the beginning of the simulation. A natural period of 700 s was observed to be a maximum value, and natural periods above this value did not reduce the commanded yaw moment that much more. As illustrated in Figure 6.15a, guidance is implemented in yaw in this simulation to create a smoother trajectory in yaw towards zero. The smoothened trajectory was observed to save some control energy in yaw when large initial angles were simulated, but as the largest force in the yaw controller is the D-force which is proportional to the speed, smoothing the attitude error did not provide that much control energy reduction.

6.11 Drop with Buoyancy Tank

6.11.1 Description

In this simulation, an attached buoyancy tank is used to provide hydrostatic stability by moving the centre of buoyancy above the centre of gravity, and to provide extra buoyancy to the structure. The attached buoyancy tank is shaped like a symmetric cylinder located on top of the ITS structure, and it's assumed to provide a buoyancy force of

$$B_{cyl} = \frac{D_{cyl}^2}{4}\pi L_{cyl}\rho g \tag{6.10}$$

The attached buoyancy cylinder is also assumed to provide extra drag damping according to Equation 6.11.

$$D_{cyl}^q = 0.47\frac{1}{2}\rho L_{cyl} D_{cyl} \tag{6.11}$$

where the drag coefficient $Cd_{cyl} = 0.47$ for a cylinder in fluid flow is used. The drag coefficient corresponding to the buoyancy tank is added to the quadratic damping matrix according to Equation 6.12.

$$D_{33}^q = D_{33ITS}^q + D_{cyl}^q \tag{6.12}$$

The simulation parameters are shown in the Table 6.19 and 6.20 . The main results are presented in 6.11.2, and the rest of simulation plots are shown in B.9.

Table 6.19: Individual loop parameters buoyancy tank

	Surge	Sway	Roll	Pitch	Yaw
Initial Conditions η_0	0	0	40 [deg]	40 [deg]	30 [deg]
Natural period control loop T_N	1500	2500	-	-	700
Relative damping ratio control loop ζ	0.707	0.707	-	-	0.707
Integrator gain Ki^*	$\frac{1}{5}Kp_{Surge}$	$\frac{3}{5}Kp_{Sway}$	-	-	0
Cutoff period low pass filter T_C	350	350	-	-	7
Saturation control force/moment τ_{max}	300 [kN]	150 [kN]	-	-	500 [kNm]

Table 6.20: Simulation parameters buoyancy tank

Desired installation position $[\eta_d^{North}, \eta_d^{East}]^T$	$[50, 40]^T$ [m]
Steady state drop velocity w	0.76 [m/s]
Total current velocity V_c	1 [m/s]
Current direction β	30 [deg]
Current profile	Constant
Installation depth	3000 m
Centre of buoyancy $r_b = [x_b, y_b, x_b]^T$	$[0, 0, -7.85]^T$
Centre of gravity $r_g = [x_g, y_g, z_g]^T$	$[0, 0, 0]^T$
Buoyancy tank diameter D_{cyl}	4 [m]
Buoyancy tank length L_{cyl}	15 [m]

6.11.2 Result

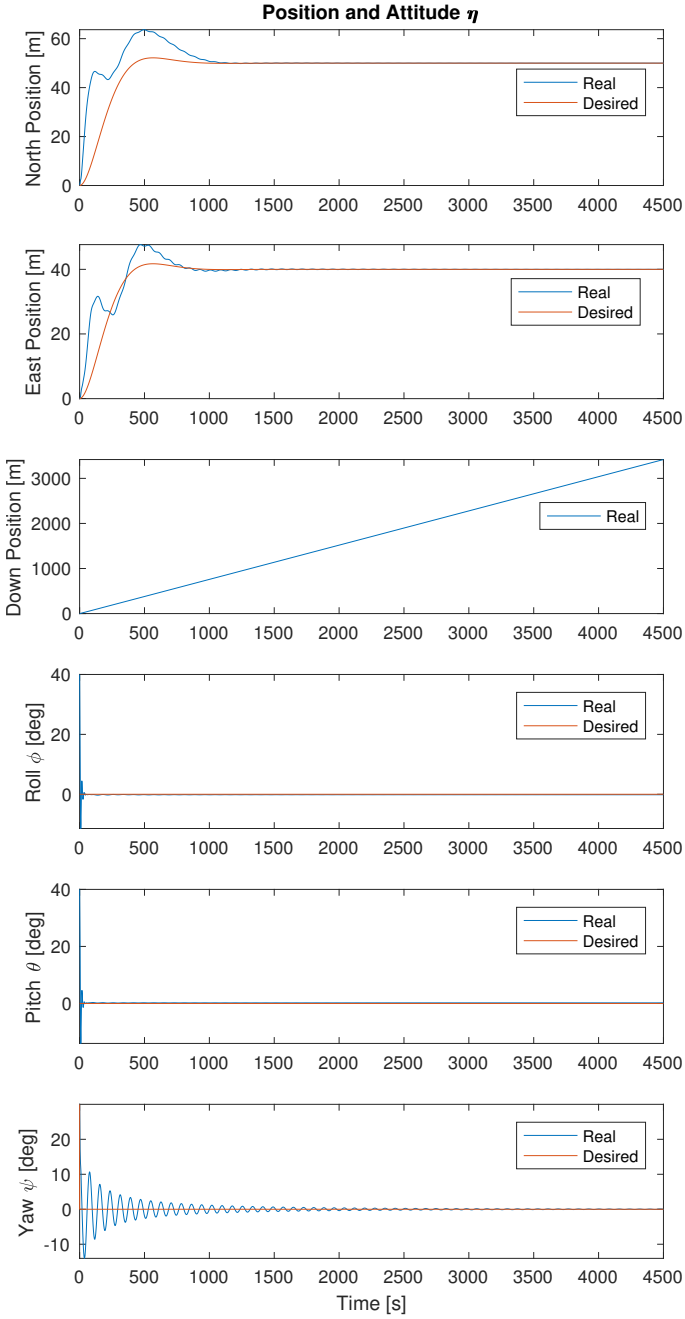

(a) Position and attitude

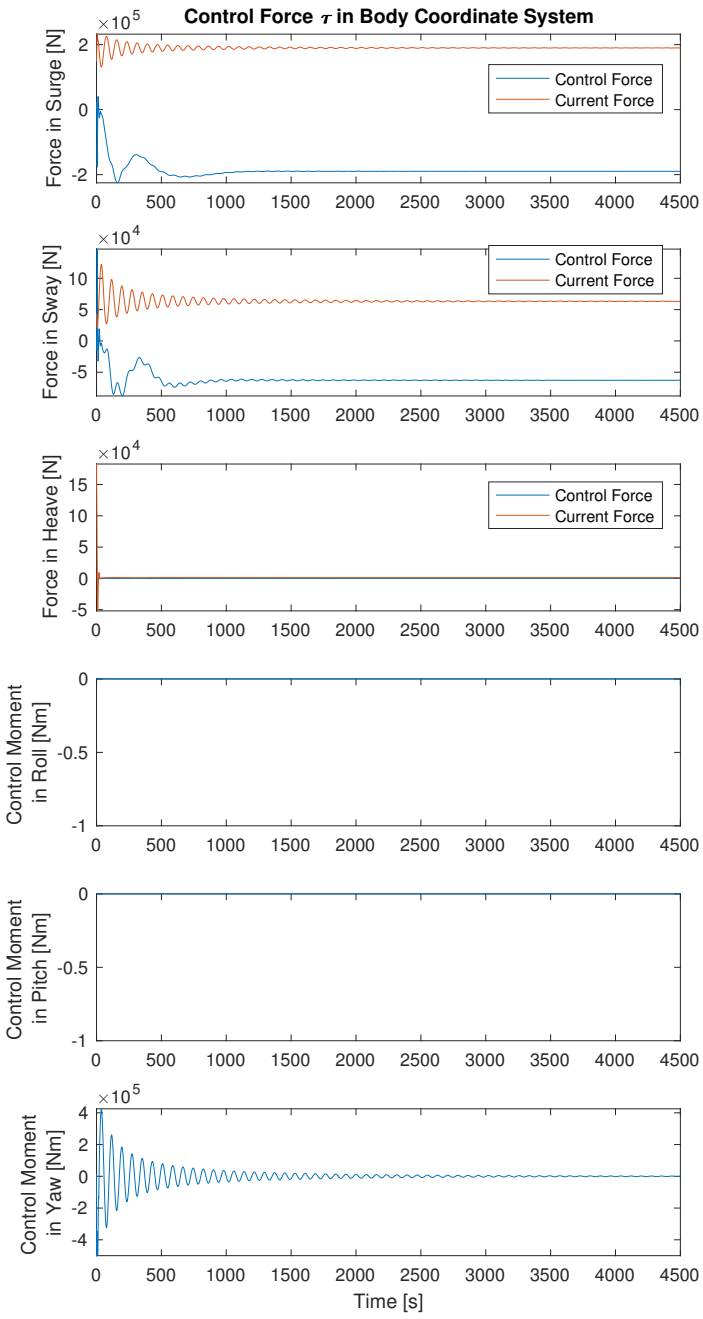

(b) Commanded control force

Figure 6.16: Free drop with attached buoyancy tank

6.11.3 Discussion

The simulated buoyancy tank is the only component able to reduce the drop velocity below 1 m/s. In this simulation, the drop velocity is 0.76 m/s which is giving the controller a long time to position the structure in the horizontal plane, and the impact velocity at the sea floor is very low. The dimensions used on the buoyancy tank is also reasonable, considering the size of the Johan Sverdrup ITS structure. Figure 6.16a shows that the structure is positioned in the correct position in the horizontal plane long before it reaches 3000 m depth. Tuning parameters similar to the parachute drop are used, and only 200 kN of thrust is used in surge, and approximately 100 kN is used in sway to achieve great horizontal positioning.

Figure 6.16a also illustrates how fast the structure is stabilized in roll and pitch, using the hydrostatic restoring moment provided by the buoyancy tank. The buoyancy tank is considered to be the best method to stabilize the structure, as few uncertainties are related to stabilization using hydrostatic restoring moment. Coupled oscillations caused by the decaying spring stabilization from the parachute are also no longer an issue when the buoyancy tank is used.

The commanded yaw moment reaches saturation very fast in the beginning of the simulation, and a lot of control energy is still required in yaw to stabilize the structure. Using a saturation limit of 500 kNm which is considered feasible for the large Johan Sverdrup ITS structure, the controller is able to stabilize the structure in yaw. Further investigation of the commanded yaw moment, including the actuator dynamics is still required.

6.12 Drop Using Scaled Structure Parameters

6.12.1 Description

It was desirable to assess the behaviour of a smaller and more compact structure, using the "Drop and Forget" installation method. In order do this, reasonable scaling is done on the Johan Sverdrup structure parameters and hydrodynamic coefficients. The scaled structure parameters, and corresponding scaled rigid body and hydrodynamic matrices is shown in Table 6.21 and Matrix 6.13 - 6.16.

Modified Structure Parameters

Table 6.21: Scaled Johan Sverdrup ITS dimensions (ref: [26])

	Suction Anchor	Structure Body	Total
Mass [Kg]	$12.5 * 10^3$	$40 * 10^3$	$90 * 10^3$
Wet mass [Kg]	$10.875 * 10^3$	$34.8 * 10^3$	$78.3 * 10^3$
Height [m]	3.25	4.5	7.75
Length/Diameter [m]	6	9	15
Breadth/Diameter [m]	6	9	15
COG [m]	2	4.25	3

Mass rigid body

$$\boldsymbol{M_{RB}} = \begin{bmatrix} 90000 & 0 & 0 & 0 & 0 & 0 \\ 0 & 90000 & 0 & 0 & 0 & 0 \\ 0 & 0 & 90000 & 0 & 0 & 0 \\ 0 & 0 & 0 & 1130625 & 0 & 0 \\ 0 & 0 & 0 & 0 & 1130625 & 0 \\ 0 & 0 & 0 & 0 & 0 & 3645000 \end{bmatrix} \tag{6.13}$$

Added mass

$$\boldsymbol{M_A} = \begin{bmatrix} 654250 & 0 & 0 & 0 & 695750 & 0 \\ 0 & 654250 & 0 & -695750 & 0 & 0 \\ 0 & 0 & 593250 & 0 & 0 & 0 \\ 0 & -695750 & 0 & 12088750 & 0 & 0 \\ 695750 & 0 & 0 & 0 & 12088750 & 0 \\ 0 & 0 & 0 & 0 & 0 & 26497125 \end{bmatrix} \tag{6.14}$$

Linear damping

$$\boldsymbol{D_l} = \begin{bmatrix} 0 & 0 & 0 & 0 & 0 & 0 \\ 0 & 0 & 0 & 0 & 0 & 0 \\ 0 & 0 & 142000 & 0 & 0 & 0 \\ 0 & 0 & 0 & 2875500 & 0 & 0 \\ 0 & 0 & 0 & 0 & 2875500 & 0 \\ 0 & 0 & 0 & 0 & 0 & 0 \end{bmatrix} \tag{6.15}$$

Quadratic damping

$$\boldsymbol{D_q} = \begin{bmatrix} 79250 & 0 & 0 & 0 & 2750 & 0 \\ 0 & 79250 & 0 & -2750 & 0 & 0 \\ 0 & 0 & 44250 & 0 & 0 & 0 \\ 0 & -2750 & 0 & 109750 & 0 & 0 \\ 2750 & 0 & 0 & 0 & 109750 & 0 \\ 0 & 0 & 0 & 0 & 0 & 10137656 \end{bmatrix} \tag{6.16}$$

6.12.2 Simulation Parameters

The simulation parameters are presented in the Table 6.22 and 6.23. The main results are presented in 6.12.3, and the rest of the simulation plots are shown in B.10.

Table 6.22: Individual loop parameters scaled structure

	Surge	Sway	Roll	Pitch	Yaw
Initial Conditions η_0	0	0	-5 [deg]	5 [deg]	10 [deg]
Natural period control loop T_N	1500	2500	10	7	200
Relative damping ratio control loop ζ	0.707	0.707	0.9	0.9	0.707
Integrator gain Ki^*	$\frac{1}{2}Kp_{Surge}$	$0.7Kp_{Sway}$	0	0	0
Cutoff period low pass filter T_C	200	200	3	3	7
Saturation control force/moment τ_{max}	100 [kN]	100 [kN]	-	-	-

Table 6.23: Simulation parameters scaled structure

Desired installation position $[\eta_d^{North}, \eta_d^{East}]^T$	$[50, 30]^T$ [m]
Steady state drop velocity w	2.87 [m/s]
Total current velocity V_c	1 [m/s]
Current direction β	30 [deg]
Current profile	Constant
Installation depth	3000 m
Centre of buoyancy $r_b = [x_b, y_b, x_b]^T$	$[0, 0, 0]^T$
Centre of gravity $r_g = [x_g, y_g, z_g]^T$	$[0, 0, 0]^T$

6.12.3 Result

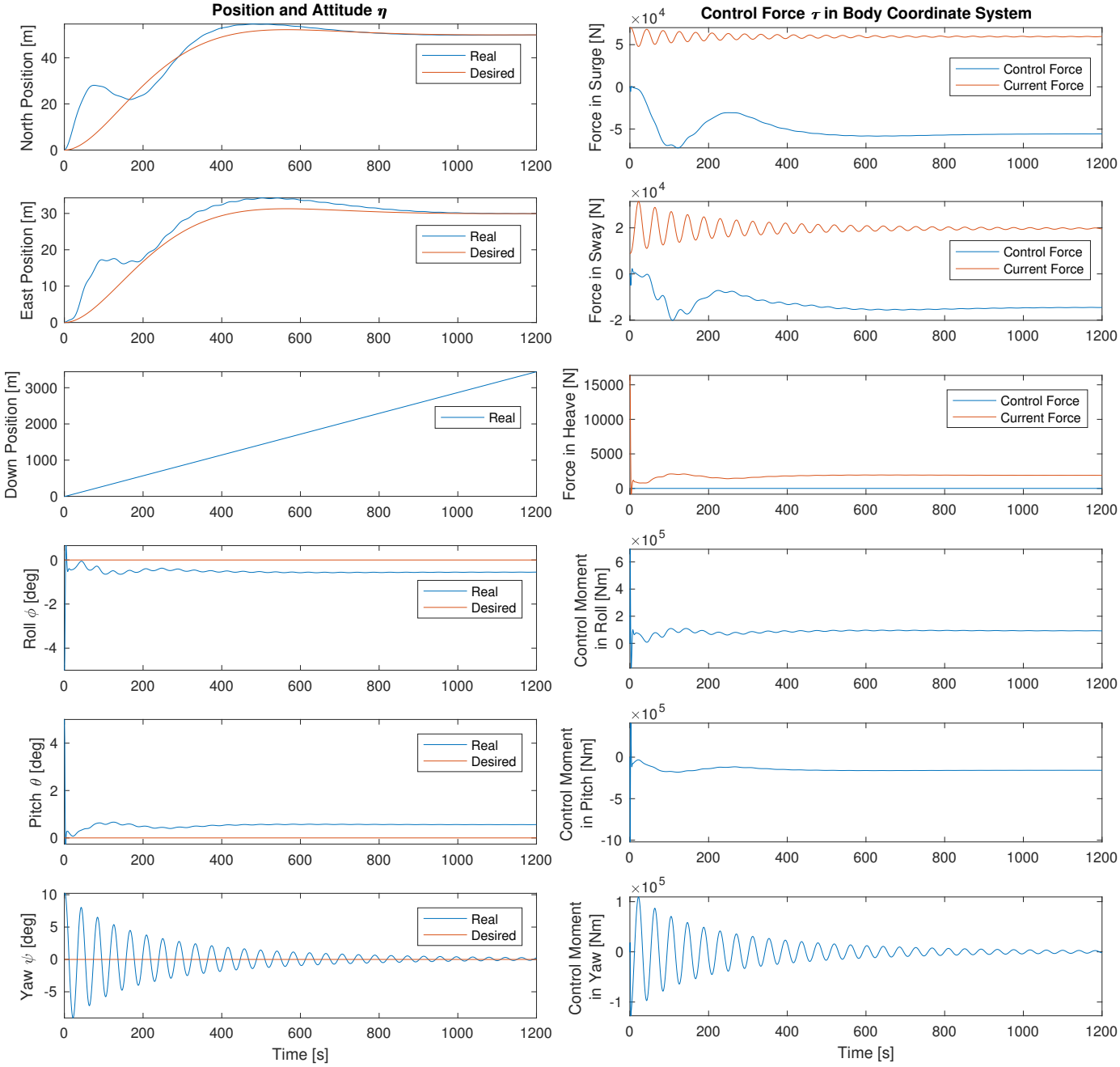

(a) Position and attitude

(b) Commanded control force

Figure 6.17: Drop with scaled structure parameters

6.12.4 Discussion

As expected, Figure 6.17b shows that less control force is required to position the structure in the horizontal plane. Only 20 kN is required in sway, and approximately 70 kN in surge which can be provided by two thrusters of moderate size. In this simulation, the surge and sway control force actually never reaches saturation.

Another interesting observation in Figure 6.17b, is that a very large moment is still required in roll and pitch to stabilize the structure. Several simulations also showed that the commanded moment must be delivered faster on than scaled structure, in order to stabilize it. The maximum arm the propellers can have to the origin of the structure on the scaled structure, is 4.5 m. Hence, providing the commanded control force of 1000 kNm will require a 250 kN thruster at the edge of the structure. Even for a much smaller structure, stabilization of the roll and pitch motion looks to be problematic, and even more problematic than for the full scale Johan Sverdrup ITS structure. Simulations showed that the controller was able to stabilize the structure when it was saturated at 200 kNm in roll and pitch, but the commanded control force had to be delivered within a second, something that is unfeasible to provide by a thruster.

Figure 6.17b shows that the commanded yaw moment is relatively high, even for the scaled structure. It's still considered feasible to deliver this moment by several thrusters attached on top of the structure, and simulations using saturation in yaw showed that stabilization in yaw also is possible using less thrust.

In Figure 6.17a, a steady state error is present in roll and pitch as only PD control is used in these motions. The steady state error was removed in the full scale simulation by using a small integrator force in the roll and pitch controller, even though a steady state error of 1 degree in roll and pitch is assumed to be acceptable.

Chapter 7

Conclusion and Further Work

7.1 Conclusion

Based on the results from Chapter 6, the "Drop and Forget" installation method is considered feasible to preform. Analysis shows that the required control force to position the structure in the horizontal plane is within reasonable values, considering the size of the simulated installation object. Active control to stabilize the structure in roll and pitch is considered unfeasible, and in the best case very risky to preform. The complicated geometry of the structure, because of the heavy suction anchors located far from the centre of gravity makes it problematic to stabilize the structure in roll and pitch by using active control of thrusters. Methods where active control of thrusters are used to keep the structure stable, if it's stabilized after the splash zone by some other component can be considered.

The results in Chapter 6 shows that the tuning parameters used in the controller is very dependent on the current profile at the installation site. Short natural period in surge and sway has to be used if rapid changing current profiles are expected, to be sure the controller can handle change in ocean current as the structure submerges. Smarter guidance trajectories can instead be included, in order to save control energy. Individual control tuning to the expected current profile is beneficial.

The simplest, and most realistic installation skid presented in Chapter 4, is the installation skid with the attached buoyancy tank or buoyancy foam block on top of the structure. Hydrostatic stability is considered to be the safest method to stabilize the structure with few uncertainties related to the very critical motions, roll and pitch. A buoyancy tank will also reduce the drop velocity to a reasonable impact velocity at the sea floor. If hydrostatic pressure is making the use of a buoyancy tank/block on top of the installation object impossible, methods where the buoyancy tank/block is released after it has stabilized the structure can be explored. The results in Chapter 6 shows that it's possible to keep the structure stable at steady state using propellers, as long as the propellers don't have to bring it to steady state. Based on the presented installation skids in Chapter 4, the recommended skid to further explore is the following

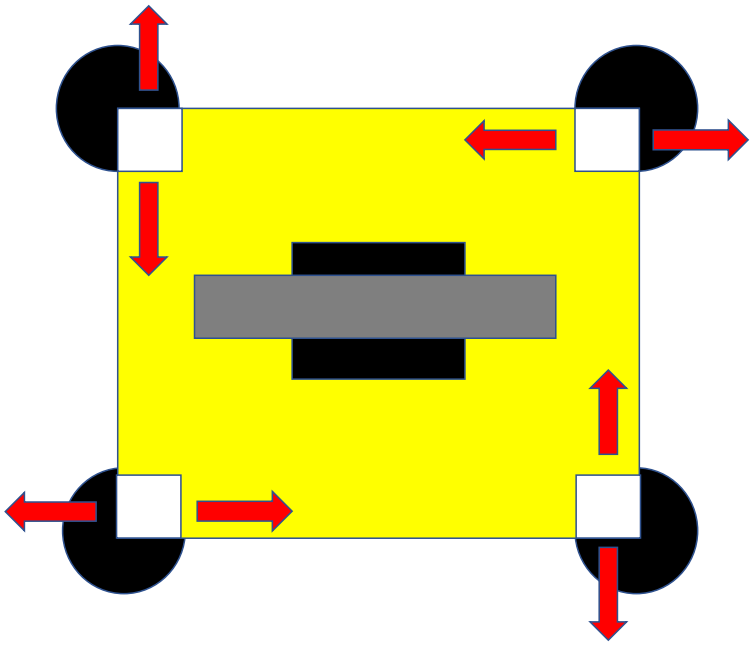

Figure 7.1: Best installation skid

If propellers or water jets, able to produce 150 - 200 kN of thrust are placed with position and thrust direction as illustrated in Figure 7.1, they will be able to produce the required control force and moment to control the surge, sway and yaw motion of the structure. The buoyancy tank will control roll, pitch and the drop velocity. Figure 7.1 illustrates a good start to further develop the "Drop and Forge" installation method, and modifications can be made if problems related to the proposed set up are discovered.

7.2 Further Work

Hydrodynamics

1. Hydrodynamic analysis related to the parachute, where methods to release and assemble the parachute in water is explored. CFD analysis of the fluid dynamics around a submerging structure with an attached parachute is also recommended, to assess the behaviour of a submerging structure with an attached parachute. The parachute is powerful tool if it can be used with low uncertainty.
2. Analysis of the dynamics of the structure with the attached installation skid in the splash zone.
3. More accurate calculations of the rigid body and hydrodynamic matrices using more advanced computer tools, or experimental testing.
4. Passive methods to reduce yaw motion can be explored.

Structure Analysis

1. Analysis of the impulse loading on structure upon impact at the sea floor to assess the maximum tolerated impact velocity. Impact with tilt angles in roll and pitch, or angular momentum in yaw is also something that should be analysed to asses the potential maximum damage if something goes wrong.

2. Analysis on how the structure with the attached installation skid handles the hydrodynamic forces in the splash zone.

Control System Improvements

1. Smarter control methods where the controller is able to handle different current profiles without manually changing the tuning parameters can be explored. Adaptive control, a suitable machine learning algorithm or a hybrid controller could be beneficially used.
2. Smarter use of the controller or guidance system to reduce the required control energy.

Bibliography

[1] [Online]. Available: http://akersolutions.com/what-we-do/products-and-services/subsea-production-systems/

[2] K. Larsen, "Lectrue notes in marine operations," tMR4225.

[3] [Online]. Available: https://medium.com/@eugenepribytkov/optimization-of-integrated-template-structures-for-arctic-subsea-production-systems-cce4f4d4d75a

[4] [Online]. Available: https://safety4sea.com/deepocean-contracted-for-statoils-snorre-expansion-project/

[5] [Online]. Available: https://chesssubseaengineering.com/wp-content/uploads/2015/04/Pic-2.jpg

[6] D. Myrhaug, "Compendium marine dynamics," 2014, tMR 4180.

[7] T. I. Fossen, *Handbook of Marine Craft Hydrodynamics and Motion Control*. Willey, 2011.

[8] O.M.Faltinsen, *Sea Loads On Ships and Offshore Structures*. Camebridge University Press, 1990.

[9] K. J.Eik, "Heidrun metocean design basisl," 1992.

[10] "Marine operations general," DNV GL, Tech. Rep., October 2011.

[11] "Modelling and analysis of marine operations," DNV GL, Tech. Rep., February 2014.

[12] A. Wang, Y. Yang, and S. Zhu, "Latest progress in deepwater installation technologies," June 2012.

[13] A. Wang, S. Zhu, and X. Zhu, "Pendulous installation method and its installation analysis for deepwater manifold in south china sea," 2013.

[14] Y. Cao, X. Hu, S. Zhang, and S. Xu, "Design of a novel installation device for a subsea production system," May 2016.

[15] R. Nelson, "Heave compensated landing system - a novel tool for subsea intervention," May 1997.

[16] A. Joensen and D. Paul, "A low tech, low risk system for the installation of large structures in deep water," *SPE 145461*, September 2011.

[17] K. A. Tofteng, "Efficient installation of subsea equipment in deep water," December 2017, project thesis.

[18] "Propulsion systems for optimal operations under all conditions," Rolls-Royce Commercial Marine, Tech. Rep.

[19] M. Ludvigsen, "Underwater engineering," August 2017, lecture Notes TMR4120.

[20] P.H.Milne, *Underwater Acoustic Positioning Systems*. Gulf Publishing Co., 1983.

[21] F. Dukan, "Rov motion control," Ph.D. dissertation, Norwegian University of Science and Technology, 2014.

[22] J. G. Bellingham, *Handbook of Ocean Engineering*. Springer, 2016.

[23] N. S. Bjørn Jalving, Karstein Vestgård, "Detailed seabed surveys with auv," march 2003.

[24] T. Fossen and T. Peres. Marine systems simulator (mss). http://www.marinecontrol.org.

[25] A. J. Sørensen, "Marine control systems," 2013.

[26] "Properties of new concept for subsea marine operations," SINTEF Ocean, Tech. Rep., December 2017.

[27] "Metocean data for brazilian water," Equinor internal document, Tech. Rep., 2018.

[28] [Online]. Available: https://www.grc.nasa.gov/www/k-12/VirtualAero/BottleRocket/airplane/rktvrecv.html

Appendix A

Rigid Body and Hydrodynamic Matrix Calculation

The simplified method used to find the 6x6 matrices describing the dynamics of the structure is shown here. In general, the method is to divide the structure into 5 parts, where the 5 parts is the main body and the 4 attached suction anchors. Each part is assumed to be a point mass where the translational forces are providing a moment about the total COG of the structure. The moment of each point mass about its own axis is neglected, including the moment of inertia of each pint mass about its own COG.

A.1 Structure

Structure and hydrodynamic information about the Johan Sverdrup ITS structure is taken from [26], and is shown in Table A.1 and A.2.

Table A.1: Johan Sverdrup ITS dimensions (ref: [26])

	Suction Anchor	Structure Body	Total
Mass [Kg]	$M_A = 25 * 10^3$	$M_S = 160 * 10^3$	$260 * 10^3$
Wet mass [Kg]	$21.75 * 10^3$	$139.2 * 10^3$	$226.2 * 10^3$
Height [m]	6.5	4.5	11
Length/Diameter [m]	6	18	24
Breadth/Diameter [m]	6	18	24
COG [m]	4	7.5	6.15

Table A.2: Translational hydrodynamic coefficients Johan Sverdrup ITS structure (ref: [26])

	Surge (i=1)	Sway (i=2)	Heave (i=3)
Added mass main structure A_{Sii} $[Kg]$	$217 * 10^3$	$217 * 10^3$	$181 * 10^3$
Added mass suction anchor A_{Aii} $[Kg]$	$300 * 10^3$	$300 * 10^3$	$274 * 10^3$
Linear damping main structure D^l_{Sii} $[N/(m/s)]$	0	0	0
Linear damping suction anchor D^l_{Aii} $[N/(m/s)]$	0	0	$71 * 10^3$
Quadratic damping main structure D^q_{Sii} $[N/(m/s)^2]$	$189 * 10^3$	$189 * 10^3$	$177 * 10^3$
Quadratic damping suction anchor D^q_{Aii} $[N/(m/s)^2]$	$16 * 10^3$	$16 * 10^3$	0

The horizontal and vertical plane of the Johan Sverdrup ITS structure is shown in Figure A.1 and A.2.

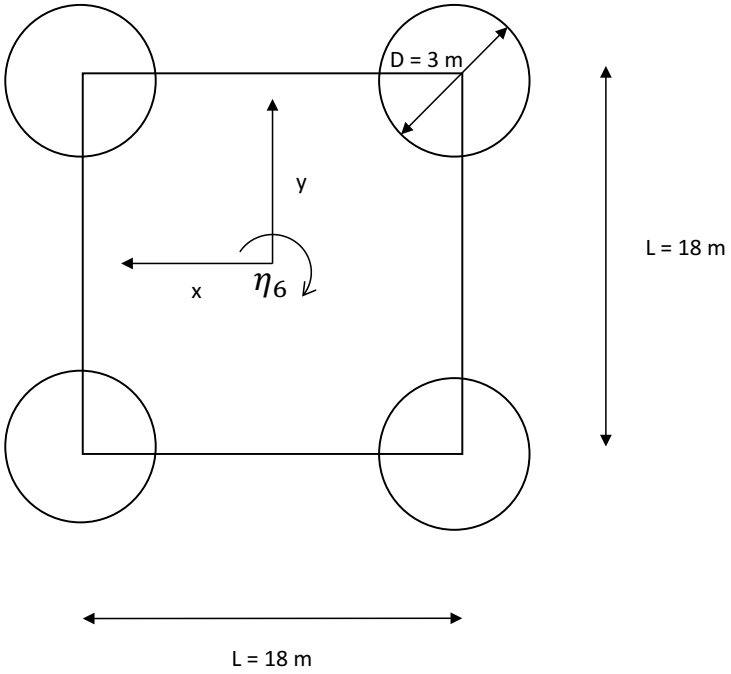

Figure A.1: Johan Sverdrup ITS structure in the horizontal plane

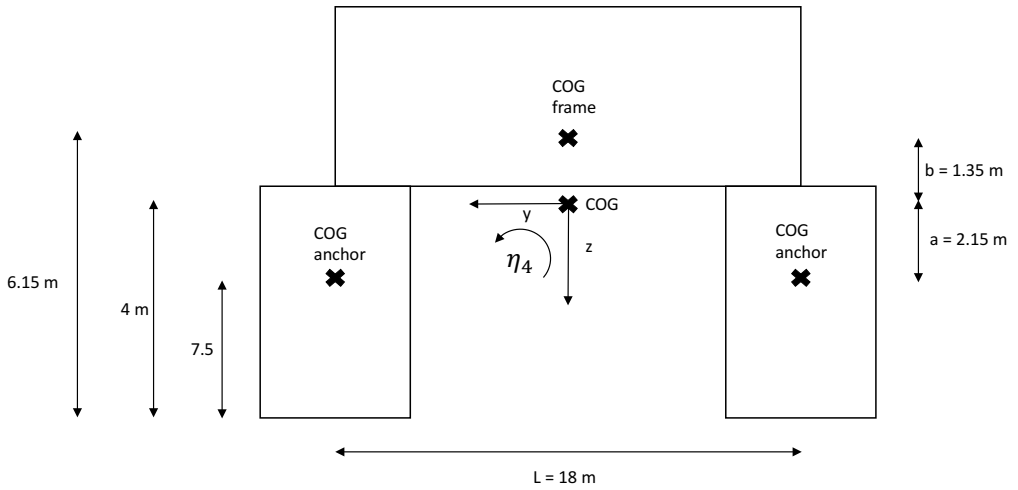

Figure A.2: Johan Sverdrup ITS structure in the vertical plane

The 6 degrees of freedom motion of the ITS structure is shown in Figure A.3.

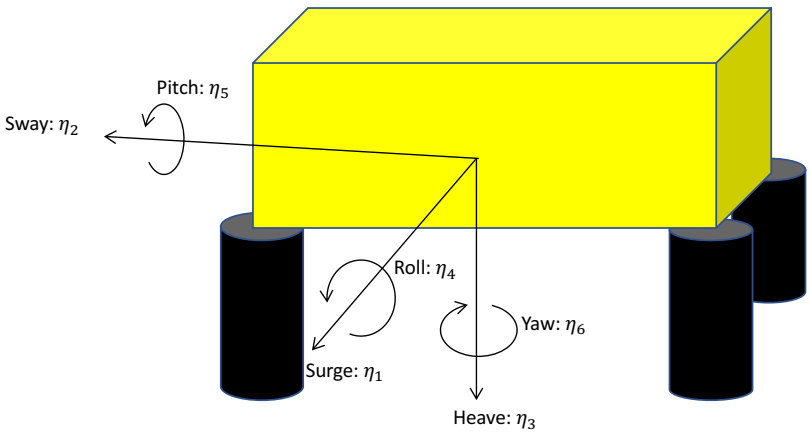

Figure A.3: 6 DOF motion of the Johan Sverdrup ITS structure

If the ITS structure is gaining velocity or acceleration in the 6 DOF described in Figure A.3, a point located at coordinate (x, y, z) on the ITS structure will gain velocity and acceleration in surge (1), sway (2) or heave (3) according to Equation A.1 and A.2.

$$\begin{aligned} \dot{s_1} &= (\dot{\eta_1} + z\dot{\eta_5} - y\dot{\eta_6}) \\ \dot{s_2} &= (\dot{\eta_2} - z\dot{\eta_4} + x\dot{\eta_6}) \\ \dot{s_3} &= (\dot{\eta_3} + y\dot{\eta_4} - x\dot{\eta_5}) \end{aligned} \tag{A.1}$$

$$\begin{aligned} \ddot{s_1} &= (\ddot{\eta_1} + z\ddot{\eta_5} - y\ddot{\eta_6}) \\ \ddot{s_2} &= (\ddot{\eta_2} - z\ddot{\eta_4} + x\ddot{\eta_6}) \\ \ddot{s_3} &= (\ddot{\eta_3} + y\ddot{\eta_4} - x\ddot{\eta_5}) \end{aligned} \tag{A.2}$$

Using the velocity and acceleration of a point on the ITS structure together with the translational rigid body and hydrodynamic coefficients, the 6 DOF matrices describing the motion of the ITS structure is calculated as shown in A.2, A.3 and A.4.

A.2 XY-plane

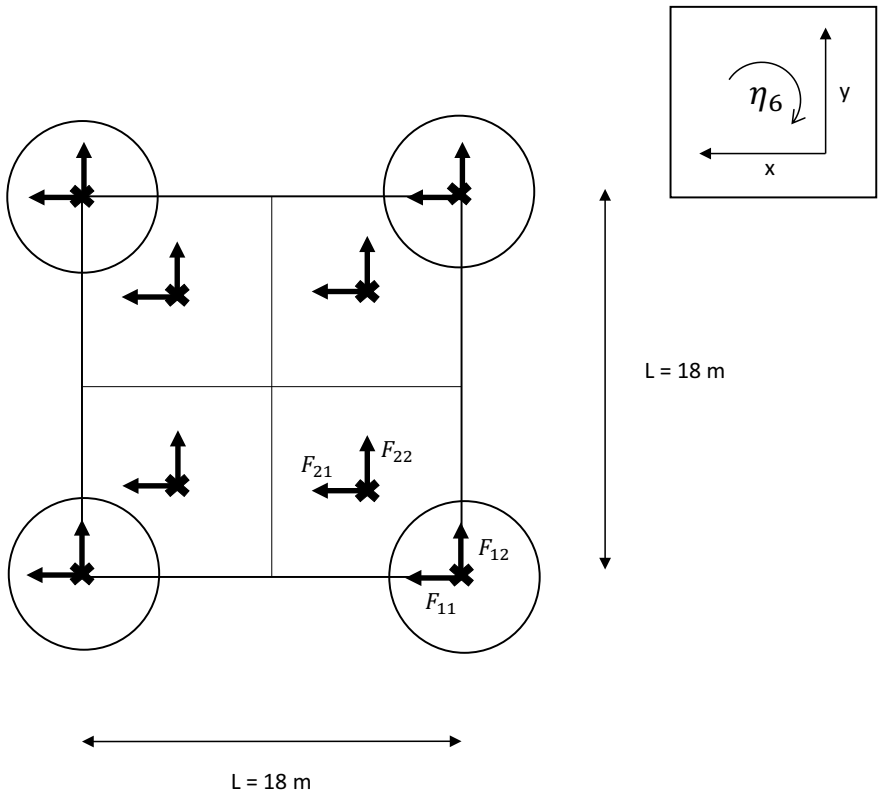

Figure A.4: Forces in the xy plane

Mass Rigid Body

$$
\begin{aligned}
F_{11} &= M_A * \ddot{s_1}|_{y=-\frac{L}{2}} = M_A * \frac{L}{2}\ddot{\eta_6} \\
F_{12} &= M_A * \ddot{s_2}|_{x=-\frac{L}{2}} = -M_A * \frac{L}{2}\ddot{\eta_6} \\
F_{21} &= M_S * \ddot{s_1}|_{y=-\frac{L}{4}} = M_S * \frac{L}{4}\ddot{\eta_6} \\
F_{22} &= M_S * \ddot{s_2}|_{x=-\frac{L}{4}} = -M_S * \frac{L}{4}\ddot{\eta_6}
\end{aligned}
$$

$$
\begin{aligned}
M_{COG} &= 4\frac{L}{2}F_{11} - 4\frac{L}{2}F_{12} + 4\frac{L}{4}F_{21} - 4\frac{L}{4}F_{22} \\
&= 2L^2 M_A\ddot{\eta_6} + \frac{L^2}{2}M_S\ddot{\eta_6} \\
&= I_{66}\ddot{\eta_6}
\end{aligned}
\tag{A.3}
$$

Added Mass

$$
\begin{aligned}
F_{11} &= A_{A11} * \ddot{s_1}|_{y=-\frac{L}{2}} = A_{A11} * \frac{L}{2}\ddot{\eta_6} \\
F_{12} &= A_{A22} * \ddot{s_2}|_{x=-\frac{L}{2}} = -A_{A22} * \frac{L}{2}\ddot{\eta_6} \\
F_{21} &= A_{S11} * \ddot{s_1}|_{y=-\frac{L}{4}} = A_{S11} * \frac{L}{4}\ddot{\eta_6} \\
F_{22} &= A_{S22} * \ddot{s_2}|_{x=-\frac{L}{4}} = -A_{S22} * \frac{L}{4}\ddot{\eta_6}
\end{aligned}
$$

$$
\begin{aligned}
M_{COG} &= 4\frac{L}{2}F_{11} - 4\frac{L}{2}F_{12} + 4\frac{L}{4}F_{21} - 4\frac{L}{4}F_{22} \\
&= L^2(A_{A11} + A_{A22})\ddot{\eta_6} + \frac{L^2}{4}(A_{S11} + A_{S22})\ddot{\eta_6} \\
&= A_{66}\ddot{\eta_6}
\end{aligned}
\tag{A.4}
$$

Linear Damping

$$
\begin{aligned}
F_{11} &= D^l_{A11} * \dot{s_1}|_{y=-\frac{L}{2}} = D^l_{A11} * \frac{L}{2}\dot{\eta_6} \\
F_{12} &= D^l_{A22} * \dot{s_2}|_{x=-\frac{L}{2}} = -D^l_{A22} * \frac{L}{2}\dot{\eta_6} \\
F_{21} &= D^l_{S11} * \dot{s_1}|_{y=-\frac{L}{4}} = D^l_{S11} * \frac{L}{4}\dot{\eta_6} \\
F_{22} &= D^l_{S22} * \dot{s_2}|_{x=-\frac{L}{4}} = -D^l_{S22} * \frac{L}{4}\dot{\eta_6}
\end{aligned}
$$

$$
\begin{aligned}
M_{COG} &= 4\frac{L}{2}F_{11} - 4\frac{L}{2}F_{12} + 4\frac{L}{4}F_{21} - 4\frac{L}{4}F_{22} \\
&= L^2(D^l_{A11} + D^l_{A22})\dot{\eta_6} + \frac{L^2}{4}(D^l_{S11} + D^l_{S22})\dot{\eta_6} \\
&= D^l_{66}\dot{\eta_6}
\end{aligned}
\tag{A.5}
$$

Quadratic Damping

$$
\begin{aligned}
F_{11} &= D^q_{A11} * (\dot{s_1}|_{y=-\frac{L}{2}})|\dot{s_1}|_{y=-\frac{L}{2}}| = D^q_{A11} * \frac{L^2}{4}\dot{\eta_6}|\dot{\eta_6}| \\
F_{12} &= D^q_{A22} * (\dot{s_2}|_{x=-\frac{L}{2}})|\dot{s_2}|_{x=-\frac{L}{2}}| = -D^q_{A22} * \frac{L^2}{4}\dot{\eta_6}|\dot{\eta_6}| \\
F_{21} &= D^q_{S11} * (\dot{s_1}|_{y=-\frac{L}{4}})|\dot{s_1}|_{y=-\frac{L}{4}}| = D^q_{S11} * \frac{L^2}{16}\dot{\eta_6}|\dot{\eta_6}| \\
F_{22} &= D^q_{S22} * (\dot{s_2}|_{x=-\frac{L}{4}})|\dot{s_2}|_{x=-\frac{L}{4}}| = -D^q_{S22} * \frac{L^2}{16}\dot{\eta_6}|\dot{\eta_6}|
\end{aligned}
$$

$$
\begin{aligned}
M_{COG} &= 4\frac{L}{2}F_{11} - 4\frac{L}{2}F_{12} + 4\frac{L}{4}F_{21} - 4\frac{L}{4}F_{22} \\
&= \frac{L^3}{2}(D^q_{A11} + D^q_{A22})\dot{\eta_6}|\dot{\eta_6}| + \frac{L^3}{16}(D^q_{S11} + D^q_{S22})\dot{\eta_6}|\dot{\eta_6}| \\
&= D^q_{66}\dot{\eta_6}|\dot{\eta_6}|
\end{aligned}
\tag{A.6}
$$

A.3 YZ-plane

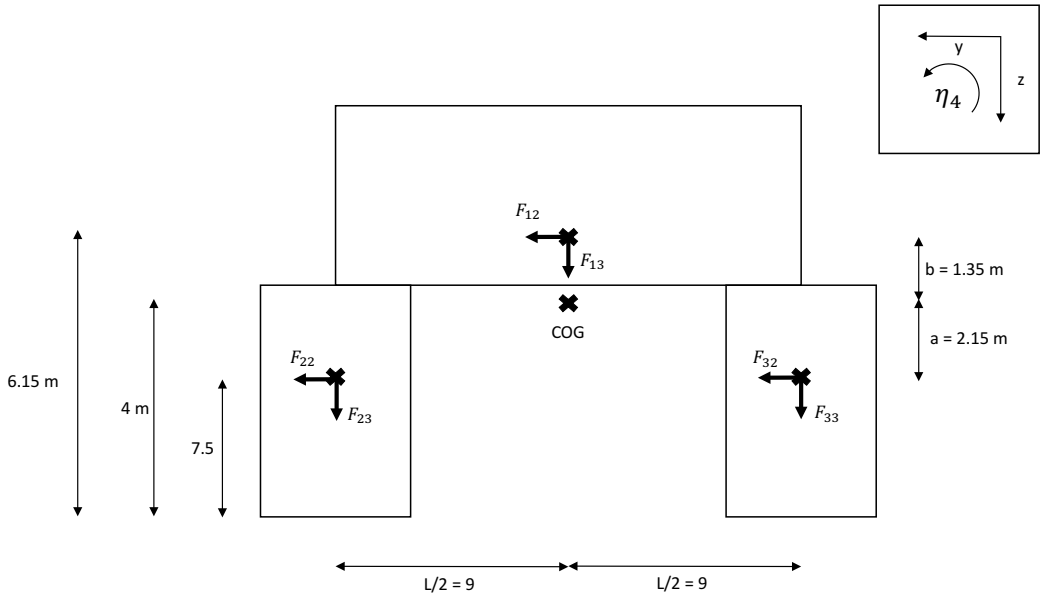

Figure A.5: Forces in the yz plane

Mass Rigid Body

As the origin is placed in the centre of gravity of the structure, the structure is assumed to have uncoupled mass inertia forces.

$$
\begin{aligned}
F_{12} &= M_S * \ddot{s_2}|_{z=-b} = M_S * b\ddot{\eta_4} \\
F_{13} &= M_S * \ddot{s_3}|_{y=0} = 0 \\
F_{22} &= M_A * \ddot{s_2}|_{z=a} = M_A * -a\ddot{\eta_4} \\
F_{23} &= M_A * \ddot{s_3}|_{y=\frac{L}{2}} = M_A * \frac{L}{2}\ddot{\eta_4} \\
F_{32} &= M_A * \ddot{s_2}|_{z=a} = M_A * -a\ddot{\eta_4} \\
F_{33} &= M_A * \ddot{s_3}|_{y=-\frac{L}{2}} = M_A * -\frac{L}{2}\ddot{\eta_4}
\end{aligned}
$$

$$
\begin{aligned}
M_{COG} &= bF_{12} - 2aF_{22} - 2aF_{32} + 2\frac{L}{2}F_{23} - 2\frac{L}{2}F_{33} \\
&= b^2 M_S\ddot{\eta_4} + 4a^2 M_A\ddot{\eta_4} + L^2 M_A\ddot{\eta_4} \\
&= I_{44}\ddot{\eta_4}
\end{aligned}
\tag{A.7}
$$

Added Mass

$$
\begin{aligned}
F_{12} &= A_{S22} * \ddot{s_2}|_{z=-b} = A_{S22} * b\ddot{\eta_4} \\
F_{13} &= A_{S33} * \ddot{s_3}|_{y=0} = 0 \\
F_{22} &= A_{A22} * \ddot{s_2}|_{z=a} = A_{A22} * -a\ddot{\eta_4} \\
F_{23} &= A_{A33} * \ddot{s_3}|_{y=\frac{L}{2}} = A_{A33} * \frac{L}{2}\ddot{\eta_4} \\
F_{32} &= A_{A22} * \ddot{s_2}|_{z=a} = A_{A22} * -a\ddot{\eta_4} \\
F_{33} &= A_{A33} * \ddot{s_3}|_{y=-\frac{L}{2}} = A_{A33} * -\frac{L}{2}\ddot{\eta_4}
\end{aligned}
$$

$$
\begin{aligned}
F_{tot2} &= F_{12} + 2F_{22} + 2F_{32} = bA_{S22}\ddot{\eta_4} - 4aA_{A22}\ddot{\eta_4} = A_{24}\ddot{\eta_4} \\
F_{tot3} &= F_{13} + 2F_{23} + 2F_{33} = 2A_{A33}\frac{L}{2}\ddot{\eta_4} - 2A_{A33}\frac{L}{2}\ddot{\eta_4} = 0
\end{aligned}
\tag{A.8}
$$

$$
\begin{aligned}
M_{COG} &= bF_{12} - 2aF_{22} - 2aF_{32} + 2\frac{L}{2}F_{23} - 2\frac{L}{2}F_{33} \\
&= b^2A_{S22}\ddot{\eta_4} + 4a^2A_{A22}\ddot{\eta_4} + L^2A_{A33}\ddot{\eta_4} \\
&= A_{44}\ddot{\eta_4}
\end{aligned}
\tag{A.9}
$$

Linear Damping

$$
\begin{aligned}
F_{12} &= D^l_{S22} * \dot{s_2}|_{z=-b} = D^l_{S22} * b\dot{\eta_4} \\
F_{13} &= D^l_{S33} * \dot{s_3}|_{y=0} = 0 \\
F_{22} &= D^l_{A22} * \dot{s_2}|_{z=a} = D^l_{A22} * -a\dot{\eta_4} \\
F_{23} &= D^l_{A33} * \dot{s_3}|_{y=\frac{L}{2}} = D^l_{A33} * \frac{L}{2}\dot{\eta_4} \\
F_{32} &= D^l_{A22} * \dot{s_2}|_{z=a} = D^l_{A22} * -a\dot{\eta_4} \\
F_{33} &= D^l_{A33} * \dot{s_3}|_{y=-\frac{L}{2}} = D^l_{A33} * -\frac{L}{2}\dot{\eta_4}
\end{aligned}
$$

$$
\begin{aligned}
F_{tot2} &= F_{12} + 2F_{22} + 2F_{32} = bD^l_{S22}\dot{\eta_4} - 4aD^l_{A22}\dot{\eta_4} = D^l_{24}\dot{\eta_4} \\
F_{tot3} &= F_{13} + 2F_{23} + 2F_{33} = 2D^l_{A33}\frac{L}{2}\dot{\eta_4} - 2D^l_{A33}\frac{L}{2}\dot{\eta_4} = 0
\end{aligned}
\tag{A.10}
$$

$$
\begin{aligned}
M_{COG} &= bF_{12} - 2aF_{22} - 2aF_{32} + 2\frac{L}{2}F_{23} - 2\frac{L}{2}F_{33} \\
&= b^2D^l_{S22}\dot{\eta_4} + 4a^2D^l_{A22}\dot{\eta_4} + L^2D^l_{A33}\dot{\eta_4} \\
&= D^l_{44}\dot{\eta_4}
\end{aligned}
\tag{A.11}
$$

Quadratic Damping

$$
\begin{aligned}
F_{12} &= D^q_{S22} * (\dot{s_2}|_{z=-b})|\dot{s_2}|_{z=-b}| = D^q_{S22} * b^2\dot{\eta_4}|\dot{\eta_4}| \\
F_{13} &= D^q_{S33} * (\dot{s_3}|_{y=0})|\dot{s_3}|_{y=0}| = 0 \\
F_{22} &= D^q_{A22} * (\dot{s_2}|_{z=a})|\dot{s_2}|_{z=a}| = D^q_{A22} * -a^2\dot{\eta_4}|\dot{\eta_4}| \\
F_{23} &= D^q_{A33} * (\dot{s_3}|_{y=\frac{L}{2}})|\dot{s_3}|_{y=\frac{L}{2}}| = D^q_{A33} * \frac{L^2}{4}\dot{\eta_4}|\dot{\eta_4}| \\
F_{32} &= D^q_{A22} * (\dot{s_2}|_{z=a})|\dot{s_2}|_{z=a}| = D^q_{A22} * -a^2\dot{\eta_4}|\dot{\eta_4}| \\
F_{33} &= D^q_{A33} * (\dot{s_3}|_{y=-\frac{L}{2}})|\dot{s_3}|_{y=-\frac{L}{2}}| = D^q_{A33} * -\frac{L^2}{4}\dot{\eta_4}|\dot{\eta_4}|
\end{aligned}
$$

$$
\begin{aligned}
F_{tot2} &= F_{12} + 2F_{22} + 2F_{32} = b^2 D^q_{S22}\dot{\eta_4}|\dot{\eta_4}| - 4a^2 D^q_{A22}\dot{\eta_4}|\dot{\eta_4}| = D^q_{24}\dot{\eta_4}|\dot{\eta_4}| \\
F_{tot3} &= F_{13} + 2F_{23} + 2F_{33} = 2D^q_{A33}\frac{L^2}{4}\dot{\eta_4}|\dot{\eta_4}| - 2D^q_{A33}\frac{L^2}{4}\dot{\eta_4}|\dot{\eta_4}| = 0
\end{aligned}
\tag{A.12}
$$

$$
\begin{aligned}
M_{COG} &= bF_{12} - 2aF_{22} - 2aF_{32} + 2\frac{L}{2}F_{23} - 2\frac{L}{2}F_{33} \\
&= b^3 D^l_{S22}\dot{\eta_4}|\dot{\eta_4}| + 4a^3 D^l_{A22}\dot{\eta_4}|\dot{\eta_4}| + \frac{L^3}{2}D^l_{A33}\dot{\eta_4}|\dot{\eta_4}| \\
&= D^q_{44}\dot{\eta_4}|\dot{\eta_4}|
\end{aligned}
\tag{A.13}
$$

A.4 XZ-plane

The structure is symmetrical in the horizontal plane, so the xz-plane is identical to the yz-plane. Hence, the rotational moment in pitch is identical to the roll moment. To find the coupled hydrodynamic coefficients in pitch and surge, the equation for the coupled hydrodynamic constants in roll and sway are used with opposite sign.

A.5 Resulting Equations for Rotational Rigid Body and Hydrodynamic Coefficients

Rigid Body

$$I_{44} = b^2 M_S + 4a^2 M_A + L^2 M_A$$

$$I_{55} = b^2 M_S + 4a^2 M_A + L^2 M_A$$

$$I_{66} = 2L^2 M_A + \frac{L^2}{2} M_S$$

Added Mass

$$A_{42} = A_{24} = bA_{S22} - 4aA_{A22}$$

$$A_{44} = b^2 A_{S22} + 4a^2 A_{A22} + L^2 A_{A33}$$

$$A_{51} = A_{15} = -bA_{S11} + 4aA_{A11}$$

$$A_{55} = b^2 A_{S11} + 4a^2 A_{A11} + L^2 A_{A33}$$

$$A_{66} = L^2(A_{A11} + A_{A22}) + \frac{L^2}{4}(A_{S11} + A_{S22})$$

Linear damping

$$D^l_{42} = D^l_{24} = bD^l_{S22} - 4aD^l_{A22}$$

$$D^l_{44} = b^2 D^l_{S22} + 4a^2 D^l_{A22} + L^2 D^l_{A33}$$

$$D^l_{51} = D^l_{15} = -bD^l_{S11} + 4aD^l_{A11}$$

$$D^l_{55} = b^2 D^l_{S11} + 4a^2 D^l_{A11} + L^2 D^l_{A33}$$

$$D^l_{66} = L^2(D^l_{A11} + D^l_{A22}) + \frac{L^2}{4}(D^l_{S11} + D^l_{S22})$$

Quadratic damping

$$D^q_{42} = D^q_{24} = b^2 D^q_{S22} - 4a^2 D^q_{A22}$$

$$D^q_{44} = b^3 D^q_{S22} + 4a^3 D^q_{A22} + \frac{L^3}{2} D^q_{A33}$$

$$D^q_{51} = D^q_{15} = -b^2 D^q_{S11} + 4a^2 D^q_{A11}$$

$$D^q_{55} = b^3 D^q_{S11} + 4a^3 D^q_{A11} + \frac{L^3}{2} D^q_{A33}$$

$$D^q_{66} = \frac{L^3}{2}(D^q_{A11} + D^q_{A22}) + \frac{L^3}{16}(D^q_{S11} + D^q_{S22})$$

A.6 Resulting Rigid Body and Hydrodynamic Matrices

Mass Rigid Body

$$\boldsymbol{M_{RB}} = \begin{bmatrix} 260000 & 0 & 0 & 0 & 0 & 0 \\ 0 & 260000 & 0 & 0 & 0 & 0 \\ 0 & 0 & 260000 & 0 & 0 & 0 \\ 0 & 0 & 0 & 8853850 & 0 & 0 \\ 0 & 0 & 0 & 0 & 8853850 & 0 \\ 0 & 0 & 0 & 0 & 0 & 42120000 \end{bmatrix} \tag{A.14}$$

Added Mass

$$\boldsymbol{M_A} = \begin{bmatrix} 1417000 & 0 & 0 & 0 & 2287050 & 0 \\ 0 & 1417000 & 0 & -2287050 & 0 & 0 \\ 0 & 0 & 1277000 & 0 & 0 & 0 \\ 0 & -2287050 & 0 & 94718483 & 0 & 0 \\ 2287050 & 0 & 0 & 0 & 94718483 & 0 \\ 0 & 0 & 0 & 0 & 0 & 229554000 \end{bmatrix} \tag{A.15}$$

Linear Damping

$$\boldsymbol{D_l} = \begin{bmatrix} 0 & 0 & 0 & 0 & 0 & 0 \\ 0 & 0 & 0 & 0 & 0 & 0 \\ 0 & 0 & 284000 & 0 & 0 & 0 \\ 0 & 0 & 0 & 23004000 & 0 & 0 \\ 0 & 0 & 0 & 0 & 23004000 & 0 \\ 0 & 0 & 0 & 0 & 0 & 0 \end{bmatrix} \tag{A.16}$$

Quadratic Damping

$$\boldsymbol{D_q} = \begin{bmatrix} 253000 & 0 & 0 & 0 & -48613 & 0 \\ 0 & 253000 & 0 & 48613 & 0 & 0 \\ 0 & 0 & 177000 & 0 & 0 & 0 \\ 0 & 48613 & 0 & 1101067 & 0 & 0 \\ -48613 & 0 & 0 & 0 & 1101067 & 0 \\ 0 & 0 & 0 & 0 & 0 & 231093000 \end{bmatrix} \tag{A.17}$$

Appendix B

Case Simulation Plots

B.1 Drop with Unlimited Control Force

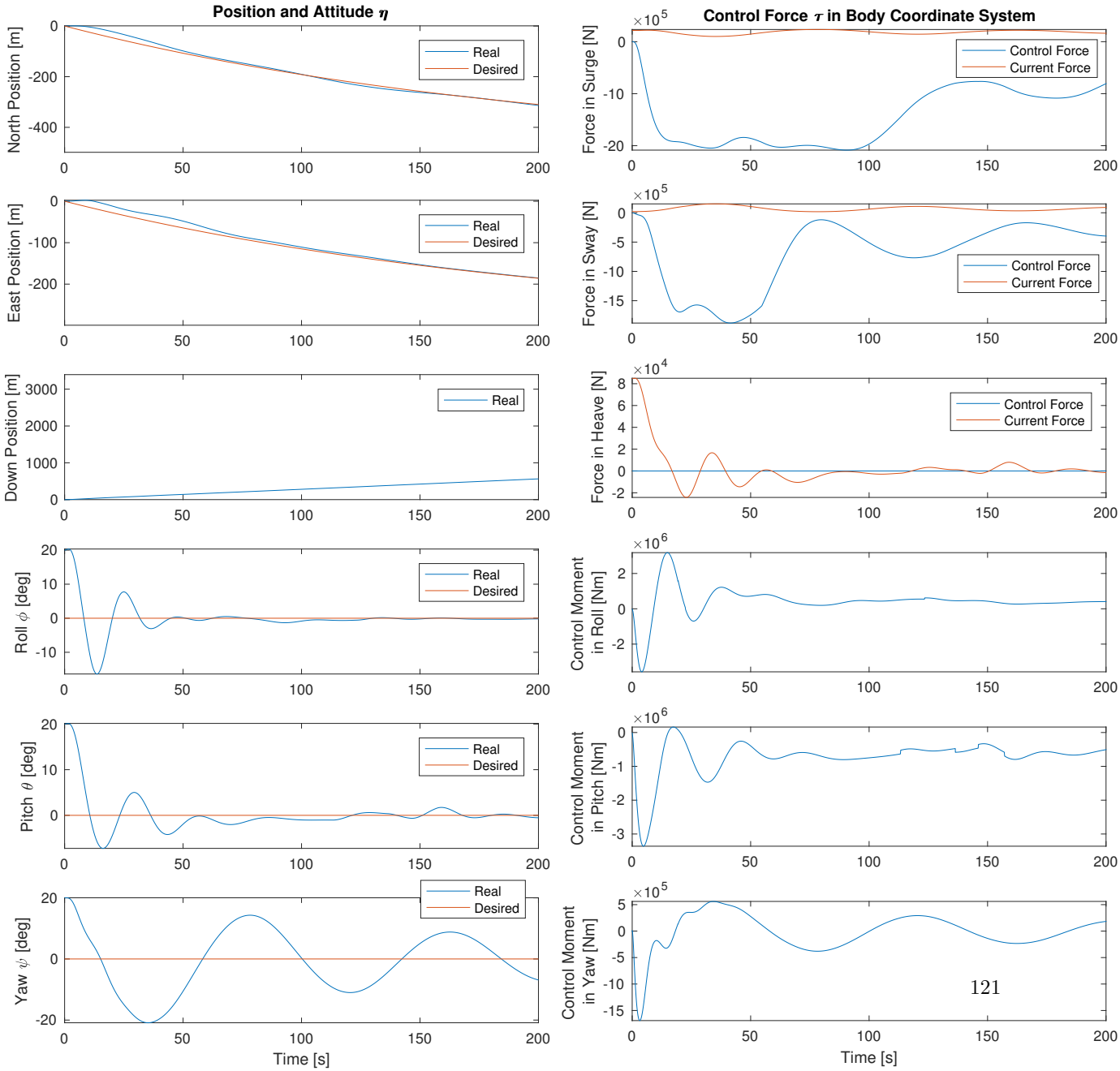

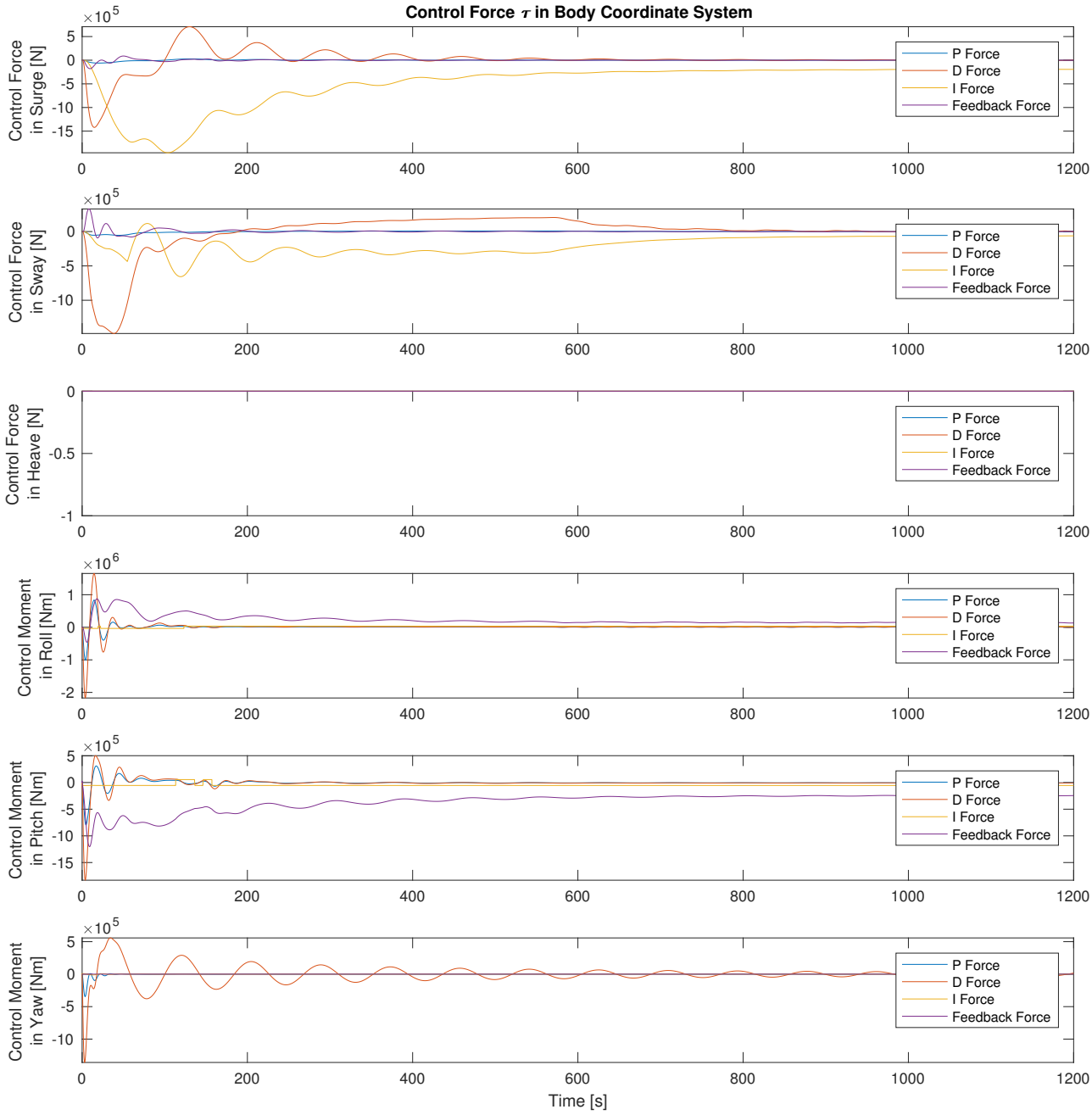

Figure B.2: Advanced control force plot unlimited control force

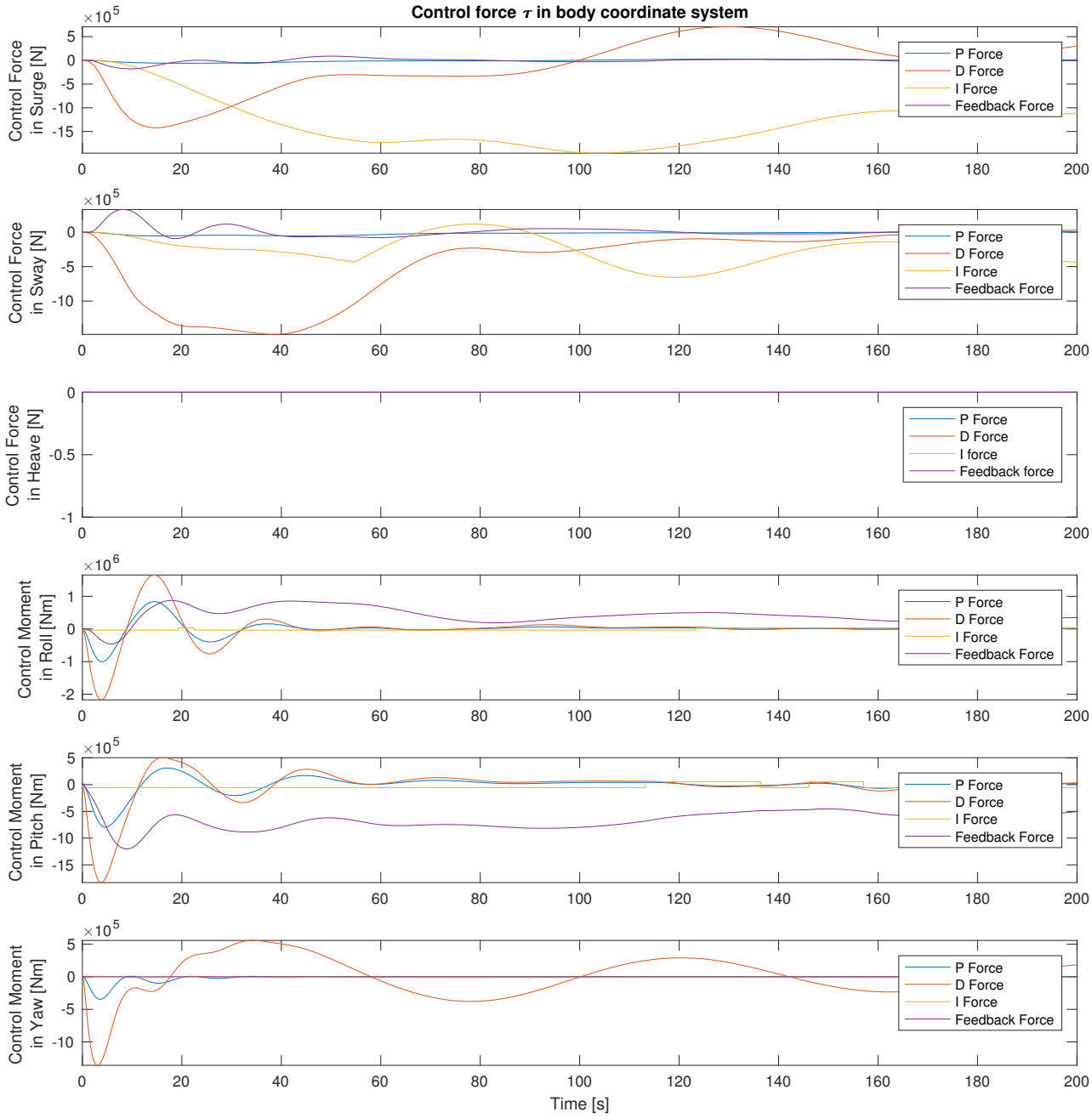

Figure B.3: Transient advanced control force plot unlimited control force

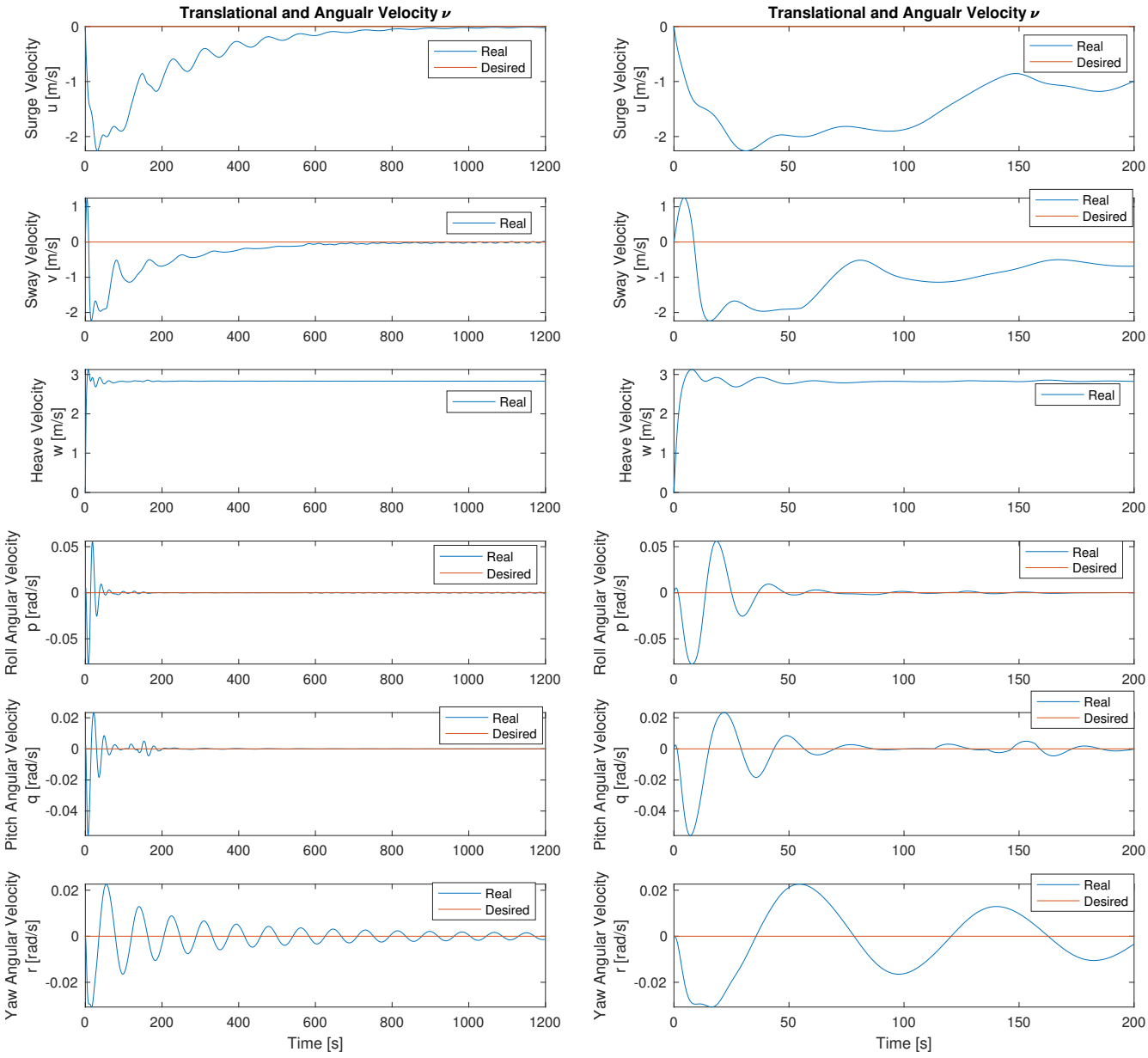

Figure B.4: Velocity plot unlimited control force

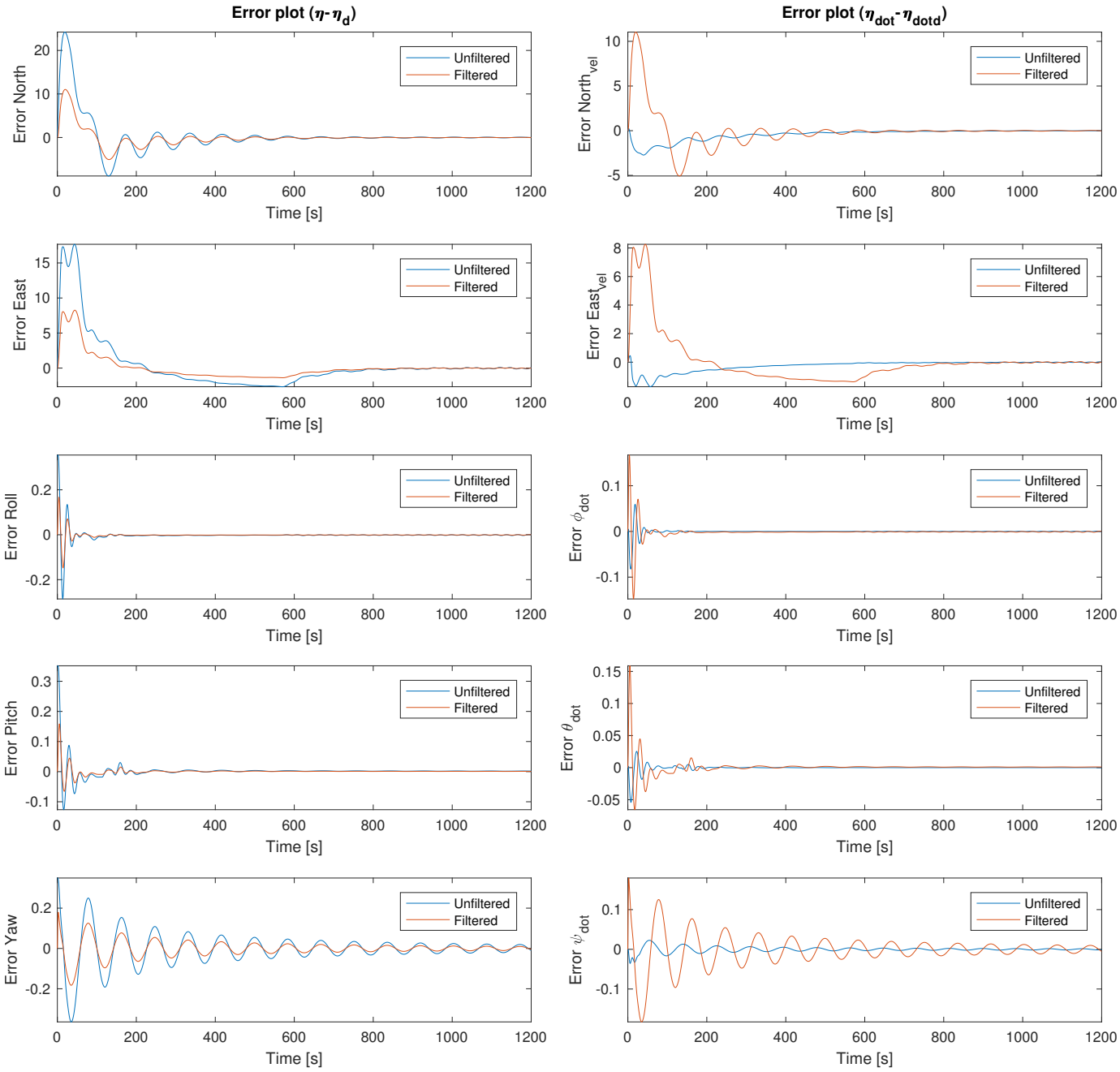

Figure B.5: Error plot unlimited control force

B.2 Drop with Saturated Control Force

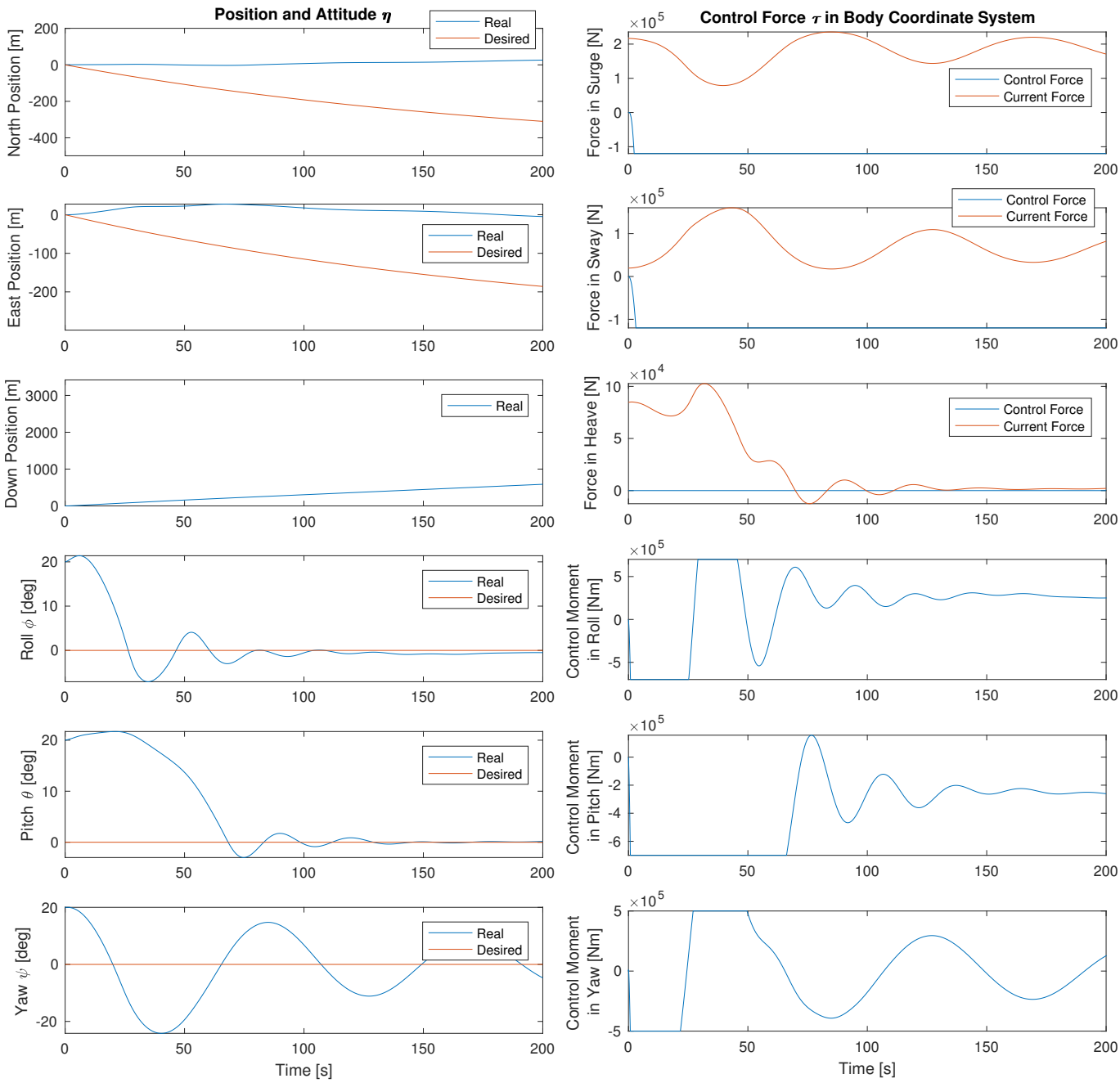

Figure B.6: Transient position and control force saturated control force

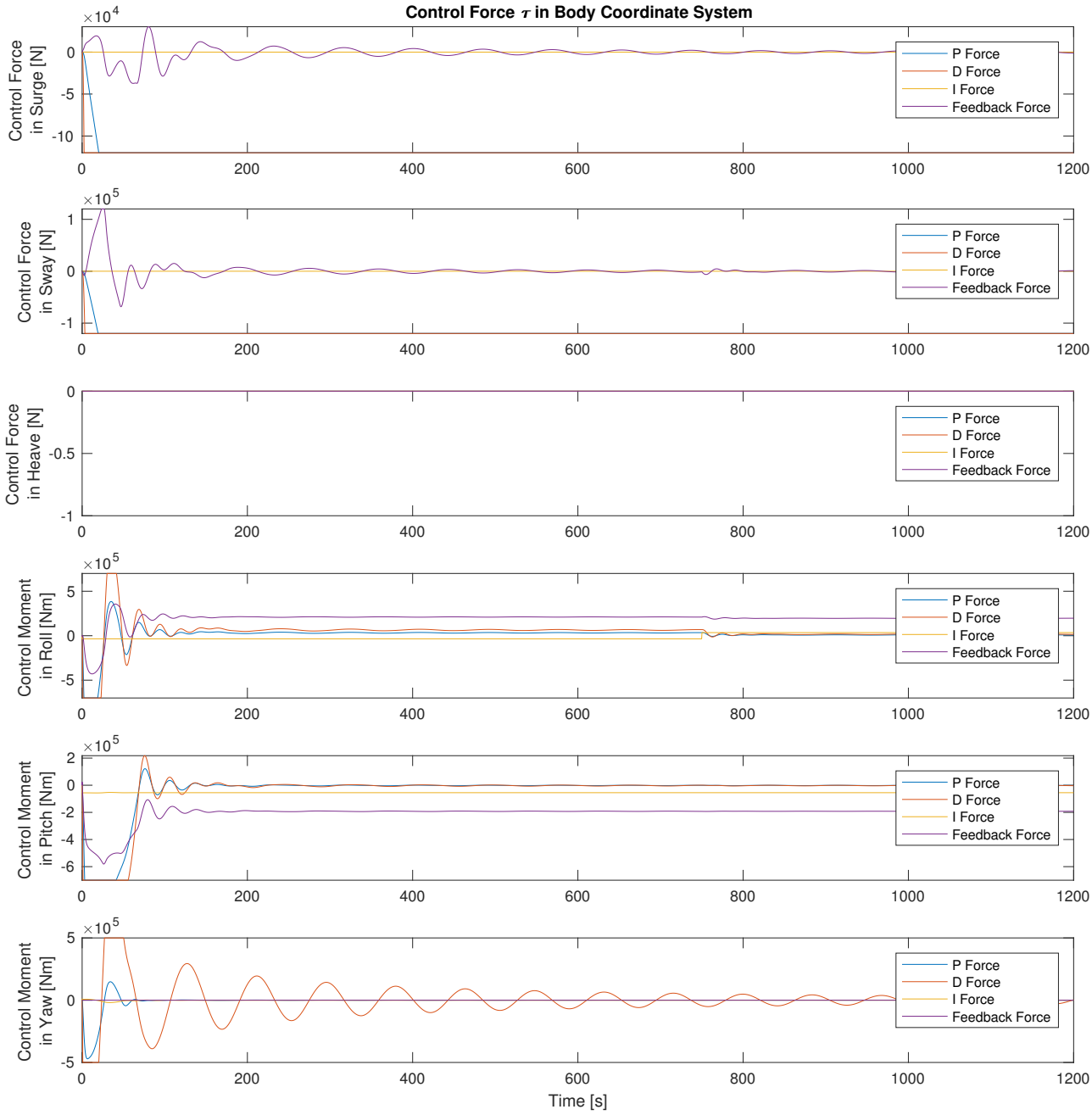

Figure B.7: Advanced control force plot saturated control force

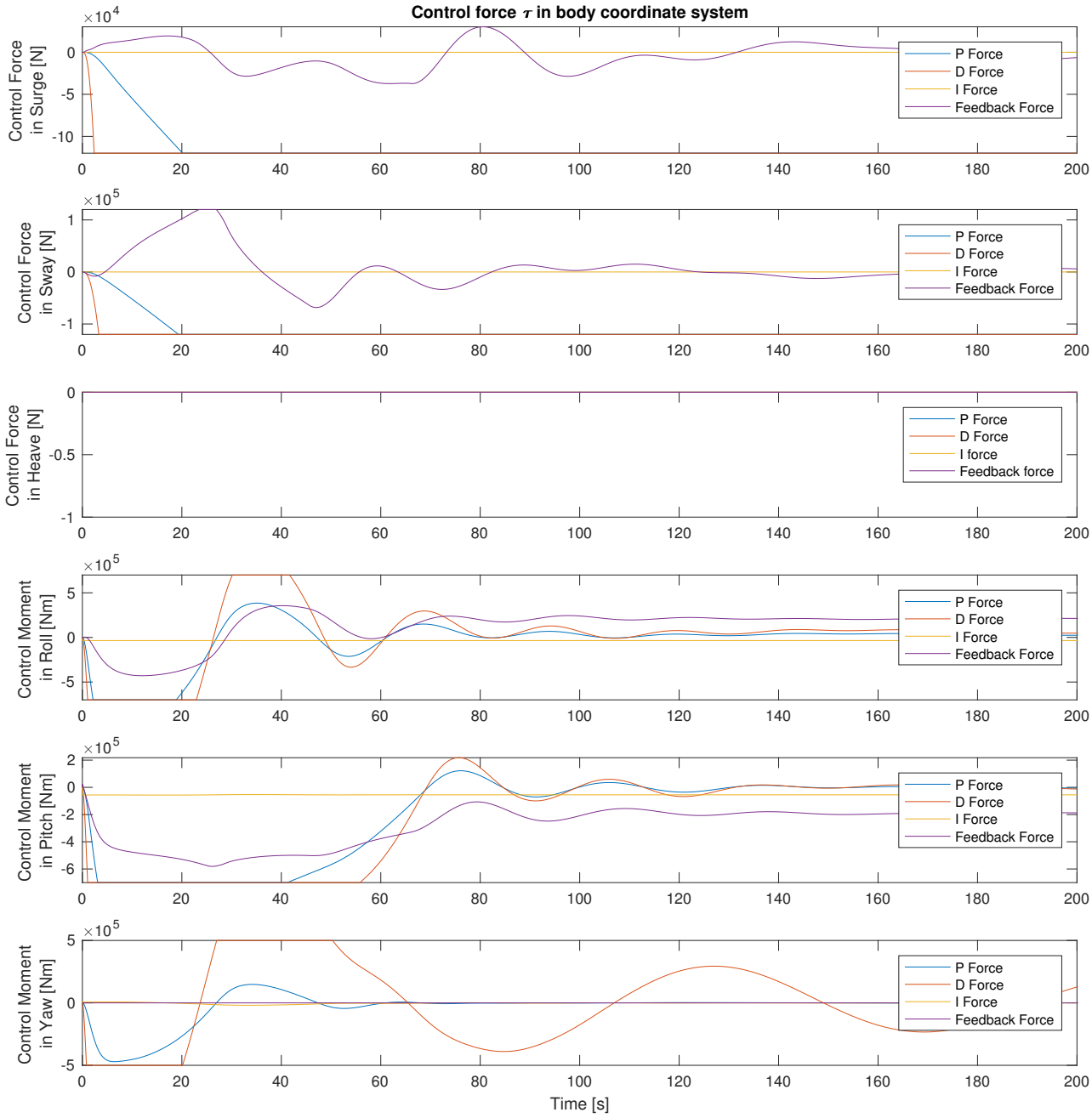

Figure B.8: Transient advanced control force plot saturated control force

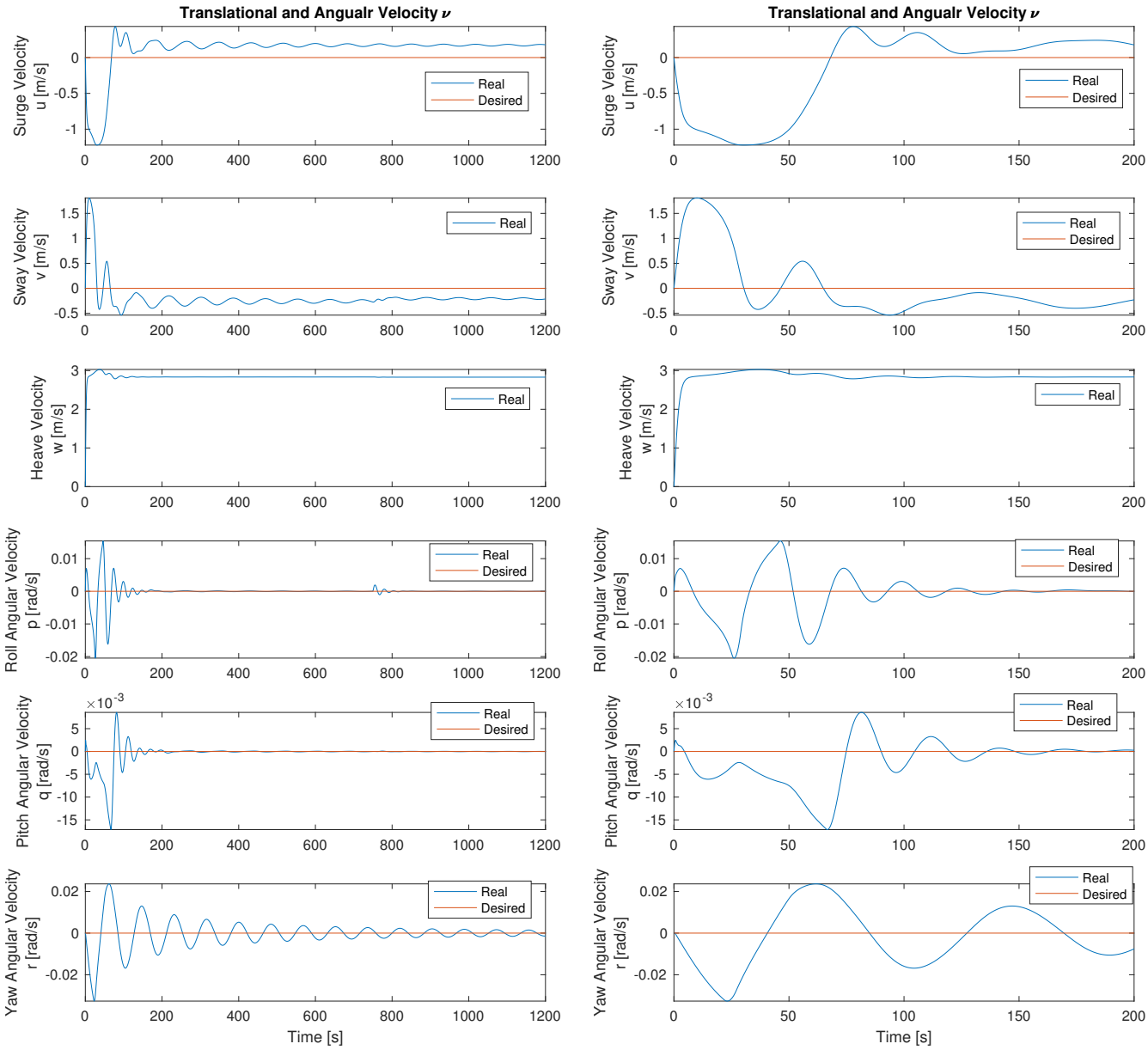

Figure B.9: Velocity plot saturated control force

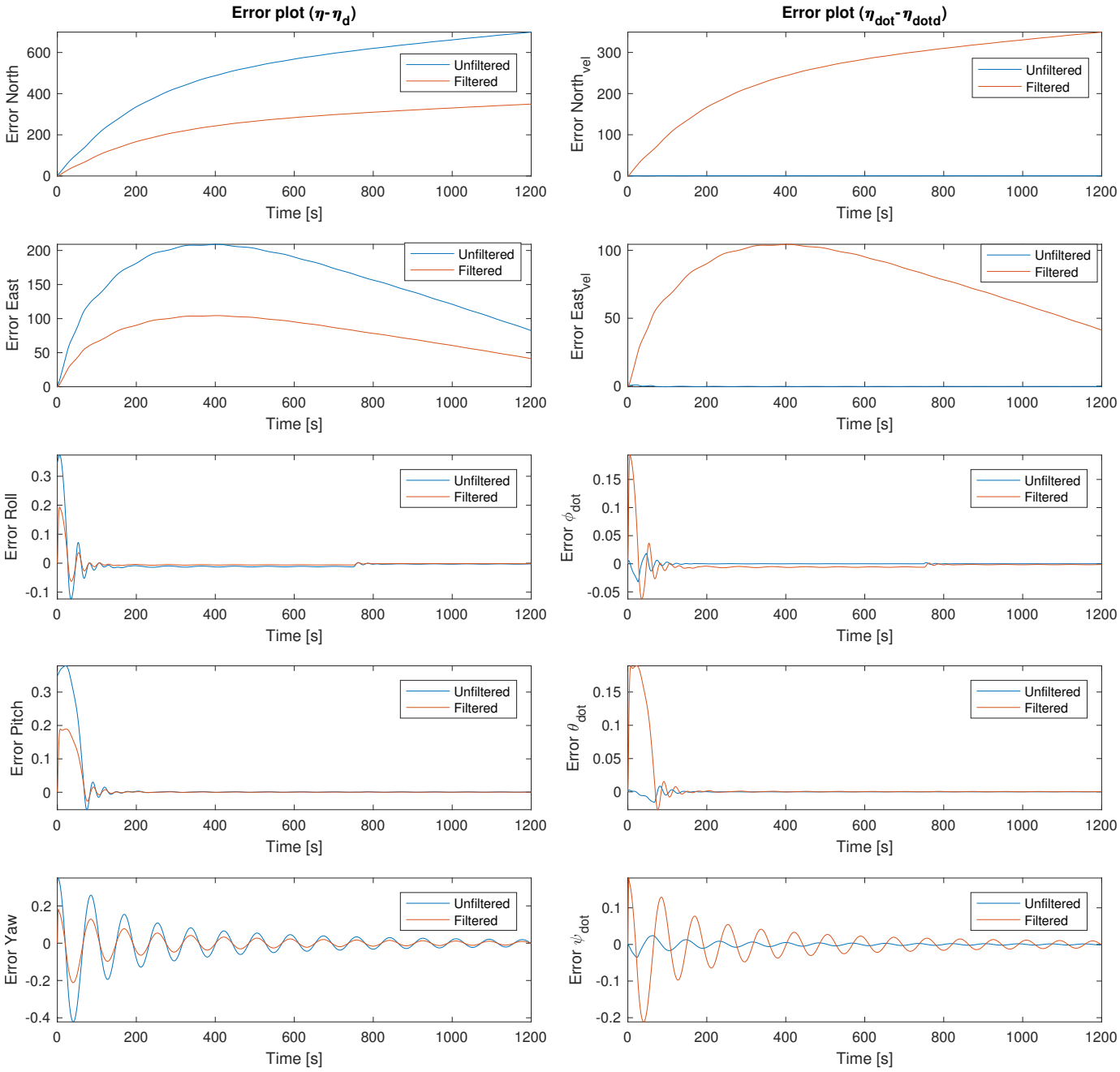

Figure B.10: Error plot saturated control force

B.3 Drop in Brazil Current Profile

Seabed is at 2000m water depth

Sample distribution of non-exceedance (%) of current speed

Current speed < cm/s	Surface to 30 m	258 m	450 m	876 m	1578 m	5 m above seabed
< 5	1.32	5.49	10.21	27.75	44.60	32.34
< 10	5.85	21.11	35.82	74.20	87.06	76.83
< 15	13.09	41.11	60.25	93.38	98.21	94.91
< 20	22.40	59.35	78.86	98.98	99.69	99.04
< 25	33.11	74.72	90.40	99.92	99.94	99.87
< 30	44.20	85.34	96.68	99.97	100.00	99.99
< 35	54.79	92.58	99.00	100.00		100.00
< 40	64.54	96.73	99.68			
< 45	72.60	98.68	99.87			
< 50	79.38	99.45	99.95			
< 55	84.96	99.73	99.99			
< 60	89.10	99.87	100.00			
< 65	92.30	99.94				
< 70	94.75	99.95				
< 75	96.27	99.97				
< 80	97.26	99.99				
< 85	97.97	100.00				
< 90	98.53					
< 95	98.95					
< 100	99.30					
< 110	99.70					
< 120	99.84					
< 130	99.96					
< 140	99.99					
< 150	100.00					
Total	**100**	**100**	**100**	**100**	**100**	**100**
Mean (cm/s)	**35**	**18**	**14**	**7**	**6**	**7**
Maximum (cm/s)	147	**81**	**58**	**34**	**28**	**31**

Figure B.11: Current data from Brazil (ref: [27])

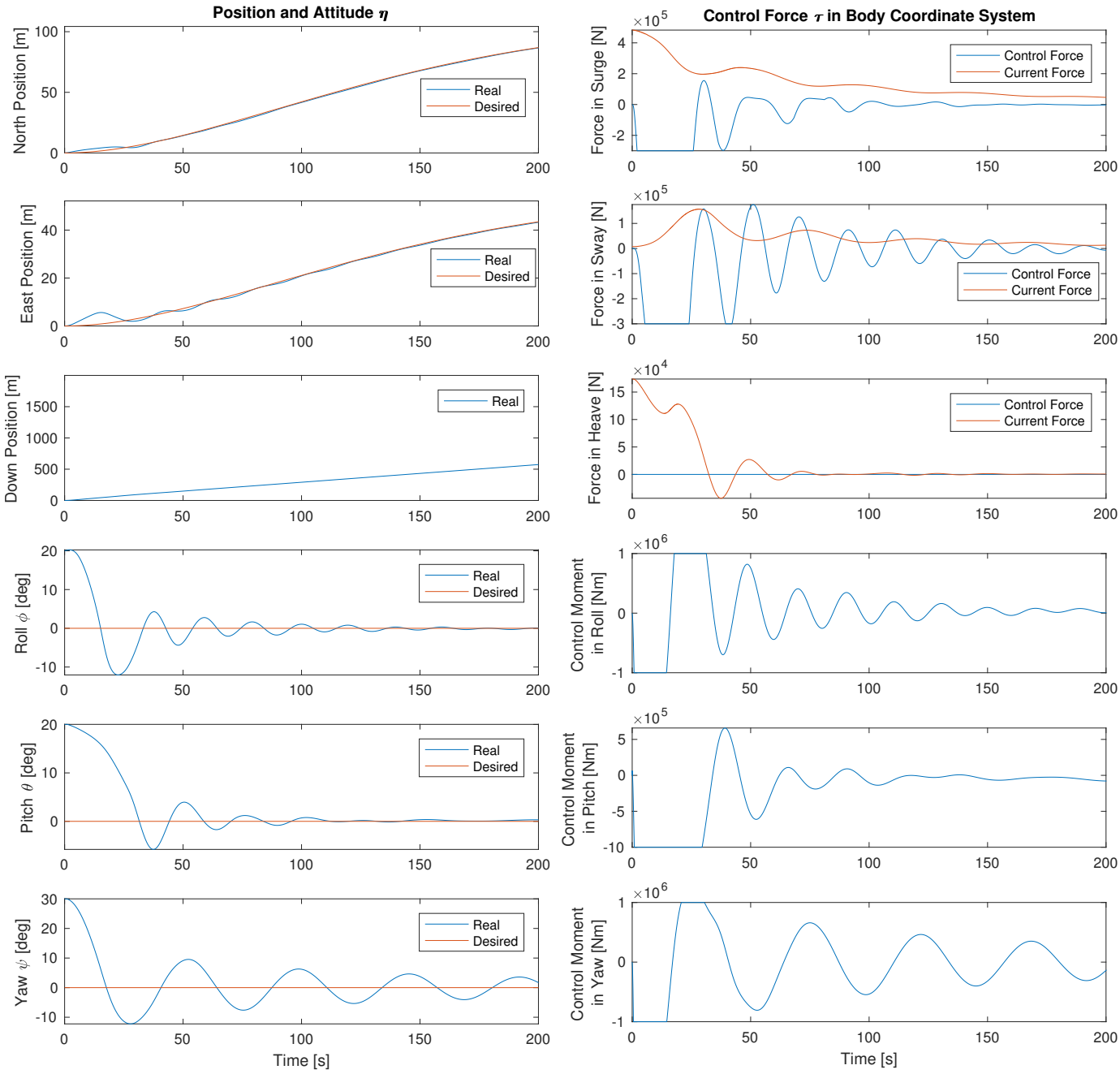

Figure B.12: Transient position and control force Brazil

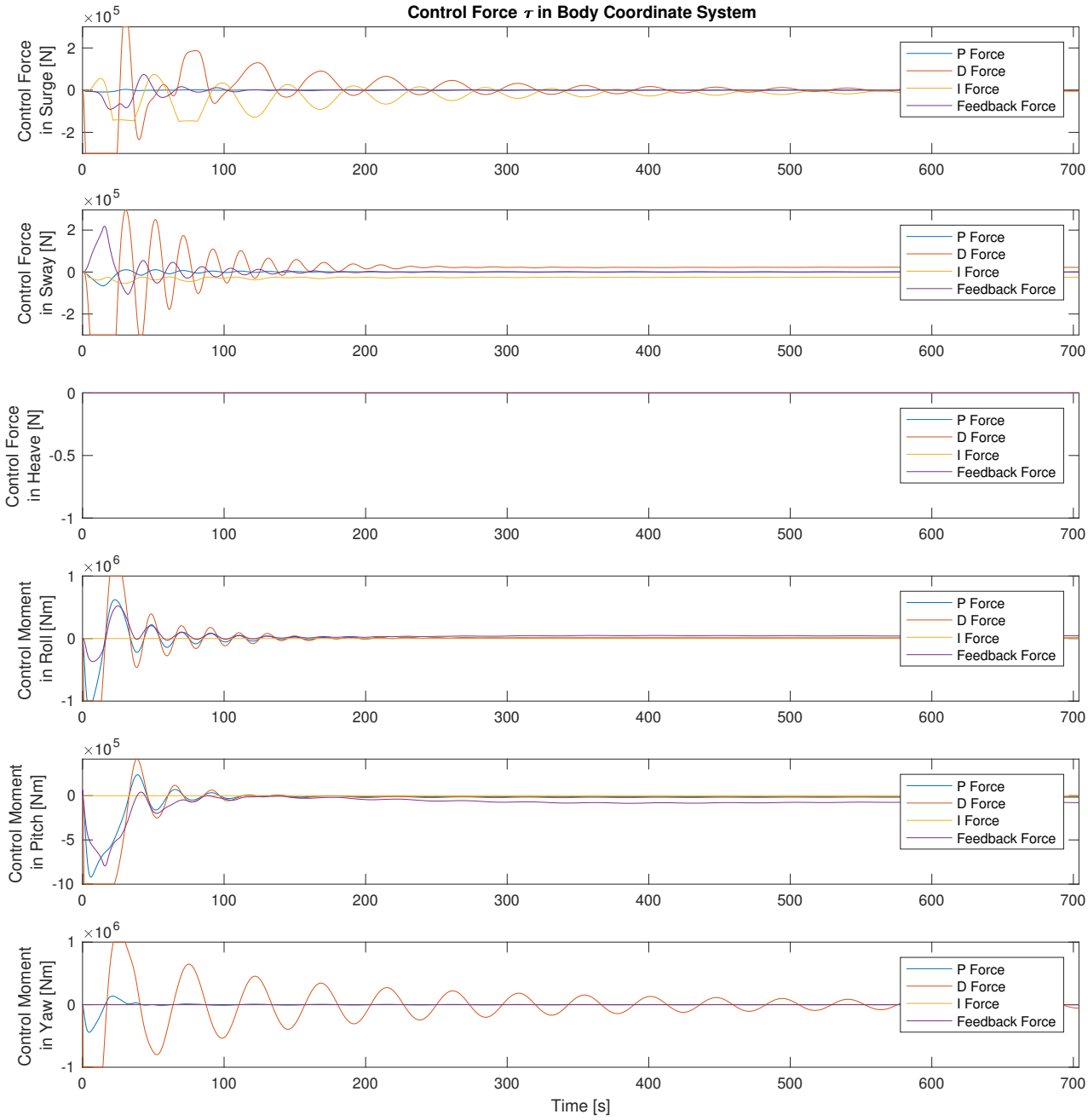

Figure B.13: Advanced control force plot Brazil

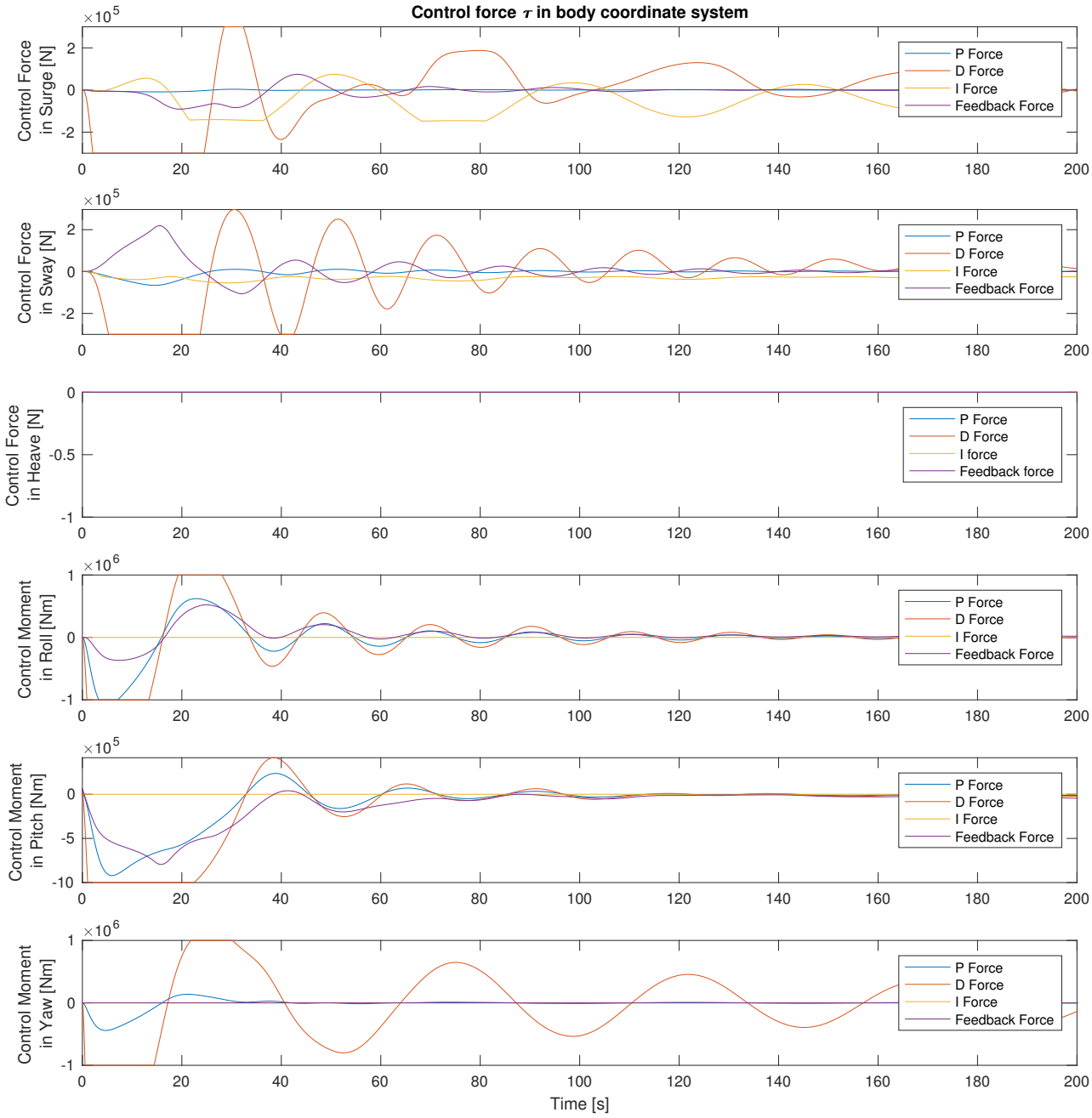

Figure B.14: Transient advanced control force plot Brazil

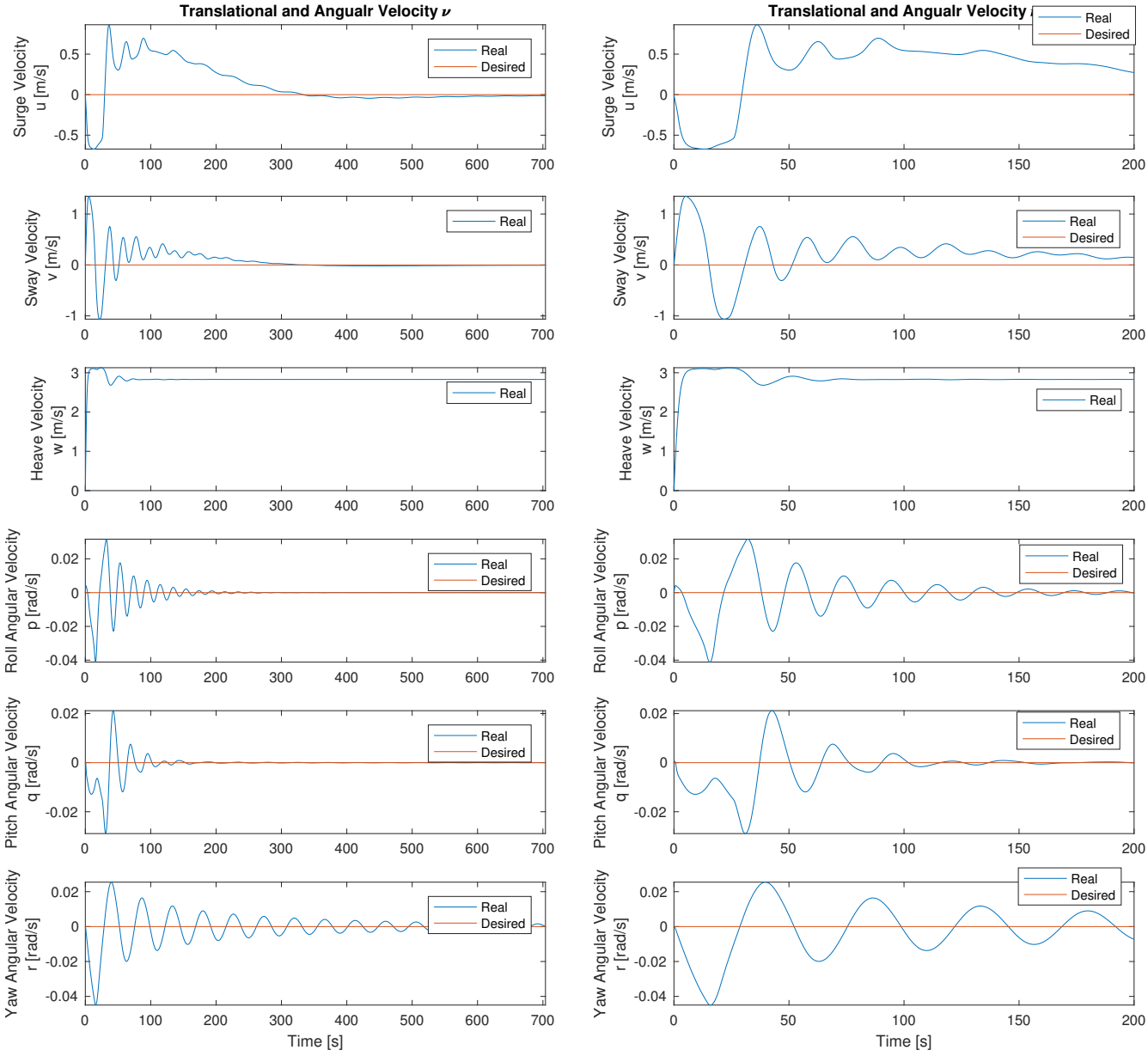

Figure B.15: Velocity plot Brazil

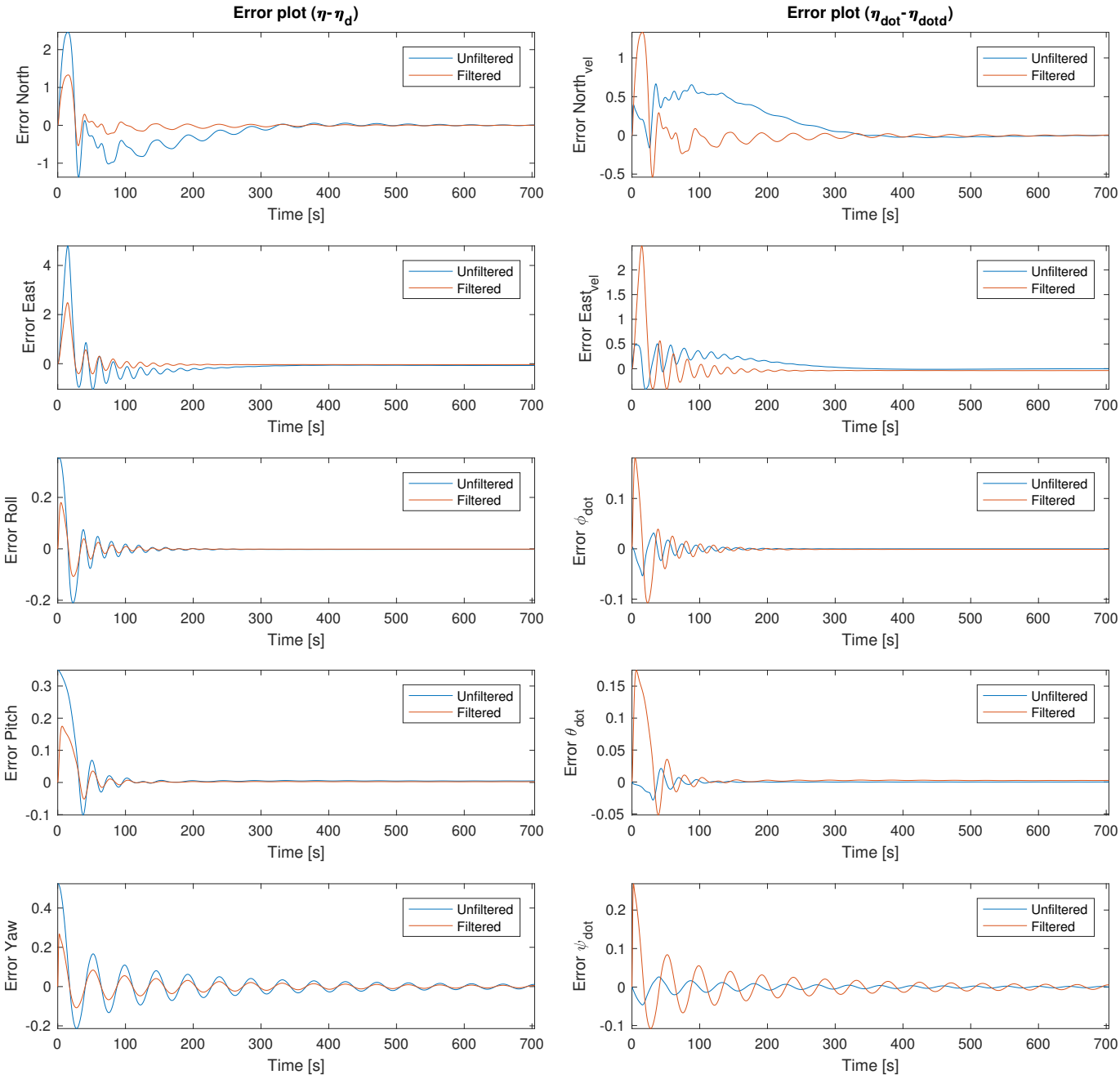

Figure B.16: Error plot Brazil

B.4 Drop in 3D Current Profile

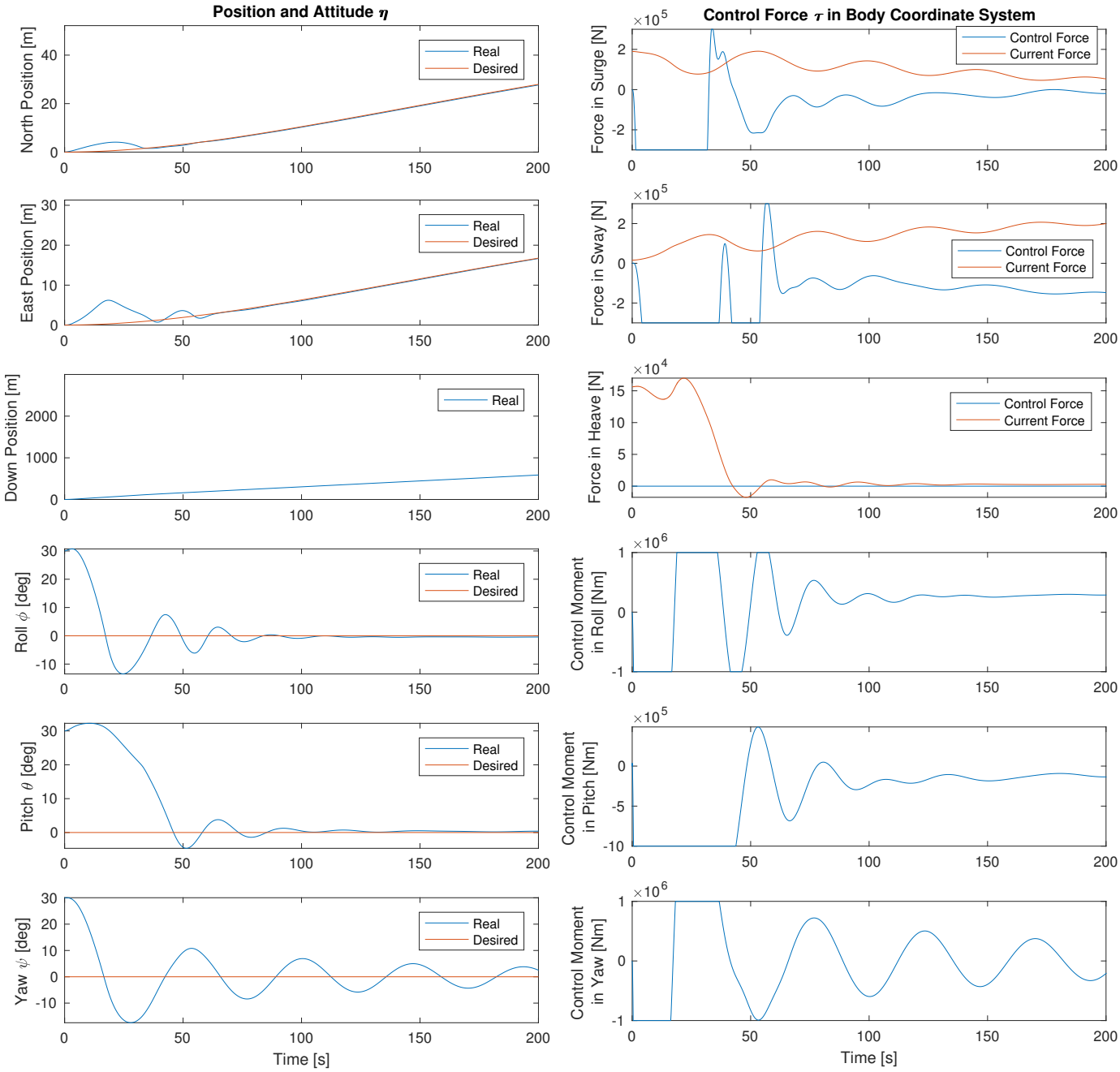

Figure B.17: Transient position and control force 3D

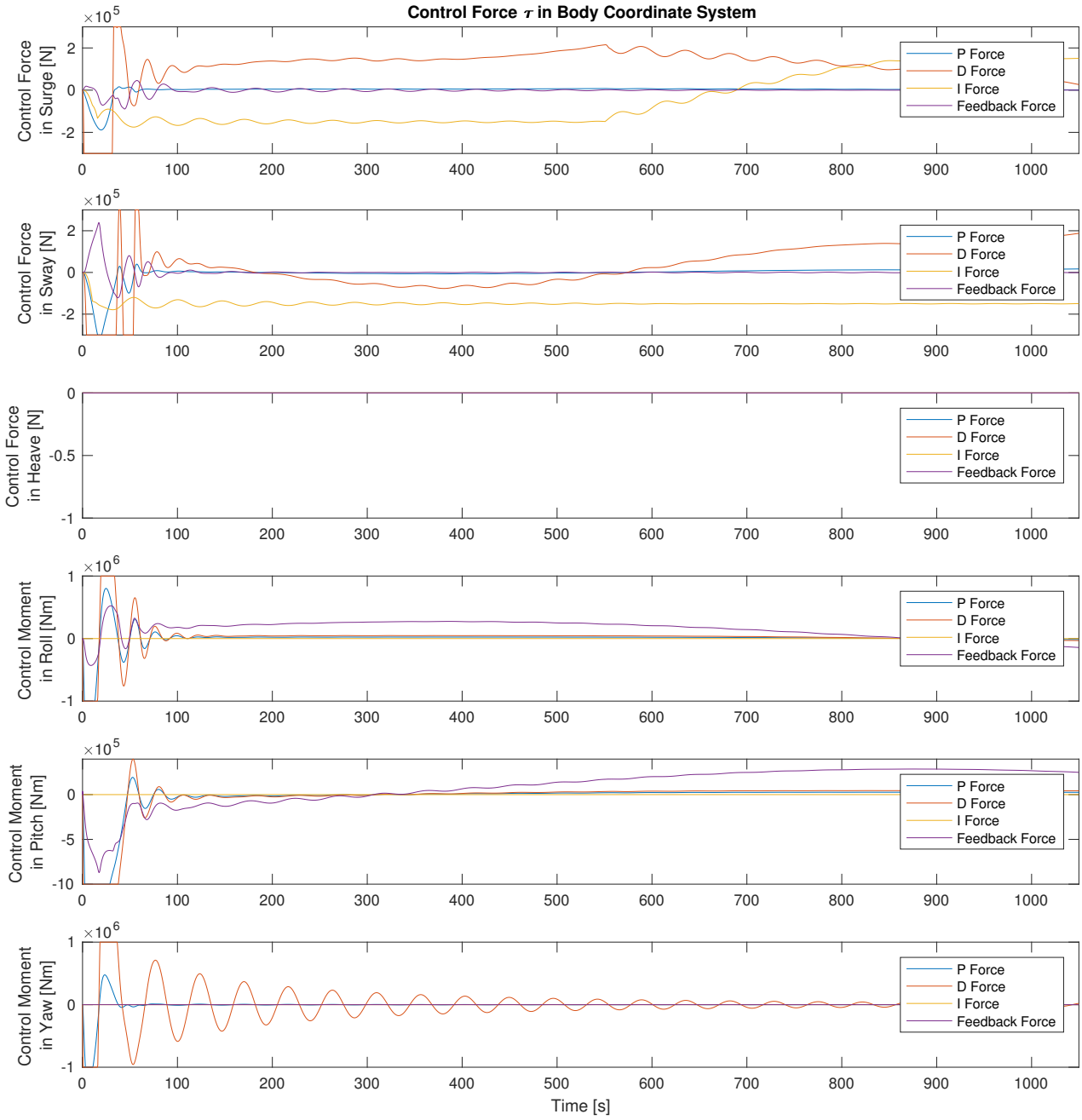

Figure B.18: Advanced control force plot 3D

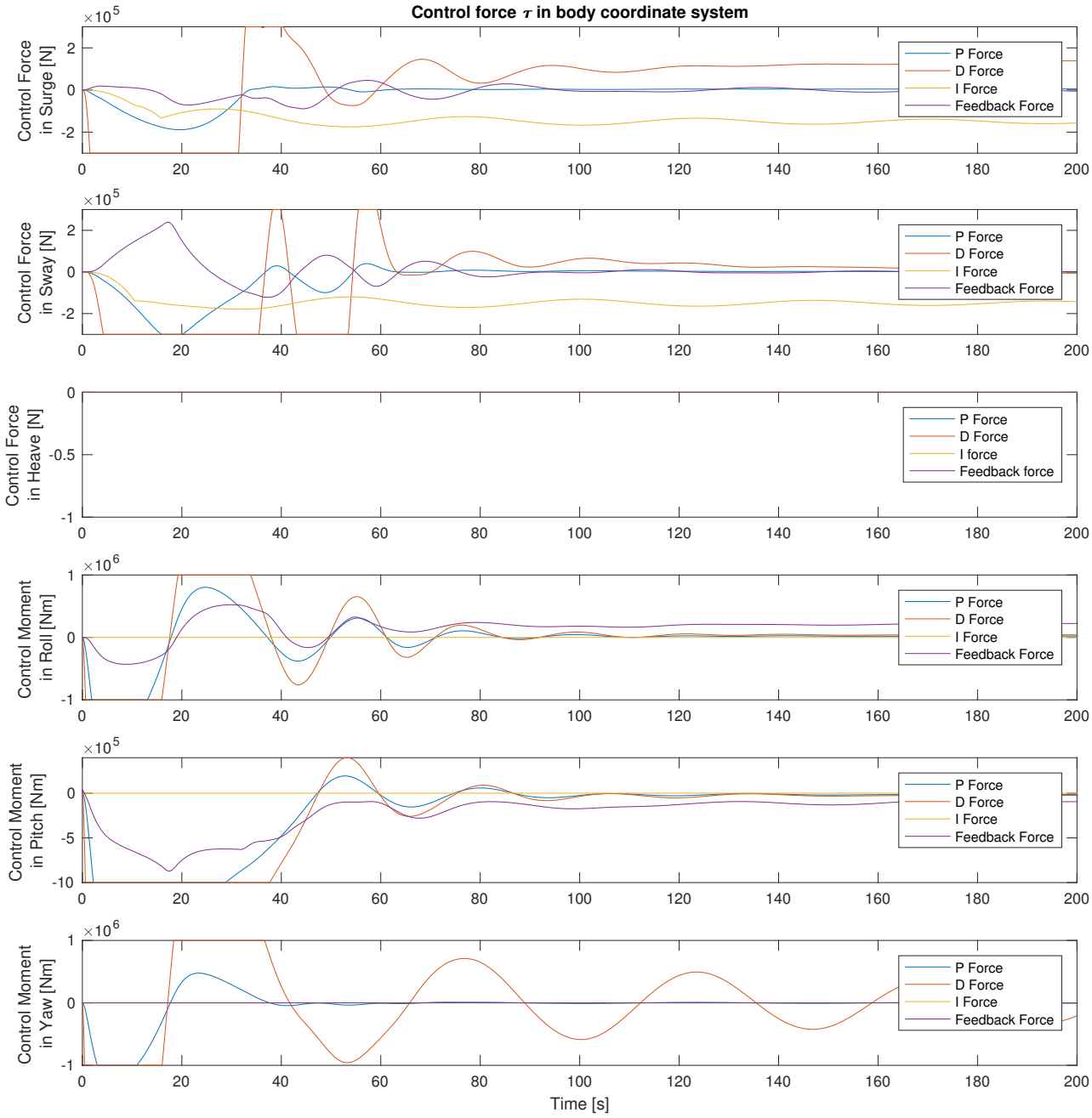

Figure B.19: Transient advanced control force plot 3D

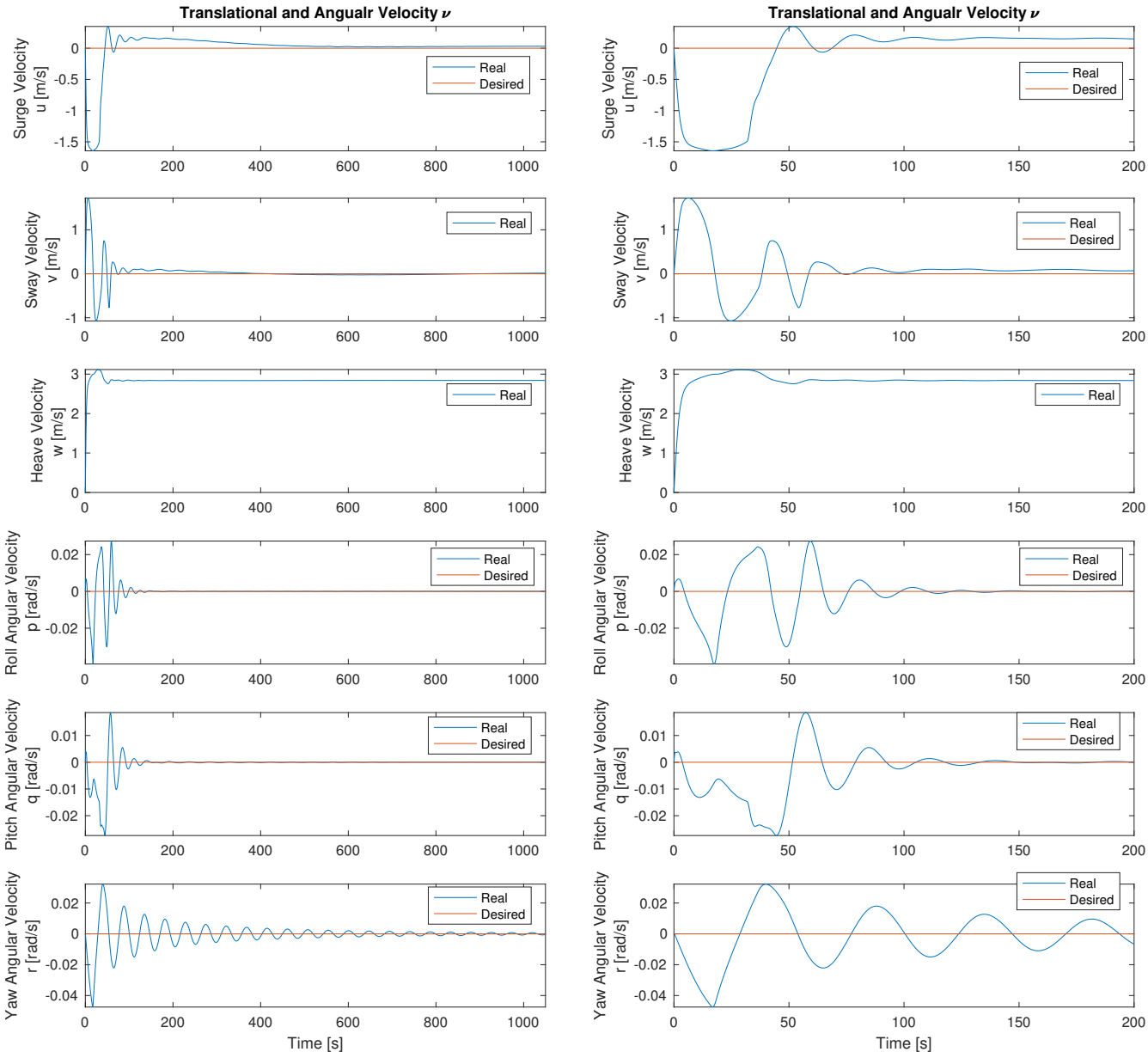

Figure B.20: Velocity plot 3D

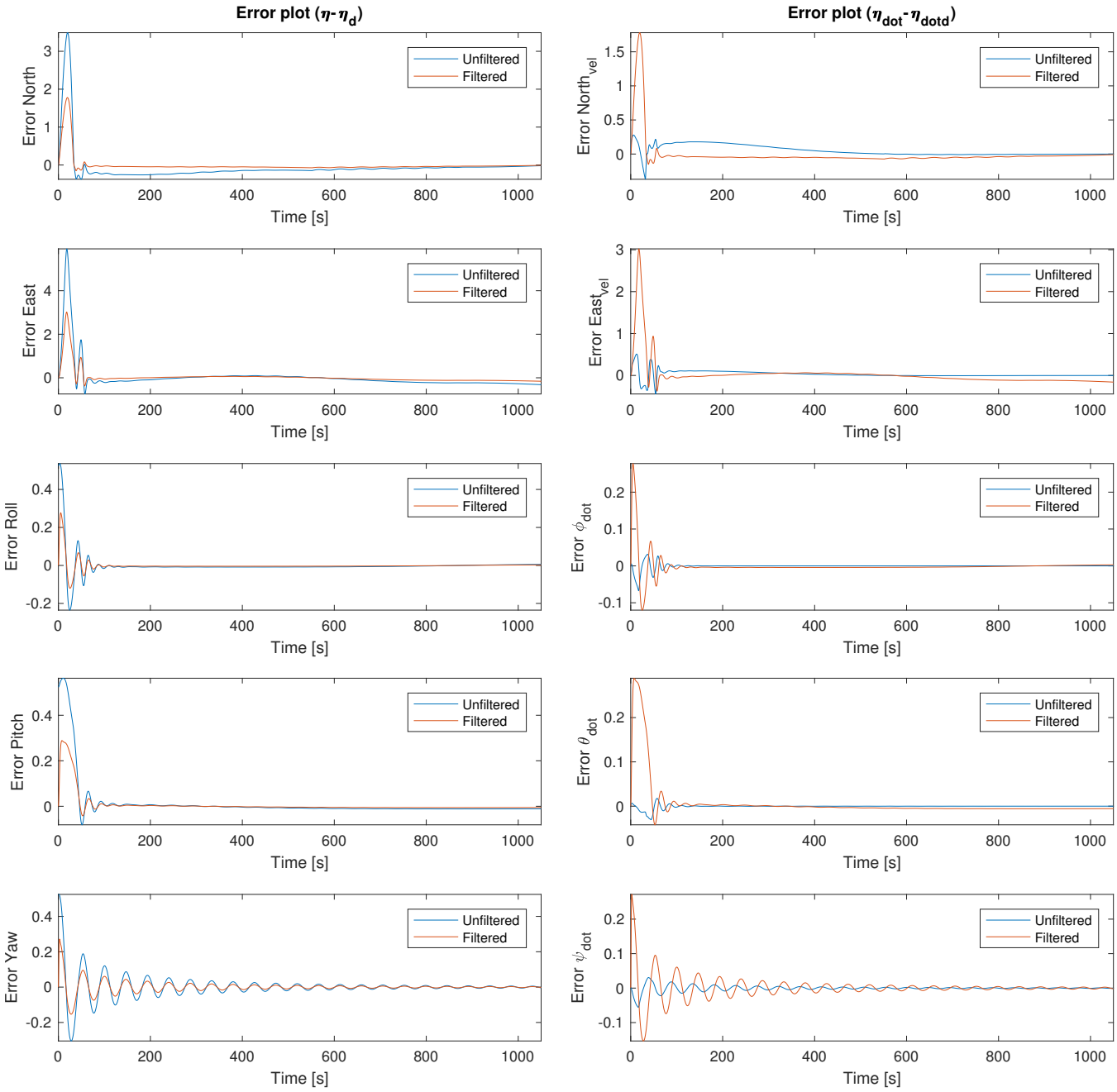

Figure B.21: Error plot 3D

B.5 Drop in Bidirectional Current Profile

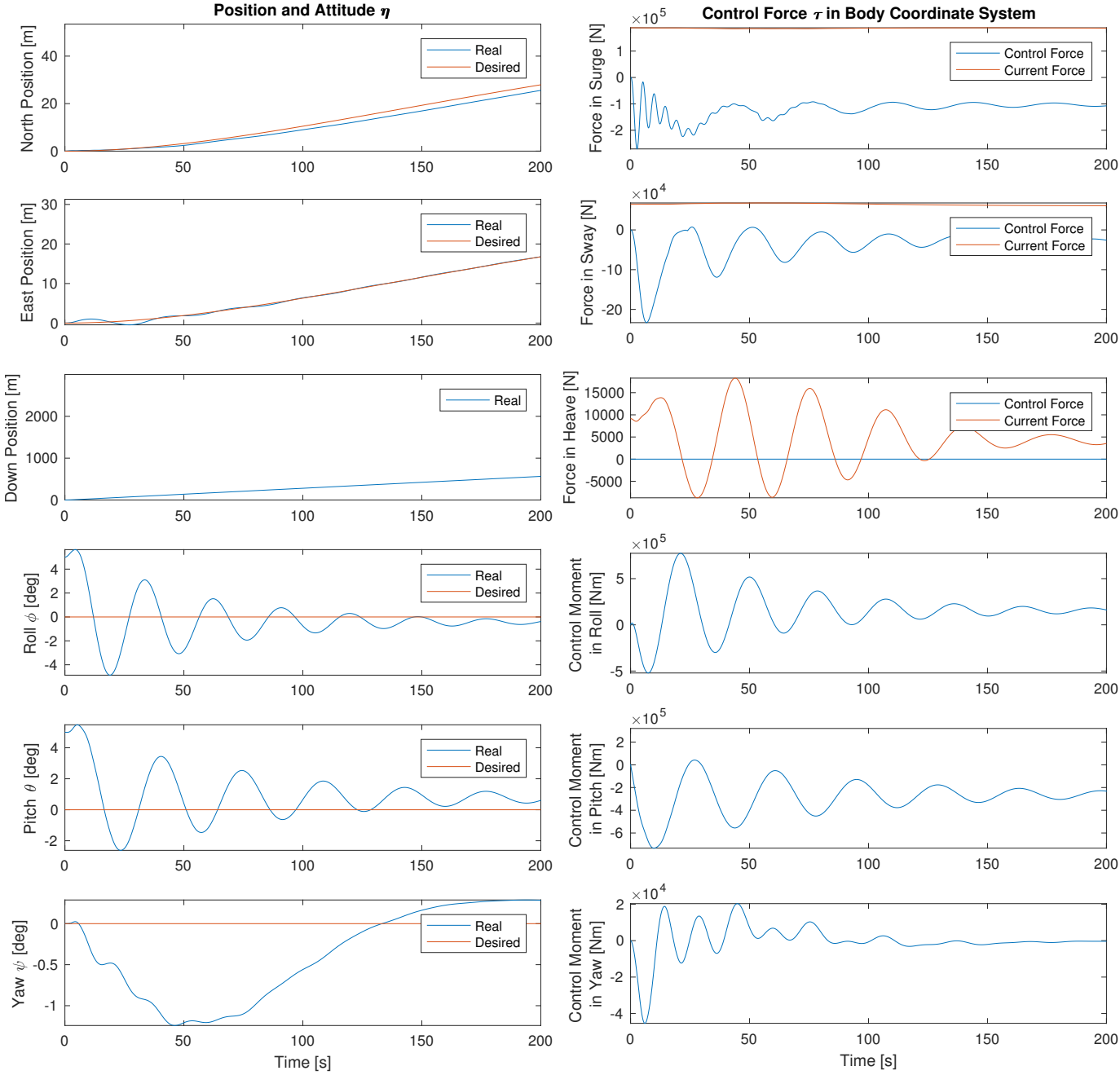

Figure B.22: Transient position and control force bidirectional

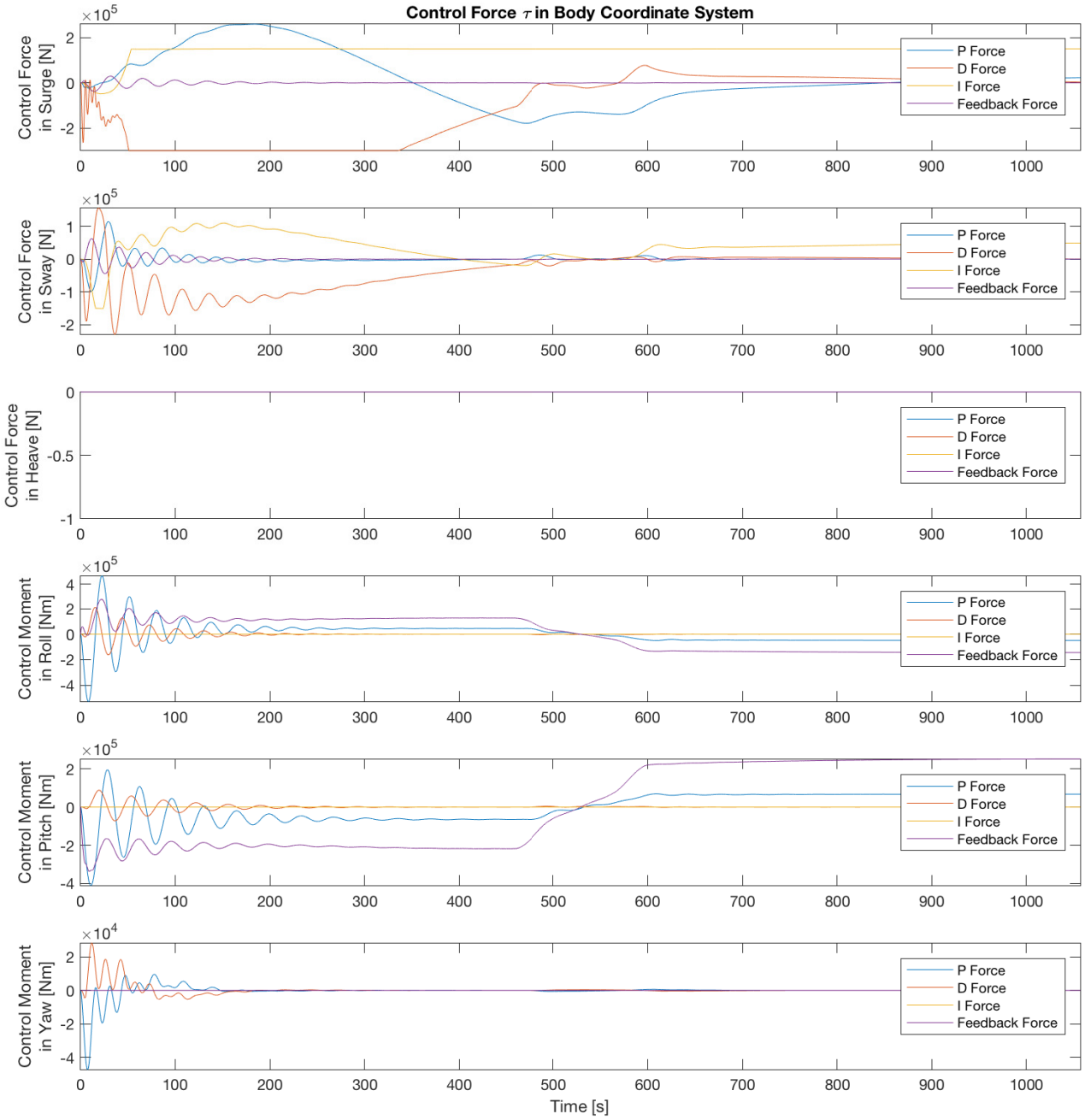

Figure B.23: Advanced control force plot bidirectional

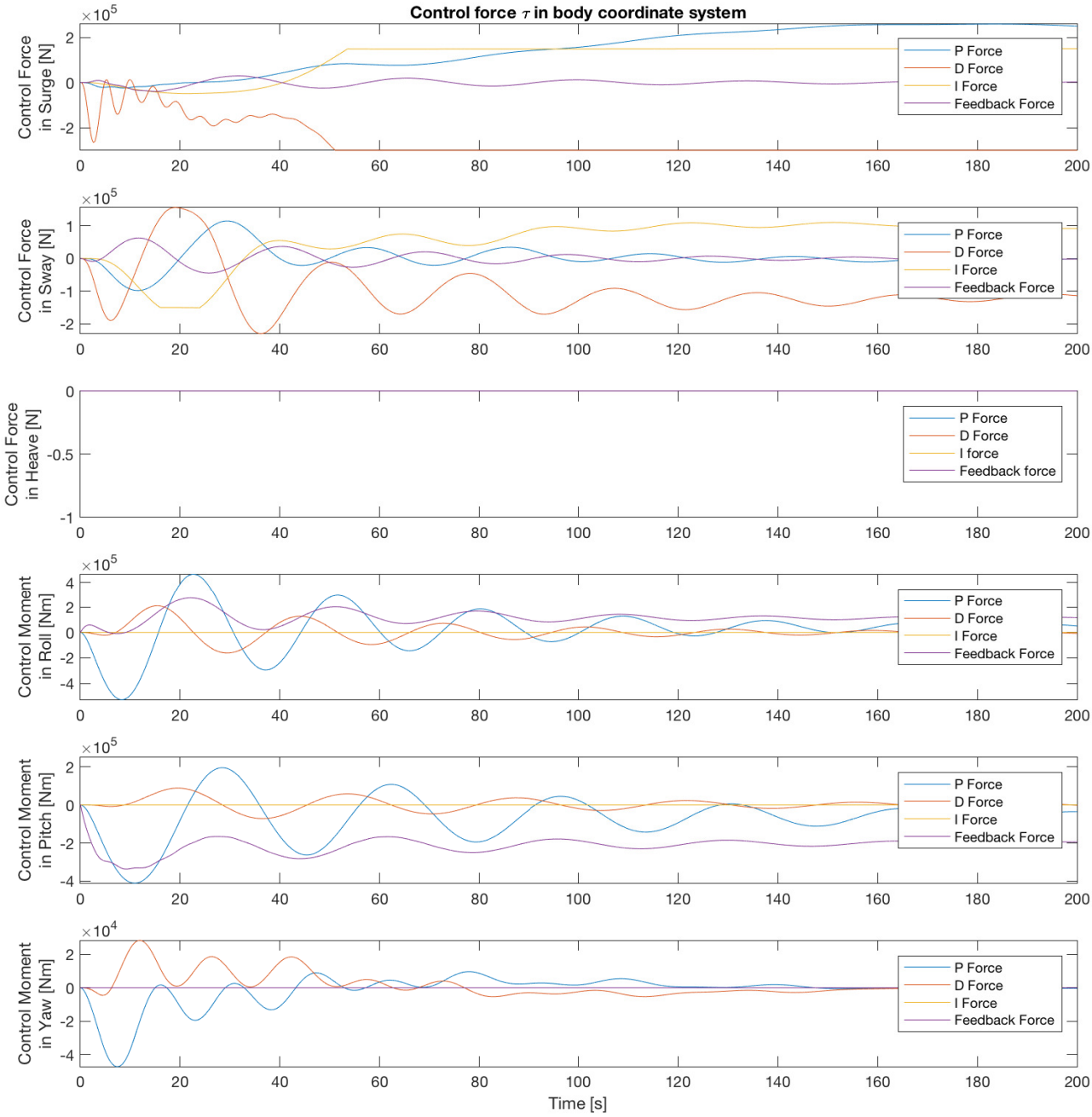

Figure B.24: Transient advanced control force plot bidirectional

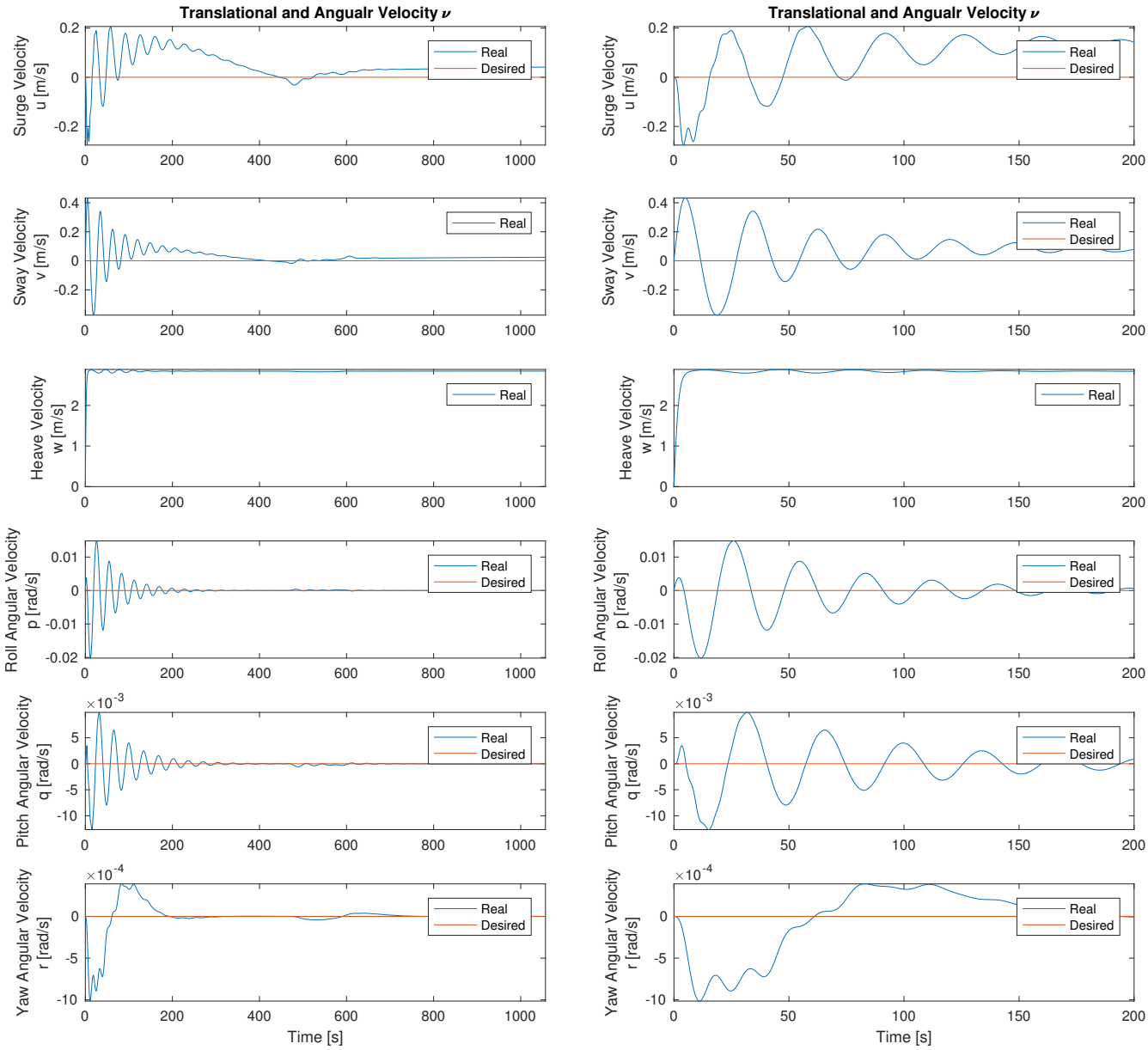

Figure B.25: Velocity plot bidirectional

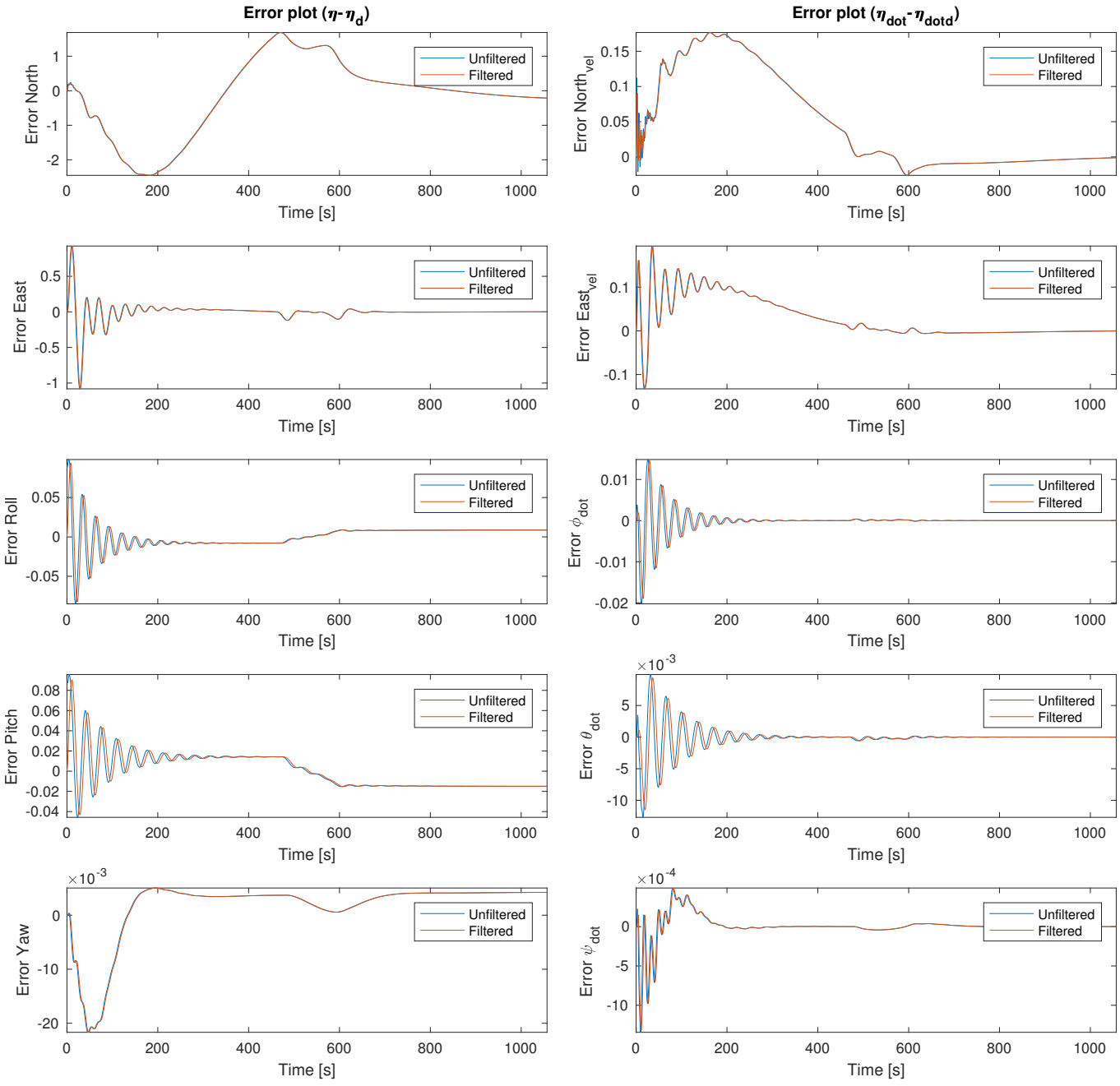

Figure B.26: Error plot bidirectional

B.6 Drop in Divided Current Profile

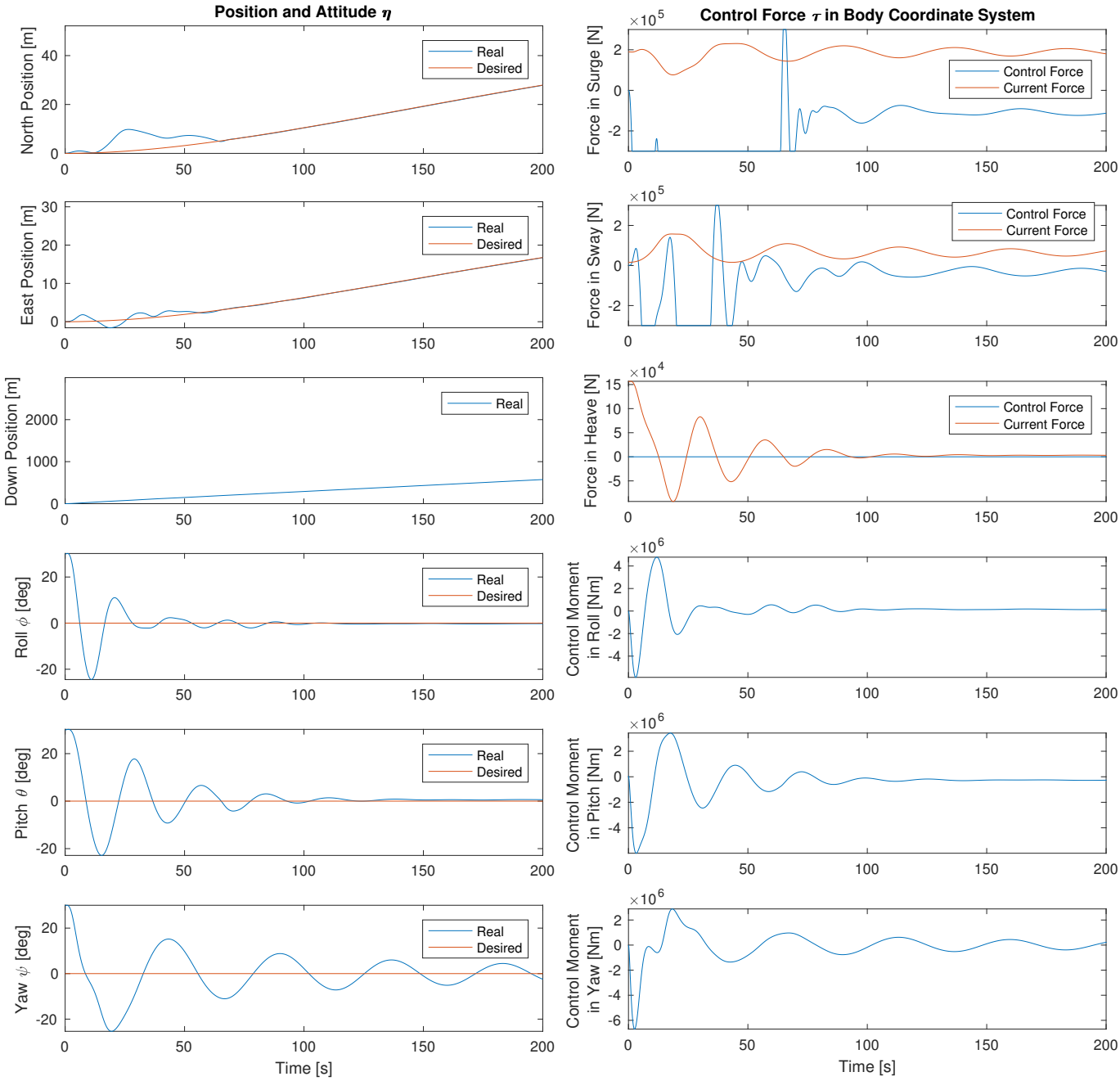

Figure B.27: Transient position and control force divided

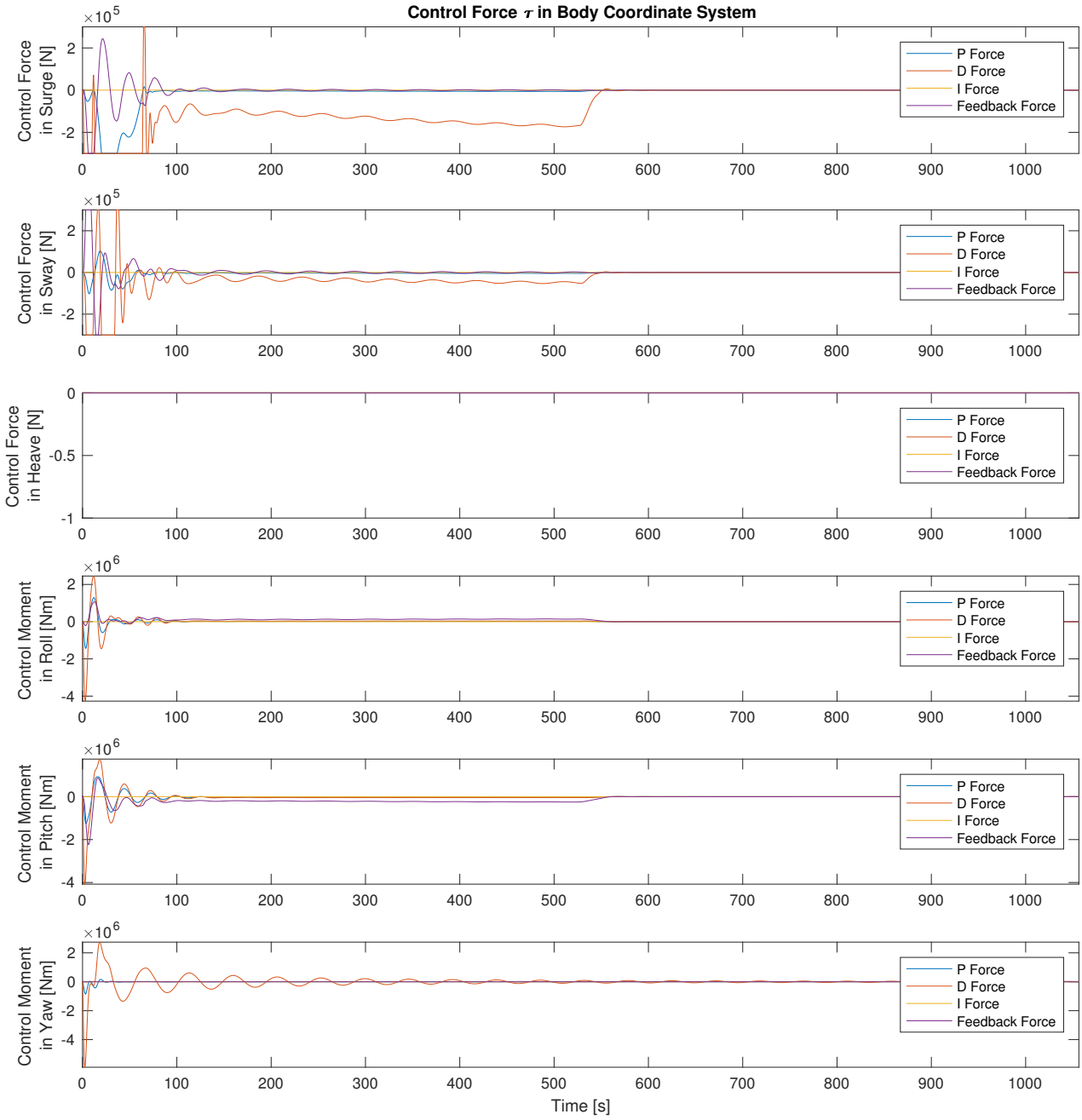

Figure B.28: Advanced control force plot divided

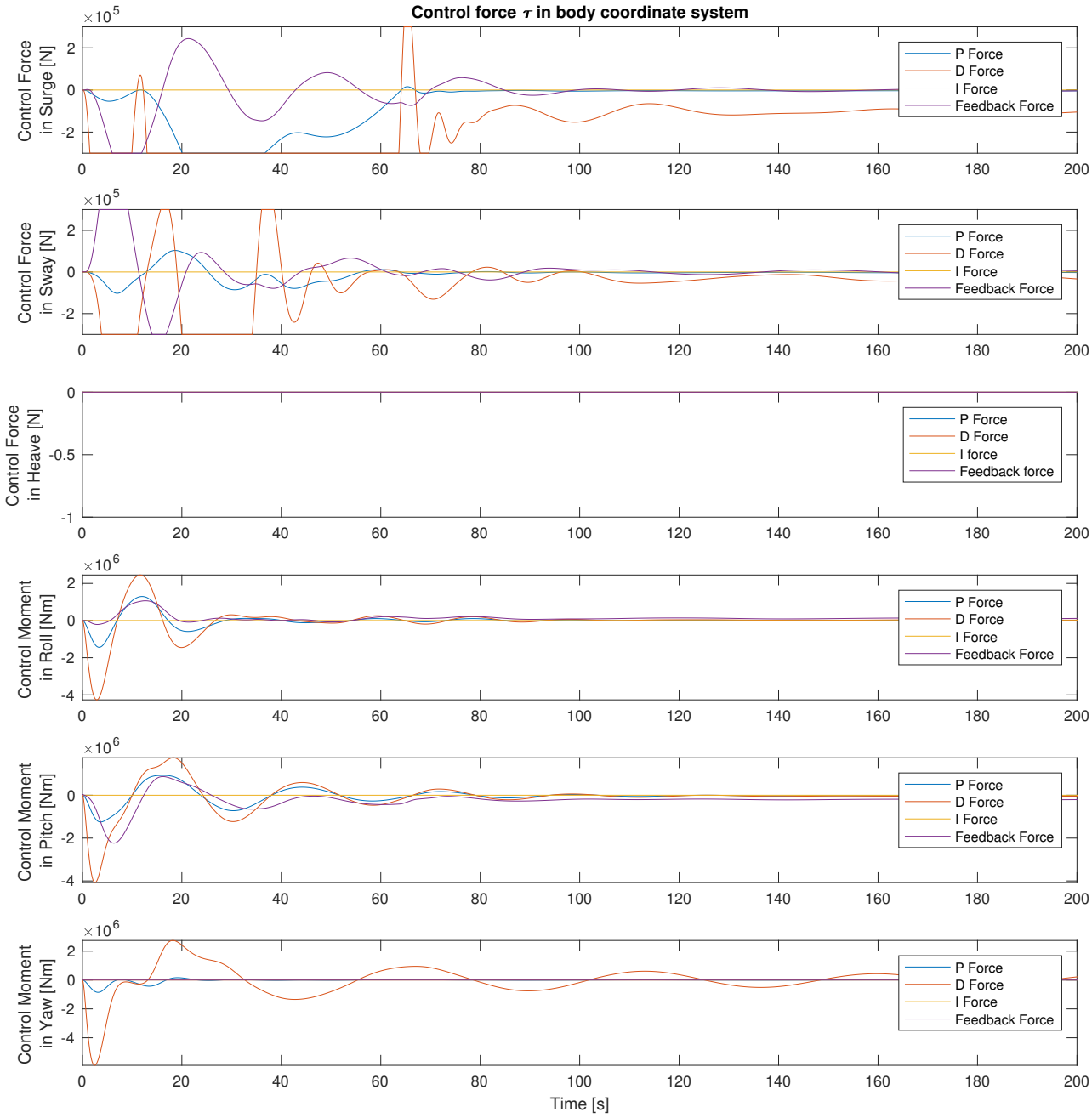

Figure B.29: Transient advanced control force plot divided

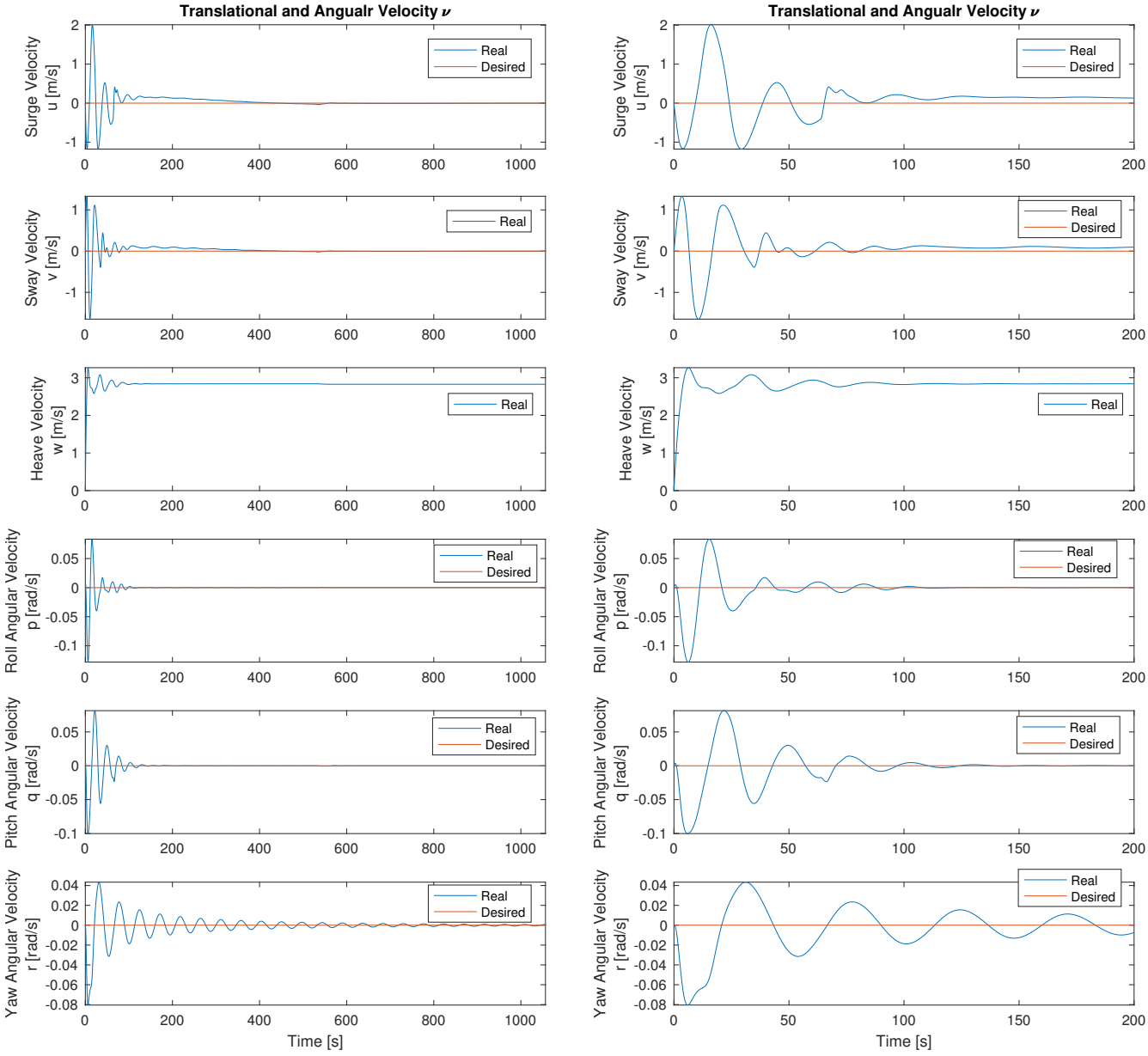

Figure B.30: Velocity plot divided

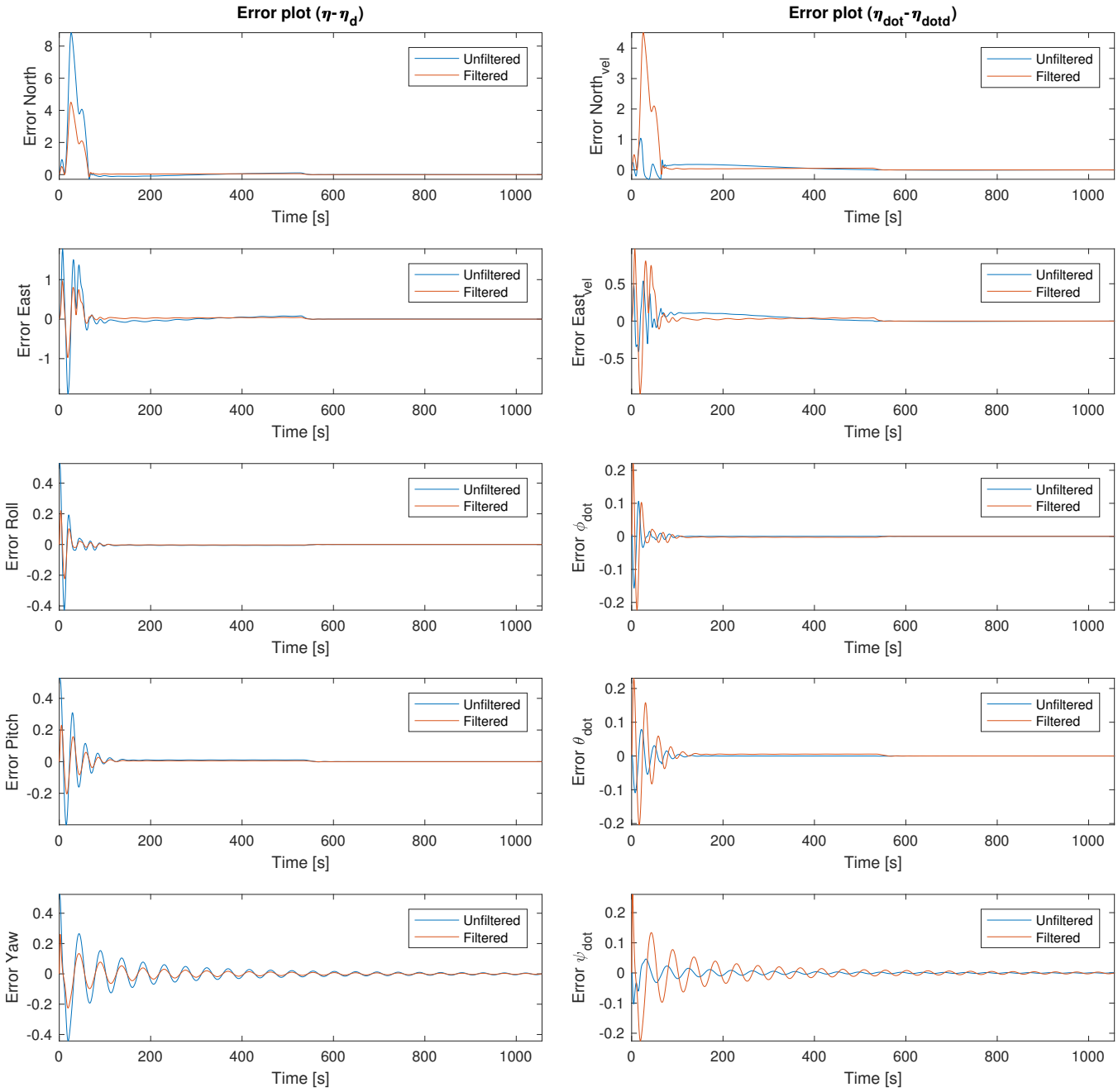

Figure B.31: Error plot divided

B.7 Drop in Shear Current Profile

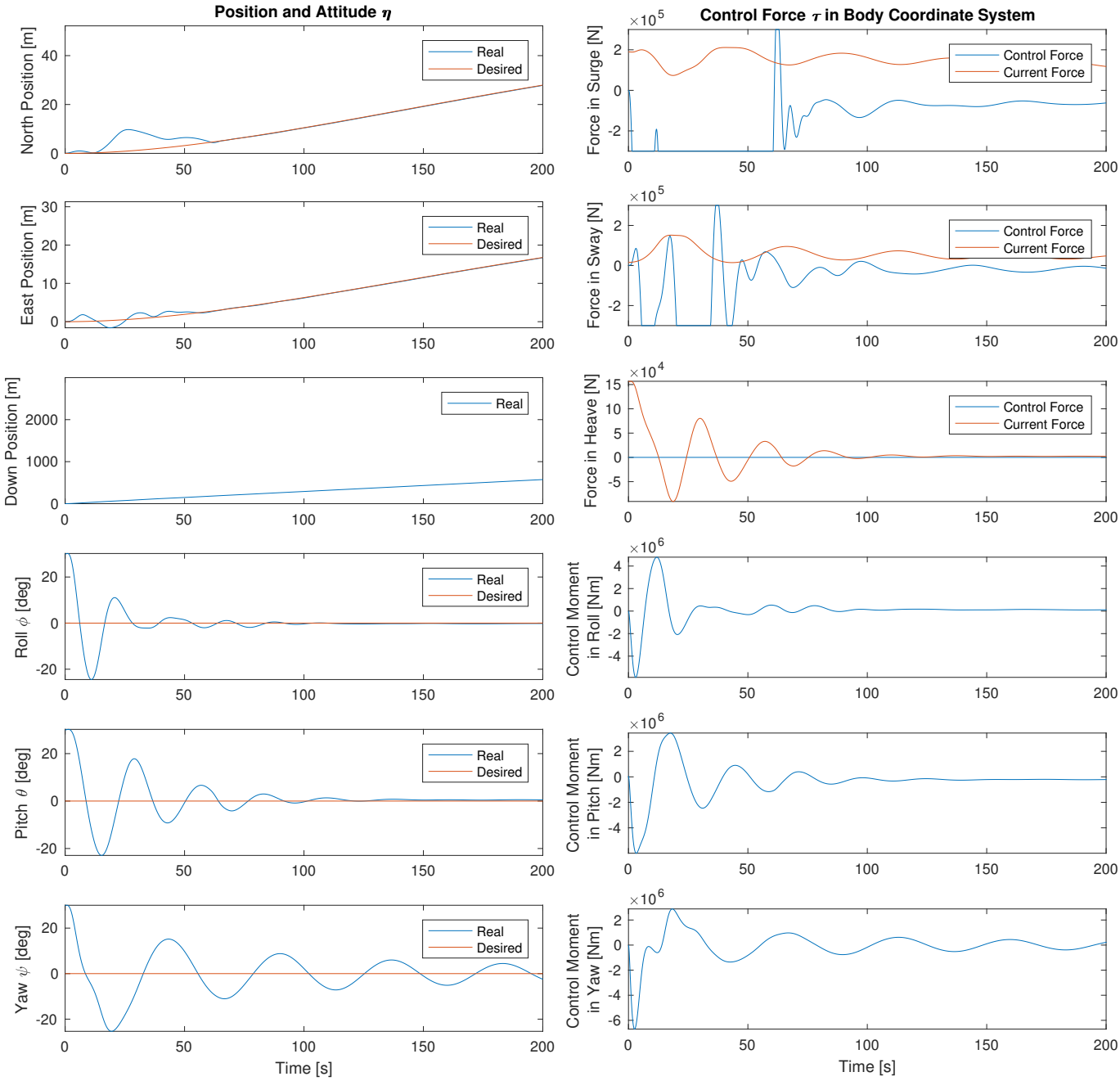

Figure B.32: Transient position and control force shear

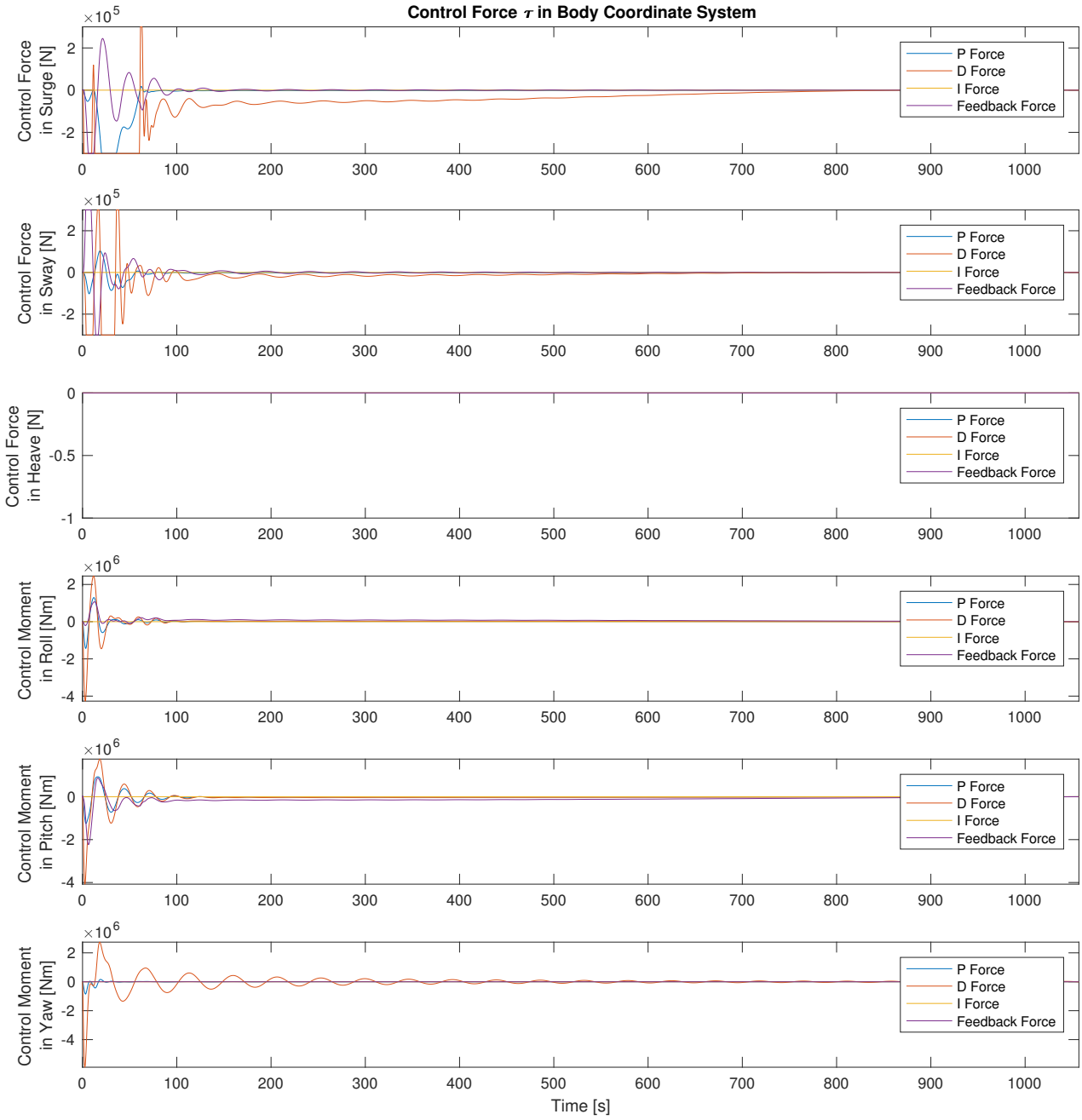

Figure B.33: Advanced control force plot shear

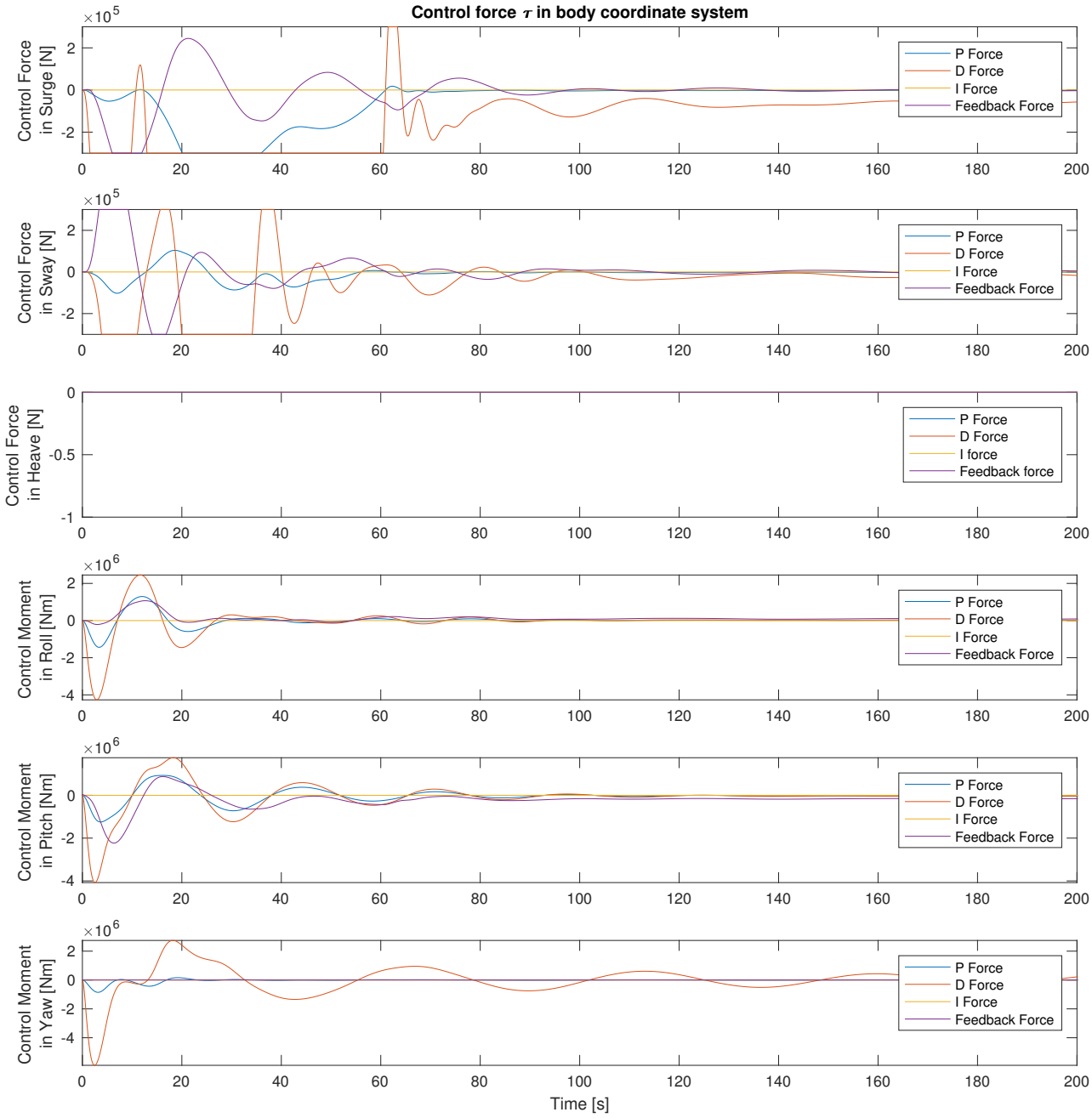

Figure B.34: Transient advanced control force plot shear

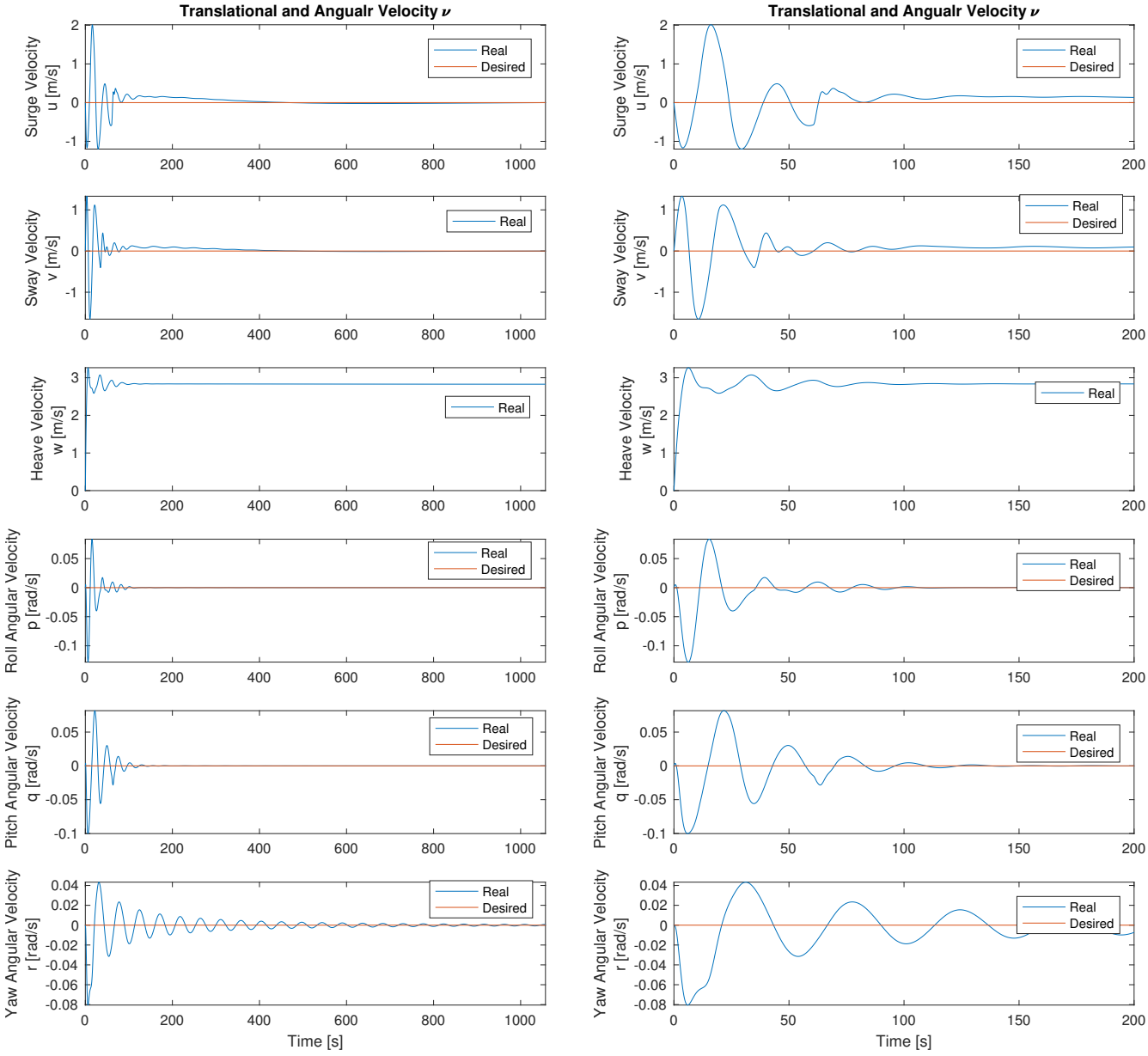

Figure B.35: Velocity plot shear

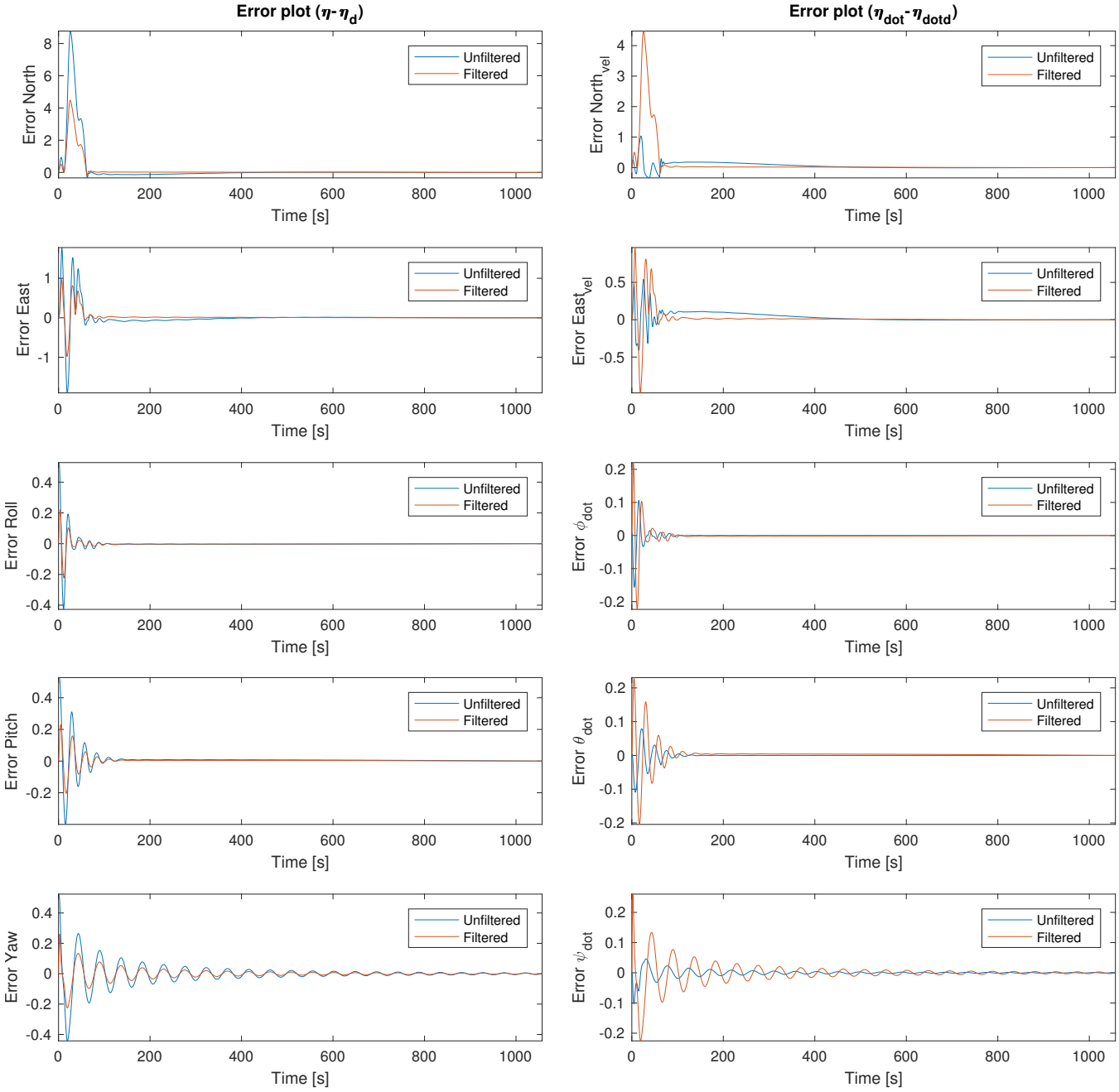

Figure B.36: Error plot shear

B.8 Parachute Drop

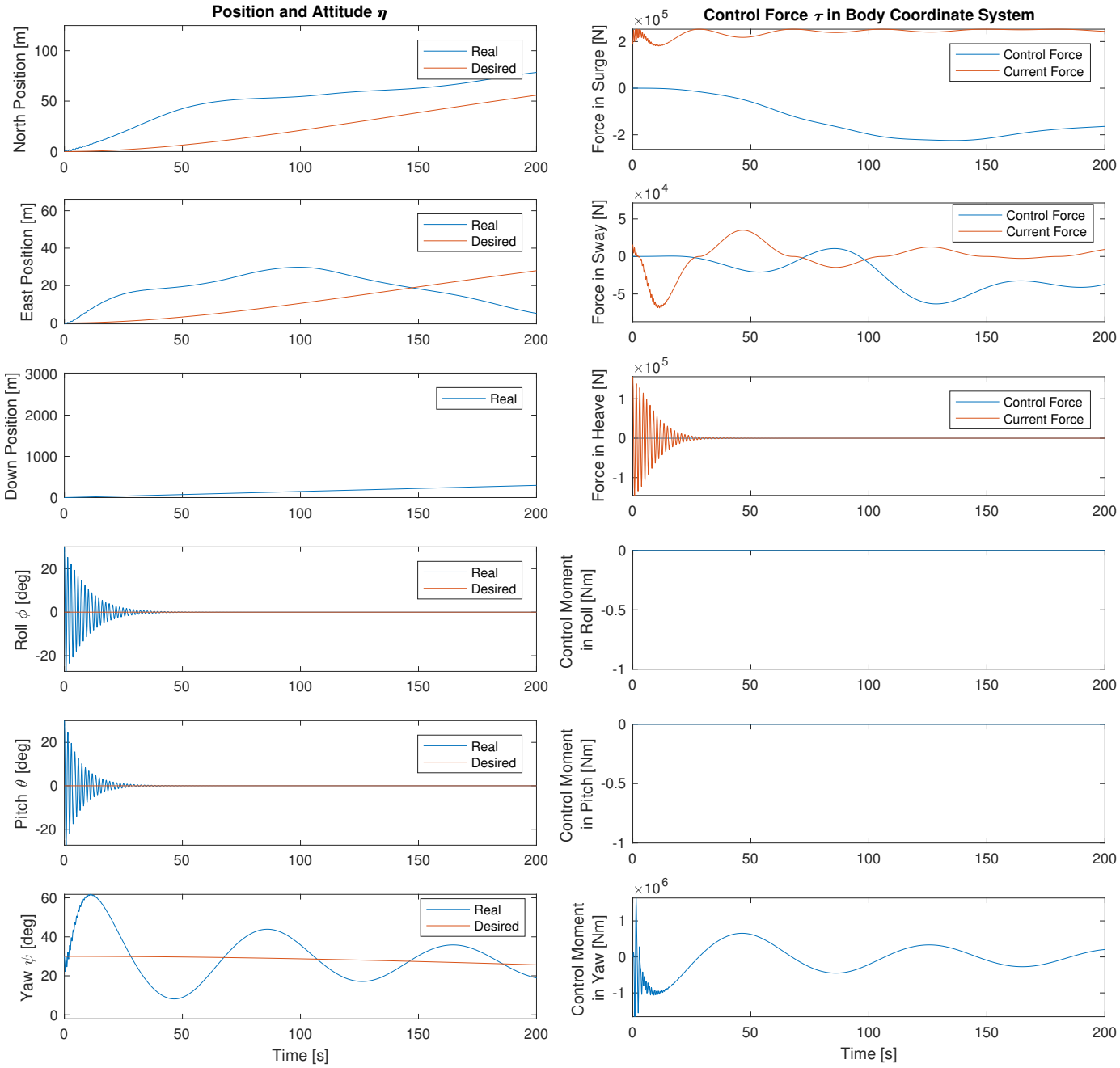

Figure B.37: Transient position and control force parachute

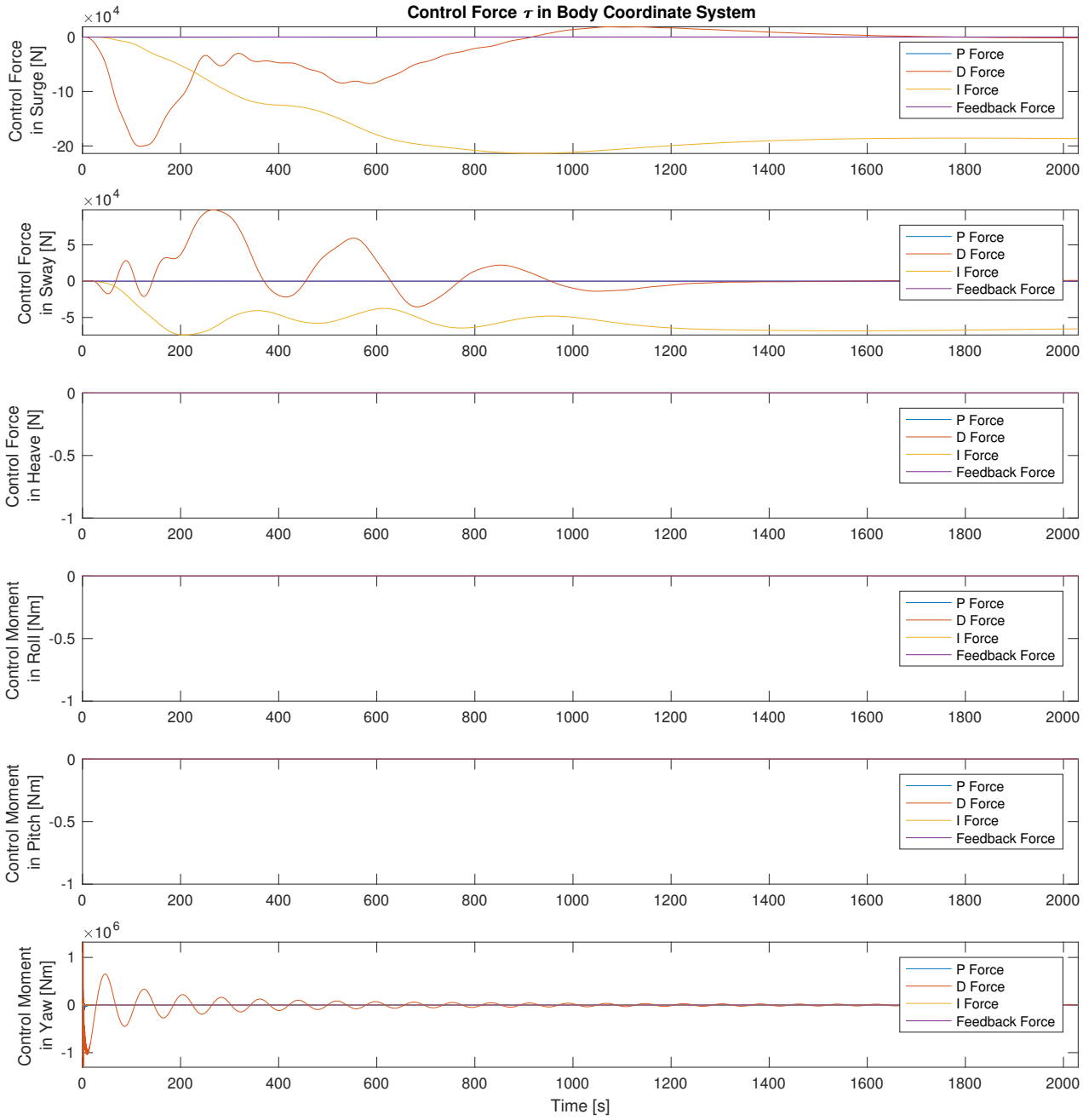

Figure B.38: Advanced control force plot parachute

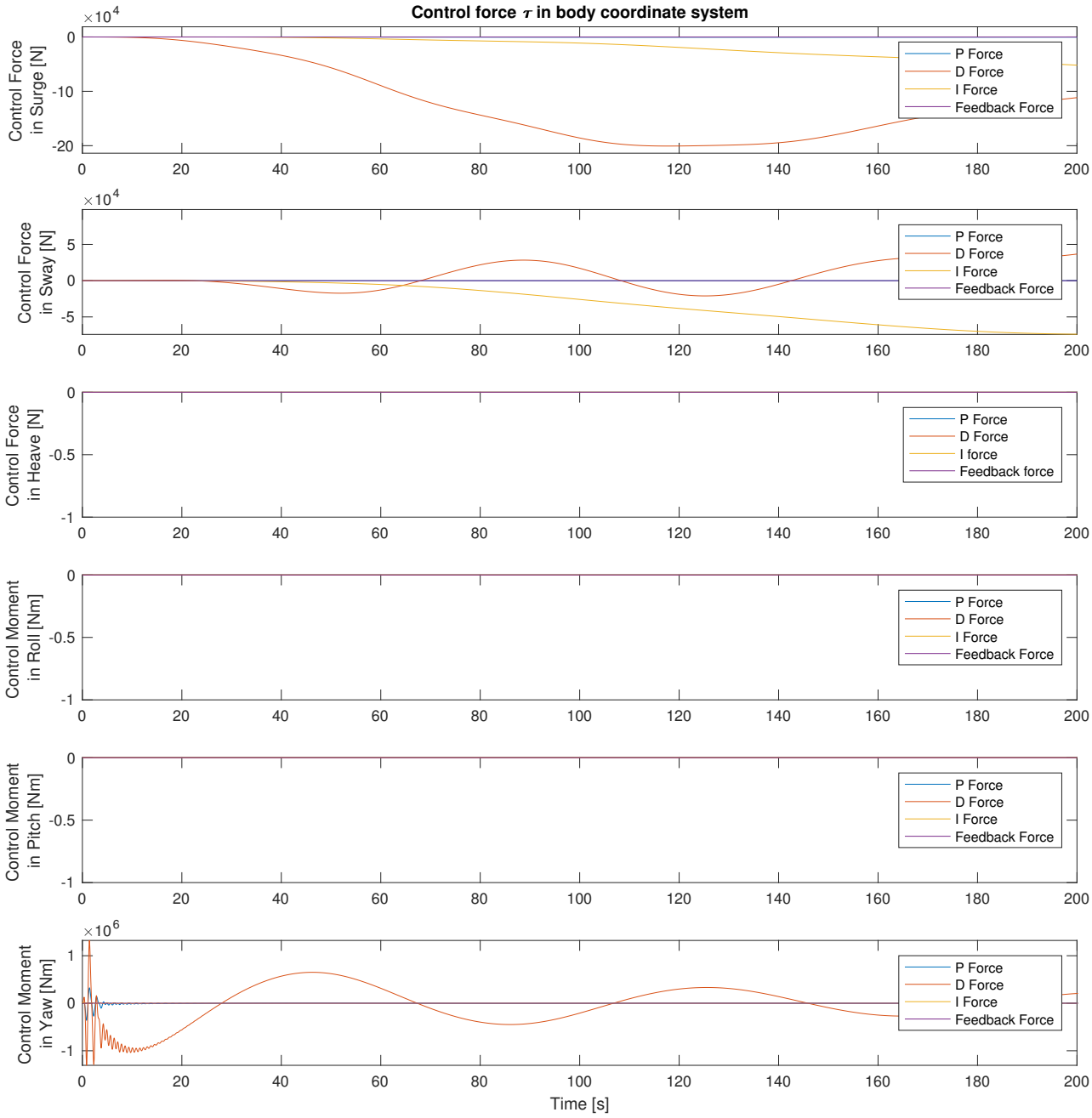

Figure B.39: Transient advanced control force plot parachute

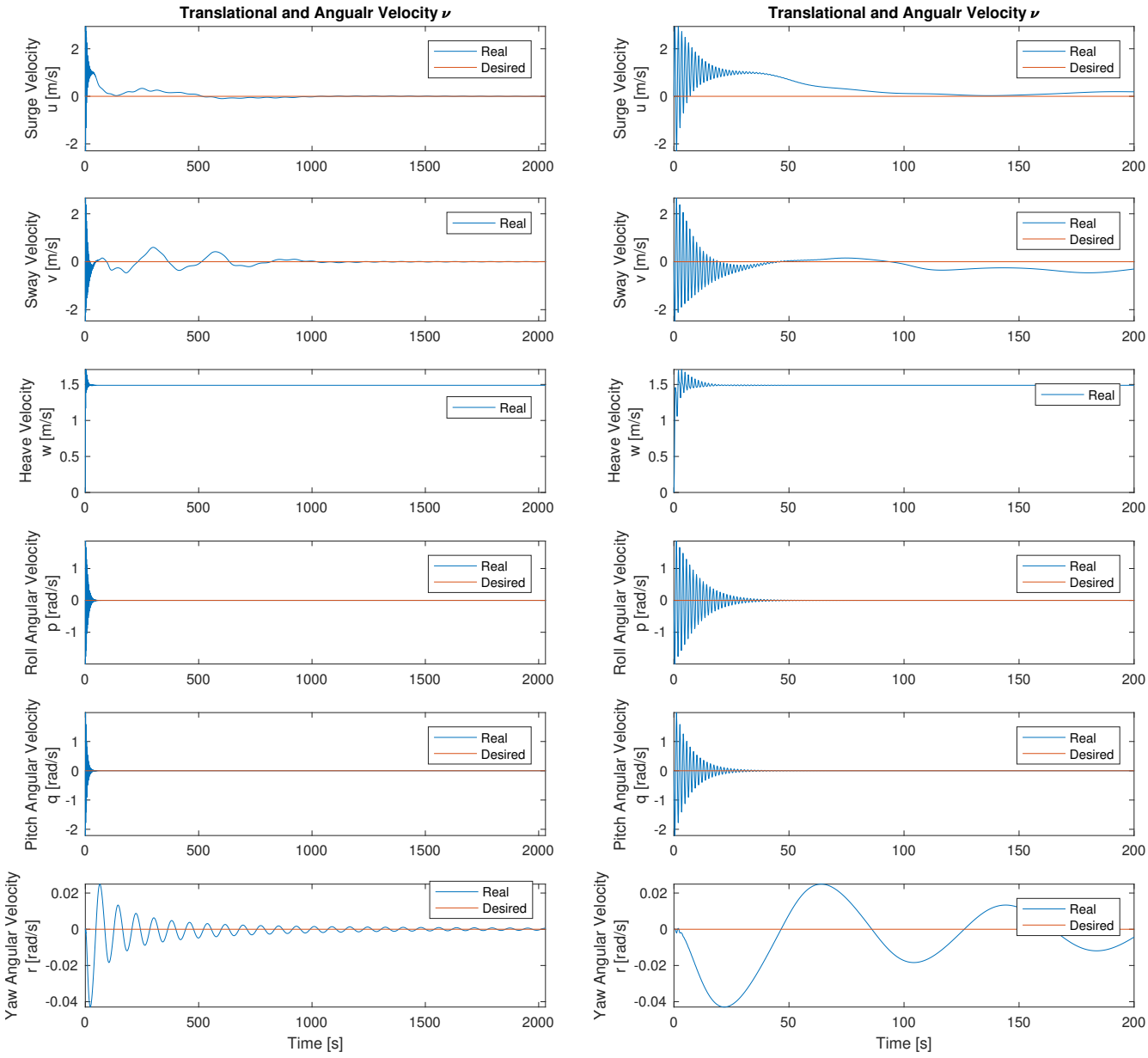

Figure B.40: Velocity plot parachute

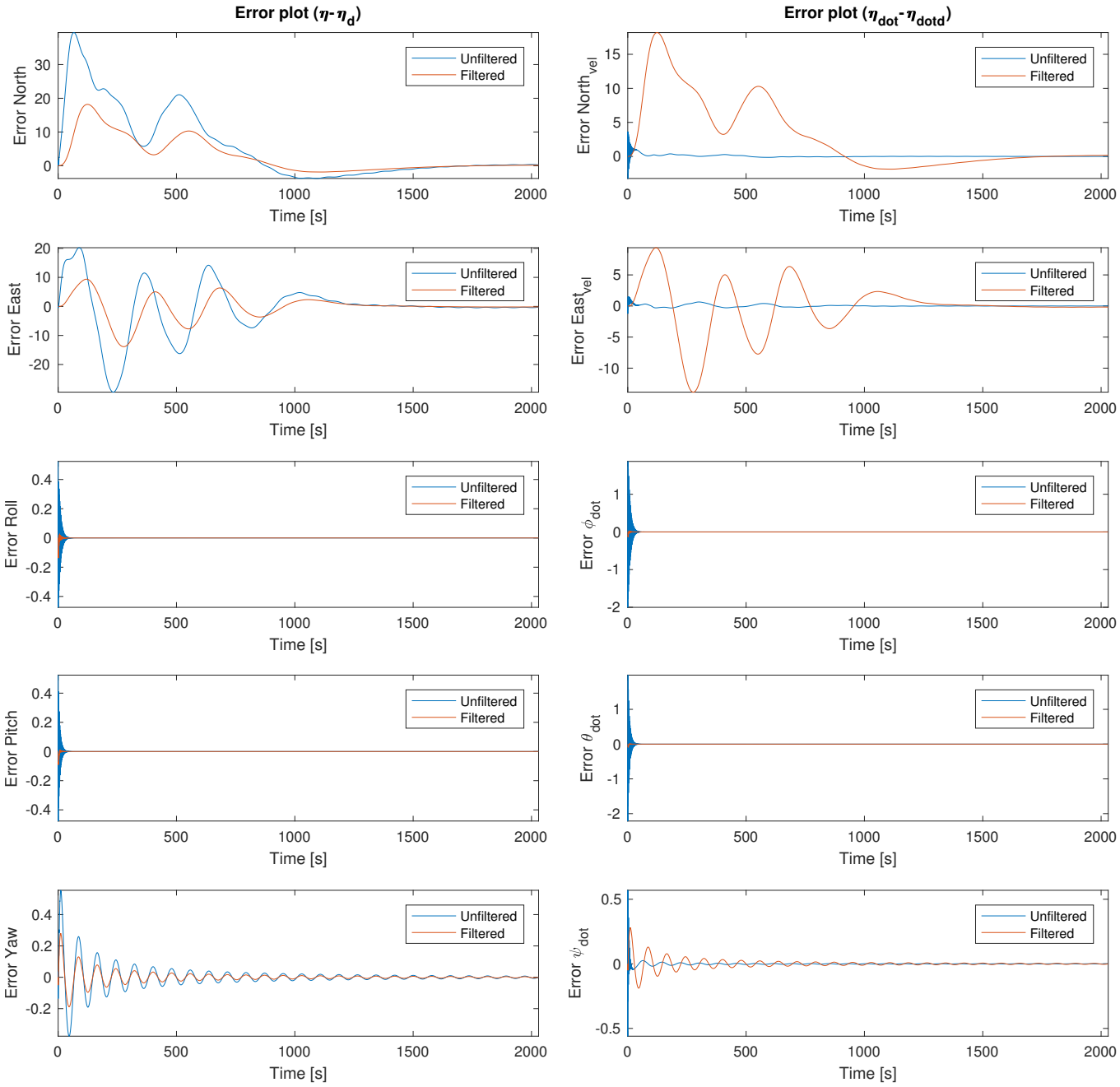

Figure B.41: Error plot parachute

B.9 Drop with Buoyancy Tank

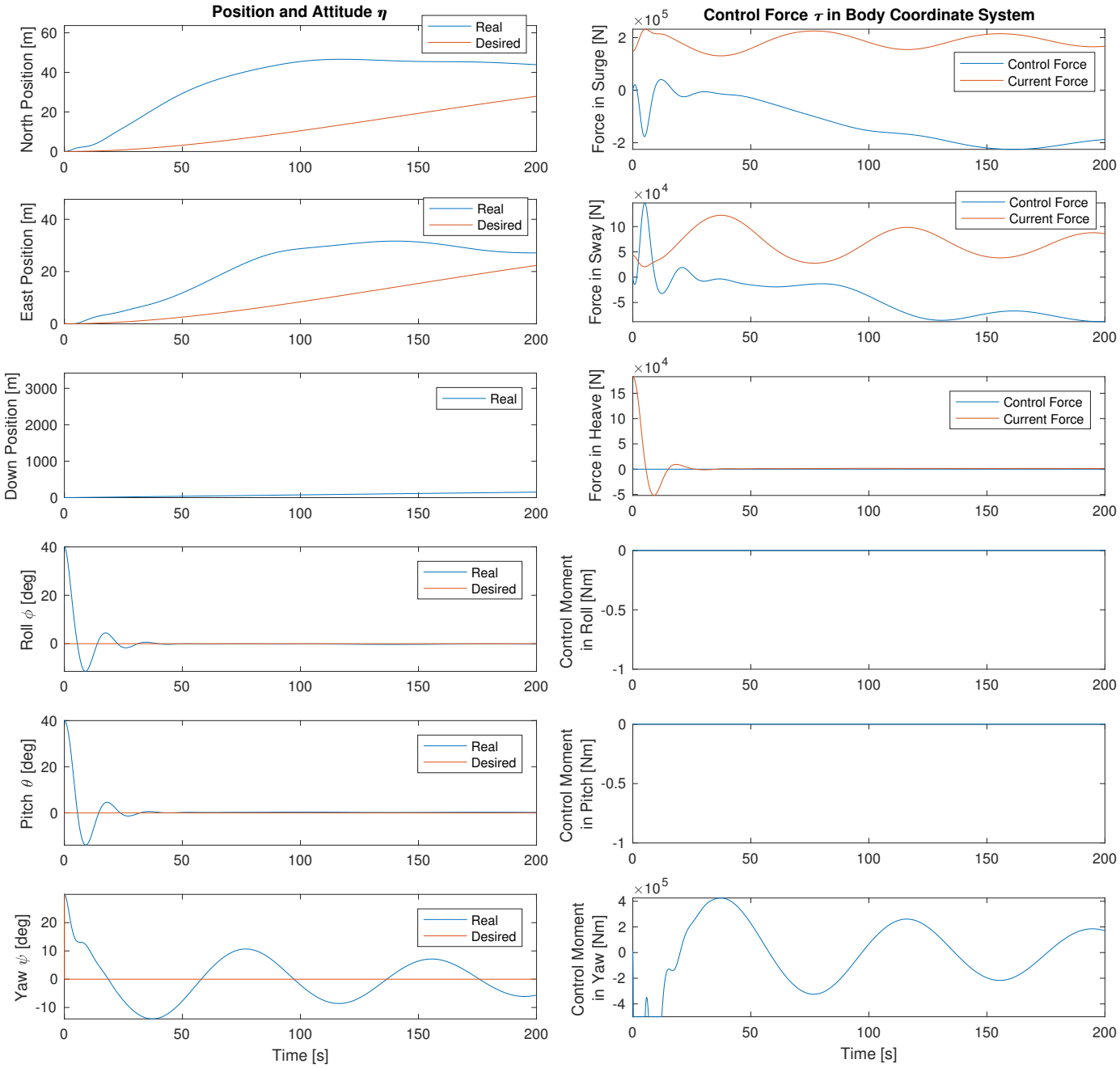

Figure B.42: Transient position and control force buoyancy

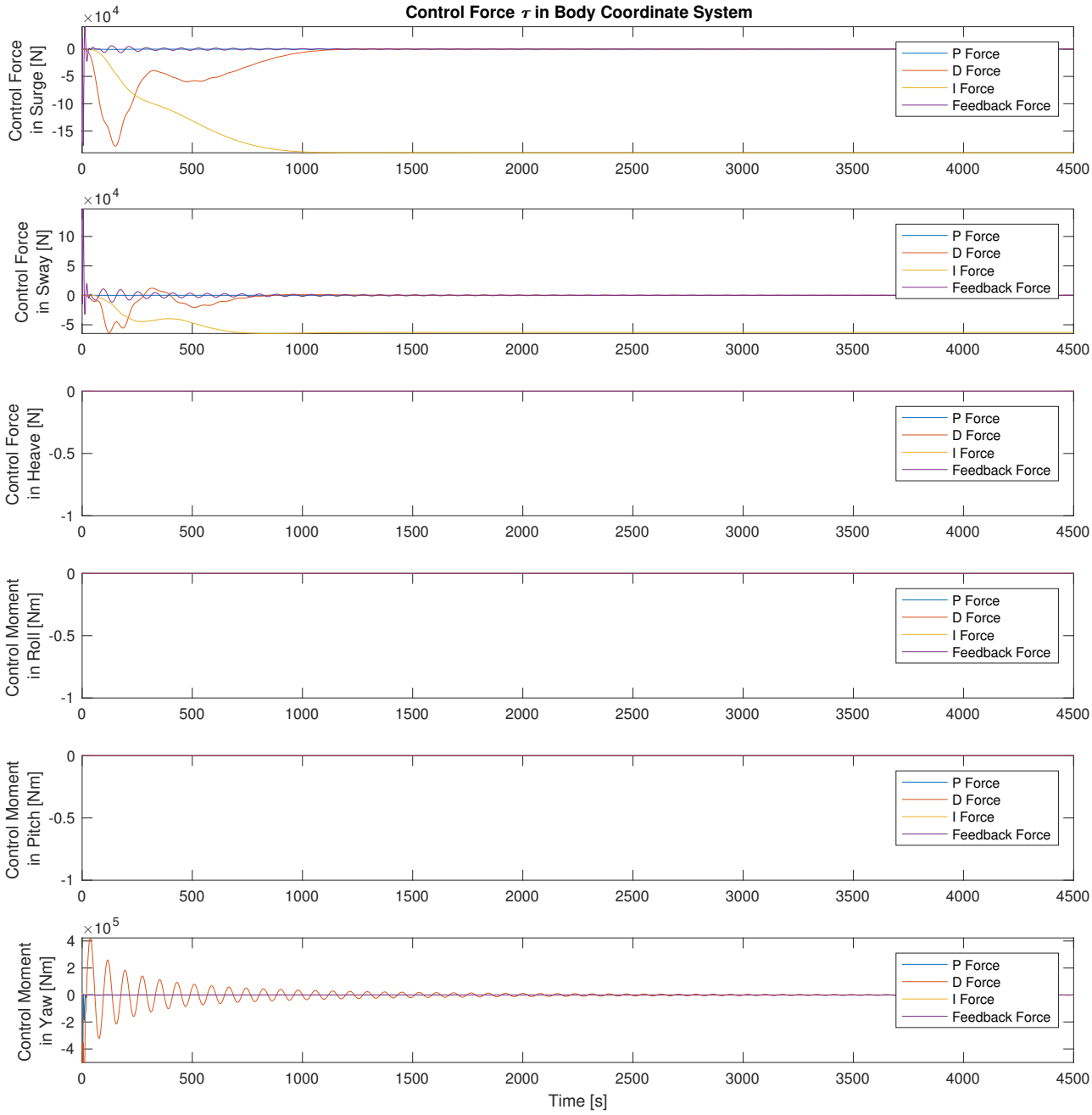

Figure B.43: Advanced control force plot buoyancy

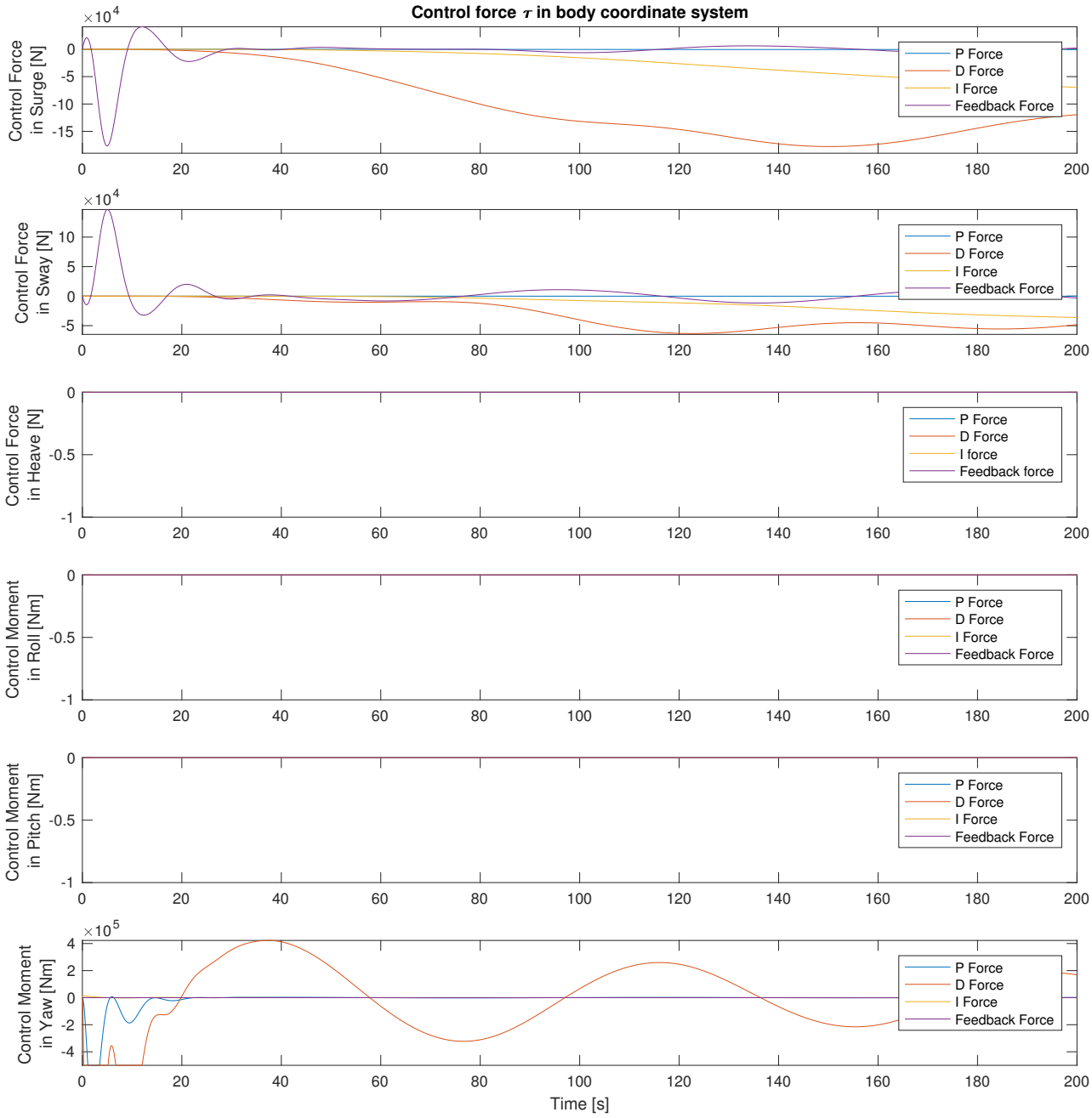

Figure B.44: Transient advanced control force plot buoyancy

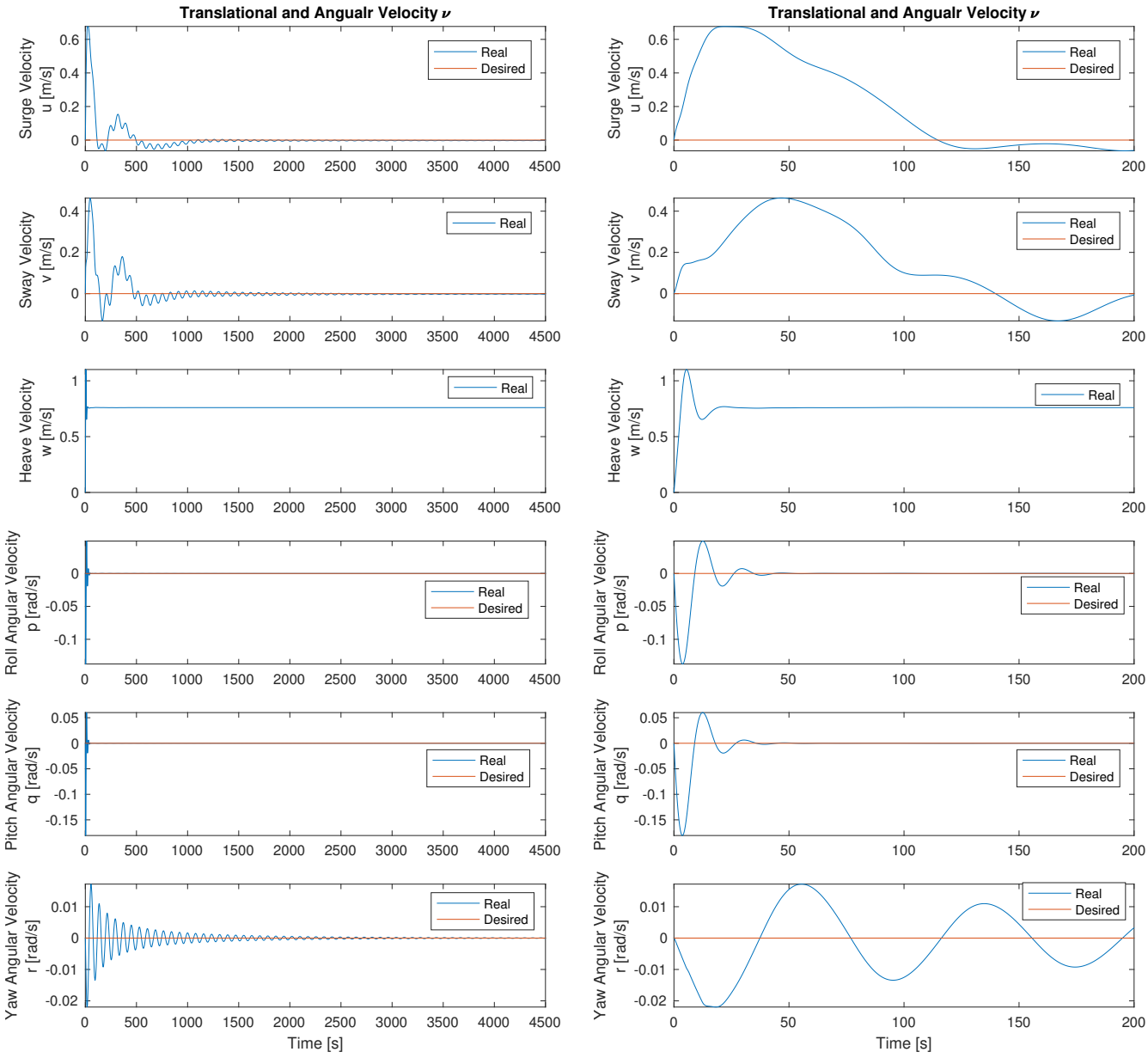

Figure B.45: Velocity plot buoyancy

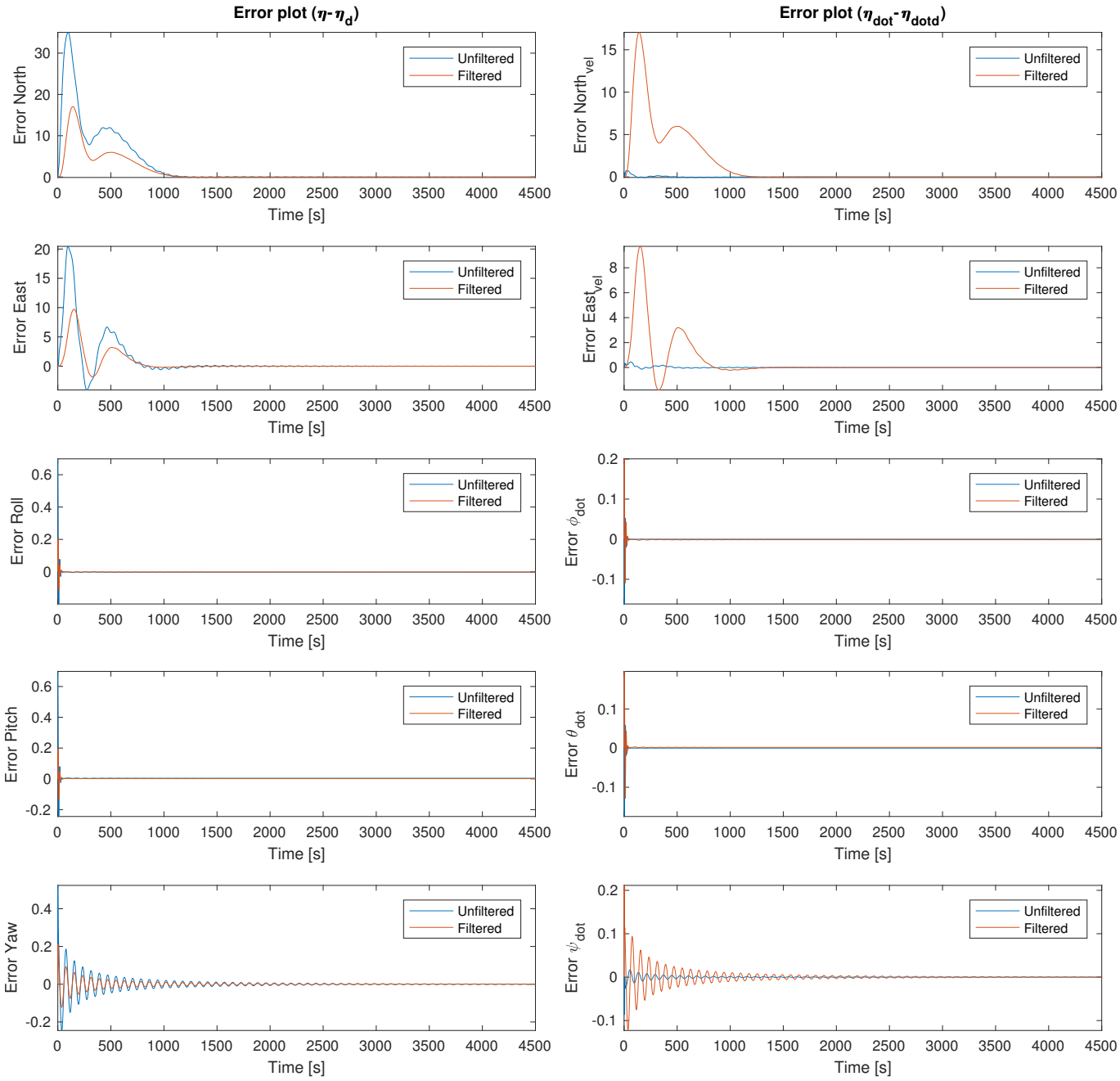

Figure B.46: Error plot buoyancy

B.10 Drop Using Scaled Structure Parameters

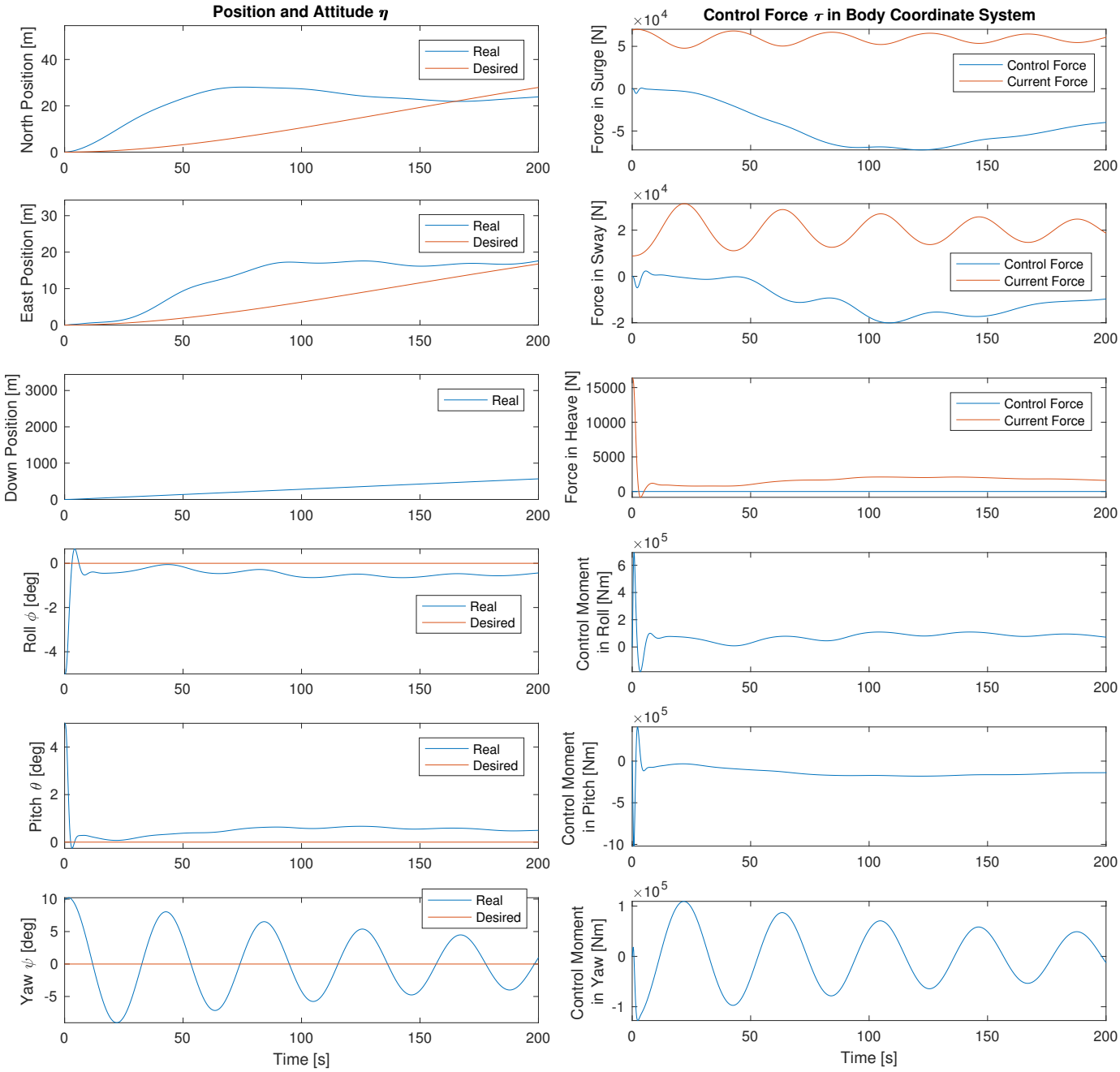

Figure B.47: Transient position and control force scaled

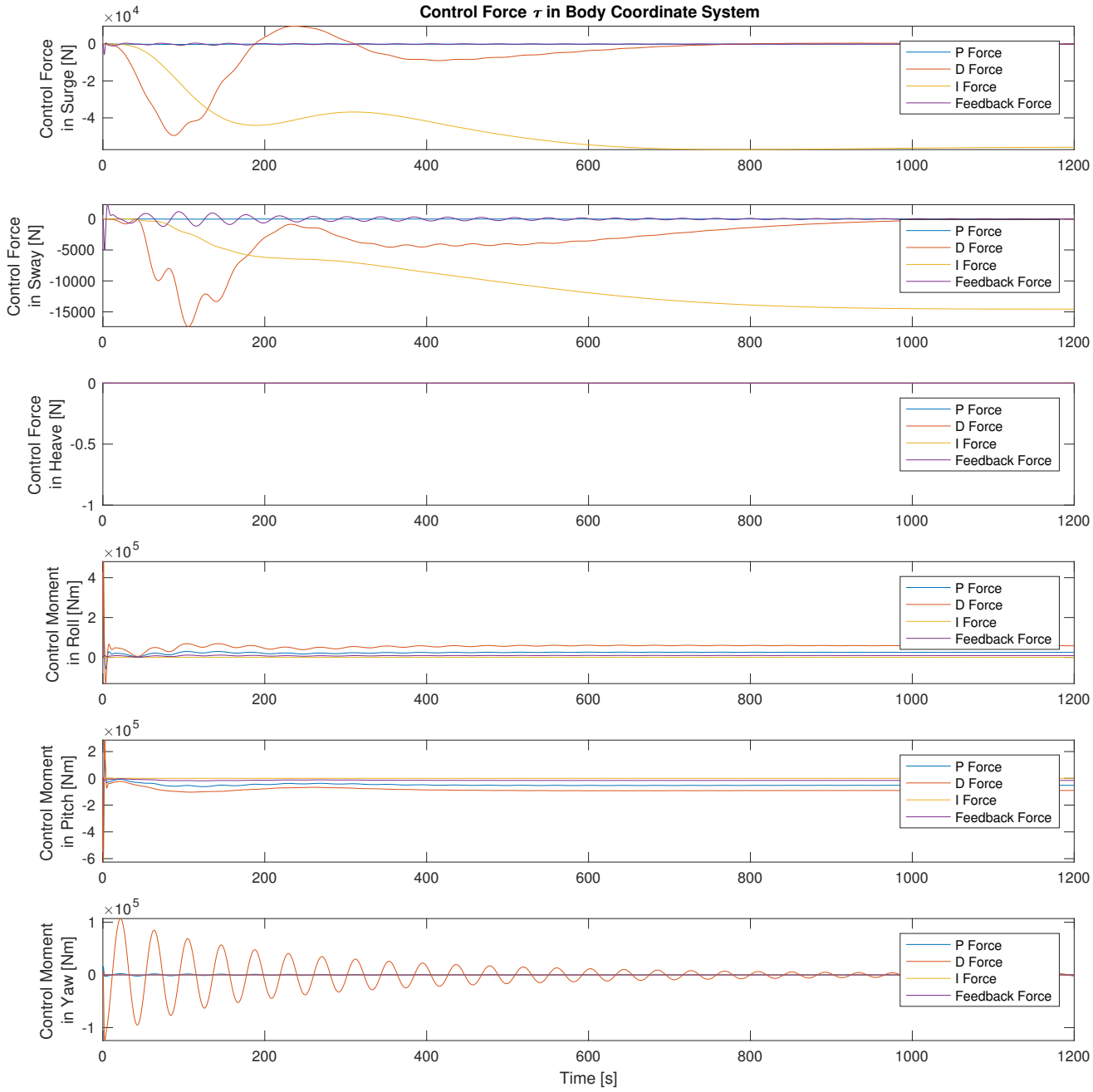

Figure B.48: Advanced control force plot scaled

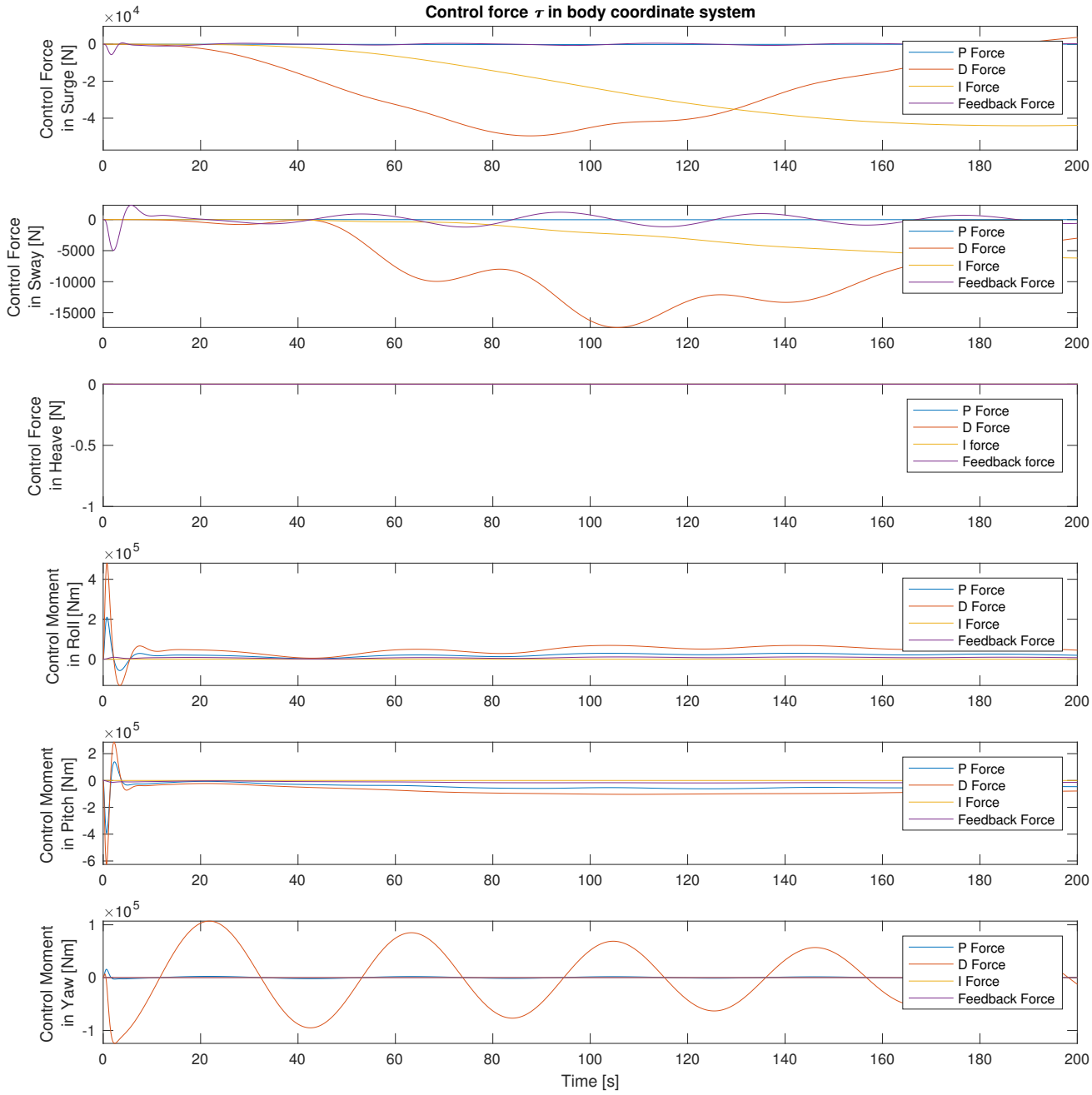

Figure B.49: Transient advanced control force plot scaled

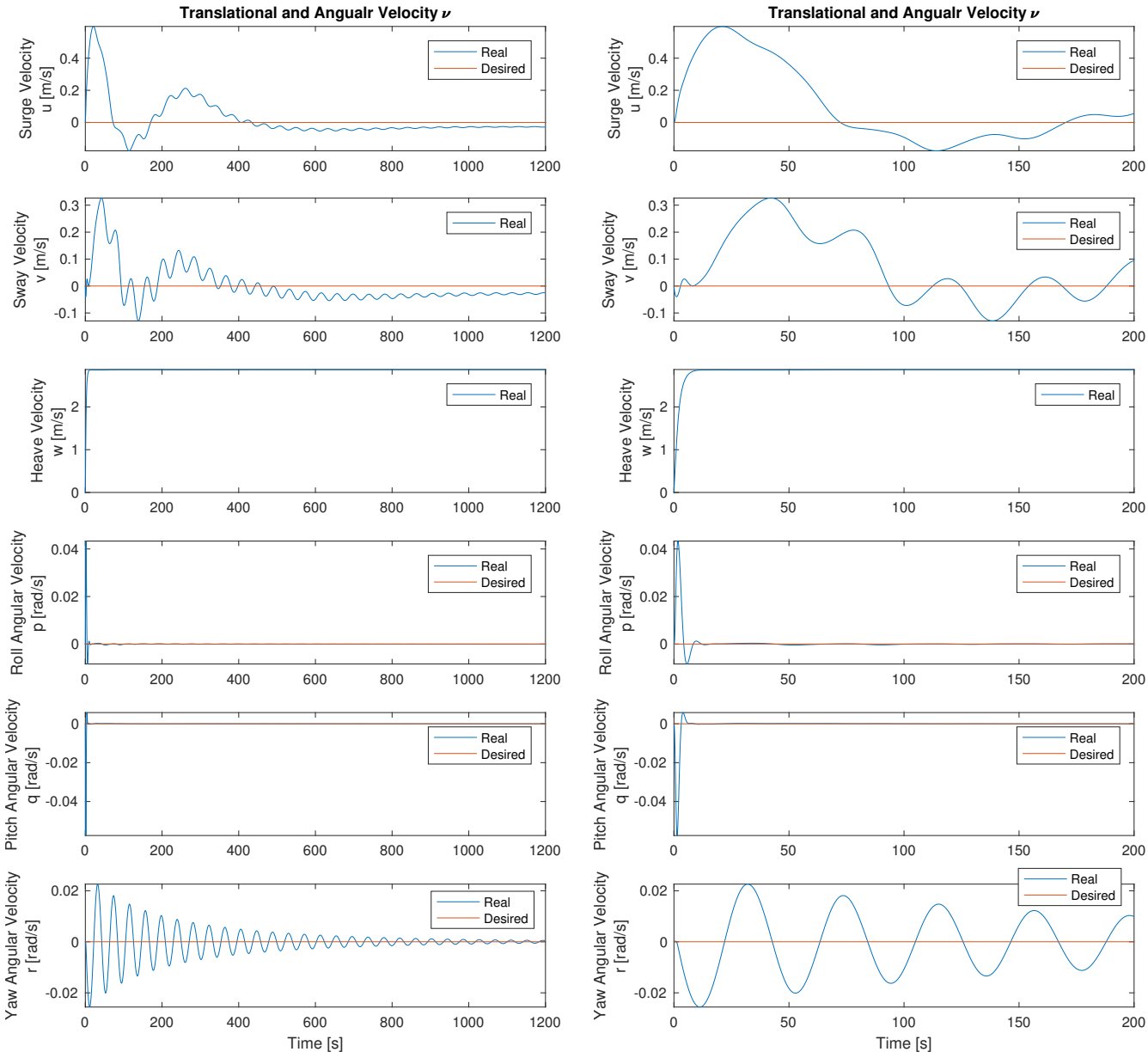

Figure B.50: Velocity plot scaled

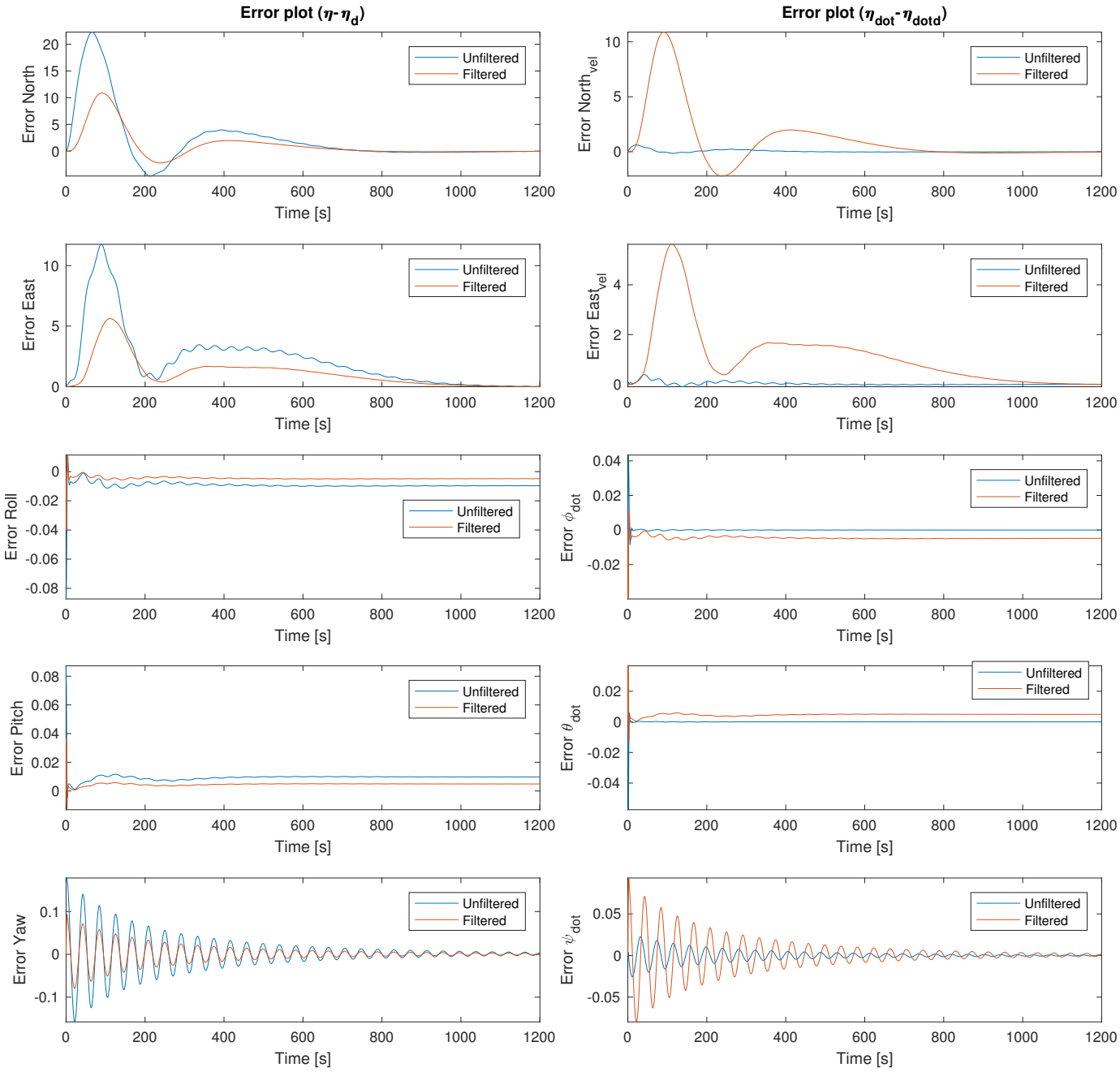

Figure B.51: Error plot scaled

Appendix C

3D

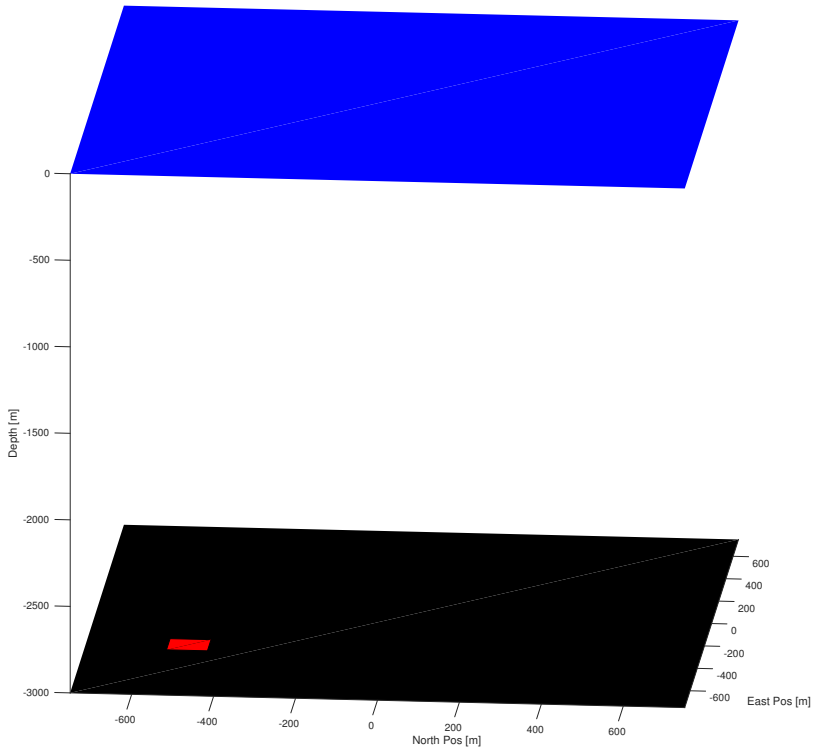

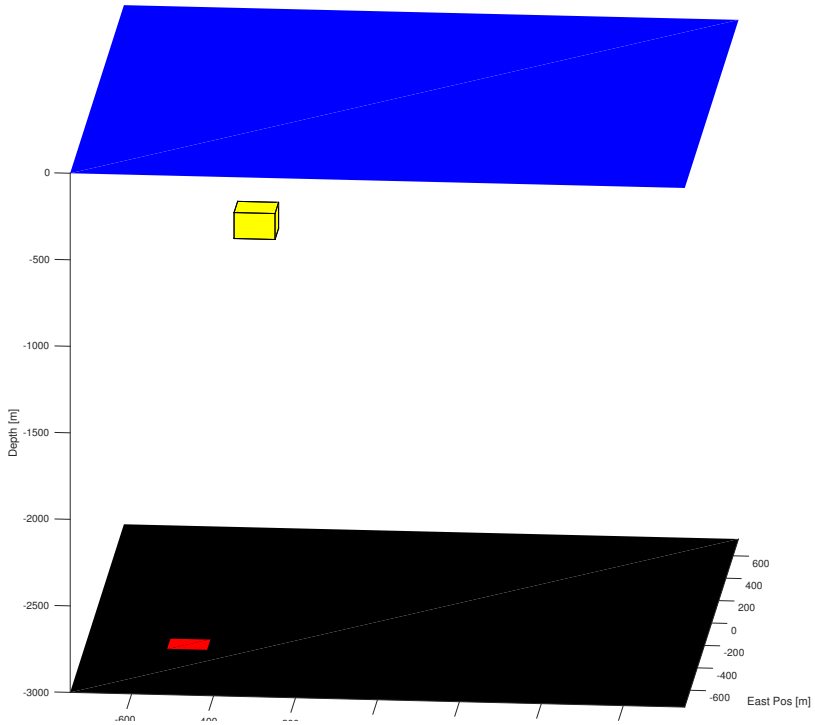
0
-500
-1000
-1500
-2000
-2500
-3000
Depth [m]
600
400
200
0
-200
-400
-600
East Pos [m]

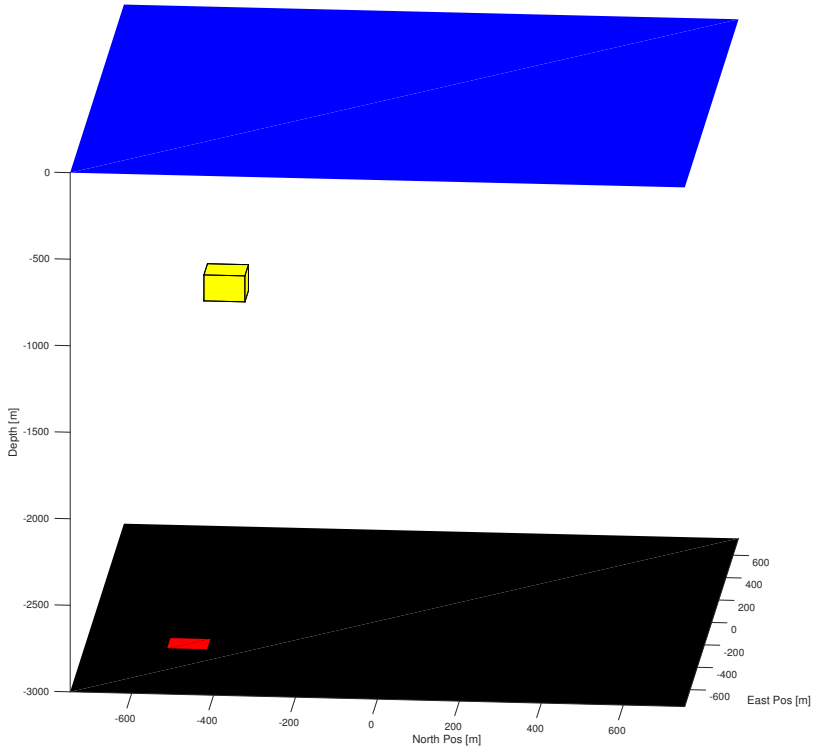
0
-500
-1000
-1500
-2000
-2500
-3000
Depth [m]
-600
-400
-200
0
200
400
600
North Pos [m]
600
400
200
0
-200
-400
-600
East Pos [m]

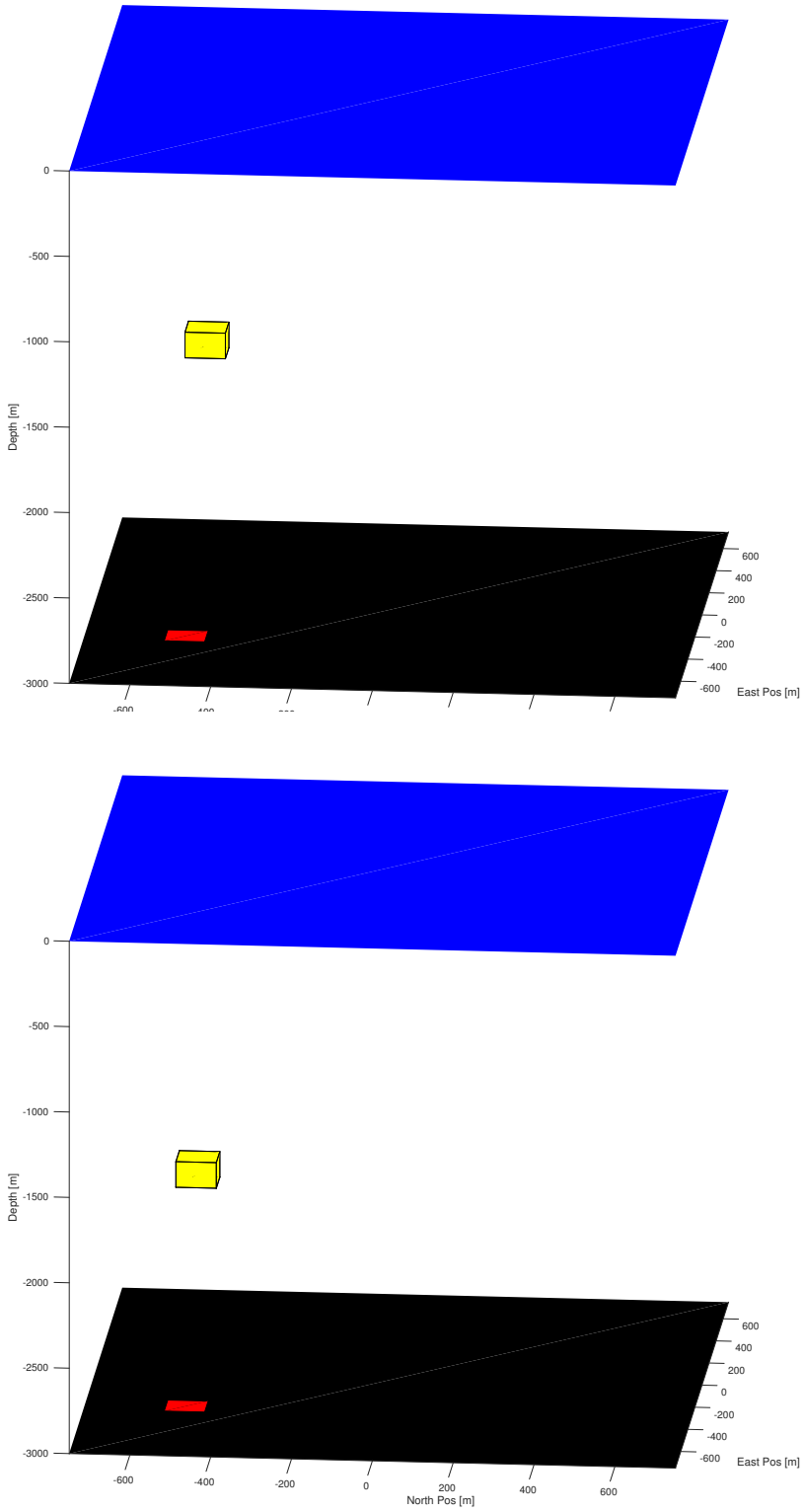
0
-500
-1000
-1500
-2000
-2500
-3000
Depth [m]
600
400
200
0
-200
-400
-600
East Pos [m]
-600
-400
-200
0
200
400
600
North Pos [m]

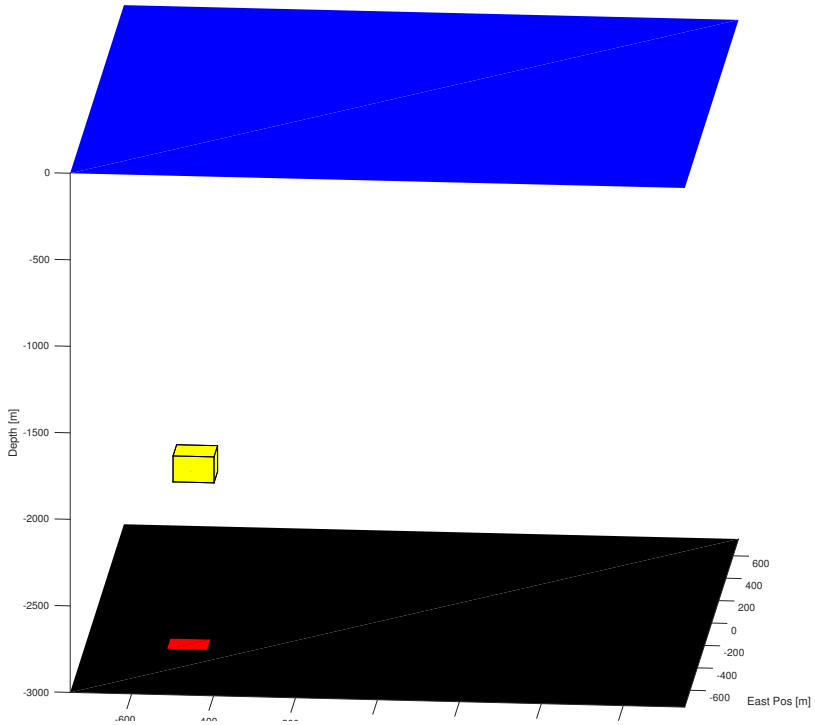
0
-500
-1000
-1500
-2000
-2500
-3000
Depth [m]
600
400
200
0
-200
-400
-600
East Pos [m]

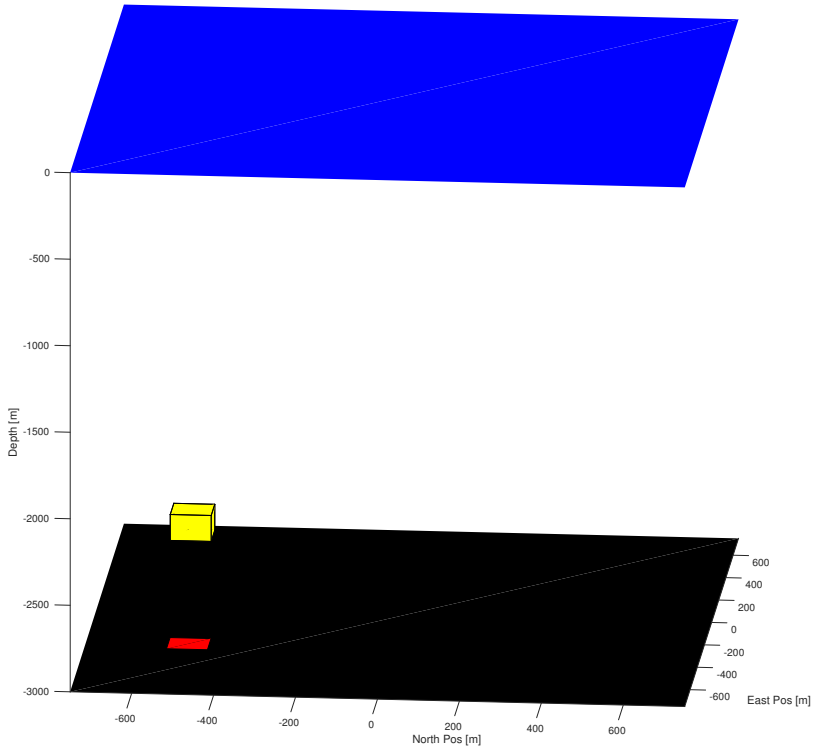
0
-500
-1000
-1500
-2000
-2500
-3000
Depth [m]
-600
-400
-200
0
200
400
600
North Pos [m]
600
400
200
0
-200
-400
-600
East Pos [m]

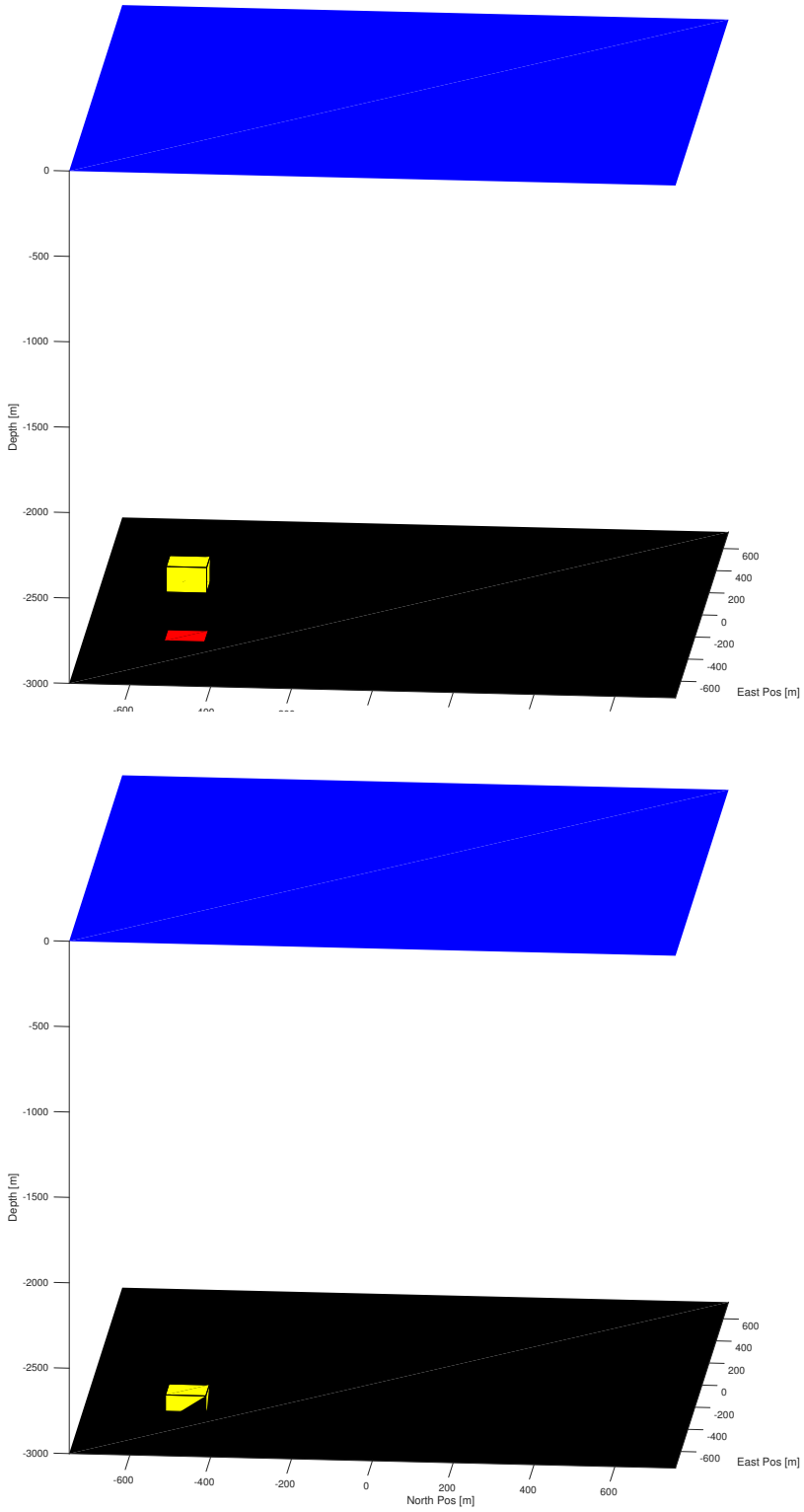
0
-500
-1000
-1500
-2000
-2500
-3000
Depth [m]
600
400
200
0
-200
-400
-600
East Pos [m]
0
-500
-1000
-1500
-2000
-2500
-3000
Depth [m]
-600
-400
-200
0
200
400
600
North Pos [m]
600
400
200
0
-200
-400
-600
East Pos [m]

Appendix D

Electronic Appendix

An explanation of the folders in the delivered electronic appendix is given here.

D.1 Simulation Folder

The simulation folder contains the MATLAB code to run the case simulated in 6.3.

D.1.1 mss Folder

The mss folder contains the mss toolbox, used to calculate the hydrostatic and Coriolis and Centripetal matrix in the simulation model [24].

D.1.2 Case1 Folder

- **Main.m:** initiates the simulation.
- **simulate.m:** runs through the time iteration.
- **control_tuning.m:** Sets the relative damping ration and natural period, and calculates the controller gain matrices.
- **lowpass_filter.m:** Sets the cutoff period in the lowpass filter, and time iterates the filter.
- **guidance.m:** Calculates the guidance trajectory.
- **current.m:** Calculates the current.
- **plotter.m:** Generates the plots.
- **fall_3D.m:** Generates the 3D simulation.
- **save_plot.m:** Saves the plots to folder.
- **controller.m:** Calculates the commanded control force/moment.
- **added_mass.m:** Calculates the added mass matrix.
- **rigid_body.m:** Calculates the rigid body matrix.
- **linear_damping.m:** Calculates the linear damping matrix.
- **nonlinear_damping.m:** Calculates the nonlinear damping matrix.

D.2 Poster Folder

Contains the poster presented in the master thesis exhibition.